Biophysical Investigations of Photosynthetic Reaction Centres from *Rhodobacter sphaeroides*.

by

Paul Kelman Fyfe

A Thesis Submitted for the Degree of Doctor of Philosophy

University of Glasgow

Division of Biochemistry & Molecular Biology

Institute of Biomedical & Life Sciences

June 1997

Declaration

This thesis is an original composition which describes work performed entirely by myself unless otherwise cited or acknowledged. Its contents have not been previously submitted for any other degree. The research for this thesis was performed between October 1993 and October 1996.

Signed ..

Paul K. Fyfe

Date: 30th, June, 1997.

Abstract.

Site-directed mutagenesis was used to produce a series of mutant reaction centres from the purple bacterium *Rb. sphaeroides*. These mutants were investigated using a combination of functional assays and X-ray crystallography in order to correlate structure/function relationships. In particular the effect of the protein environment on the carotenoid pigment in the reaction complex has been investigated. The carotenoid is held within a largely hydrophobic pocket within the reaction centre complex, assuming a twisted 15,15' *cis* conformation. A small number of polar amino acid residues are positioned towards one end, forming almost a ring around the pigment molecule. Each of these amino acids was replaced with a non-polar residue of an approximately similar size: Trp M115-Phe, Ser M119-Ala, Met M122-Leu, Trp M157-Phe and Tyr M177-Phe. The mutant reaction centres were expressed in a background lacking light-harvesting complexes, permitting observation of the spectral characteristics of the complex in the bacterial cell and chromatophores. A range of techniques were then applied to attempt to identify the effects of the mutations on the reaction centre carotenoid. One additional mutant complex was investigated, in which an amino acid in close proximity to the BChl special pair was mutated (Phe to Arg M197). Limited investigation of this mutant complex had already identified altered spectral characteristics, although the precise mechanism by which this spectral shift was produced by the mutation was unclear.

The investigations performed fell into three groups. The initial focus was concentrated on establishing whether the mutant reaction centre complexes were still being properly assembled by the bacteria. To this end, the ability of the bacteria to insert complexes into the membrane, the stability of the complexes upon removal from the membrane, and the ratio of pigments bound within the complex were determined. All of the strains were determined to be assembling correctly, and alterations of the absorption spectrum characteristics were confined to the special pair band of the Phe M197-Arg mutant complexes. The second group of investigations utilised specialised spectroscopic techniques. Circular dichroism studies showed that the carotenoid was apparently binding in a similar fashion in the mutant and wild-type complexes, and that the blue-shifted P band in the absorption spectra of RM197 strains was also manifested in the CD spectra. Resonance Raman spectroscopy provided perhaps the most sensitive probe of the carotenoid and the binding pocket. The results did identify some apparent alterations in the carotenoid

signals, although as there was no prior information regarding the RR spectra of spheroidenone, the information that could be extracted from these studies was limited. ESR was the final spectroscopic technique utilised. It was used to investigate the ability of the various RC complexes to transfer the triplet energy from BChl to carotenoid. All the carotenoid binding site mutants returned wild-type signals. However, those carrying the RM197 mutation showed marked differences from the wild-type. The mutation at RM197 affected the values of the ESR field splitting parameters, and allowed the triplet energy to be transferred at temperatures much lower than that determined for the wild-type.

X-ray crystallography was used to determine the atomic structures of each of the mutants. Initial work concentrated on obtaining a protocol which would be capable of reliably producing high quality crystals, i.e. single crystals, diffracting to high resolution. Optimisation of the purification and crystallisation protocols ultimately led to being able routinely obtain crystals which would diffract to ~2.2Å at the Daresbury synchrotron. Data sets were collected for the wild-type complex, for four of the carotenoid mutants (two of which contained the second mutation at M197), and for the single RM197 mutant. Resolution of the models ranged from 3.2Å to 2.3Å. Several points of interest have arisen as regards the carotenoid binding site and wild-type models. Firstly, the alteration of the amino acid side chains around the carotenoid pocket led to minimal structural alteration. Secondly, a residue was identified (Trp M75) which may be important for the selection of carotenoids bearing a methoxy or hydroxy terminal group (xanthophylls) by the RC. Finally, in one of the models (FM115/RM197), water molecules were observed to have entered the pocket filling the void created by replacement of a tryptophan with a smaller phenylalanine.

All three models of the RM197 complex showed identical structure with minor differences probably the result of the variation in the diffraction data quality. The replacement of the wild-type Phe residue had led to an unexpected reorientation of the M197 side chain, with the Arg side-chain now pointing up towards the periplasm and interacting with a surface residue (Asp L155). This rearrangement appears to be possible due to the positioning of this residue at the interface between the L and M subunits at the base of a crevice in the periplasmic face of the complex. As was observed in one of the carotenoid models, water molecules had entered the complex, filling the void created by removal of the M197 side chain from the region surrounding BChl P_M. The precise structure of the water

chain was the only difference observed among the three models. Concomitant with the insertion of water was a rotation of the 2-acetyl group of P_M of either 20° or 160° from the position assigned in the WT structure. The precise mechanism by which these alterations produced the spectral characteristics remains unclear. However, it is likely to be the cumulative effect of rotation of the 2-acetyl and the alteration in the dielectric constant in the region surrounding the special pair. In addition, some alteration in the distances / angles separating the two BChls of the special pair cannot be discounted.

Acknowledgements

I wish to take this opportunity to thank all those people who have given me their help, advice and friendship over the last few years. Firstly I would like to thank my supervisor Prof. Richard Cogdell for guiding me through what has been a stimulating and very interesting series of investigations and for giving me the opportunity to spend some time working in other laboratories and the financial ability to attend conferences and meetings abroad.

I am also deeply indebted to Dr. Mike Jones for introducing me to the world of molecular biology during time spent in Sheffield, and for the discussions and advice proffered throughout my Ph.D. I must also thank the ever growing Jones family for welcoming me into their home on numerous occasions. Back in Glasgow University I would like to thank Prof. Neil Isaacs for the use of the X-ray detector and computing facilities of the Protein Crystallography Group.

The crystallography sections would not have been nearly so succesful without the help and advice given on numerous occasions by Dr. Katherine McAuley-Hecht. I would also like to acknowledge Dr. Gunter Fritzsch and the members of his lab in the Max-Planck Institut for Biophysics (Frankfurt am Main, Germany) for their help and friendship during my visit there in Spring 1996. In addition, I wish to acknowledge Dr. Gunter Fritszch, Dr. Roy Lancaster and Dr Ullrich Ermler for providing the topology and parameter files used to perform all the crystallographic refinements reported in this thesis. This visit was made possible only through the award of an ESF short term fellowship grant. I must also thank the staff at Daresbury Synchrotron Radiation Source for assistance with the operation of beamlines 9.6 and 9.5.

I am very grateful to Prof. Harry Frank and Dr. Date Chynwat (University of Connecticut) for performing the ESR spectroscopy investigations, and for help in the interpretation of the obtained spectra. Likewise I must acknowledge Dr. Bruno Robert and Dr. Andy Gall (CEA Saclay, Paris) for carrying out the resonance Raman investigations and the cryo-cooled circular dichroism spectroscopy. The room temperature circular dichroism was performed closer to home at Stirling University with the assistance of Dr. Nick Price and Dr. Sharon Kelly.

There are a number of other people who have offered their help, advice and friendship whom I would like to take this opportunity to thank. In alphabetical order, so as to avoid any claims of favouritism, I wish to acknowledge Juan Arellano, Jehan Bakht, Stuart Barrett, Ailsa Carmichael, Gaye Dahler, Peter Dominy, Niall Fraser, Alistair Gardiner, Evelyn Halloren, Tina Howard, Janet Laird, Chris Law, Gerry McDermott, Steve Prince, Justin Ridge, Adrian Simmons, Sarah Thomas and finally the past and present members of the Botany Tea Room.

I would like to thank the SERC/BBSRC for funding this work and my attendance at the 10th International Photosynthetic Congress, Montpellier, France. I also attended the ESF summer school "Biophysical Techniques in the Study of Photosynthesis" (Saclay, Paris) in the summer of 1994, the funding for which was provided by the ESF.

Finally I would like to thank Alex for her support and encouragement throughout, and to Mum and Dad for all their support, not least for unsplitting my infinitives and my english good sound.

INTRODUCTION

MATERIALS & METHODS

C. RESULTS

DISCUSSION & CONCLUSIONS

APPENDICES

Abbreviations

Å	Angstroms
ATP	Adenosine 5' triphosphate
β-OG	β-octyl glucoside
BChl	Bacteriochlorophyll
BD	(R,R)-2,3-Butanediol
bp	Base pairs.
BPheo	Bacteriopheophytin
CD	Circular Dichroism spectroscopy
Crt	Carotenoid
DAD	Diode Array Detector
EM	Electron Microscopy
EPR	Electron Paramagnetic Resonance spectroscopy
FPLC	Fast Protein Liquid Chromatography
fs	Femtoseconds
FT	Fourier Transform
HPLC	High Pressure Liquid Chromotography
Hpt	Heptane-1,2,3-triol
Hxt.	Hexane-1,2,3-triol
ICM	Intracytoplasmic membrane
KPi	Potassium Phosphate
LB	Luria Bertani
LDAO	N-lauryl-N,N-dimethylamine-N-oxide
LH	Light-harvesting complex
MAD	Multiple Wavelength Anomalous Dispersion
MES	2-(N-Morpholino) ethanesulphonic acid
MIR	Multiple Isomorphous Replacement
μs	Microseconds
ms	Milliseconds
nm	Nanometres
NIR	Near Infra-Red
ODS	Octadecylsilyl
ps	Picoseconds
PSU	Photoynthetic Unit
Rb.	*Rhodobacter*
RC	Reaction centre
RCO2	Reaction Centre Only strain of *Rhodobacter sphaeroides*

Rps.	*Rhodopseudomonas*
RR	Resonance Raman spectroscopy
SDS	Sodium dodecyl sulphate
Spo	Spheroidenone
TEAP	Triethylammonium phosphate buffer.
TEMED	NNN'N'-tetramethylethylene diamine
Tris	Tris (hydroxymethyl) aminoethane
Ubi	Ubiquinone

IUPAC-IUB One and Three Letter Amino Acid Codes.

A	Ala	Alanine
C	Cys	Cysteine
D	Asp	Aspartate
E	Glu	Glutamate
F	Phe	Phenylalanine
G	Gly	Glycine
H	His	Histidine
I	Ile	Isoleucine
K	Lys	Lysine
L	Leu	Leucine
M	Met	Methionine
N	Asp	Asparagine
P	Pro	Proline
Q	Glu	Glutamine
R	Arg	Arginine
S	Ser	Serine
T	Thr	Threonine
V	Val	Valine
W	Trp	Tryptophan
Y	Tyr	Tyrosine

Table of Figures

A. INTRODUCTION

CHAPTER 1.

The Evolution and Taxonomy of Photosynthesis.

Photosynthetic organisms form one of the earliest groups of living organisms. The precise dating of the appearance of photosynthetic life has been the subject of much discussion over many years, and has sought evidence from many different sources. Perhaps the most obvious indicator of the emergence of photosynthetic organisms is the build up of oxygen in the atmosphere of the earth. A date has indeed been suggested for this, resulting in the claim that oxygenic photosynthesis has been occurring on earth for over 3500 million years (Awramik, 1992). This date has been based largely on evidence gathered from banded iron formations in rocks which date back to this period. The formation of such quantities of insoluble oxides of iron would suggest a massive and relatively rapid increase in the quantity of oxygen within the atmosphere. While this might seem to be very strong evidence, there are two reasons for disputing the dating of the emergence of photosynthesis from this time.

Alternative mechanisms, by which these banded iron formations could have been formed by non-biological processes, have been suggested by several groups. Proposed alternatives include the photodissociation of water in the atmosphere (Walker et al, 1983), photochemical reactions that extract oxygen from sea water (Cairns-Smith, 1978), and inverse segregation (Lambert et al, 1978). The inverse segregation theory proposes that solar radiation impinging upon the early Precambrian atmosphere could set off a series of complex reactions, leading ultimately to the reduction of iron into its insoluble ferric and ferrous forms. As a result, iron would precipitate out of the sea water, forming layers of iron sediments on the sea-bed. These alternative theories illustrate how the 3500 million year dating of the emergence of photosynthesis has been challenged.

However, the sheer extent of the iron-banded rock formations has led to the widely accepted belief that the only process capable of producing the required levels of oxygen is oxygenic photosynthesis. The strongest argument against the 3500 million year dating, is that it would seem unlikely that oxygenic photosynthesis would predate its anoxygenic relative. The photosynthetic process is often falsely regarded as exclusively an oxygenic one. In purely evolutionary terms, the emergence of photosynthesis, like all other biological processes, would be expected to be through a simple pathway. That photosynthesis could have begun with the oxygen evolving phototrophs, with the highly specialised protein:pigment complexes that this requires, seems paradoxical. It is perhaps more likely that the development of photosynthetic apparatus proceeded by way of a simpler photosystem, possibly via something equivalent to today's heterodimeric purple bacterial system or the homodimeric green-sulphur bacterial system discussed later in Section 1.2. If this was indeed the case, the date of appearance of the first photosynthetic organism can be pushed back further than 3500 million years. Schidlowski (1988), places the appearance of the first anoxygenic phototroph on earth at around 3800 million years ago, 300 million years before its more "technically" advanced oxygenic cousin.

This revised dating of 3800 million years was based upon more direct methods for determining biological activity. Reliance on measuring down-line effects of the bi-product of oxygenic photosynthesis, i.e. molecular oxygen, is open to alternative explanations and dating based on the theories discussed above. Another approach is to attempt to gather evidence that can be directly related to the activity of photosynthetic organisms. Such evidence is available in two forms. Firstly, Schidlowski (1988) provides evidence for the existence of C^{12}-fixation, dating back 3800 million years. The incorporation of CO_2 into biological material is biased towards the utilisation of the lighter C^{12} isotope. Biological material becomes enriched in C^{12}, leaving its surroundings with elevated levels of the heavier isotope, C^{13}. This phenomenon can be used in the analysis of deposits of kerogen. Kerogen is a form of high molecular weight organic matter, that is stable over geological time, and is believed to represent the end point of the burial of biogenic organic matter. This type of investigation, described in Schidowlski (1988), suggests that carbon from

CO_2 was being actively incorporated into biological materials as early as 3,800 million years ago.

The kerogen investigations provide evidence of CO_2 fixation apparently attributable to bacterial photosynthesis. Unfortunately, kerogen does not preserve any of these ancient organisms; the presence of such preserved organisms combined with the chemical evidence would produce a much more convincing set of results. However, there exists further evidence that, it has been claimed, shows ancient photosynthetic organisms preserved within structures formed by the sediment trapping, binding and precipitation activities of microbes. These structures, called stromatolites, have been intensively studied, and Schopf and Packer (1987) claim to have isolated the fossilised remains of cyanobacterial-like cells. One of the big debates surrounding this discovery of cyanobacterial-like cells concerns whether this is a true reflection of the original microbial ecology of the area, or rather of the different abilities of organisms to "survive" fossilisation. There is also debate as to whether the stromatolite "fossils" are even of biological origin. The "date-of-birth" of photosynthesis remains controversial due, in large degree, to difficulty in determining definitively the bio-genic origin of fossilised specimens.

1.1. Taxonomy of Photosynthetic Life.

Attempts to establish the period during which photosynthetic life first appeared constitute, then, one focus of research into the evolution of these organisms. Also of great interest are the attempts to order those photosynthetic organisms that exist in the present day, in both taxonomic and evolutionary terms. The universal problems met in classifying bacterial species have been encountered in attempts to classify photosynthetic bacteria. For example, if a species is defined as "any of the taxonomic groups into which a genus is divided, the members of which are capable of interbreeding" (McLeod & Hanks, 1984), then as *Rb. sphaeroides* and *Escherischia coli* can mate they would have to be regarded as being within the same species. This ability to mate is in fact utilised in investigations described later in this thesis to introduce into *Rb. sphaeroides* reaction centre genes manipulated in *E. coli*. Schemes depicting the evolution of photosynthetic organisms on Earth have been

based on the results of investigations using a range of techniques. Separation into families has been traditionally undertaken by using pigment analysis, investigating the internal cell structure (Section 2.1) and noting the types of metabolic processes the organism can perform (Pfennig & Trüper, 1983). Another classification scheme has been developed (Woese, 1987) based on the levels of similarity of the 16S ribosomal RNA shown by the organisms studied. This procedure has been widely applied in modern taxonomic studies. It has led to the proposal that all forms of life fall within three kingdoms: the eukaryotes, the eubacteria and the archaebacteria. The 16S rRNA classification for phototrophic bacteria shows high similarities with classifications using more traditional methods. However there are some important exceptions to this generalisation.

The eubacteria can be split into ten phyla, five of which have photosynthetic members. Most of these contain both photosynthetic and non-photosynthetic organisms (Figure 1). It has been suggested that the common ancestor of most or all of the phyla had photosynthetic capability, and that certain groups have lost the capability over time (Blankenship, 1992).

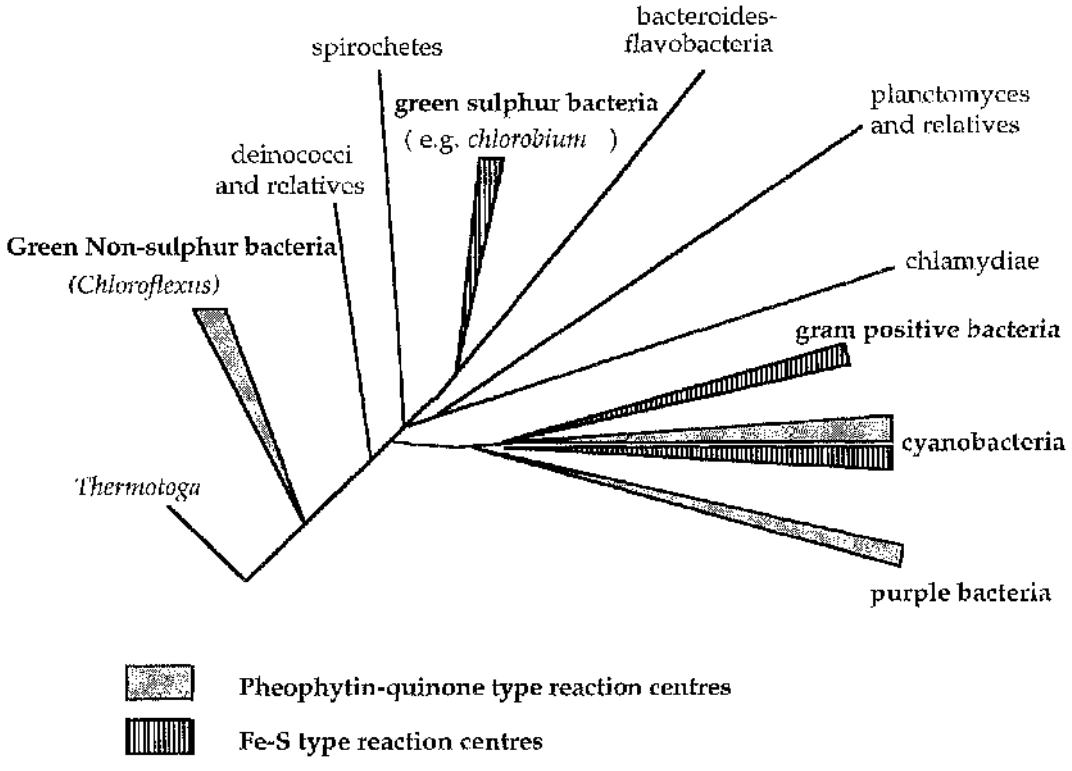

Figure 1: Evolutionary tree of the eubacteria, based on 16S rRNA analysis. Also depicted is the class of reaction centre present in the groups which contain photosynthetic members (Adapted from Woese 1987).

1.2. Classification by Structural and Functional Similarities.

The classification of organisms must also take into account functional and structural similarities. These are not revealed by 16S rRNA analysis. For photosynthetic organisms, the most commonly used basis for structure/function classification is perhaps analysis of the reaction centre complex (Kirmaier & Holten, 1987; Barber, 1987; Nitschke et al, 1987; Michel & Deisenhofer, 1988; Nitschke & Rutherford, 1991). Photosynthetic organisms can be readily divided into three groups depending on the type of reaction centre they contain: those which contain a pheophytin-quinone reaction centre; those which contain an Fe/S reaction centre; or those which contain both. The 16S RNA based evolutionary tree indicates that the purple bacteria are most closely related to the gram positive bacteria and the cyanobacteria (Woese et al, 1987). However, when reaction centre content is taken into account, purple bacteria seem more closely related to the green non-sulphur bacteria. A similarly close relationship between the gram positive bacteria and the green sulphur bacteria is revealed through

reaction centre analysis, and yet this relationship is not easily recognised when only the 16S rRNA groupings are considered (Figure 1).

The evolution of the reaction complex is itself another focus of investigation. The purple bacterial reaction centre is composed of three protein subunits, within which are held a number of pigment molecules (see Section 2.3). Two of the protein subunits, L and M, form a dimeric structure, responsible for the binding of the pigments. The third subunit, H, plays no part in pigment binding. The cyanobacterial and plant Photosystem II (PS II) has long been likened to the purple bacterial reaction centre (Michel & Diesenhofer, 1988; Komiya et al, 1988). PS II and the purple bacterial reaction centre share a number of common features. They are both members of the iron-quinone class of reaction centres (unlike PS I of cyanobacteria and plants which is of the iron-sulphur system), and the two putative "core" subunits of PS II show a relatively high level of sequence homology with the purple bacterial L and M subunits.

The transmembrane domains of L and M share a 20% sequence homology with their putative counterparts in PS II, having 66 identical amino acid residues (Trebst, 1986; Ruffle et al, 1992; Xiong et al, 1996; Svensson et al, 1996). This level is not sufficiently high to provide conclusive evidence that the core of the PS II complex will assume a similar folding pattern as the purple bacterial reaction centre core. However, other evidence is available which strengthens the argument that this may nonetheless be the case. This evidence includes functional analogies with the purple bacterial reaction centre, the fact that the herbicide azidoatrazine binds to both the D1 and L subunits affecting Q_B binding, and the presence of analogous point mutations in both systems which can confer resistance to the action of this herbicide (Sinning et al, 1989; Sinning, 1992; Xiong et al, 1996). Immunological experiments have also provided evidence that the D1 and D2 proteins each span the membrane five times (Sayre et al, 1986). Structural information for the PS II complex is currently, and will probably remain for some time, restricted to predictions and modelling based on sequence analysis in combination with information gathered from other complexes. The major barrier to progress is the current inability to purify the intact complex in a sufficiently stable form. However, some progress has been made with the use of 2-D crystallisation and cryo-electron microscopy (Holzenburg et al

1993; Santini et al, 1994; Nakazato, 1996). The data obtained from 2-D crystals of PS II from spinach, appears to show a core structure similar to the L/M core found in purple bacterial reaction centres.

However, modelling of the structure is ongoing. Ruffle et al (1992) presented a model structure of PS II from *Pisum sativum*, Xiong et al (1996) a model for the D1/D2 proteins and the cofactors for the PS II complex from the cyanobacterium *Synechcystis sp.* PCC 6803, while Svenson et al (1996) report similar work, but fail to mention which species they worked on. The modelling carried out by these groups followed very similar lines. They used the crystal structures of the *Rps. viridis* and *Rb. sphaeroides* reaction centres as a starting point. The ancestral relationship between the bacteria and higher plant sequences allowed both the L and M subunits to be used as structural templates for the modelling. Modelling of the less conserved extra-membranous regions was performed using a combination of database searches for regions of sequence homology, and using the results as the basis for building of these sections. Finally computational techniques that utilise databases of information regarding the favoured rotameric states of amino acid side-chains, can perform "refinement" by calculating interactions within the model and carry out energy minimisations of these.

A structure similar to the dimeric subunit "core" described above is also being uncovered in the Photosystem I complex (see Fromme, 1996, for a current review of the work on the structure of PS I). Crystals of this complex have been obtained from the cyanobacterium *Synechococcus elongatus* from which a model to 4Å resolution has been produced. Diffraction has been observed to much greater resolution (~2.5Å, Fromme, P., 1996, personal communication). However, this level of resolution has only been observed in one dimension of the crystals (in the plane of the membrane). Unlike the PS II situation, the availability of pure and stable protein would suggest that it should be possible to construct models equal in quality to those developed for the purple bacterial reaction centres. However, the 4Å resolution model (Krauß et al, 1996) has been sufficient to reveal a core region remarkably similar to the L and M subunit configuration of the purple bacteria. Two sets of five transmembrane α-helical spans can be clearly observed, and appear essentially identical to L and M. The remainder of the structure does not show any other obvious

regions of homology, although as the models improve this situation may change. This was a relatively unexpected. It had been thought that the reaction centres would be split into two groups: the Fe-S photosystem (i.e. PS I), and the Fe-Q systems (i.e. purple bacteria and PS II). This recent information about PS I might suggest otherwise. The full impact of the crystal structure of PS I on the discussions of the evolution of photosynthesis has yet to be seen. This area has been recently reviewed by Fromme et al (1996).

The evolutionary advantage of the heterodimeric structure probably lies in the formation of the (bacterio)chlorophyll special pair (Blankenship, 1992). The ancient ancestor to the photosynthetic community presumably consisted of a monomeric reaction centre. The emergence of a heterodimeric structure perhaps arose through the developing ability of monomeric proteins to form homodimers. Indeed, a homodimeric reaction centre can in fact be seen today in the green-sulphur bacteria, for example in *Chlorobium* (Nitschke & Rutherford, 1991). It may be that the green-sulphur bacteria represent the end-point in the evolution of homodimeric reaction centres. While the green-sulphur bacteria continued to follow the homodimer structure, other groups branched off, forming the current species containing heterodimeric reaction centres.

For homodimer and subsequently for heterodimer formation to have occurred there must have been some form of selective pressure. One of the most striking features of the modern purple bacteria reaction centre is the presence of the BChl special pair (Figure 2). The elucidation of the significance of this special pair is the focus of a large volume of work (See Woodbury & Allen (1995) for a recent review of the research into the special pair). It can be argued that this arrangement of BChl pigments is vital for the high efficiency of the modern reaction centre. This suggests that the ancient monomeric reaction centre, whilst functional, was not particularly efficient. The formation of the homodimer may have provided some of the advantages of the BChl special pair. Subsequent gene duplication and the divergence of the subunits permitted further refinement of the reaction centre over time.

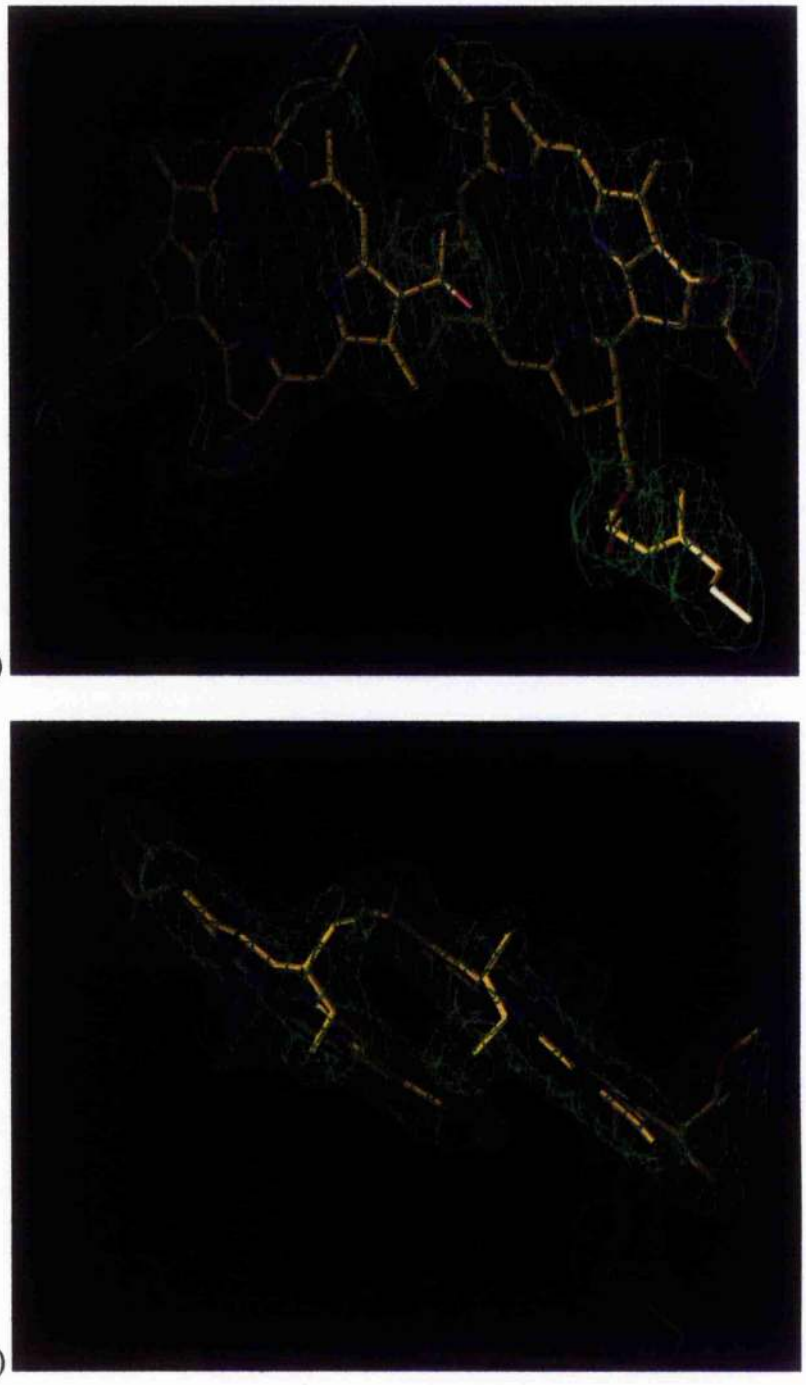

Figure 2: The special pair of bacteriochlorophylls in the photosynthetic reaction centre from *Rhodobacter sphaeroides* WT red (this work), (a) side on view; (b) viewed looking down upon the reaction centre from the periplasmic side of the membrane. The WT red 2Fo-Fc map is contoured at the 1 sigma level.

The evolution of the reaction centre is one part in the development of an efficient photosynthetic system. The light harvesting capability of the reaction centre is poor, and so other pigment:protein complexes had to be created, or perhaps some existing complex adapted, to make more efficient use of this new form of "proton pump". Light harvesting has become the domain of specialised complexes which give a remarkable increase to the light capturing capabilities of the organism. *Rb. sphaeroides* can produce two different forms of light harvesting complexes, LHI and LHII. The antenna complexes are discussed in more detail later, but for a recent review of progress in research into these pigment-protein complexes see Fyfe & Cogdell (1996).

Production of an efficient reaction centre surrounded by light-harvesting complexes does not in itself produce a successful photosynthetic system. These protein:pigment complexes must be co-expressed in carefully controlled ratios to one another, and also in conjunction with other complexes that are able to make use of the proton gradient produced. All this had to occur within a single membrane structure, "gradient-former and gradient-harvester" had to span the same membrane. This was probably not such a great obstacle, as the respiratory chain had presumably already been functioning within such a structure. However, since the original hijacking of the membrane systems by the photosynthetic complexes, the structure of the membrane would appear to have been drastically altered. A recent report by Sturgis & Niederman (1996) has provided evidence that the LHII complex may be partly responsible for the internal membrane structure found in purple bacteria. They hypothesise that the B800-850 complex of *Rb. sphaeroides* both drives development of the vesicular intracytoplasmic membranes (see Section 2.1.) and determines the size of these membrane vesicles. However, the vesicular chromatophore structure of *R. rubrum*, which does not synthesise LHII, demonstrates that additional processes must also be involved. The details of the internal membrane structure of photosynthetic organisms are still being uncovered. The recent elucidation of atomic structures for light-harvesting complexes has refocussed some attention back onto this area. Some of the current theories are described in the next section, which begins with a discussion of the internal membranes found inside purple photosynthetic bacteria.

CHAPTER 2.

Structure and Function of the Photosynthetic Apparatus

The apparatus which allows organisms to perform photosynthesis has been intensively studied over many years. While recent investigations have tended to become more detailed with the recent availability of high resolution structural data, and the application of increasingly sensitive spectroscopic techniques, much remains unknown about the system as a whole. The structural data now gathered has reflected attention back onto how the photosynthetic "super-complexes" might be arranged in the membrane, a problem that was first examined in the 1930s by Emerson & Arnold (1932) in their discussions of the photosynthetic unit (PSU). The PSU is the combination of antenna light-harvesting complexes and the reaction centre. The system can be seen as functioning in an analogous manner to a satellite dish, the light-harvesting complexes forming the dish, capturing energy and feeding it into the central receptor, i.e. the reaction centre. This section will discuss the current ideas regarding the PSU and the protein-pigment complexes involved. In addition, discussion into the structure and roles of the carotenoid pigments in photosynthetic organisms is included, setting the scene for the investigations into the carotenoid binding pocket carried out in the research reported in later chapters.

2.1. Structure and Organisation of the Internal Membranes of Purple Bacteria.

The electron microscope made possible the detailed investigation of the internal structure of cells. Studies of photosynthetic bacteria using electron microscopy began in the early 1950's (Pardee et al, 1952; Schachman et al 1952), with Vatter & Wolfe (1958) the first to publish analyses of the internal structure of a range of photosynthetic bacteria. These

investigations revealed an unusual arrangement of membranes inside the bacteria (intracytoplasmic membrane or ICM). It has been shown that the major protein components of these ICMs are the photosynthetic protein supercomplexes (Figure 3), and that the ICM organisation differs depending upon the species of photosynthetic bacteria.

As would be expected of gram negative bacteria, the photosynthetic bacteria all posses an outer membrane that appears under the electron microscope as two electron dense lines separated by an electron transparent middle zone. The thickness of this membrane is approximately 75-100Å (Cohen-Bazire & Kunisawa, 1963) Inside the outer membrane lies the cytoplasmic membrane (CM). It is this membrane that functions as the selective barrier to the environment surrounding the protoplast. Electron microscopy has shown that this membrane has the same apparent structure as the outer membrane, again showing up as a double track structure (Cohen-Bazire & Kunisawa, 1963; Boatman, 1964; recently reviewed by Drews & Golecki, 1995). Held within the CM are the components of the respiratory chain, along with additional energy transducing components and transporters. However the pigment-protein components of the light reactions of photosynthesis are restricted to the ICM (Holt & Marr, 1965).

The ICM itself is believed to be formed from invagination of the CM (Drews & Giesbrecht 1963; Hickman & Frenkel, 1965; Tauschel & Drews 1967). The ICM and CM appear to form a continuous system. This has been demonstrated in several of the photosynthetic bacteria (Drews & Giesbrecht, 1963; Cohen-Bazaire & Kunishawa, 1963; Boatman 1964; Holt & Marr 1965; Tauschel & Drews, 1967). Despite the apparently continuous nature of these two membrane systems, there are distinct differences in their chemical and structural composition and in their physical properties.

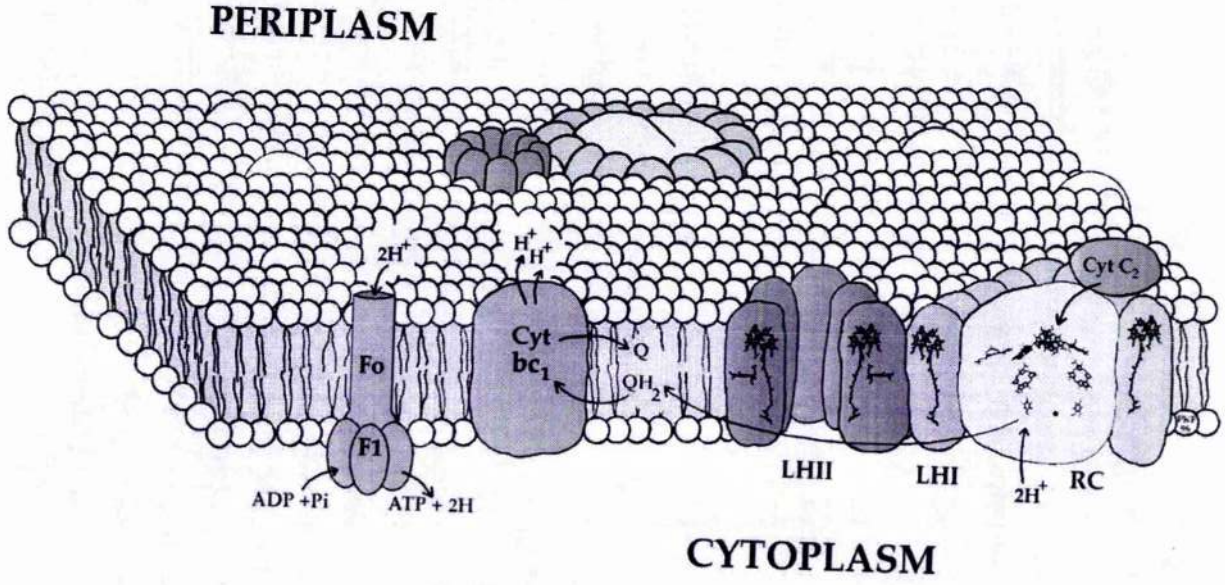
PERIPLASM
2H+
H+ H+
Cyt C2
Fo
Cyt bc1
Q
QH2
F1
LHII
LHI
2H+
RC
ADP +Pi
ATP + 2H
CYTOPLASM

[Facing Page]

Figure 3: Model of the photosynthetic apparatus as typically found in the intracytoplasmic membrane of a photosynthetic bacterium such as *Rb. sphaeroides*. The reaction centre is surrounded by a 16 subunit ring of LHI (B850) forming the "core" complex. Positioned adjacent to this LHI ring are the nonameric rings of LHII (B800-850) antenna complexes. The charge separation events within the reaction centre lead to the release of dihydroquinone into the membrane. The membrane-bound cytochrome bc_1 complex oxidises the quinone, releasing the protons into the protoplasm, while the electrons are shuttled back to the reaction centre via the soluble cytochrome C_2. At the same time the ATPase complex uses the proton gradient to provide the energy for ATP synthesis. In this way, the light energy is converted into a chemical form of energy which can supports a large number of processes within the bacterium.

One of the most distinctive markers which can be used to determine the bacterial species is the structuring of the ICM within the cells. This alters greatly and specifically across different strains of bacteria. The ICM adopts one of four structures (Figure 4). Firstly there is the vesicle type structure found in bacteria such as *Chromatium vinosum*, *Rhodobacter capsulatus*, *Rhodobacter sphaeroides*, *Rhodospirillum rubrum*, *Thiocapsa roseopersicina* and some other species. Secondly, there are ICMs that consist of tubules e.g. *Thiocapsa pfennigii*. Thirdly there are the flat thylakoid-like membranes found in *Ectothiorhodospira shaposhnikovii*. and *Rhodospirillum molischianum*. Finally there are the large thylakoid-like membranes, partially stacked but irregularly arranged. This final form is found in bacteria such as *Rhodopseudomonas viridis* and *Rhodopseudomonas palustris* (Drews & Imhoff, 1991).

1: *Rhodobacter sphaeroides*

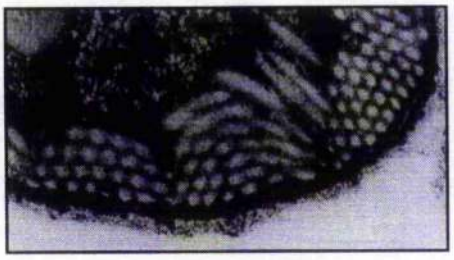

2: *Thiocapsa pfennigi*

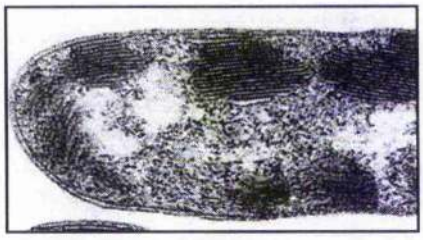

3: *Ectothiorhodospira shaposhinikovii*

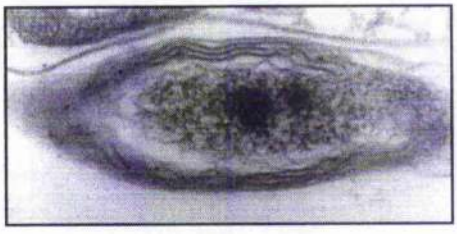

4: *Rhodopseudomonas palustris*

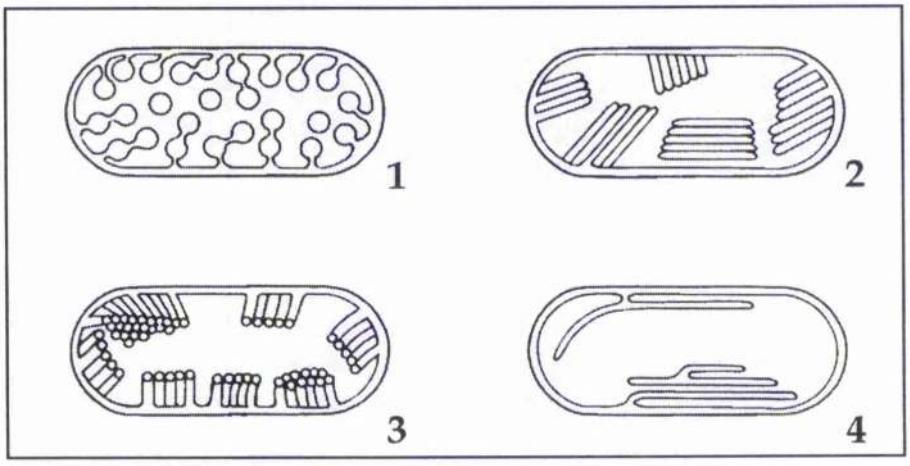

Figure 4: Electron micrographs and cartoon representations of the four basic structures and arrangements of intracytoplasmic membranes (ICM) that carry the protein:pigment apparatus for photosynthesis: **1.** *Rhodobacter sphaeroides* ; **2.** *Thiocapsa pfennigii* ; **3.** *Ectothiorhodospira shaposhinikovii* ; **4.** *Rhodopseudomonas palustris.* (electron micrographs 1, 2 & 4 adapted from Gall (1994), EM. 3 and cartoons adapted from Drews & Golecki (1995).

The biosynthesis of ICM is strictly controlled in most bacteria (Lascelles, 1959; Cohen-Bazaire & Kunisawa, 1963; Marrs & Gest, 1973; Schumacher & Drews, 1979; Lee & Kaplan, 1992a, b; Bauer, 1995). Under aerobic conditions, where chemotrophic growth is dominant, most purple bacteria do not produce ICM. The exceptions to this rule, found to date, are

Rhodobacter capsulatus and a group of aerobic photosynthetic bacteria, recently reviewed by Shimada (1995). *Rhodobacter capsulatus* will continue to produce a small amount of ICM even under high oxygen concentrations. However, the aerobic photosynthetic bacteria, such as *Erythrobacter, Roseobacter* and *Acidiphilum* species will only synthesise the photosynthetic apparatus in the presence of oxygen, and cannot grow in anaerobic conditions even in the light. The regulation of the synthesis of the photosynthetic apparatus in the aerobic photosynthetic bacteria remains unresolved.

Despite some differences in the expression of the ICM systems in different bacteria there remains a common theme. Photosynthetic bacteria can greatly increase the surface area of the internal membrane when grown in an environment conducive to photosynthetic growth, although the precise conditions to produce this effect can be very different. Bound within this extensive membrane system are the pigment-protein complexes responsible for the light reactions of photosynthesis. There are in addition a range of complexes responsible for the utilisation of the products of the light reactions, e.g. the ATPase complex, utilising the generated H^+ gradient. The organisation of these complexes within the ICM of photosynthetic bacteria is an area of research which has taken a great leap forward in recent years, with the elucidation of the atomic structure of two LHII (McDermott et al, 1995; Koepke et al 1996) complexes, along with the 8Å map for an LHI complex (Karrasch et al, 1995). To complete the system to atomic detail a model LHI was produced by combining the details known about LHI with the crystal structure of the *Rps. acidophila* LHII structure. Attempts to build models of the entire RC-LHI-LHII complex, i.e. to build a model of the photosynthetic unit (PSU) (Hunter et al, 1989; Papiz et al, 1996; Hunter, 1995; Hu et al, 1997), has opened up research leading to more accurate understanding of how each of the individual components of the system interact with each other.

Into this membrane are inserted the protein-pigment complexes which comprise the photosynthetic apparatus. A number of developmental studies have revealed that during photosynthetic membrane genesis, the reaction centres are inserted first, followed by the LHI complexes, and only then are the LHII complexes introduced (Aagaard & Sistrom, 1972; Takemoto, 1974; Niederman et al, 1976; Drews et al, 1977; Firsow & Drews,

1977; Pradel et al, 1978; Schumacher & Drews, 1978; Hunter et al, 1982; Inamine et al, 1984). In addition to this, it was shown that the synthesis of the reaction centre and the LHI complexes are co-ordinated, whereas the LHII synthesis is essentially independent from the LHI/RC synthesis (Aagaard & Sistrom, 1972; Lien & Gest, 1973; Niederman et al, 1976).

2.2. The Structure and function of the Photosynthetic Unit of the Purple Bacteria.

The Photosynthetic unit (PSU) was first proposed by Emerson & Arnold in 1932. The PSU (reviewed in Cogdell et al, 1996) is made up of the pigment-containing protein complexes that are involved in the light-reactions of photosynthesis. These pigment-protein complexes take one of two forms, the antenna complexes and the reaction centres. The reaction centre is the complex responsible for charge separation events, producing a chemical gradient across the ICM. The function of the antenna, or light-harvesting (LH), complexes is to capture light and transfer the light energy rapidly and efficiently to the reaction centre. In the purple bacteria there is only a single type of reaction centre, and, indeed, in some species such as *Rps. viridis* and *Rhodospirillum rubrum* there is only a single form of antenna complex, LHI. However, in many other species, including *Rb. sphaeroides*, there are two forms of antenna complex, namely LHI and LHII.

LHI and LHII light-harvesting complexes absorb light of different wavelengths (see Hunter et al, 1989; Olsen & Hunter, 1994; Hunter, 1995; Fyfe & Cogdell, 1996; Pullerits & Sündstrom, 1996 for reviews on light-harvesting complexes). LHI is generally referred to as the B875 complex, and LHII as the B800-850 complex due to their distinctive absorption bands in these regions. Those species which possess the ability to synthesise both forms of antenna complex, LHI and LHII, can use this as a method by which they can react to changes in the light environment.

The core of the PSU, a reaction centre surrounded by a ring of LHI, represents the maximum size of the unit in species such as *Rps. viridis* and *Rhodospirillum rubrum* which are incapable of synthesising LHII. However, in the other species, such as *Rb. sphaeroides*, it represents the

minimal unit of the PSU. In these species, additional LHII molecules assemble around the circumference of this core, in variable levels of LHII per reaction centre (or per core). This kind of system was first described by Aagaard & Sistrom (1972). They showed that the size of the PSU in *Rb. sphaeroides* varied from about 30 BChls in high light to 200-250 BChls in low light. Certain bacteria can therefore increase the levels of BChl surrounding each reaction centre, raising the light-capturing capabilities of the PSU. This increase in BChl levels is the result of stimulation of, or increase in LHII synthesis. In other species such as *Rhodopseudomonas acidophila* and *Rhodopseudomonas cryptolactis* the absorption characteristics of the synthesised LHII complex can also be altered. When grown in light of very low intensities, *Rps. cryptolactis* has been observed to produce the B800-820 complex as well as, or instead of, B800-850 (Hawthornthwaite & Cogdell, 1991). However, in species which can only produce LHI, the response is limited simply to the insertion of more RC:LHI complexes into the membrane.

Despite differences in their light absorption characteristics, the light harvesting complexes described above, are all constructed in a very similar manner. They consist of super-complexes built around a common two-subunit module. For example, the LHII complex from *Rps. acidophila* (McDermott et al, 1995), is made up of nine repeats of a common α-β polypeptide dimer (See Figure 5). The α-β polypeptides form transmembrane α-helices, one per polypeptide, with the top of the structure closed off by the C- and N-termini of each, which fold back over and interact with each other. The subunits are arranged such that two rings are formed, the α-polypeptides forming a ring "inside" the β-polypeptide ring. Within the two rings are bound two sets of BChl pigments, the 18 B850 BChl molecules, and the 9 B800 BChl molecules. Two molecules of carotenoid (rhodopin glucoside) are also held, almost traversing the membrane, in contact with both the B800 and the B850 BChl's. The B800 BChl molecules form a ring with the pyrol rings oriented parallel to the membrane. The B850 BChl's are oriented so that their pyrol rings are perpendicular to the plane of the membrane, lying towards the periplasmic side of the B800 BChl's. Whilst there is no interaction between the individual B800 BChl's, the B850 molecules form a very tightly coupled system, with the Mg-Mg distance rings of ~8.7Å within each α-β protomer unit, and ~9.7Å between adjacent protomers. It has been

proposed that this general structure is repeated throughout the light harvesting systems of purple bacteria, although the size of the ring may differ from species to species. The structure of the LHII complex from *R. molischianum* (Koepke et al 1995), for example, is made up of only 8 of the α-β pairs. The same modular construction would appear to be present in the LHI complexes (Karrasch et al, 1995), although they only carry one ring of BChl, equivalent in position to the B850 ring of LHII.

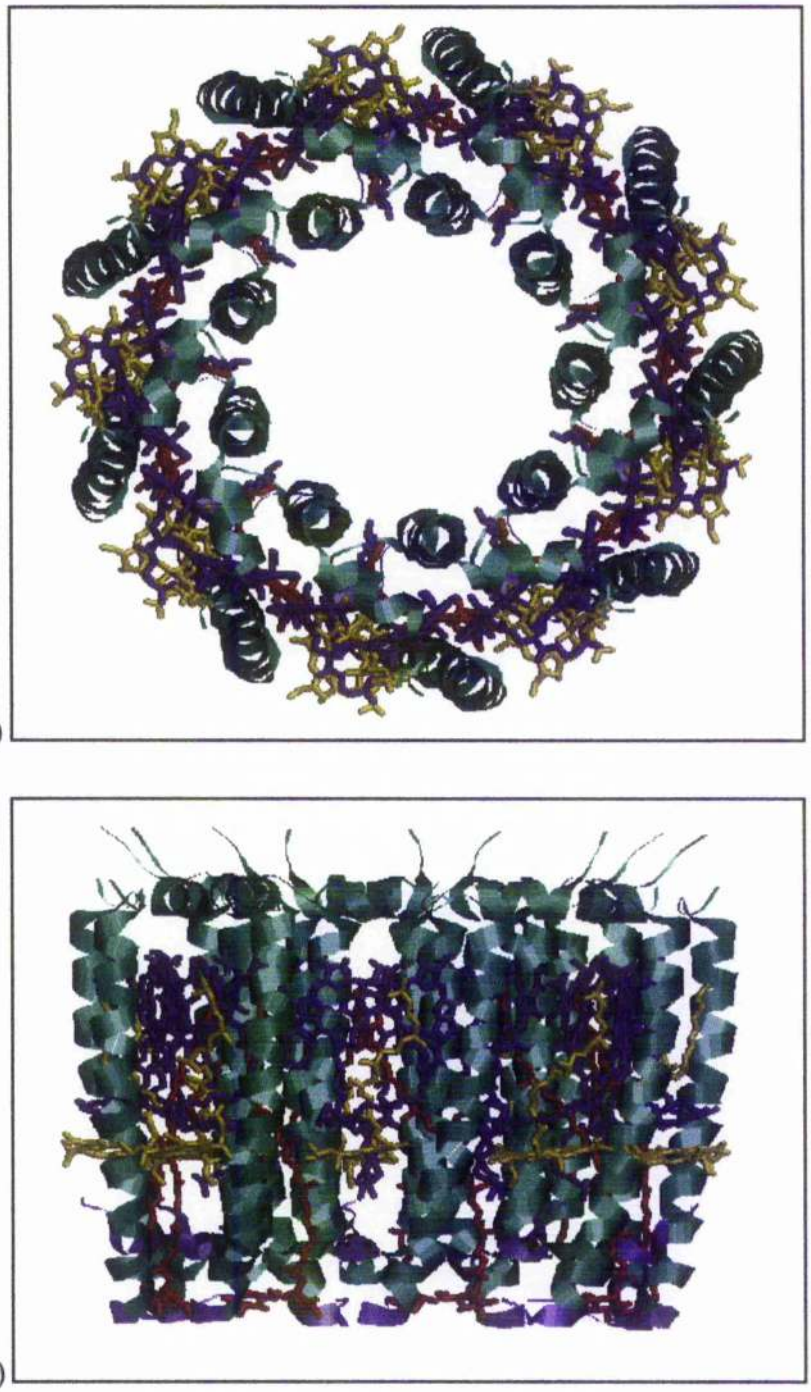

Figure 5: Model of the LHII complex of *Rhodopseudomonas acidophila* 10050 (McDermott et al, 1995). a) The complex viewed from the periplasmic side of the membrane; b) viewed perpendicular to the symmetry axis. The B800 BChl's are coloured yellow; the B850 BChl's are coloured purple; the carotenoid (rhodopin glucoside) in red.

2.3. Photosynthetic Reaction Centres: A General Introduction.

The primary photochemical reactions of photosynthesis are carried out in pigment-protein complexes called photosynthetic reaction centres. These macromolecules are responsible for the conversion of absorbed light energy into chemical energy. This chemical energy can then be utilised by other protein complexes to generate molecules, such as ATP or $NADPH_2$, vital energy units for the organism.

Plants and algae contain two types of photosynthetic reaction centres referred to as Photosystem I (PS I) and Photosystem II (PS II). PS II is responsible for the extraction of electrons from water and for raising them to a negative potential sufficient for reducing plastiquinone (PQ) to plastiquinol (PQH_2). The PQH_2 interacts with a cytochrome bf complex, where the electrons are transferred to plastocyanin. Plastocyanin, in turn acts as the donor of electrons to PS I. The function of PS I is to raise the energy of the electrons sufficiently to permit the reduction of ferredoxin (Fd), an Fe/S protein. The enzyme ferredoxin-$NADP^+$ oxidoreductase then acts to produce NADPH from the reduced ferredoxin. This "Z-scheme" of photosynthesis in PS I and PS II containing phototrophs is shown diagrammatically in Figure 6.

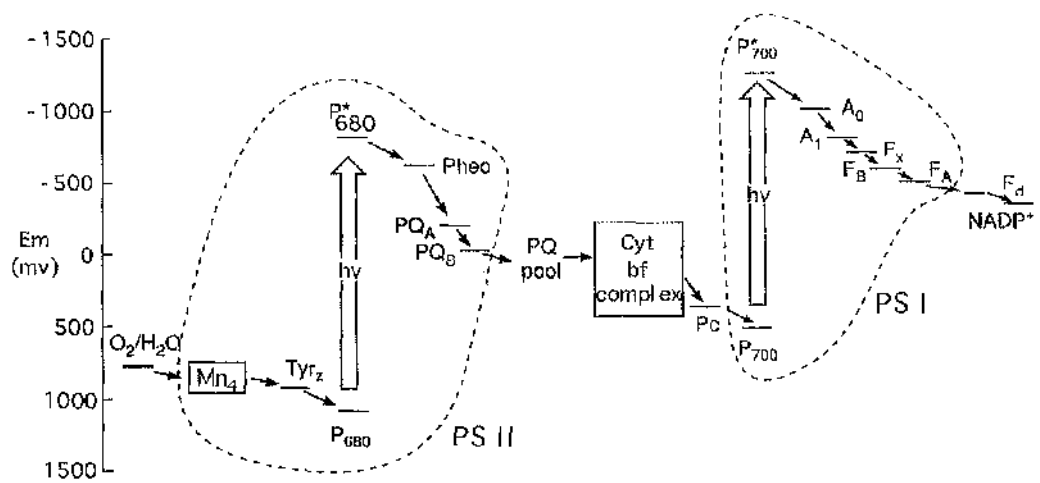

Figure 6. PS. I and PS. II perform two light driven reactions in tandem to drive electrons from water to $NADP^+$, in the series of reactions commonly known as the "Z-scheme." (Adapted from Nicholls & Ferguson, 1992)

The bacterial photosynthetic reaction centre is an integral membrane pigment-protein complex. As discussed in section 1.2., it is believed to be most closely related to PS II in plants and algae, although it does not catalyse the oxidation of water. The photosynthetic reaction centre of the purple bacteria has been intensively studied, the pinnacle of this research arguably being the elucidation of its atomic structure by X-ray crystallography. This was the first time the structure of a membrane protein had been resolved, a feat that ultimately led to the award of the Nobel Prize for Chemistry to Johann Deisenhofer, Robert Huber and Hartmut Michel in 1988. The structure of the reaction centre of *Rhodopseudomonas viridis* was the first structure solved, initially to a resolution of 3.0Å (Deisenhofer, J., Epp, O., Miki, K., Huber, R., & Michel, H. 1984, 1985). The reaction centre structures from a number of different strains of *Rb. sphaeroides* have since been determined (Allen et al, 1986, 1990; Arnoux et al, 1995; Chang et al, 1991, Chirino et al, 1994; El-Kabanni et al, 1991; Ermler, et al 1994; McAuley-Hecht et al, 1997; Stowell et al, 1997; Yeates et al, 1988) with models to 2.2Å for *Rb. sphaeroides* 2.4.1. reaction centres (Stowell et al, 1997) and 2.3Å for *Rps. viridis* (Deisenhofer et al, 1995) reaction centres being the highest resolution structures published to date. Details on the recent 2.2Å model (Stowell et al 1997) are limited, with the single publication detailing structural changes in the Q_B site upon illumination of the reaction centre crystal and the with co-ordinates yet to be released by the Brookhaven Protein Structure Database. For this reason, much of the following discussions are based on the previous highest resolution structure of Ermler et al (1994) at 2.65Å.

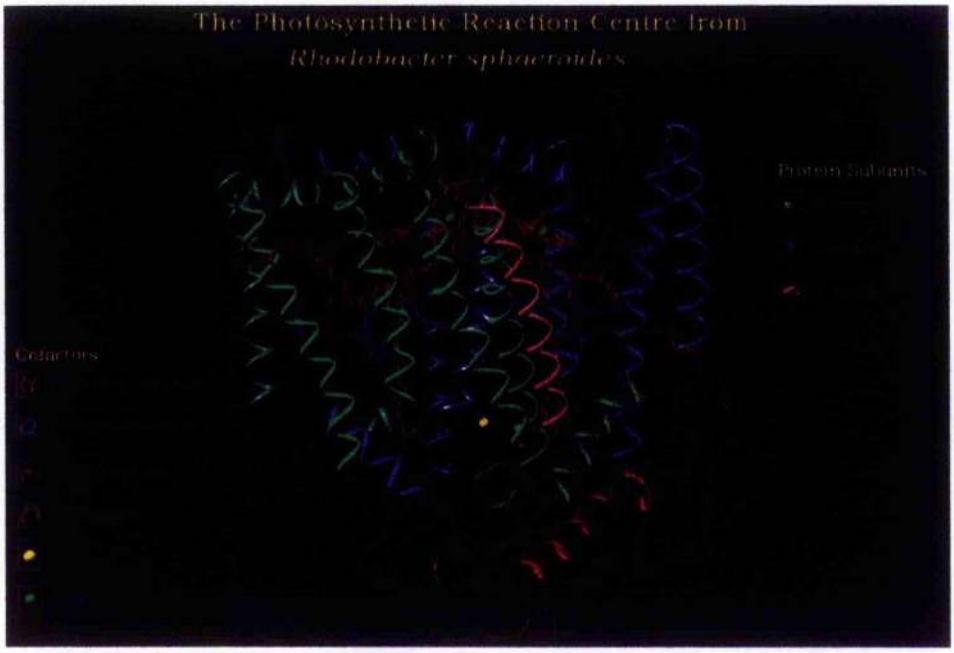

Figure 7: The photosynthetic reaction centre from *Rhodobacter sphaeroides* NCIB 8253 (WT red, this work).

The photosynthetic reaction centres from purple bacteria are composed of three polypeptides which have been named the H (heavy), M (medium) and L (light) subunits on the basis of their apparent molecular weights when run on SDS polyacrylamide gel electrophoresis: 28,000kDa (±1000), 24,000kDa (±1000) and 21,000kDa (±1000) respectively (Feher, 1971; Reiss-Husson & Jolchine, 1972; Jolchine & Reiss-Husson, 1974; Okamura et al, 1974). Table 1 presents the amino acid content along with the apparent and actual masses (Williams et al, 1983, 1984) of each of the reaction centre polypeptides. Subunits L and M both possess five transmembrane α-helices, with the H subunit containing only a single transmembrane section, again α-helical in structure. In certain bacteria, such as *Rps. viridis*, an additional cytochrome complex is bound onto the periplasmic surface of the reaction centre. The cytochrome in *Rb. sphaeroides* is a soluble cytochrome, although the reaction centre and cytochrome complex has been co-crystallised (Adir et al, 1996). The bulk of the H-subunit is found on the cytoplasmic side of the membrane (see Figure 7). The pigments are held within a protein cage formed exclusively by the M and L subunits.

Purple bacterial reaction centres normally contain the following pigments: four bacteriochlorophylls, two bacteriopheophytins, two quinones, one non-haem Fe^{2+} and a single carotenoid pigment molecule. The cofactors are arranged in two branches (A and B), approximately related by a two-fold symmetry axis, the exception being the carotenoid molecule (Figure 8). The carotenoid lies on one side of the two-fold axis. The primary donor (P), usually referred to as the special pair, consists of two bacteriochlorophyll molecules. The two BChl molecules which compose the special pair, P, are known as P_L and P_M. These overlap at the ring I position with a separation of approximately 3Å. The absorption spectrum produced by the reaction centre protein:pigment complex is shown in Figure 9. The absorption bands shown in the spectrum can be attributed to specific pigments, the origin of each absorption peak is marked.

Table 1: Amino acid content and masses of the three reaction centre polypeptides from *Rb. sphaeroides.*

Subunit	Mass from SDS-PAGE (±1000)kDa	Actual Mass kDa	Amino acid content
L	21,000	31,319	281
M	24,000	34,265	302
H	28,000	28,534	250

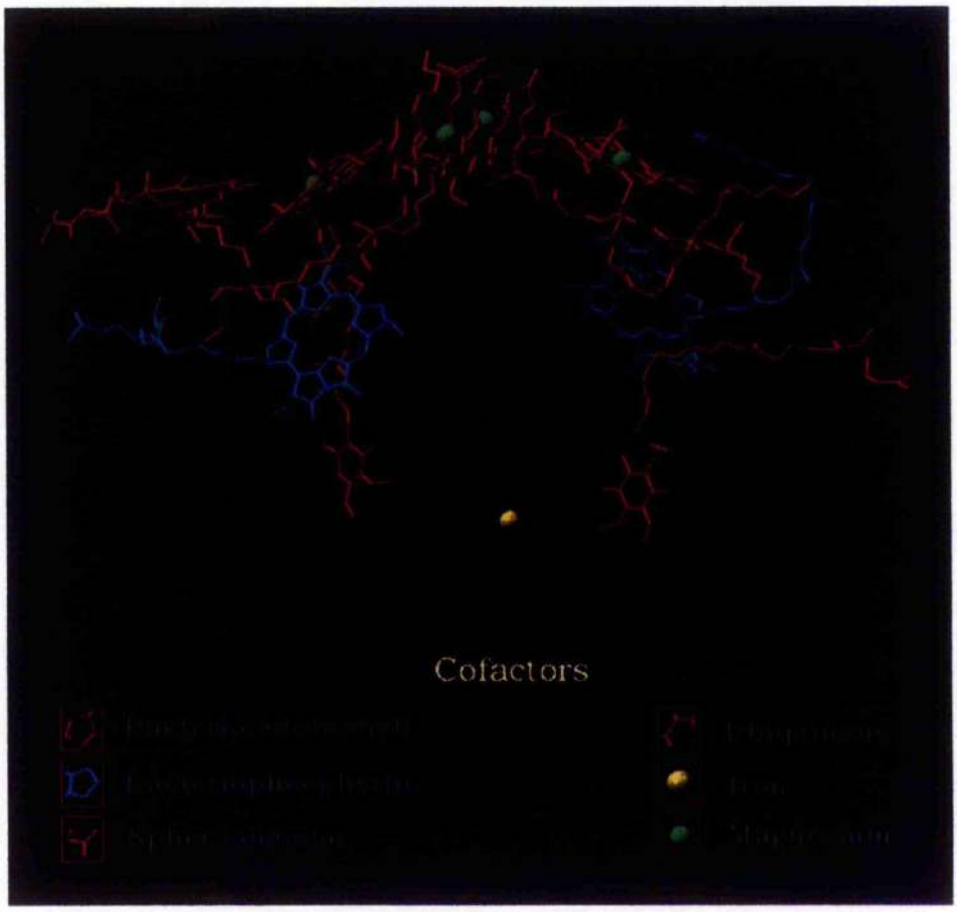

Figure 8: The arrangement of the pigments of the WT RCO2 *Rhodobacter sphaeroides* reaction centre.

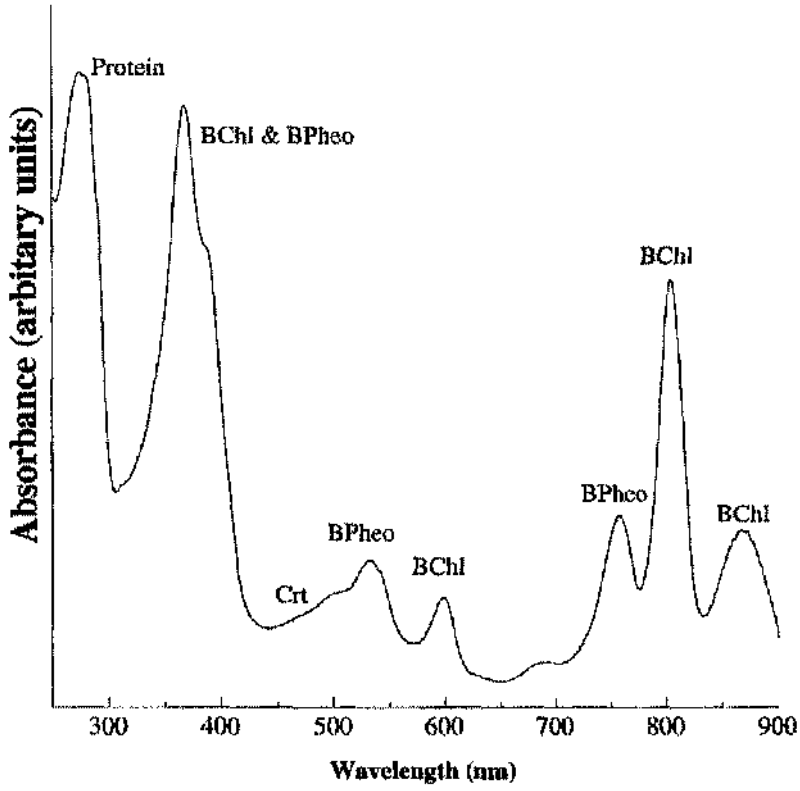

Figure 9: The absorption spectrum at room temperature of the photosynthetic reaction centre isolated from *Rhodobacter sphaeroides* NCIB 8253 (WT red, this work).

Despite the high degree of similarity between the two pigment arms, only one arm (A) carries out the charge transfer process (Figure 10). Absorption of a photon excites the primary electron donor (P), causing it to form the excited state P*. An electron is then released from P* and transferred onto the primary acceptor, a bacteriopheophytin molecule (H_A). The movement onto H_A occurs in approximately 4ps (Zinth et al, 1985, Martin et al, 1986; Breton et al, 1986 a, b; Flemming et al, 1988). The speed of this transfer over approximately 7Å, has led to the suggestion that a bridging intermediate must be involved. The most likely candidate for this bridging intermediate is the accessory bacteriochlorophyll, B_A, located between P* and H_A (Zinth et al, 1985; Holzapfel, 1990; Dressler et al, 1991; Arlt et al, 1993). The electron is thus transferred from P* to B_A in ~3.5ps, followed by a faster step for transfer from B_A to $H_A$of ~0.9ps (Creighton et al, 1988; Dressler et al, 1991; Hamm et al, 1995). The electron then passes on to Q_A in approximately 200ps (Kirmaier & Holten, 1987) before transfer to Q_B in about another 100µs (Debus et al, 1986). The nature of the role of the Fe^{2+}, lying between Q_A and Q_B, remains to be explained. Remarkably,

Chirino et al (1994) performed an investigation into one mutant of *Rb. sphaeroides* reaction centre in which the Fe atom was excluded, with no apparent effect on the characteristics of the complex.

A single electron is transferred across the membrane for each photon absorbed, but to complete the process a second electron has to be shuttled through the system to Q_B. Before a second electron transfer process can occur, P has to be re-reduced by a cytochrome molecule. In *Rb. sphaeroides* the cytochrome is a soluble c_2 type heme-protein complex which interacts with the complex (Rich, 1984), meanwhile in *Rps. viridis*, the cytochrome is bound to the reaction centre protein (Deisenhofer et al, 1985). With P re-reduced, a second excitation process can occur, and another electron shuttled to Q_B, (Wraight, 1979; Kleinfeld et al, 1984, 1985; Dracheva et al, 1988) forming a double reduced species Q_B^{2-} (Dracheva et al, 1988). The Q_B^{2-} molecule acquires two protons from the cytoplasm, after which it dissociates from the reaction centre. The precise mechanism of proton uptake is another area of debate, centred on whether each reduction step is immediately followed by protonation, or whether both protons are bound once the double reduced quinone is formed (Wraight, 1979; Kleinfeld et al, 1984, 1985). What is clear from the high resolution X-ray crystal structure of *Rb. sphaeroides* reaction centres is the pathway through which the protons travel through the protein to the Q_B site. There exists an unbroken chain of water molecules, running from the cytoplasmic surface of the reaction centre complex to Q_B (Ermler et al, 1994). The striking level of conservation in the positions of these water molecules between the different structures supports the hypothesis that it is this channel that the protons "use" to reach the quinone.

The released QH_2 molecule is then oxidised by a cytochrome bc_1 complex, (Gabbelini et al, 1982; Dutton, 1986) the protons being released into the periplasm and the electrons accepted by cytochrome c_2 for return to the reaction centre, thus completing the cycle. This combination of reactions leads to the formation of a system capable of performing vectorial transport of protons across the membrane, generating a pH gradient. This gradient is exploited by complexes such as the ATPase complex (also situated in the ICM) to convert the proton gradient into a more useful form of chemical energy, in this case ATP. The empty

quinone binding pocket in the reaction centre is refilled by an exogenous quinone from the membrane pool (Crofts & Wraight, 1983).

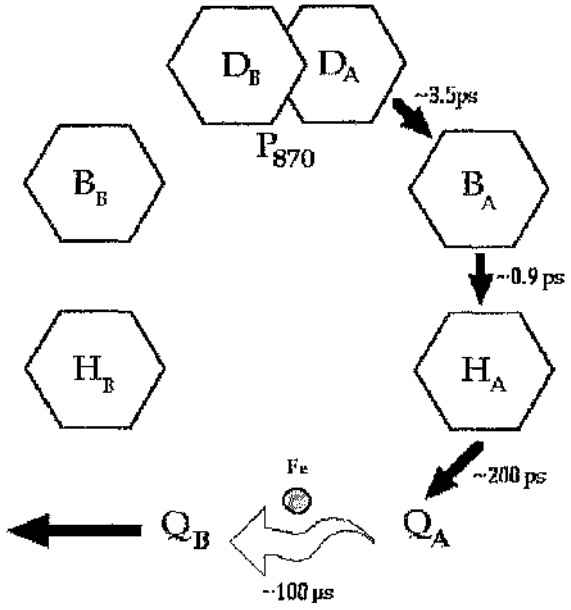

Figure 10: The electron transfer network in *Rb. sphaeroides* reaction centres, and the electron transfer times for each step (Adapted from Deisenhofer et al, 1985). References for the kinetics are in the text above. The special pair BChls are labelled in the alternative format of D_A and D_B which equate to P_L and P_M respectively.

2.4. Carotenoids in Photosynthesis.

Carotenoids are widely distributed in nature, occuring in microorganisms, plants and animals (See Bendich & Olsen, 1989, for a short review of the function of carotenoids in animal systems). It has been hypothesised that carotenoids carry out five functions in photosynthetic organisms, namely photoprotection, light harvesting, scavenging of singlet oxygen, dispersion of excess energy and structure stabilisation / assembly. The methods by which the carotenoid fulfils these roles will now be discussed, beginning with an introduction to the structure and synthesis of carotenoids in purple bacteria.

2.4.1. The Structure and Biosynthesis of Carotenoids.

The carotenoids are carotenes, a class of hydrocarbons, and their oxygenated derivatives, the xanthophylls. They consist of eight isoprenoid

units joined together with a reversal of the bond structure at the centre of the molecules (Isler et al, 1971). All the carotenoids are derived from the first C_{40} intermediate of the carotenoid biosynthesis pathway, phytoene. The more complex carotenoids found in purple bacteria are formed from phytoene by a combination of desaturation, hydroxylation, methylation and hydration (Figure 8) (Britton, 1993). In the 1950s researchers began to uncover the pathways by which carotenoids are synthesised in purple bacteria (Griffiths et al, 1955; Griffiths & Stanier, 1956; Sistrom et al, 1956; Cohen-Bazaire et al, 1956). A mutant of *R. rubrum*, with a block in the carotenoid biosynthetic pathway was discovered. This strain could only produce the carotenoid phytoene, the enzymatic defect interpreted as lying at some point between phytoene and phytofluene (Jensen et al, 1966). The same paper reported on the isolation of a number of carotenoid biosynthetic pathway mutants in *Rb. sphaeroides*, the investigation of which led to a proposed biosynthetic pathway. This pathway has now been completely resolved in two purple bacterial species, with each step attributed to specific genes/gene products (Figure 11). The genetics and the molecular biology of the carotenoid biosynthesis pathway has been recently reviewed in detail by Armstrong & Hearst (1996), and Armstrong (1985)

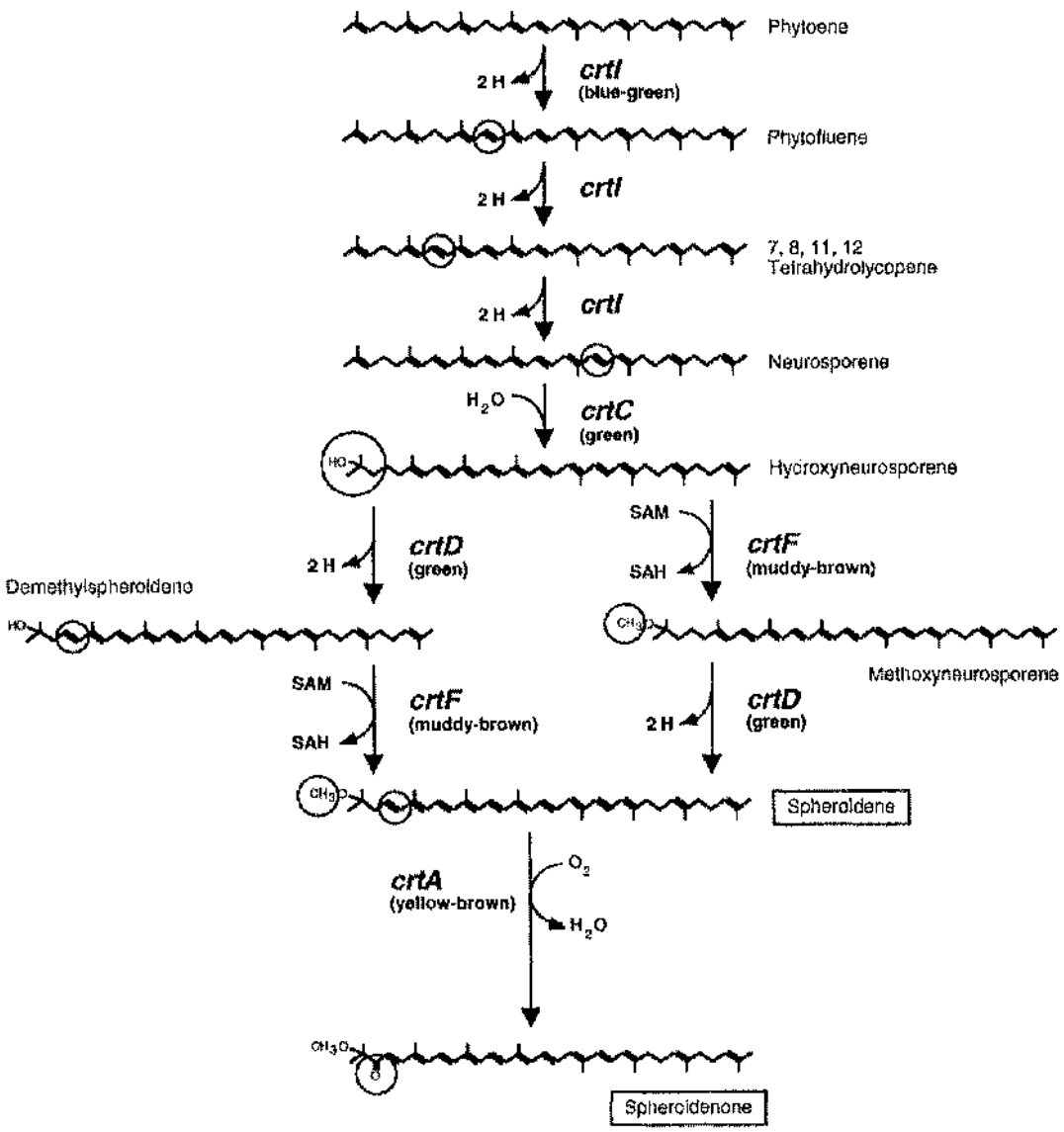

Figure 11: The biosynthesis of the complex carotenoids found in *Rb. sphaeroides.* [Adapted from Armstrong, (1995)] The sites of the biosynthetic conversions are circled. The *crt* genes and functions are as follows: *crtA*, monooxidation; *crtB*, 1'-2,3 prenylphosphate condensation and 1'-1 rearrangement; *crtC*, hydration; *crtD*, 3,4 dehydrogenation; *crtE*, 1'-4 prenylphosphate condensation; *crtF*, O-methylation; *crtI*; dehydrogenation.

2.4.2. *Carotenoid Energy Levels.*

Carotenoids, and polyenes through which much of the knowledge about carotenoid energy levels has been derived, posses two low-lying excited singlet states. These are denoted the 1^1B_u and the 2^1A_g states. The major absorption band of carotenoids, in the visible region of the spectrum

(Figure 12a), is due to the allowed 1^1A_g ground state to 1^1B_u state transition. This transition decreases in energy as the extent of π-conjugation within the carotenoid increases (Figure 12b). The carotenoids carrying a short conjugated chain (3-6) are of sufficiently high energy to be colourless to the eye. Only when the conjugated system reaches seven, do they appear coloured to the human eye. The energy of the 1^1B_u state can be determined from the absorption spectrum and decreases to an almost constant value in the longer conjugated chain carotenoids (Figure 12).

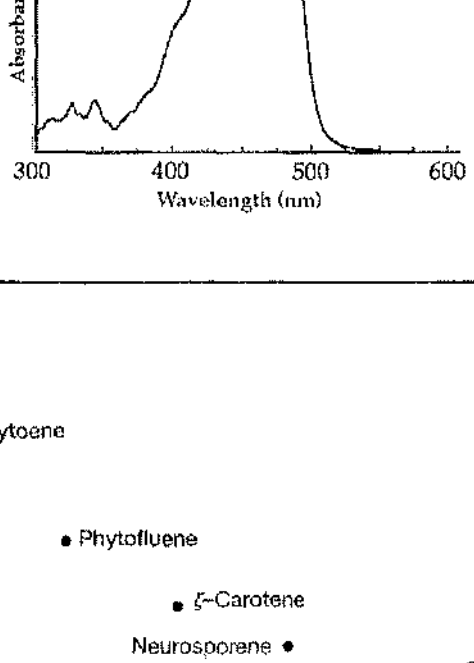

a)

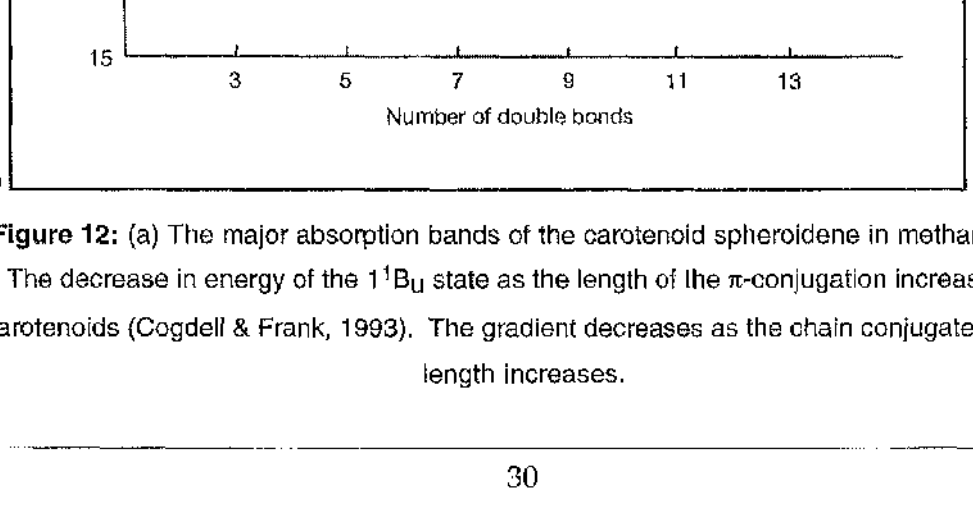

b)

Figure 12: (a) The major absorption bands of the carotenoid spheroidene in methanol; (b) The decrease in energy of the 1^1B_u state as the length of the π-conjugation increases in carotenoids (Cogdell & Frank, 1993). The gradient decreases as the chain conjugated chain length increases.

Another excited state, additional to the 1^1B_u state has been proposed, that of the 2^1A_g (D'Amico et al, 1980; Hudson et al, 1982) The investigation of 2^1A_g in long polyenes has only relatively recently begun. Investigation was initially proposed because the 1^1B_u state could not satisfy all the observed spectral characteristics of polyenes. This led to the proposal that the lowest energy excited state was not the 1^1B_u state, but was the 2^1A_g state. Data from analysis of short chain polyenes have provided experimental evidence for the existence of the 2^1A_g state (e.g. D'Amico et al, 1980). However, although the existence of this low lying Ag state is a widely accepted characteristic of polyenes and carotenoids, measurements of the energies of the 2^1A_g state in long chain carotenoids remain ill-defined. This is due to the fact that the longer chain carotenoids (greater than 8 conjugated C=C bonds) have a strong tendency to only fluoresce from their 1^1B_u states, making direct measurement of the 2^1A_g state very difficult.

The energy of the 2^1A_g state is an important element in our understanding of the processes involved in the function of carotenoids in photosynthetic apparatus. The energy of this state must be determined before the mechanisms of energy transfer by carotenoids can be fully understood. This has led a number of groups to attempt to determine the energies using a range of techniques (e.g. Thrash et al , 1977; Anderson et al 1992; DeCoster et al, 1992; Frank et al, 1993; Chynwat & Frank, 1995). The 2^1A_g state energies as derived by Chynwat & Frank (1995) are given below in Table 2.

Table 2: The 2^1A_g state energies for a range of "long-chain" carotenoids, as determined by Chynwat & Frank (1995)

Carotenoid	Length of Conjugated System	Calculated 2^1A_g state energy (cm^{-1})
Canthaxanthin	13	13 300±150
Zeaxanthin	11	13 935±10
Spheroidene	10	14 100±250
β-Carotene	11	14 100±150
Antheraxanthin	11	14 510±5
Violoxanthin	9	15 120±3

2.4.3. Light Harvesting.

Carotenoids have a role in light-harvesting. They absorb light in a region of the visible spectrum where the major light-harvesting pigments, the (bacterio)chlorophyll molecules, do not exhibit strong absorption. Thus, carotenoids allow the organism to utilise an otherwise almost unobtainable part of the light spectrum. This role might be especially valuable for those organisms whose natural habitats are in areas starved of light in a particular region of the spectrum. Many photosynthetic organisms inhabit areas where the light reaching them may be heavily depleted by organisms lying above them. Thus the ability to tap into as wide a range of the spectrum as possible is of great importance. Indeed a recent report into the determination of the crystal structure of a soluble light-harvesting complex from the dinoflaggelate *Amphidinium carterae,* showed a complex in which the carotenoid peridinin is the major light-harvesting pigment (Hoffmann et al, 1996). The high-resolution (2.0 Å) X-ray structure of this peridinin-chlorophyll-protein, reveals a trimer configuration of polypeptides, each containing an unusual fold of the alpha-helical terminal domains. This unusual structure produces a scaffold with pseudo-twofold symmetry surrounding a hydrophobic cavity which is filled by two lipid, eight peridinin, and two Chl*a* molecules. The efficient energy transfer from the peridinin molecules to the Chl*a*'s is due to the clustering of peridinins around the chlorophylls in the structure, van der Waals distance apart. These organisms live where blue-light is the major source of light energy. By adopting a light-harvesting system with the carotenoid as the major pigment, these organisms are ideally adapted to growth in these conditions.

The transfer of singlet energy from the carotenoid to the BChl, such as is found in the light-harvesting role of carotenoids, requires that the two pigments are in close proximity. This requirement, due to the short lifetime of the carotenoid excited state, is satisfied in the light-harvesting complexes and the reaction centre. This is not of course the only requirement. The nature of the carotenoid is also of great importance. For example, the B800-850 complex in *Rb. sphaeroides* contains different ratios of spheroidene and spheroidenone depending on the growth conditions. In anaerobic growth the major carotenoid is spheroidene (92%), which

transfers the singlet energy to BChl with ~90-100% efficiency (Cogdell et al, 1981; van Grondelle et al, 1982; Noguchi et al, 1990). When grown in semi-aerobic conditions spheroidenone becomes the major carotenoid (98%) and the efficiency of transfer has been determined to drop to ~75% (Cogdell et al, 1981). However, several other factors have also been seen as important. These include the geometry of the two pigments relative to each other, the stereochemistry of the carotenoid, the position and nature of the electronic states of both pigments, the spectral overlap between the two pigments, the magnitudes of the transition moment dipoles of the donor and acceptor, and the dynamics of the participating states (Frank & Cogdell, 1996).

2.4.4. Triplet States and Photoprotection.

The elevation of (B)Chl by light into an excited state must be followed by the dispersion of the gathered energy. This usually occurs in the form of energy transfer over the photosynthetic apparatus to the reaction centre and then electron transfer within the reaction centre system, leading to charge separation. However, under conditions of over-excitation it is also possible for the singlet (B)Chl to undergo internal conversion to form triplet (B)Chl (Parson et al, 1975). If the reaction centre system is excited by light when the primary quinone is absent or chemically reduced, the electron transfer from the BPheo is blocked. When this situation arises a back reaction can occur between the oxidised special pair and the reduced BPheo. One of the possible products of this reaction is triplet state of the special pair.

The formation of the BChl triplet changes the orientation of the spin of the excited electron so that it enters a relatively long lived state. The triplet state of the special pair from *Rb. sphaeroides* R-26 decays back to ground state in a rate of approximately 50μsecs (Cogdell et al, 1975). This is because loss of energy from triplet states by relaxation back to the ground state can only proceed at a rather slow rate (this type of internal conversion is forbidden according to the Pauli exclusion principle). This length of time is long enough for the triplet state to react with molecular oxygen.

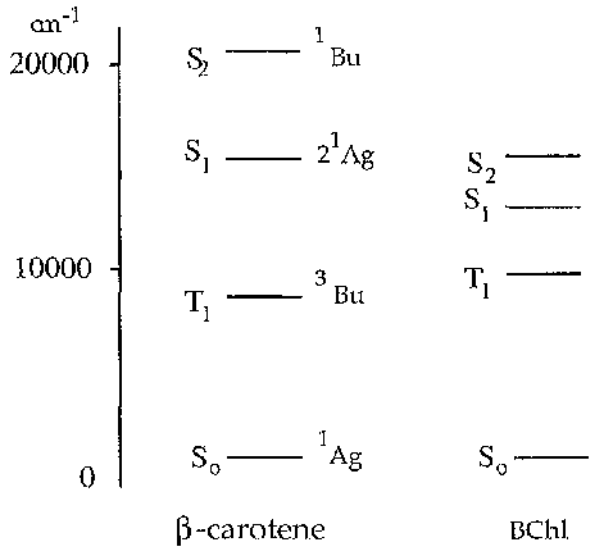

Figure 13: Energy diagram of all trans β-carotene and BChla (Koyama, Y. 1991)

Potentially, the formation of the special pair triplet state in vivo in the presence of oxygen can lead to the formation of singlet oxygen. Singlet oxygen is an extremely efficient oxidising agent. Once formed within a cell it can cause damage, possibly terminal, to the organism. It is a powerful enough oxidising agent to react with lipids, proteins and nucleic acids (Foote, 1968). Indeed this is one process which macrophages in the immune systems of mammals have utilised to kill invading microrganisms (Krinsky, 1966). Singlet (B)Chl has a sufficiently short lifetime (ns range, Krinsky, 1966) to effectively exclude the possibility of it reacting with molecular oxygen. The lifetime of triplet (B)Chl is much longer (~50μs at room temperature, Cogdell et al, 1975), because the decay back to the S_0 ground state is symmetry forbidden. The long lifetime of the (B)Chl triplet state makes a reaction with molecular oxygen possible, via simple diffusion. This reaction would lead to the (B)Chl returning to the ground state but only with the concomitant formation of singlet oxygen (See Equations 1-3 below). Hence, the (B)Chl triplet state is particularly dangerous for an organism to harbour, any organism containing (B)Chl must contain a system by which it can protect itself from this danger.

$BChl + h\nu \rightarrow {}^1BChl^*$ *Equation 1.*

${}^1BChl^* \rightarrow {}^3BChl^*$ *Equation 2.*

${}^3BChl^* + {}^3O_2 \rightarrow BChl + \Delta_g O_2^*$ *Equation 3.*

All wild-type photosynthetic organisms possess a mechanism for quenching the triplet states of (B)Chl to prevent the possibility of the formation of highly reactive singlet oxygen molecules. The photoprotective system adopted is based on the inclusion of carotenoid molecules in the photosynthetic systems. This role of carotenoids in photosynthetic organisms was first suggested by Griffiths et al (1955) and Sistrom et al (1956) They noted that in experiments using different strains of *Rb. sphaeroides*, those containing carotenoids did not display the "photosensitization" observed for carotenoidless strains. They (Griffiths et al, 1955) stated "Since carotenoid-containing strains of the same organism (*Rb. sphaeroides*) do not show such a photosensitization the conclusion that they are protected by the carotenoids seems inescapable". The ability of carotenoids to quench triplet Chl and singlet oxygen in solution was demonstrated by Mathis (1969), Foote & Denny (1968) and Foote et al, (1970) respectively. However, to be able to carry out the protective role, carotenoids must be in close proximity to the (B)Chl molecules (Krinsky, 1966). Transfer of the triplet state requires the transfer of electrons, this requires that the donor and acceptor molecules be in close proximity to each other. The high resolution models determined for the reaction centre protein (Deisenhofer et al, 1984, 1985; Allen et al, 1987a, 1987b, 1988, 1989; Komiya et al, 1988; Ermler, et al 1994; McAuley-Hecht et al, 1997) and the light harvesting proteins (McDermott et al, 1995; Hu et al, 1996; Koepke et al, 1996) of photosynthetic organisms all reveal carotenoid molecules lying in close proximity to the (B)Chl molecules.

The carotenoid pigments can effectively scavenge the triplet states of (B)Chl when adjacent to these molecules. However, this function also depends upon the type of carotenoid bound or, more specifically, the number of conjugated double bonds in the molecule. *In vivo*, when (B)Chl molecules return to the ground state, the triplet state energy is transferred to the carotenoid. The rate of this transfer has been estimated to be around 10-30 nsecs at room temperature (Cogdell et al, 1975). This is sufficiently rapid to prevent the energy being transferred to molecular oxygen. Obviously, the triplet state of the carotenoids must not itself present the organism with the same problems as the BChl equivalent. To be successful in the scavenging role the energy of the carotenoid triplet state must be equal to or lower than the energy of singlet oxygen, 7855cm^{-1}

(Claes, 1960; Foote et al, 1970). This requirement is satisfied by carotenoids bearing 7 or more conjugated C=C double bonds (Claes, 1960; Foote et al 1970). Spheroidene, the major carotenoid in *Rb. sphaeroides* 2.4.1. (possessing 10 C=C conjugated bonds) has a triplet energy of approximately 6560cm^{-1} and neurosporene, the major carotenoid in *Rb. sphaeroides* G1C (possessing 9 C=C conjugated bonds) a triplet energy of approximately 7285cm^{-1} (Bensasson et al, 1976). Thus the energy level of the carotenoid triplet state produced in these conditions is lower than that required to produce singlet oxygen, and hence this energy can be safely lost via intersystem crossing (non-radiative relaxation) back to the ground state, losing the excess energy as heat.

^{3}(B)Chl* + ^{1}Car $\rightarrow$ ^{1}(B)Chl + ^{3}Car* *Equation 4*

^{3}Car* $\rightarrow$ ^{1}Car + heat *Equation 5*

The effectiveness of the carotenoid in carrying out this photoprotective role can be dramatically demonstrated using a carotenoidless mutant. For example, Boucher et al (1977), demonstrated the effect of light in the presence of oxygen on the mutant, *R. rubrum* strain G9. By illuminating preparations of reaction centres from strain G9 with a range of light intensities, they showed that P_{800} can be irreversibly bleached. However, this effect is prevented by placing the G9 reaction centre preparation in an anaerobic environment (in this case by bubbling with N_2), or in the presence of the carotenoid (spirilloxanthin) in wild type *R. rubrum* reaction centres. Similar levels of photoprotection were also observed when G9 reaction centres reconstituted with spirilloxanthin were analysed.

As with transport of the electron from P to the active branch bacteriopheophytin, the triplet state energy of the special pair is most likely transferred to the carotenoid via an accessory bacteriochlorophyll, this time on the inactive pigment branch in the purple bacterial reaction centre. This idea has been tested using transient absorption and electron spin resonance spectroscopy (Frank & Violette, 1989). They measured the spectra of spheroidene incorporated into intact and BChl(B_M) deficient reaction centres from *Rb. sphaeroides* R-26. When the accessory BChl

molecule was absent, the formation of triplet spheroidene was inhibited, while the intact reaction centre continued to transfer the triplet state as normal. Transient absorption spectroscopy, and also analysis by CD spectroscopy, suggested that the "incomplete" reaction centre complex was binding the carotenoid molecule in the normal way. Therefore, it was assumed that the inhibition of the transfer of the triplet state was due entirely to the removal of the accessory BChl.

2.4.5. Selective Binding of Carotenoids in Purple Bacterial Reaction Centres.

The binding of carotenoids within purple bacterial reaction centres is unusual in at least two respects. Firstly, the carotenoids bound have been shown by raman spectroscopy to take up an unusual twisted 15, 15'-*cis* conformation (Lutz et al, 1978; Koyama et al, 1982; Kok et al 1994). This assignment of the structure of the reaction centre bound carotenoids has still to be backed by X-ray crystallographic evidence, although it has been confirmed by Magic Angle Spinning NMR spectroscopy (DeGroot et al, 1992). To date the resolution of the published X-ray crystallographic data has not been sufficient to discriminate between the two proposed conformations of 13-*cis and 15-cis* (Ermler et al, 1994). Higher resolution structures will be required before X-ray crystallography will be capable of solving this problem. Secondly, purple bacterial reaction centres display a strong preference for binding methoxy or hydroxy-carotenoids, such as spheroidene, spheroidenone and methoxyneurosporene (Chadwick & Frank, 1986; Cogdell, 1985; Agadilis et al 1980). The precise nature of the selection method remained unclear until recent crystallographic data became available. The new model structures pointed towards a single amino acid residue, Trp M75, as potentially responsible for this selection protocol (See Results, Section 13.1.2. and Discussion, 14.2.1.).

CHAPTER 3

History and Theory of the Techniques.

The first two sections of the introduction have briefly described the field of bacterial photosynthesis. The position photosynthetic organisms and in particular the purple bacteria hold in the evolutionary scale, and the general taxonomy of these bacteria were discussed. The apparatus involved in the light reactions of photosynthesis was described, and the increasing understanding of how these individual components combine to form the PSU was then discussed in some detail. Finally, the potential roles of the carotenoid pigments in these organisms were mooted, introducing the areas where research into this pigment may prove to be valuable.

Research in photosynthesis has become a field which requires an increasingly multi-disciplinary approach. Few topics combine fields as diverse as biochemistry, biophysics, chemistry, molecular biology, and physics to the extent required in the study of photosynthesis. The work carried out for this thesis is similarly multi-disciplinary in its approach. A wide range of techniques has been utilised to investigate different aspects of the mutant reaction centres produced. The following sections attempt description and discussion of some of the more specialised techniques used, pointing to the history, the theory, and the potential applications of each technique within photosynthetic research.

Discussion begins with a relatively brief introduction to the X-ray crystallographic determination of protein structures, a topic which would perhaps normally demand more than just sub-section status. Three spectroscopic techniques will then be discussed, each capable of providing information about the chromaphores held within the reaction centre

complexes. Resonance raman spectroscopy probes the structure of the pigment molecules within their protein environment, and provides highly detailed information about specific interactions between the pigment and the protein. Electron paramagnetic resonance spectroscopy detects "lone" unpaired electrons within a system. The photosynthetic system provides a number of such species which can be probed in this manner, for example the triplet states of (B)Chl and carotenoid molecules. Finally, circular dichroism is described. This is widely used to gather information into the secondary structure of proteins but can be used to investigate the fine structure of chromophores bound within the photosynthetic pigment:protein complexes.

3.1. X-Ray Crystallography: Theory.

3.1.1. The Laws of Laue and Bragg.

The processes underlying the phenomenon of diffraction of X-rays by crystals were first described in 1912 by Max von Laue. He showed that the process of X-ray diffraction parallels that of diffraction of light from a three-dimensional grating. By hypothesising a one-dimensional crystal in the form of a linear array of unit cells with repeat distance **a**, an equation can be obtained which describes the conditions required for scattering to be observed:

$$\mathbf{a} \,.\, \mathbf{S} = h \qquad \textit{Equation 6}$$

where $\mathbf{S} = \mathbf{s}$ *(vector describing direction of incident radiation)* $- \mathbf{s_0}$ *(vector describing direction of scattered radiation)*, and h is an integer. The expression of diffraction from a crystal, a three-dimensional array of atoms, can be captured by the using three Laue equations:

$$\mathbf{a} \,.\, \mathbf{S} = h \qquad \textit{Equation } 7_1$$
$$\mathbf{a} \,.\, \mathbf{S} = k \qquad \textit{Equation } 7_2$$
$$\mathbf{a} \,.\, \mathbf{S} = l \qquad \textit{Equation } 7_3$$

The equations accord with the three crystallographic axes required to define the three-dimensional atomic arrangement of the crystal.

The Laue equations, whilst providing a precise, mathematical description of diffraction, are difficult to use in practical situations. An alternative approach to the phenomenon of diffraction of X-rays by crystals, based on Bragg's law, has provided the standard theory underlying current crystallographic techniques. The remainder of this section, therefore, gives an explanation of diffraction as described by Bragg's law. Bragg (1913) produced equations to express the process of diffraction. The theoretical basis of Bragg's description differs from that of Laue. Bragg observed that the process of diffraction is governed by principles similar to that of ordinary reflection. He perceived crystals as being built up of layers or planes, each of which could act as a semi-transparent mirror. When a crystal is exposed to an X-ray beam, some of the X-rays will be reflected off a given plane with an angle of reflection equal to that of the incident beam, but the remainder of the beam passes on to be reflected by subsequent planes or to traverse through the crystal unimpeded. This treatment of diffraction allowed Bragg to produce simple equations to encapsulate the process, treating diffraction as reflections of the X-rays from the lattice planes of the crystal.

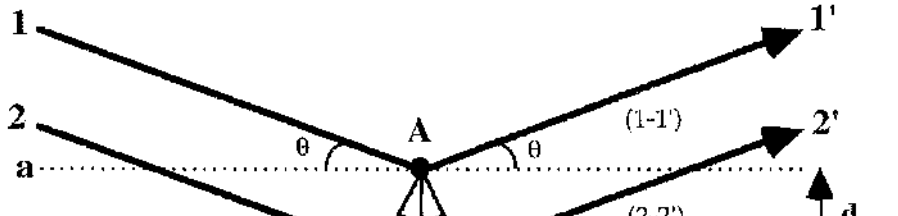

Figure 14: Conditions required to produce a strongly diffracted X-ray.

The derivation of Bragg's law is demonstrated in figures 14 and 15. Figure 14 shows an X-ray beam of wavelength λ, impinging upon a crystal at an angle θ. The X-rays are reflected from planes a and b, at an angle equal to that of the angle of incidence. The Bragg law defines when the diffracted beams from planes a and b will interfere constructively and lead

ultimately to the formation of a spot in the diffraction pattern from a crystal. Beam 22′ (the beam travelling from 2 to 2′ after "reflection" from point y) has to travel a longer distance (xyz) than that of beam 11′ (the beam travelling from 1 to 1′ after "reflection" from point A). Hence, for beams 1′ and 2′ to interact constructively this distance must equal a whole number of wavelengths. This distance allows the two beams 11′ and 22′ to return to a state in which they are in phase with each other. In figure 15, the interplanar distance, d, and the angle of incidence, θ, are related to the distance xy by the equation:

$$xy = yz = d \sin\theta \qquad \textit{Equation 8}$$

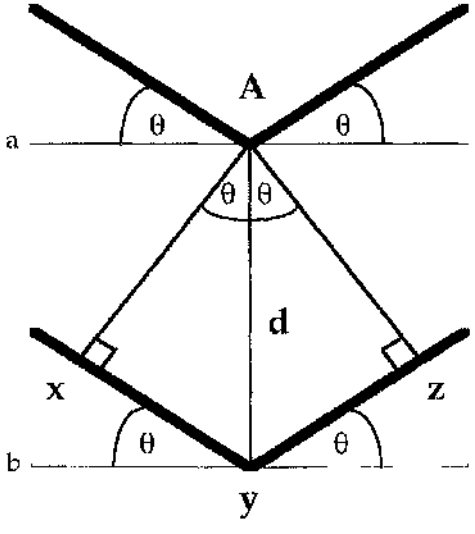

Figure 15: Diagram showing the interplanar distance d, and the angle of incidence θ, and the derivation of the equation 8 which relates the two.

However, constructive interference requires that:

$$xyz = n\lambda \qquad \textit{Equation 9.}$$

Expanding equation 9 gives:

$$2d \sin\theta = n\lambda \qquad \textit{Equation 10.}$$

(Bragg's Law)

Constructive interference of the reflected beams only occurs when the above equation is satisfied. If the X-ray beam impinges at any angle other than the Bragg angle the reflected beams are out of phase, leading to destructive interference or cancellation. In real crystals, containing thousands of such planes, Bragg's law imposes stringent conditions on the angles at which reflection can occur, with very little movement required to lead to the cancellation of reflected beams. Bragg's law does require the acceptance of some strictly untenable assumptions. It is known, for example, that atoms do not reflect X-rays but instead scatter them in all directions and X-rays are diffracted as the result of an interaction between the X-rays and atoms. However, despite the apparently highly simplified treatment Bragg's law provides, it leads to the same results as those generated by the more stringent mathematical treatments.

3.1.2. *The Reciprocal lattice.*

The process of diffraction can be described and understood by the laws discussed above. However, how does the image created from an X-ray diffraction experiment relate to the structure of the molecule under investigation? While a microscope gives a view of a real structure, a diffraction pattern gives a picture of what is known as the reciprocal lattice.

When rewritten as in equation 11, Bragg's law shows that θ relates directly to the inverse of d:

$$\sin\theta = {}^{n\lambda}/_{2}.{}^{1}/_{d} \qquad \textit{Equation 11}$$

This direct relationship has great practical significance, as will be illustrated later. The formation of the reciprocal lattice allows this direct relationship to be made. This lattice is produced in the following manner (Figure 16).

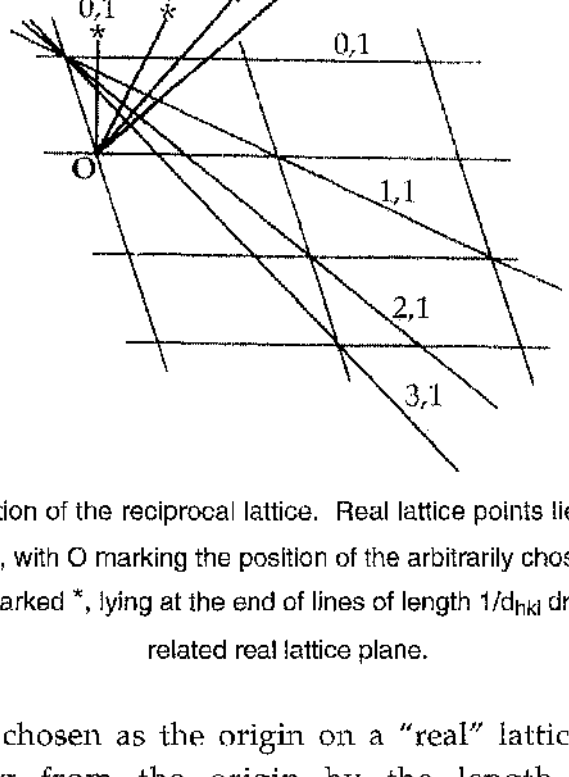

Figure 16: Construction of the reciprocal lattice. Real lattice points lie at the intersection of the planes (thin lines), with O marking the position of the arbitrarily chosen origin. Reciprocal lattice points are marked *, lying at the end of lines of length $1/d_{hkl}$ drawn normal to their related real lattice plane.

A point, O, is chosen as the origin on a "real" lattice. Lines are then drawn extending from the origin by the length $^{1}/_{d_{hkl}}$, which are perpendicular to each respective lattice plane. The points at the ends of each of these lines are the reciprocal lattice points. Each plane in the real lattice is represented by a single point in the reciprocal lattice. The diagram above gives a two-dimensional representation of a reciprocal lattice. Lines could be drawn from all of the remaining real lattice points, building up a lattice of points. It can be imagined that in three-dimensions a similar process would occur, leading to the construction of a three-dimensional reciprocal lattice. The reciprocal lattice, when interpreted in association with Bragg's law, produces a picture of what happens during X-ray diffraction experiments.

3.1.3. The Reciprocal Lattice and Bragg's Law.

Taken together, Bragg's law and the construction of reciprocal lattices allow the visualisation of the situation existing when the criteria for diffraction from points in a crystal are satisfied. Consider a crystal oriented in an X-ray beam of wavelength λ, such that the beam is trained along one

of the reciprocal lattice planes. Figure 17 illustrates the relationship between the diffracted beam and the reciprocal lattice.

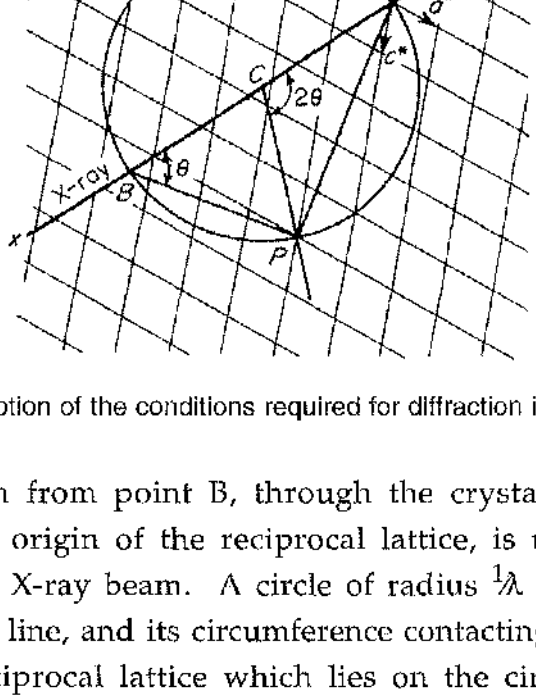

Figure 17: Description of the conditions required for diffraction in reciprocal space.

A line is drawn from point B, through the crystal, and a point, O, determined as the origin of the reciprocal lattice, is marked. This line corresponds to the X-ray beam. A circle of radius $1/\lambda$ is drawn, with its centre lying on the line, and its circumference contacting the point O. P is a point on the reciprocal lattice which lies on the circumference of the circle. The angle OPB has to be 90° because it lies within a semi-circle. Therefore, it can be seen that:

$$\sin\theta = {}^{OP}/_{OB} = {}^{OP}/_{2(1/\lambda)} \qquad \textit{Equation 12.}$$

Rearranging gives the equation:

$$2\,{}^{1}/_{OP}\sin\theta = \lambda \qquad \textit{Equation 13.}$$

However, a line from the origin of the reciprocal lattice to a point on that lattice must, by definition, have the length ${}^{1}/_{d_{hkl}}$. Therefore, the above equation can be rewritten as:

$$2\,d_{hkl}\sin\theta = \lambda \qquad \textit{Equation 14.}$$

However, a line from the origin of the reciprocal lattice to a point on that lattice must, by definition, have the length $^1/_{d_{hkl}}$. Therefore, the above equation can be rewritten as:

$$2\, d_{hkl} \sin\theta = \lambda \qquad \textit{Equation 14.}$$

The above equation is the Bragg law equation (see Equation 7), when n is equal to 1. Any point in the reciprocal lattice which comes in contact with the circumference of the circle satisfies the criteria described by Bragg's law and diffraction will occur. In three dimensions a sphere, rather than a circle, is used to describe the diffraction requirements. Any point in the three-dimensional reciprocal lattice which contacts the surface of the sphere will satisfy the Bragg equation and will give rise to diffraction. The sphere is commonly called the sphere of reflection, or the Ewald Sphere. The direction of diffraction can also be defined. A line drawn from the origin to a reciprocal lattice point lies exactly 90° away from the real-planes. Consequently the line BP, which is perpendicular to the line OP (the line from the origin to the reciprocal lattice point), is parallel to the real planes which have produced the reflection P. A line parallel to the line BP, through the centre of the circle, represents a plane which reflects the X-ray beam under these conditions. The beam impinges on the plane with the angle θ, and is diffracted with an equal angle. Thus, the diffracted beam is reflected away from the line OB by 2θ, i.e. with angle θ from the line representing the real-plane.

3.2. X-Ray Crystallography: Determination of the Structure of a Biological Macromolecule.

The methods used to collect X-ray diffraction data and the calculation of atomic co-ordinates from this data are discussed in detail in the Materials and Methods section (9.2 and 9.3). However, at this point it may be useful to outline the overall procedures involved in obtaining an atomic model of a macromolecule by X-ray crystallography.

of biological interest. The group led by Max Perutz followed a couple of years later with the structure of haemoglobin (Cullis et al, 1962) initially to a lower resolution of ~5.5Å. In the decades that have followed the determination of structures has accelerated (Figure 18), so that there are now over five thousand structures held in the Brookhaven Protein Structure Data Bank, the vast majority of which have been elucidated by X-ray Crystallography.

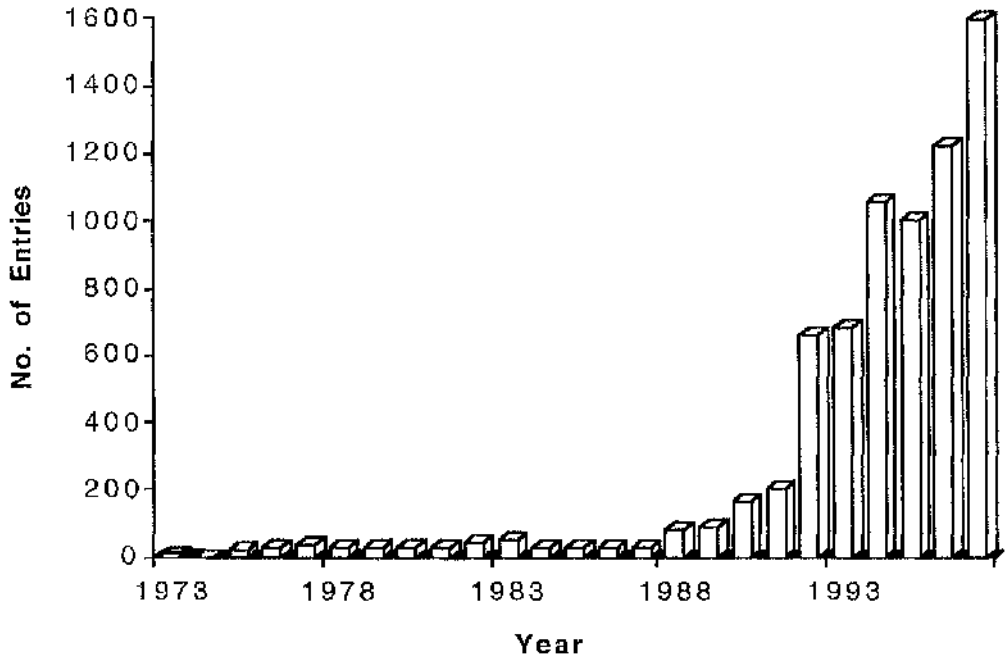

Figure 18: The dramatic increase in the number of structures deposited in the Brookhaven Protein Structure Database since 1973. The figure given for 1997 was based upon the number which had been deposited by 1st April 1997.

A successful protein crystallography investigation can be split into six stages: obtaining sufficient pure and stable protein; growth of high quality crystals; collection of X-ray data; obtaining phase information; map interpretation and finally refinement. Assuming there is no problem in obtaining adequate samples to work on, the two most problematical stages are obtaining quality crystals, especially when membrane proteins are concerned, and obtaining phase information for the maps.

3.2.1. *Crystallisation Theory.*

Crystallisation is one of several means by which a metastable supersaturated solution can reach a stable lower energy state by reduction of solute concentration (Weber, 1991), the others being non-specific aggregation and precipitation. The general processes by which substances crystallise are similar for molecules of both microscopic (salts and small organics) and macroscopic (proteins, DNA, RNA) dimensions. There are three stages of crystallisation common to all systems: nucleation, growth, and cessation of growth.

Nucleation is the process by which molecules or non-crystalline aggregates (dimers, trimers, etc.) which are free in solution come together in such a way as to produce a thermodynamically stable aggregate with a repeating lattice. Crystallisation is known to lower the free energy of proteins by ~3-6 kcal/mole relative to the solution state (Drenth and Haas, 1992). However, the formation of crystalline aggregates from supersaturated solutions does not necessitate the formation of macroscopic crystals. Instead, the aggregate must first exceed a specific size, "the critical size", defined by the competition of the ratio of the surface area of the aggregate to its volume (Feher and Kam, 1985; Boistelle and Astier, 1988). Once the critical size is exceeded, the aggregate becomes a supercritical nucleus capable of further growth. The formation of non-specific aggregates and non-crystalline precipitation from a supersaturated solution does not involve the competition between surface area and volume, and thus generally occurs on a much faster time scale than crystallisation.

The degree to which nucleation occurs is determined by the degree of supersaturation of the solutes in the solution. The extent of supersaturation is in turn related to the overall solubility of the potentially crystallising molecule. Higher solubility allows for a greater number of collisions by diffusion. Thus, higher degrees of supersaturation produce more stable aggregates (due to higher probability of collision of diffusing molecules) and therefore increase the likelihood of the formation of stable nuclei. In the case of a finite number of solute molecules, this condition generally results in the production of a large number of small crystals. At lower solute concentrations the formation of individual stable nuclei

increases in rarity, thus favouring the formation of single crystals. Crystal growth generally starts at solute concentrations sufficient for nucleation to occur, and continues at concentrations beneath the nucleation threshold. The rate of growth is determined by a combination of the nature of the growing crystal surface and the rate of diffusion. Addition of molecules to a rough surface requires less energy than addition to a smooth surface, where surface nucleation is required for addition. The growth of crystals from nuclei is also strongly influenced by effects of diffusion and convection. As with nucleation, increased solubility results in increased growth rates. Again, this is a function of the rate at which protein molecules reach the growing surface of the protein crystal.

Feher and Kam, through the use of ultraviolet microscopy, have been able to demonstrate that the regions surrounding growing crystals are lowered in protein concentration relative to the surrounding solution (Feher and Kam, 1985). The rate of diffusion of proteins in and out of these regions around the growing crystal provides a growth limiting factor. The formation of regions of lowered solute concentration around growing crystals also has the effect of producing density gradients in these areas. These in turn, under the effects of gravity, result in the formation of convection currents which may dominate the rate of simple diffusion and adversely effect crystal growth (Rosenberger & Meehan, 1988). As the formation of concentration gradients around growing crystals is directly proportional to the rate at which molecules add to the surface (the crystal growth rate), slower growth results in decreased convection currents. This may be accomplished by growing crystals in porous gels (Robert and Lefaucheux, 1988). Crystal growth in zero (effective) gravity may also be used to remove sedimentary effects, and effects due to convection (Littke and John, 1986; DeLucas et al, 1986).

Cessation of growth of crystals can occur for a multitude of reasons. The most obvious is the decrease in concentration of the crystallising solute to the point where the solid and solution phases reach exchange equilibrium. In this case, the addition of more solute can result in continued crystal growth. However, some crystals reach a size beyond which growth does not proceed irrespective of solute concentration. This may be a result either of cumulative lattice strain effects or poisoning of the growth surface. Lattice strain effects in tetragonal lysozyme crystals have been

demonstrated by Kam et al (1978). Halved crystals of hen egg white lysozyme, when placed in fresh crystallisation solutions, grew to precisely the same size as the original crystal. This suggests that the long range propagation of strain in the lattice effectively prevents addition of molecules to the surface once a particular critical volume is reached. Crystals affected by lattice strain are therefore inescapably size limited.

Poisoning of growing faces occurs when foreign or damaged molecules are incorporated into the growing crystal face resulting in successive defects which interrupt the crystal lattice. An example of this might be the incorporation of a proteolytically knicked protein onto the face of an otherwise perfect protein crystal. If the knicked molecule is unable to form the same lattice contacts with newly added molecules as would the perfect protein, then its incorporation will cause local defects in the growing lattice. Since the growth of crystal lattices typically selects for perfect over damaged or incorrect molecules, the concentration of these defective molecules relative to perfect molecules tends to increase as growth proceeds. Thus, as crystals grow larger the likelihood of incorporation of defective molecules into the lattice increases (an effect to which the increase in surface area also contributes).

3.2.2. *Crystallisation Methodology.*

By and far the most important factor in crystallisation is the purity of the sample to be crystallised. Although crystal growth, by nature, tends to exclude impurities (such as in PS I where a crystallisation step is used to perform the final purification; Witt et al, 1992). The presence of high concentrations of impurities in small volumes, as are present in vapour diffusion and dialysis experiments, will undoubtedly lead to contamination of the crystal lattice, and ultimately poorer crystals. Lin and co-workers recommend the use of FPLC (or HPLC) for general purification of proteins and to assure homogeneity on both macroscopic and microscopic levels (Lin et al., 1992). Lin notes several cases where the use of FPLC techniques has improved the reproducibility of crystallisation as well as the maximum resolution to which protein crystals diffract. A similar finding was observed during this project, with FPLC being adopted at an early stage as the best method for purifying protein intended for crystallisation.

As noted earlier, molecules crystallise from metastable supersaturated solutions as a means of lowering the overall solution free energy. Chemical precipitants are by and far the most widely used method of achieving supersaturation of macromolecules in order to induce crystallisation. In general, the main influence of these compounds is on the solvent (e.g. bulk water) rather than on the solute (the protein), with the notable exception of dye precipitants. For crystallisation of proteins, the major classes of precipitants may be divided into four categories: salts (e.g. Deisenhofer et al, 1984; Ermler et al, 1994); high molecular weight straight chain polymers (e.g. Polyethylene glycol (PEG), recently analysed with respect to RC crystallisation by Gaucher et al, 1997); organic solvents such as 2-methyl-2,4-pentanediol (MPD) (King et al, 1956); and deionized water (Arakawa and Timasheff, 1985; McPherson, 1990; Witt et al, 1992).

Salts are by far the most common precipitant type used to crystallise macromolecules. Historically they have been the most effective precipitants tried, although, until recently, there were few other options (McPherson, 1991). Unfortunately, the use of salts generally has the disadvantage of increasing the mean electron density of the crystallisation solution, decreasing the signal to noise ratio for crystallographic data. Salts also have a tendency to interact strongly with heavy atom compounds, making crystal derivitisation for M.I.R. phasing difficult. The efficacy of a particular salt as a precipitant is proportional to the square of the valencies of the cations and anions which make up that salt. In practice the PO_4^{3-} anion does not exist in solution within the range of pH typically used for crystallisation trials, and is present instead as HPO_4^{2-} and $H_2PO_4^-$. In addition, the NH_4^+ cation generally loses H^+ above pH 8.0 and boils off as NH_3, making NH_4^+ salts difficult to use at high pH, as well as making the pH highly unstable.

Two general categories of salts exist - those which mainly interact with water (non-chaotropic salts), and those which mainly interact with the protein (chaotropic salts). Chaotropic salts are generally not used for crystallisation due to their tendency to salt in macromolecules and to induce unfolding through interactions with secondary structural elements of proteins. Non-chaotropic salts are preferentially hydrated with respect to protein solutes. The effect of this is an increase in the surface tension of

the solvent surrounding the macromolecule, and subsequent dehydration of the protein's surface, creating excluded volume effects. These force solute molecules to form close interactions with each other. Binding of non-chaotropic salts by the protein does not generally play a role in crystallisation, although in some cases salt ions (particularly phosphates, see Results 13.2.1) are seen bound by macromolecules in crystal structures, and occasionally act as lattice contacts between molecules in the crystal.

Two other chemical factors which can be used to initiate or enhance crystallisation are viscosity altering compounds and anti-twinning/solubilising compounds (detergents and ethers). As noted in the section on crystallisation theory, the rate at which crystals grow often affects the overall quality of the crystals due to the inclusion of defective or mis-aligned molecules. By inclusion of viscosity altering compounds (notably glycerin) in the crystallisation mother liquor the rate of crystal growth may be retarded.

The use of detergents as additives in crystallisation mother liquors has most often been utilised in attempts to crystallise membrane proteins (Deisenhofer et al, 1984; Caravito et al., 1983, 1986; Gros et al., 1988; McDermott et al, 1995; Iwata et al, 1995). The hydrophobic tail of the detergent molecule binds to the hydrophobic areas of the protein which are usually embedded in the membrane, thus solubilising these areas through the exposed hydrophilic head groups of the detergent molecules. Michel (1991) noted that dialysis of β-OG detergent into crystals grown in the detergent LDAO, dramatically improved the order within the crystal. However, simply growing the crystals in β-OG did not yield results of as high quality as the "double detergent" method. At lower concentrations, detergents, as well as simple ethers like dioxane, can also be used in conjunction with other precipitants either to increase the solubility of poorly soluble molecules or to improve crystallisation habit, and particularly to reduce or eliminate twinning. In one case, McPherson et al (1986) reported an entirely new crystal form of a protein due simply to the addition of 0.1-1% β–OG to the crystallisation conditions. Crystal size also appeared to be increased, while nucleation decreased.

The most important factor in crystallising proteins other than the chemical composition of the mother liquor is the pH (McPherson, 1990).

For some proteins (including the purple bacterial photosynthetic reaction centre), crystallisation occurs over a very broad range of pH with little by way of variation in crystal morphology (6.5-9.5, this work). However, it is far more typical for crystallisation to occur over a fairly narrow range (< 1 pH unit). Crystal morphology, including various twinned and polynucleated growth forms, often is directly related to pH. Typically, there is a gradual improvement in crystal morphology as the optimal pH is approached, and a fall off of crystal quality on either side of the optimal condition.

Temperature is another factor which is of considerable importance in the crystallisation of proteins. Crystallisation of macromolecules has been accomplished in a range of roughly 60 °C to 0°C, although the vast majority of molecules are crystallised between 4°C and 22°C. Low temperature tends to act as a preservative for sensitive proteins as well as an inhibitor of bacterial growth. Solubility of proteins in salt solutions tends to increase at low temperatures (4°C), while in PEG and MPD solutions protein solubility generally decreases with decreasing temperature. By increasing or decreasing either precipitant or protein concentration, crystallisation should be possible, at least in theory, at either room temperature or 4°C, although the kinetics of crystallisation can be expected to vary in accord with temperature.

The vapour diffusion technique, which was the only method used in this work, utilises evaporation and diffusion of water between solutions of different concentration as a means of approaching and achieving supersaturation of macromolecules. The solution containing the macromolecule is mixed approximately with a solution containing the precipitant to a concentration below that at which supersaturation occurs. A drop containing the mixture of protein and precipitant is then suspended and sealed over the well solution, which contains the precipitant at the target concentration. This can be performed with either a hanging or sitting drop. Evaporation of water from the protein-containing drop slowly raises the concentration, and the supersaturated state is reached. Glass capillaries have also been successfully used to perform vapour diffusion. Capillaries containing protein and precipitant at concentrations below that required for crystallisation can be equilibrated against a well solution in a sealed test tube. DeMattei and co-workers have

shown capillary based vapour equilibration to occur at much slower rates than drop based methods, resulting in this particular case with improved crystals of isocitrate lyase (DeMattei et al, 1992). The difference in precipitant concentration between the drop and the well solution is the driving force which causes water to evaporate from the drop until the concentration of the precipitant in the drop equals that of the well solution. Since the volume of the well solution is much greater than that of the drop (1ml as compared 15µl) its dilution by the water vapour leaving the drop is negligible.

3.2.3. Crystallisation of Membrane Proteins.

In the past few years, the field of crystallisation of membrane proteins has been remarkably productive. The particular problems associated with the crystallisation of membrane proteins had kept the list of structures small. However, the list has been swelled somewhat with the structures of LHII from *Rps. acidophila* to 2.5Å (McDermott et al, 1995) and from *R. molischianum* to 2.4Å (Koepke et al, 1996); the 8Å projection map of LHI from *R. rubrum* produced from 2-D crystals; and finally models of cytochrome c oxidase from *Paracoccus denitrificans* to 2.8Å (Iwata et al, 1995) and from bovine heart mitochondria to 2.8Å (Tsukihara et al 1995). The details of the two cytochrome c oxidase structures were recently discussed by Ostermeier et al (1996). These structures follow the previous determinations of the photosynthetic reaction centre from *Rps. viridis* (Deisenhofer et al, 1985, 1995) and *Rb. sphaeroides* (Allen et al, 1987; Komiya, 1988) and various forms of porin (Garavito, 1986; Cowan et al, 1992)

The main problem encountered with membrane proteins is that they are notoriously difficult to crystallise, especially in the highly ordered state required for X-ray crystallography. There is the problem of simply obtaining sufficient quantities of high purity, stable protein to perform crystallographic analysis. Conditions for extracting the protein from the membrane and maintaining it in a stable form need to be developed. One problem unique to membrane protein crystallisation is phase separation. This is due to the tendency of the detergent to form a separate, viscous detergent phase, in which will be held the membrane proteins. Alteration of factors such as temperature, the concentration and type of salts and

detergents or even the addition of substances such as glycerol, can all be used to overcome this (Michel, 1991; Garavito, 1986).

There is also a range of additives which may prove to be useful/essential for crystallisation. The most common additives in membrane protein research are the so-called amphiphiles. These are small amphiphilic molecules, the precise role of which remains unclear. Explanations for their effect include suggestions that they combine with and reduce the size of the detergent micelle (Michel, 1983) or that the amphiphile might in some way be making the micelle more deformable and thus more suitable for packing into a three-dimensional crystal (Garavito, 1986). Crystallographic investigations are expensive in terms of the amounts of protein required, and many projects do not advance beyond the problem of obtaining sufficient protein for effective screening of the possible crystallisation conditions. Fortunately the photosynthetic apparatus is present in the purple bacterial intracytoplasmic membrane in relatively large amounts, and this last problem is not a major difficulty for the analysis of photosynthetic reaction centres.

Conditions in which the photosynthetic reaction centres from *Rb. sphaeroides* will successfully crystallise have been known for some years. A number of crystal forms have been produced and structures produced from these different forms (Table 3). Although all the structures produced are essentially identical (See Fyfe et al, 1997), the trigonal crystal form as produced in the Ermler et al structure, provides the highest published resolution data (2.65Å). Obtaining crystals of the reaction centre was not a major problem for reaction centre research. However, to realistically observe the alteration of structure in the point mutants, with quite conservative amino acid changes, the crystal quality, i.e. the resolution of diffraction, needed to be improved. Chirino et al (1994) generated x-ray data on a series of mutant reaction centres. However, the information which could be gleaned from that work was minimal due to the poor levels of resolution (between 3.0Å and 4.5Å). Only one of the five structures was actually put through a complete refinement procedure, and deposited in the Brookhaven Data Base. Therefore, it was important that for the crystallography section to be successful, or even worthwhile given the large amount of time and resources required for such a study, the resolution had at least to match the best structure (3Å) in the Chirino et al

structures was actually put through a complete refinement procedure, and deposited in the Brookhaven Data Base. Therefore, it was important that for the crystallography section to be successful, or even worthwhile given the large amount of time and resources required for such a study, the resolution had at least to match the best structure (3Å) in the Chirino et al paper. Even at this level, the amount of information available is not particularly high. It was hoped to obtain crystals which would diffract to beyond 2.5Å. This was in fact achieved, with diffraction approaching 2.0Å (See results, section 12.1.).

Table 3: The models of *Rhodobacter sphaeroides* reaction centres currently available with the crystallographic statistics for each. *The co-ordinates of this model are deposited in the PDB but have yet to be released

Model	Resoln. Range (Å)	Crystal form (space group)	No. of unique reflections	Completeness (%)	R-Factor (%)	Reference
1AIG	30.0-2.2	Tetragonal ($P4_32_12$)	335,463	86	22.0	Stowell et al, 1997*
WM115 RM197	26- 2.3	Trigonal ($P3_121$)	96,029	94	20.7	This Work
1PCR	10 - 2.65	Trigonal ($P3_121$)	56,141	90.4	18.6	Ermler et al, 1994
4RCR	8.0 - 2.8	Orthorhombic ($P2_12_12_1$)	21,992	60.0	22.7	Yeates et al, 1988
1PSS	8.0 - 3.0	Orthorhombic ($P2_12_12_1$)	21,518	68.9	22.3	Chirino et al, 1994
1PST	8.0 - 3.0	Orthorhombic ($P2_12_12_1$)	22,184	71.1	21.8	Chirino et al, 1994
1YST	7.0 - 3.0	Orthorhombic ($P2_12_12_1$)	19,630	80	22.9	Arnoux et al, 1989
2RCR	8.0 - 3.1	Orthorhombic ($P2_12_12_1$)	13,493	50.8	22.0	Chang et al, 1991

3.2.4. Data collection and Phase determination.

The techniques used to collect the diffraction images are detailed in section 9.2. of the Materials and Methods chapter, and will not be expanded

measured directly from the image, all the information regarding the phasing within the reflections is absent. As discussed above, for a spot to form in the diffraction image the constituent beams must give net constructive interference. However, the "constructed" beam, although all in-phase, could be at any position in that phase cycle. Information about the position is not carried on the diffraction pattern, and so phases must be obtained through additional investigation. This can be extremely problematic, as is demonstrated by the solution of the LHII structure from *Rps. acidophila* (McDermott et al, 1994), some years after the first crystals were reported by Cogdell et al in 1985. Typical methods used to gain phase information include multiple isomorphous replacement (MIR), the use of anomalous dispersion in anomalous scattering (or multiple wavelength anomalous scattering, MAD) and molecular replacement.

MIR is the established technique in protein crystallography. It involves soaking protein crystals, or co-crystallising, the protein with a heavy atom solution. Typical solutions used for this are platinum compounds such as K_2PtCl_4, gold compounds such as $KAu(CN)_2$, and lead compounds such as $Pb(NO_3)_2$. The method depends upon the measurements of differences in intensities that arise when the heavy atoms are bound within the protein at a limited number of specific sites. This procedure, like crystallisation itself, is very much a trial and error procedure, altering the heavy atoms solutions, the concentrations of the solutions, the length of time the crystals are soaked for, backsoaking, and so on. The technique requires that the crystal maintains an arrangement identical with the "native" and that the derivatives are formed with the heavy atom regularly placed at the same position in all of (or at least most of) the unit cells.

MAD is often used in conjunction with MIR. Elements can absorb X-rays, with characteristic absorption maxima for each element. The absorption maxima drops sharply just below the elements characteristic emission wavelengths, this sudden change in absorption as a function of wavelength is known as the absorption edge. An element will exhibit anomalous scattering when the X-ray wavelength is close to the element's absorption edge. The wavelengths used in crystallography are not close to the absorption edges of light atoms such as nitrogen, carbon and oxygen, hence these atoms do not contribute to anomalous scattering. However, the absorption edges of heavy atoms are within this range, especially if

anomalous scattering when the X-ray wavelength is close to the element's absorption edge. The wavelengths used in crystallography are not close to the absorption edges of light atoms such as nitrogen, carbon and oxygen, hence these atoms do not contribute to anomalous scattering. However, the absorption edges of heavy atoms are within this range, especially if tuneable synchrotron X-ray radiation is used to maximise the anomalous scattering effect. Anomalous scattering takes advantage of the ability of heavy atoms to absorb X-rays of specific wavelengths. The result of this absorption is to cause the *hkl* and *-h-k-l* reflections to be unequal in intensity. This inequality of symmetry related reflections is called anomalous scattering or anomalous dispersion. From this disparity in the symmetry related reflection pairs, it is possible to extract phase information. MAD is very rarely used as a method for phase determination by itself, but rather to help enhance the information made available by MIR experiments.

Molecular replacement was the technique utilised in this research project. The required phase information can be supplied by using the structures of highly homologous proteins. In the case of reaction centres from *Rb. sphaeroides* there exist a number of previously determined structures (See Table 3 above). Indeed all the models that have been produced for *Rb. sphaeroides* reaction centres have been solved by molecular replacement, the co-ordinates for the *Rps. viridis* reaction centre providing the original starting model. All the initial phase information in this research was obtained from the Ermler et al model (1994) of *Rb. sphaeroides* ATCC 17023 (1PCR).

3.2.5. Data Processing, Production of Maps and Refinement Procedures.

Once collected, the diffraction data must be processed. Processing refers to the measurement of the position and intensity of each spot on each collected diffraction image. Processing is followed by scaling of the data. This allows the merging of data from the individual images of each data set and of two or more sets of data. Protein crystals are susceptible to radiation damage, causing effects such as reduction in the resolution of diffraction. For this reason it is often necessary (in all but one case in the collection of data for this project, and even in this example, the crystal had to be translated three times during the data collection) to collect data from

in the unit cell dimensions between crystals, and differences in the power of diffraction (due to different sizes of crystal). The result is a weighted data set corrected for these factors. The processed and scaled data can then be used in conjunction with the phase information to produce the first electron density maps.

The initial co-ordinates will contain a large number of inaccuracies. Further refinement procedures are used to improve the fitting of the co-ordinates to the density. It is also important to note, that as the model co-ordinates improve, so will the electron density map. This occurs because the maps themselves are produced using the model co-ordinates as the source of the phase information. Improving the model will lead to more accurate phasing information, leading to improved maps and to a further improved model and so on. The refinement procedure ends when there is no further improvement in the fitting of the co-ordinates to the density maps. This point is determined by the observation of the results of a number of statistical analyses throughout the refinement.

As the refinement proceeds a number of parameters are checked to continuously monitor the quality/reliability of the models being produced. Perhaps the two most common and most immediately useful are the R-factors, R_{norm} and R_{free}. The R_{norm}, usually simply called the R-factor, gives an indication of how well the calculated structure factors (calculated from the model co-ordinates) fit the observed structure factors (calculated from the experimental observations, i.e. the diffraction patterns). Meanwhile a sub-set of the observed data (5% or 10% in this work, giving a total of approximately 4000 reflections) is kept out of the refinement calculations. The R_{free} statistic allows scrutiny of the extent to which this unrefined set of data matches the model calculated from the remaining 90-95% of the data (Brünger, 1992; Brünger, 1997; Kleywegt & Brünger, 1996). A successful refinement will show both the R-factor and R_{free} dropping at an approximately equal rate. If the R_{free} is observed to increase, or be decreasing at a slower rate than R_{norm}, over the progress of a refinement procedure, then the quality of the model is decreasing, and the refinement protocol must be reassessed. In addition, various other properties of the model may be investigated. Many of these investigations utilise databases of high resolution X-ray crystal structures and compare and contrast specific structural features of the model. Features of the model

investigated include checks of the peptide and protein geometry, whether the potential H-bond donors and acceptors are satisfied, side chain planarity and so on. The regions with potential problems can then be assessed with the molecular graphics and further rebuilding performed if necessary.

Refinement itself is performed in cycles. Each cycle usually contains a session of interactive modelling, followed by a series of computational steps where energy minimisation within certain constraints is performed (See Kleywegt & Jones (1997) for a discussion of good model building and refinement practice). In this project, the first step was performed using the program O (Jones et al, 1991), which also allows interactive manipulation of the model co-ordinates, essentially attempting a best fit of the atomic skeleton within the electron density contour map. The program suite X-PLOR (Brünger et al, 1987) was then used to perform the energy minimisation computations, with various programs from the CCP4 (CCP4: Collaborative Computational Project, 1994) suite also used. Additional atoms are carefully introduced into the model. In the case of the reaction centre models presented in this work, three additional molecule types were introduced; water and detergent molecules (LDAO) were introduced into all of the models, while in the higher resolution models phosphate groups were also built in.

3.3. Resonance Raman Spectroscopy.

Molecules naturally vibrate at a given frequency. The vibrational modes of a molecule are determined in turn by the structure of that molecule and by the interactions of the molecule with surrounding molecules, i.e. its environment. Raman spectroscopy provides a method by which the chemical structure of a molecule can be analysed, by probing the vibrational modes present. The Raman effect was first described by C.V. Raman in 1928. When a molecule is illuminated by light, the light which is scattered from the molecule will exhibit a range of frequencies. The majority of the scattered light will be of the same frequency as was applied. However, there will also be a very small fraction of the scattered light which will be of either lower or higher frequency. This loss or gain of frequency, or energy, is the so-called Raman effect.

A photon of light which collides with a molecule can undergo one of four processes. It may be absorbed by the molecule or reflected with its frequency unchanged. However, the photon may also be scattered from the molecule with a small decrease or increase in energy. The process of loss or gain of energy can be likened to the analogy of a ball-bearing striking the surface of a drum. If the drum surface is still then energy would be lost from the ball to the drum. The surface of the drum would be seen to vibrate, and the ball-bearing would bounce back with a lower energy. However, if the drum surface was already resonating, an alternative outcome is possible. If the ball strikes the drum surface as it flexes up towards the ball, then the ball will pick up energy from the drum, and bounce off with increased energy. A similar situation occurs if a sample is irradiated with a intense beam of light of intensity ν_o. If the frequency of the scattered light is altered, say to ν_r, then the frequency shift:

$$\Delta\nu = \nu_o - \nu_r \qquad \textit{Equation 15}$$

corresponds to the energy exchanged between the photon and the molecule with which it collided. In addition, this alteration in frequency or energy must equal that of a transition between energy levels within the irradiated molecule.

Two sets of Raman lines are produced. Lines which occur as a result of surrendering energy to the photon are called anti-Stokes lines, whilst those resulting from the molecules accepting energy from the photon are called Stokes lines. To be able to give energy to the photon, a molecule would have to be existing in a raised energetic state. Since a larger number of molecules will always exist in the lower (ground) state, the Stokes lines are by far the most intense, and it is these lines which are measured experimentally.

Classical Raman studies have been replaced in the study of photosynthetic systems by resonance Raman procedures. Resonance Raman occurs when a sample is irradiated with a monochromatic beam (a laser line) which corresponds to an absorption band region. When this

occurs, the intensity of the scattered Raman lines increases greatly ($<10^6$). The advantages of this are two-fold. Firstly the signal to noise ratio increases, making the signal much easier to detect, and secondly the selectivity of the procedure increases, because only the vibrational modes associated with the absorbing compound in the molecule are enhanced. Thus it is possible to examine the Raman spectra of individual groups of pigments held within the reaction centre protein. The vibrational frequencies of pigments are determined by bond strength, the number of atoms involved, geometry and its co-ordination environment within the complex. Detailed studies of the photosynthetic pigments have been carried out, including many which have probed the structure and conformation of the carotenoid molecule within the reaction centre.

The investigation of carotenoids in reaction centre complexes by resonance Raman has provided the strongest information regarding the conformation the molecule adopts. X-ray crystallographic analyses have failed to demonstrate conclusively whether the carotenoid adopt a 15-*cis* or a 13-*cis* conformation. A number of individual resonance Raman studies have produced agreement that it is the 15-*cis* conformation which is adopted (Lutz et al, 1978; Koyama et al, 1982; Kok et al, 1994). However, information into the carotenoid structure is not limited to this. A number of lines in the Raman spectra have now been assigned to specific structural and conformational aspects of the carotenoid.

The RR spectra of carotenoids contain four major groups of bands. They are ν_1 (1530-1540 cm^{-1}), ν_2 (1120-1260 cm^{-1}), ν_3 (~1120-1030 cm^{-1}) and ν_4 (~960 cm^{-1}). The ν_1 line has been assigned to C=C stretching; ν_2 to C-C stretching coupled with C-H in-plane deformation; ν_3 to C-H in-plane deformation coupled with C-C stretching (Rimai et al, 1970; Warshel et al, 1974; Koyama et al, 1982) and finally ν_4 has been attributed to out-of-plane bending of C-H groups and also to C-CH_3 stretching (Lutz et al, 1978). The band selected as most indicative of the cis- conformation is found at ~1240 cm^{-1}. However, the intensity of the ν_2 band has also been shown to decrease in the cis conformation relative to that of the ν_3 band, and the ν_4 band was found to increase in intensity (Lutz et al, 1978). A typical resonance Raman spectrum for spheroidene bound within a *Rb. sphaeroides* reaction centre is shown in Figure 19.

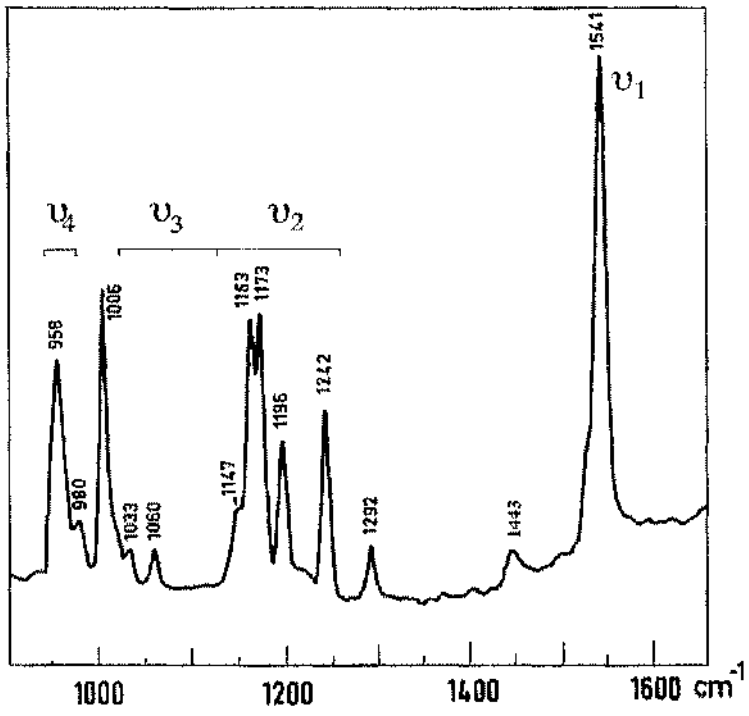

Figure 19: The Resonance Raman spectrum for spheroidene bound within a *Rb. sphaeroides* reaction centre, 30K, 496.5nm excitation, 900-1650 cm^{-1} (Robert, 1996).

Resonance Raman spectroscopy can also be utilised to examine the properties of the BChl pigments in the reaction centre (and also the light-harvesting BChl pigments). Investigation of the BChl pigments of the reaction centre involves a more complicated procedure than investigation of the carotenoid. To obtain resonance Raman spectra of the special pair it is necessary to use the technique of near-infrared (NIR) Fourier transform (FT) Raman spectroscopy. Standard resonance Raman, with excitation into the 870nm absorption band, poses huge difficulties in that the accessory BChls contribute to the generated spectrum. NIR-FT Raman spectroscopy is performed using an excitation of much lower wavelength (typically 1064nm from a Nd:YAG laser). The beam at this wavelength causes resonance excitation of P, but not of the accessory BChl's. However, the generated signal is much weaker, hence the use of FT techniques to extract the spectrum.

FT Raman spectroscopy has been used to probe the interaction of the reaction centre protein with the BChl's that comprise the special pair. Mattioli et al, (1994) analysed a range of mutations around P which had been produced in the expectation that they would be capable of either breaking the existing H-bond, or forming new H-bonds to P (Williams et al

1992). The changes in the H-bonding states were determined using FT Raman spectroscopy. Table 4 shows the mutations that had been created, the expected effect of each and the effect the mutations were observed to have on the Raman signal assigned to the carbonyl group on P (Mattioli et al, 1991).

Table 4: Mutants discussed by Mattioli et al (1994) and the results obtained. The mutations were designed to alter the hydrogen bonds to the primary donor.

Mutant	Expected result	WT frequency (cm^{-1})	Mutant Frequency (cm^{-1})	Difference in frequency (cm^{-1})	Alteration attributed to
His L168-Phe	broken $C_2 = O\ P_L$	1620	1653	+33	Broken H-bond
Phe M197-His	formed $C_2 = O\ P_M$	1653	1630	-23	Formed H-bond
Leu M160-His	formed $C_9 = O\ P_M$	1679	1657	-22	Formed H-bond
Leu M131-His	formed $C_9 = O\ P_L$	1691	1673	-18	Formed H-bond

The FT Raman studies fully confirm the formation of H-bonds to the C9 carbonyls in the M160 and M131 mutants. This confirmed earlier investigation by FTIR spectroscopy (Nabedryk et al, 1993), although there were some discrepancies in the strengths of the bonds alluded to in the two studies. The remaining mutants were found also to have characteristics suggesting that these too had broken/formed H-bonds as had been expected. These mutants, and others which influence the H-bonding nature of the protein to P have been studied intensively by many techniques other than (FT) Raman. However, the investigation reported by Mattioli et al (1994) is a clear demonstration of the power of the FT Raman techniques to examine the state of P in reaction centres.

3.4. Electron Paramagnetic Resonance Spectroscopy.

Electron Paramagnetic Resonance spectroscopy (EPR) is a technique by which molecules containing unpaired electrons can be studied. The potential uses of a such a technique would at first seem limited, if only because systems containing unpaired electrons are rare. However, this apparent disadvantage does mean that when such a situation does exist, EPR provides a highly specific probe. Systems which have been studied using EPR include those which form free radicals, those containing

transition-metal ions and also those where the triplet states of a molecule is generated. All of the above can be found in biological systems. EPR has greatly advanced the understanding of the photosynthetic process. The absorption of light by the special pair (B)Chl and the subsequent release of an electron provides a system which can be explored with EPR. In addition the formation of triplet states of the (B)Chl and the carotenoid pigments can be followed. This latter possibility has been utilised in this research project, probing the capability of the mutant complexes to transfer triplet energy from the BChl to the carotenoid.

EPR spectroscopy specifically probes the behaviour of unpaired electrons in a system. When such electrons exist in a substance their spins are aligned at random. However, when a magnetic field is applied to the sample, each paramagnetic electron will assume a particular spin direction, either $+\frac{1}{2}$ or $-\frac{1}{2}$. This can be thought of as spinning either clockwise or anti-clockwise about the field direction (Figure 20). The application of an external magnetic field to ordinary bar magnets would cause a similar observation. These two different spin orientations have slightly different energy levels, the difference between the two denoted ΔE. The paramagnetic electrons can take one of only two orientations with regards to the magnetic field, either directed parallel to the field or opposed to it (anti-parallel). The parallel orientation is of slightly lower energy than the anti-parallel, hence the difference ΔE.

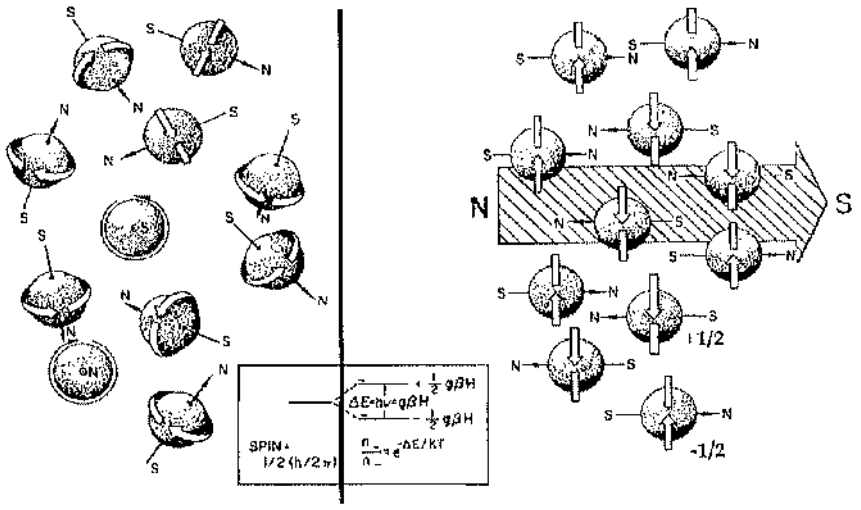

Figure 20: Diagrammatic representation of unpaired electrons and their spins. (a) The electrons assume random spin orientations of equivalent energy in the absence of an external magnetic field; (b) Upon the application of a magnetic field, the electrons assume spins $\pm\frac{1}{2}$ to the applied field. The electrons are therefore split into two groups, with a small energy difference, ΔE (Adapted from Swartz et al, 1972).

When paramagnetic electrons are split into two sets by a magnetic field, it is possible to carry out an investigation into the size of the energy difference between the two sets. Energy transitions become possible, in which the spin of electrons flip to the opposite orientation. In EPR this switching of orientation is caused by applying a second electromagnetic field to a sample with magnetic moments already lined up by the application of the first field. If the energy of the second energy field corresponds to the energy difference, ΔE, between the parallel and anti-parallel electron magnetic moments, spin transitions will occur. Electrons can "resonate" within the applied field, either accepting energy from the field or losing energy to it. Those electrons which accept energy from the field will become excited up to the higher energy spin state, i.e. the transition of parallel to anti-parallel. Meanwhile the second transition process is caused by some electrons giving up energy, causing them to switch from the anti-parallel to the lower parallel spin state. However, as in any system, the state with lower energy will tend to be more highly populated. Thus, there will exist more of the parallel oriented species within the sample. A net absorption of energy will therefore occur from the second applied field. It is this absorption which is detected as the sample signal in EPR.

The resonance condition is met when the conditions given in Equation 16 are satisfied:

$$\Delta E = h\nu = g\beta H \qquad \textit{Equation 16}$$

where g is the g-factor of an electron, and β the Bohr magneton. That is, for resonance to occur the energy difference ΔE must equal the energy of one quantum of the applied electromagnetic field, as given by hν, Planck's constant times the frequency of the field.

EPR can be used to study the triplet states of species generated by the photosynthetic apparatus. The triplet states of carotenoids were first reported by Frank et al (1980). EPR can provide information on a number of important factors. Firstly, the zero-field parameters |D| and |E| provide information regarding the molecular structure of the carotenoid (Frank et al, 1987). They are related to the extent of dipolar interaction between the two unpaired electrons that comprise the triplet state. Secondly, information can be obtained from the polarisation pattern about the mechanism by which the triplet state was formed. Carotenoid triplet states are formed via transfer of triplet energy from a triplet energy donor. The polarisation pattern reports on whether this transfer is via intersystem crossing or via the radical-pair mechanism. The results of an EPR investigation of reaction centres and light-harvesting complexes from *Rb. sphaeroides* 2.4.1. are given in Table 5 and Figure 21. These results indicate that triplet formation in reaction centres is via the radical pair mechanism (pattern *eaa eea*) whilst in the light-harvesting transfer occurs via intersystem crossing.

Table 5: Polarisation Patterns and zero-field splitting parameters from an EPR investigation of *Rb. sphaeroides* 2.4.1. reaction centres and B800-850 complex. Polarisation pattern is defined as *e.* emission and *a.* absorption.

Location of T1 carotenoid	Polarisation pattern	|D| (cm^{-1})	|E| (cm^{-1})
Reaction Centre	*eaa eea*	0.0290±0.0005	0.0044±0.0006
B800-850	*eae aea*	0.0326±0.0007	0.0036±0.0007

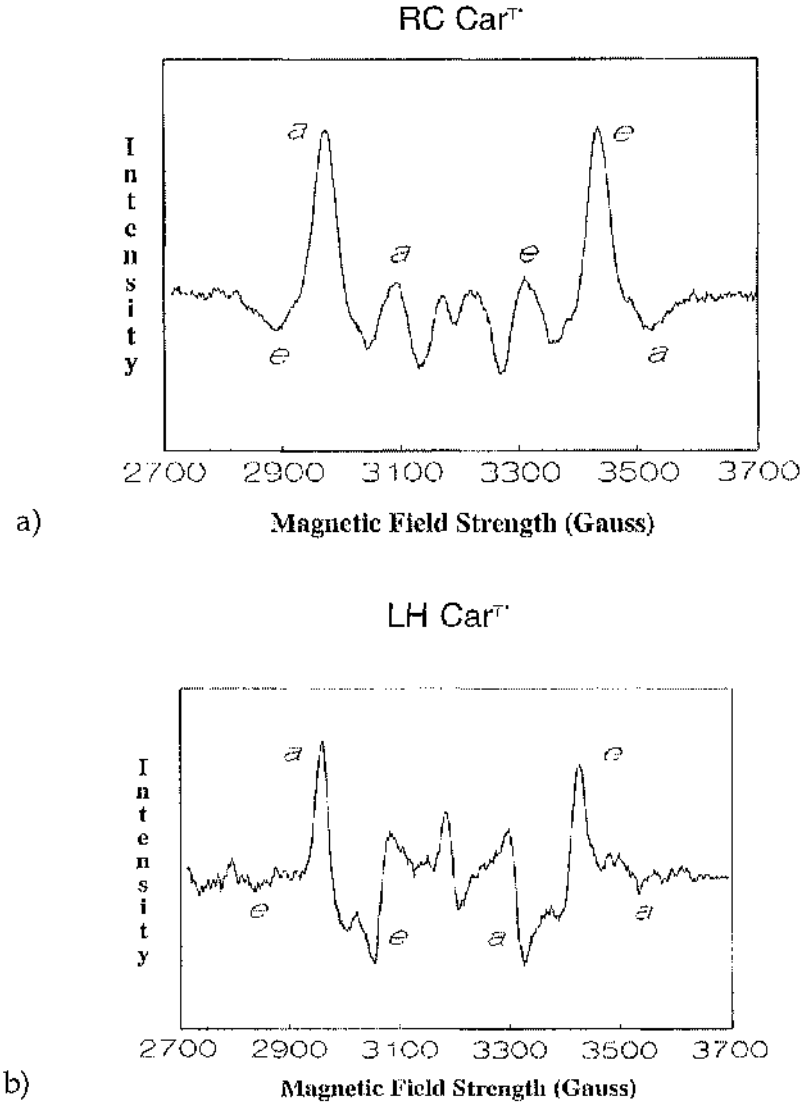

Figure 21: The EPR spectra obtained from investigation of the *Rb. sphaeroides* 2.4.1. a) reaction centre and, b) B800-850 complex (Frank, 1992).

The structure of the carotenoid can also be investigated. Table 6 shows the results of the investigation of B800-850 complexes from a range of bacteria, in which carotenoids of different lengths of π electron conjugation are present. The carotenoid with the shortest conjugated system, neurosporene, was found to have the largest |D| value, that is the greatest dipole interaction between the unpaired electrons. The |D| values were then found to decrease with increasing conjugation. Rhodopin, the carotenoid with the longest conjugated system in this investigation, had the smallest value for |D|. The zero-field parameters can therefore be used to deduce the structure of the carotenoid.

Table 6: The zero-field parameters of B800-850 complexes from a range of bacteria.

Sample	|D| (cm^{-1})	|E| (cm^{-1})	Carotenoid	No. of Conjugated π bonds.
Rb sphaeroides GA	0.0365±0.0002	0.0035±0.0002	Neurosporene	9
Rb. sphaeroides 2.4.1. (anaerobic)	0.0324±0.0002	0.0036±0.0002	Spheroidene	10
Rb. sphaeroides 2.4.1. (aerobic)	0.0318±0.0002	0.0036±0.0002	Spheroidenone	11
Rps. acidophila 7750	0.0279±0.0003	0.0029±0.0003	Rhodopin	13

3.5. Circular Dichroism Spectroscopy.

Circular dichroism (CD) refers to the differential absorption of left and right circularily polarised components of plane polarised radiation (Price, 1997). A molecule which exhibits CD, must be either intrinsically chiral, (i.e. optically active) or in an asymmetric environment. CD is commonly used to estimate the secondary structure content of proteins, and also to study the processes underlying protein folding *in vitro*. However, CD has also become of great importance to photosynthetic research. Carotenoid molecules in general do not exhibit circular dichroism when free in organic solution. However, when they are bound within protein complexes they may become twisted, resulting in the observation of optical activity.

The CD spectrum of spheroidene bound within *Rb. sphaeroides* 2.4.1 reaction centres (Figure 22) exhibits three strong peaks at 503, 472 and 446 nm (Cogdell et al 1976; Koyama & Hashimoto, 1993). However, when reaction centres from *Rb. sphaeroides* R-26 are investigated, these three bands are not observed. Absorption in this region of the spectrum is of course due to the presence of carotenoid molecules, in this case spheroidene. This, in conjunction with the result from investigation of the carotenoidless reaction centres from strain R-26 (Figure 22), makes it clear that the observed bands are due to the carotenoid molecules. A similar observation has been made with *Rps. rubrum* wild type strain (containing spirilloxanthin as the major carotenoid) and the

carotenoidless strain G9. Again, strong CD peaks were found in the carotenoid absorption bands in the wild type (~500nm) which were not observed in the carotenoidless strain. The protein must in some way be causing the carotenoid to exhibit CD behaviour. This is presumably due to the asymmetry in the binding site within the complex.

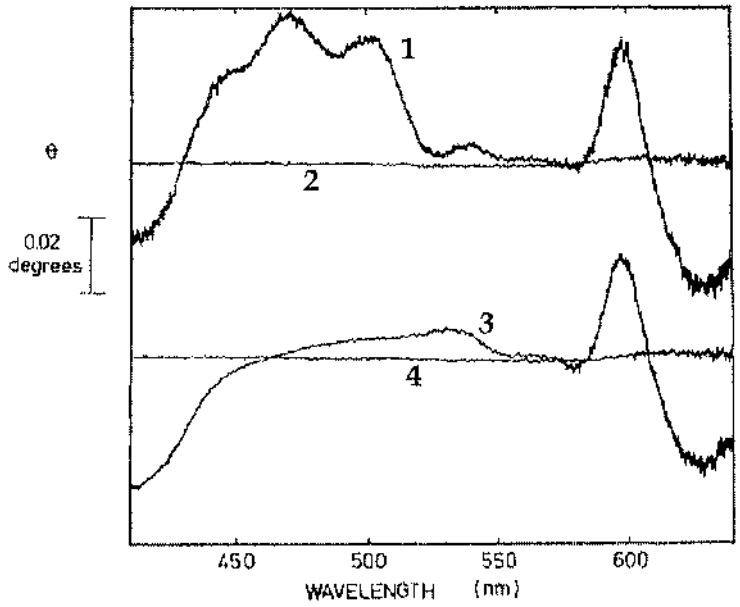

Figure 22: The CD spectra of 1. the reaction centre from *Rb. sphaeroides* 2.4.1. and 3. the reaction centre of *Rb sphaeroides* R-26. Lines 2 and 4 are baselines for the respective scans (adapted from Cogdell et al, 1976)

The information that can be gained with respect to the stereochemistry of the carotenoid from a CD spectrum is limited. Boucher et al (1977) suggested that the spectra could provide some evidence for a "cis" conformation of the carotenoid within the RC. However, they also state that spectra in the 350-400nm region must be treated with caution, as any alterations may be due to perturbation of the Soret band of BChl. They conclude that the strongest statement that can be made is that the spectra are "consistent with a *mono-cis* conformation of the carotenoid twisted in a protohelical shape". However, CD is valuable in that it can quickly provide information on the carotenoid bound within the reaction centre. If any significant alterations in the binding pocket have occurred, i.e. by the alteration of amino acids lining the pocket, they may be revealed by a CD investigation.

B. Materials and Methods

All chemicals were purchased from either Sigma or BDH unless otherwise stated.

CHAPTER 4.

Culture of Bacteria.

4.1. Bacterial Strains and Plasmids.

The bacterial strains and plasmids used are listed in Table 7.

Table 7: The Bacterial Strains and plasmids used during this research project.

Strain/Plasmid	Relevant Characteristics	Source/reference
Rb. sphaeroides		
2.4.1.	Wild-type	Cohen-Bazaire et al (1956)
G1C	Wild-type RC, in neurosporene expressing strain	Crofts et al (1974)
R-26	Wild-type RC, in carotenoid minus strain	Crounse et al (1963)
DD13	Strain NCIB 8253 with replacement of genomic *pufBALMX* operon with Km^R gene and of genomic *pucBAC* operon with Sm^R gene.	Jones et al (1992a)
RCO2	RC only producing strains. Produced in DD13 with *pufQLMX* genes supplied on pRKEH10D plasmid	Jones et al (1992b)
E. coli		
BMH 71-18 mut S	Mismatch repair incompetent strain	Kramer et al (1984)
DH5α	*supE44, ΔlacU169, (p80 lacZΔM15), hϕdR17, recA1, endA1, gyrA96, thi-1, relA1.* Mismatch repair competent strain	Sambrook et al (1989)
S17-1	*thi, pro, hsdR⁻, hsdM, recA, RP4-2* (Tc::Mu Km::Tn7) Strain of *E. coli* capable of mating with *Rb. sph.*	Simon et al (1983)
Plasmids		
pALTER-1	TcR; 5680bp mutagenesis vector	Promega
pALTPC-1	Tc^R; 549bp *PstI-SacI* encompassing codons 83-235 of the *pufM* gene in pALTER.	McMaster (1995)
pUCXB-1	Amp^R; 1841bp *XbaI-SalI-BamHI* fragment encompassing *pufLM*, in pUC19.	McMaster (1995)
pRKEH10D	TcR; derivative of broad-host range vector pRK415 containing a 6.55kb *EcoRI-HindIII* fragment encoding *pufQLMX* with engineered *XbaI* and *BamHI* sites and a unique *SalI* site.	Jones et al (1992a,b)

4.2. Long-term Storage of Bacterial Stocks.

The bacterial strains used were maintained in the form of glycerol stocks (~30% Glycerol / 70% liquid culture (v/v)), stored at -70°C. These stocks acted as a source of original material throughout the project.

4.3. Growth of *E. coli* Strains.

All inoculations and transfers of bacteria (*E. coli* and *Rb. sphaeroides* strains) were performed using standard sterile techniques in a laminar flow hood. Several strains of *E. coli* were used; BMH 71-18 mut S for original transformation of putative mutation carrying plasmids, DH5α for the post-mutation manipulations and S17-1 for mating with *Rb. sphaeroides*. Stocks of each were maintained as glycerol stocks at -70°C. The bacteria were streaked out onto LB/agar plates (LB medium is described in Appendix I) and grown at 37°C, and single colonies were used from these for further growth. Liquid cultures were obtained by picking off single colonies with sterile toothpicks, and placing these in 10mls LB liquid medium in sterile McCartney bottles. These were then grown at 37°C on an orbital shaker, supplemented with appropriate antibiotics. Larger cultures of 250mls LB medium, in 1 litre flasks, were produced by inoculating with 10ml cultures. This liquid-liquid transfer was performed as the bacteria in the starter culture neared the end of the log phase of growth.

4.4. Growth of *Rb. sphaeroides*.

The various strains of *Rb. sphaeroides* used required a range of culturing techniques. The *Rb. sphaeroides* strains 2.4.1. and G1C were grown photosynthetically, usually under anaerobic conditions. However, on occasion, aerobic cultures were prepared. The growth of *Rb. sphaeroides* 2.4.1. in aerobic conditions stimulates the production of spheroidenone as the major carotenoid, instead of spheroidene. Samples of spheroidenone, required on occasion during the project, were produced by aerobic growth of the bacteria. In both cases c-Succinate medium was used (see Appendix I). The RCO2 based strains were all grown non-

photosynthetically in semi-aerobic conditions. In this case the media used was M22+ (See Appendix I), supplemented with fructose as the carbon source. Fructose was determined by a set of experiments to provide higher cell yields and sustain faster growth rates (see Results *10.2.2*). These RCO2 strains were also grown in the presence of antibiotics. The combination of growth conditions and the antibiotics helped to minimise the chance of reversion of the site-directed mutants.

4.4.1. Growth on Agar Plates.

Initial cultures of 2.4.1 and C1C were grown in sterile petri dishes on 1.5% (w/v) agar, supplemented with 0.3% (w/v) yeast extract (DIFCO) and 0.2% (w/v) casamino acids (DIFCO). The plates were grown in anaerobic jars (MERCK), with anaerobic conditions provided by Anaerocult® A packs (MERCK). Illumination was provided by incandescent bulbs (irradiance levels were approximately 40 Wm^{-2}), with the temperature maintained at ~30°C. Once grown, single colonies were picked off the plate and used to inoculate stab cultures. Stab cultures consisted of sterile McCartney bottles, half filled with the same media used in the petri dishes. These cultures were returned to the growth chamber for a minimum of 48 hours. Liquid cultures were obtained by filling the stab culture bottles with liquid c-Succinate media. Further incubation for ~48 hours allowed growth of the bacteria out into the liquid media. This culture was then used to inoculate larger liquid cultures.

The initial cultures of the RCO2 based strains were again provided by growth on solid media in petri dishes. The media in this case were based on M22+ media (Appendix I) with 1.5% (w/v) agar, supplemented with liquid M22+ media, 0.2% (w/v) casamino acids, 1.5mM fructose (filter sterilised), and also the antibiotics required for maintenance of the plasmids (1µg mL^{-1} tetracycline and 10 µg mL^{-1} neomycin). The solid cultures were grown in dark/aerobic conditions and maintained at ~30°C. Initial liquid cultures were obtained by inoculating a sterile 100ml conical flask, containing 10mls of M22+ media. A sterile inoculating loop was used to scrape a sample of bacteria off the plate, and this scraping was transferred to the flask. The flask was then placed on an orbital shaker in

the dark at ~30°C. Growth of the bacteria overnight usually produced a culture with which larger cultures could be inoculated.

4.4.2. Large Scale Liquid Culture.

Flat-sided glass bottles (100 or 500mls) containing sterile c-Succinate medium were inoculated with 5-20mls of *Rb. sphaeroides* 2.4.1 or G1C bacterial suspension, either from a stab culture or from a previously prepared liquid culture. The cultures were maintained in high light conditions at ~30°C. Light was provided by banks of incandescent bulbs. Irradiance levels were approximately 40 Wm^{-2}. The flat side of the bottles were always facing the light source. 10 litre and 20 litre cultures were grown in Pyrex bottles. These cultures were inoculated with two 500ml cultures, and the level of liquid brought up to approximately 1cm below the neck of the bottle. Normally the bottles were then stoppered to produce anaerobic growth. Aerobic cultures were obtained by replacing the glass stopper with a sterile non-absorbent cotton wool bung. Aeration was provided by connecting a sterile glass tube to a compressed air-line via sterile rubber tubing and a 0.2µm Millex® FG_{50} inline air filter. These large cultures were again grown between banks of incandescent bulbs, but were also stirred continuously by a magnetic stirrer.

The RCO2 based strains required different culturing techniques. The 10ml cultures were used to inoculate firstly 70mls of medium, held in 250ml conical flasks and then 1litre of medium in 2 conical litre flasks. The medium in each case was M22+, supplemented with 1.5mM fructose (filter sterilised) and the antibiotics in the concentrations given above plus the addition of 5 µg mL^{-1} streptomycin. All were incubated in the dark, on an orbital shaker at ~160rpm, ~30°C. These strains were grown in 20 litre cultures using the same procedure as for *Rb. sphaeroides* 2.4.1 and G1C, although the bottles were covered in black polythene sheeting to exclude light.

CHAPTER 5

Mutagenesis of Reaction Centres.

The mutagenesis of the reaction centre protein was performed by mismatch oligonucleotide mutagenesis, using the Promega pALTER® system and an expression system described in Jones et al (1992b). This section will describe the protocol behind the production of the point mutants. An additional genetic manipulation procedure is also described, where a system was produced to ease the screening of putative mutant constructs prior to the sub-cloning required before mating into the *Rb. sphaeroides* expression strain. However, the section begins with a discussion of the protocols used to perform standard molecular biology techniques.

5.1 General Molecular Biology Techniques.

The plasmids and bacterial strains used in the work described in this section are given in Table 7 (Section 4.1.)

5.1.1. Desalting and Kinasing of Oligonucleotides.

The oligonucleotides were supplied by the Krebs Institute Biomolecular Synthesis Service at the University of Sheffield. Residual salt in the oligonucleotide solution was removed using Sephadex G-25 (Pharmacia) gel filtration media. Individual 1ml columns were prepared in 1ml plastic disposable syringe barrels, with a small amount of siliconised glass wool "plugging" the outlet. The columns were equilibrated with 6-7 washes of 200µl d.H_2O, spinning in a benchtop centrifuge with a swing-out rotor at 3,000rpm for 15 secs between each wash. Equilibration of the column was determined when the volume of d.H_2O collected in the tube after centrifugation equalled that of the volume added prior to spinning. The

oligonucleotide suspension was then added, and spun as above. The oligonucleotides were eluted in the collected solution while the salt remained held within the column. The oligonucleotides were then used to perform mutagenesis without any further purification.

The mutagenesis reaction required that the oligonucleotide be ligated to the 3′ end of the newly synthesised strand of DNA by DNA ligase. For this reaction to be instigated, the oligonucleotide has to be kinased, i.e. a phosphate group added to its 5′ end. This was performed by the incubation of 30µls of the oligonucleotide solution in 10 x kinase buffer (4µls), 0.1mM ATP (2µls) and 10u/µl T4 polynucleotide kinase (1µl). The solution was then made up to at total volume of 40µls with d.H_2O and incubated at 37°C for 30 minutes, followed by 10 minutes at 70°C. All oligonucleotides were kinased at a concentration of 5pmol/µl.

5.1.2. Determination of Oligonucleotide Concentration.

The concentration of oligonucleotides required for the mutagenesis reactions was determined from measurement of A_{260nm}. For oligonucleotides, an OD at 260nm of 1 is equivalent to 20µg/ml, as is described in Sambrook et al (1989)

5.1.3. Denaturation of Plasmids.

Denaturation of plasmid DNA splits the plasmid into its two component strands. This was required for the mutagenesis reactions to present the annealing sites to the oligonucleotides. Denaturation was performed by incubation of an equal volume of plasmid solution, with (2x) denaturation buffer (0.4M NaOH, 0.4mM EDTA) at 37°C for 30mins. After incubation, $^1/_{10}$th the volume of 3M sodium acetate (pH 4.6) and a volume of 100% ethanol equivalent to twice that of plasmid solution were added and, after mixing the tubes, placed on ice for 1 hour. Spinning in a microfuge at 13,000 rpm for 10 mins led to the production of a pellet. The excess solution was carefully removed, and the pellet resuspended in 100µl 70% ethanol, before spinning again as above. The excess solution was again carefully removed, and the remaining pellet dried using a vacuum dessicator.

5.1.4. Transformation of Plasmid DNA into E. coli .

Transformation was carried out using the following procedure. The plasmid DNA/bacteria mix was placed on ice for 40 minutes, and followed by a heat shock consisting of 1 minute at 37°C, before returning the tubes to ice for a further 5 minutes. At the end of the incubation procedure, 5 volumes of LB medium (Appendix I) were added, and the tubes incubated for a further 90 minutes at 37°C. Finally, each transformation reaction was added to a 30ml universal bottle containing 10mls of LB medium supplemented with ampicillin (1mg/ml) and tetracycline (0.1mg). This was placed at 37°C in an orbital shaker for ~16 hours. The tetracycline selects for the presence of a pALTPC-1 plasmid in the bacterium, whilst ampicillin should select for those bacteria containing pALTPC-1 plasmids which are carrying the repaired ampicillin resistance gene. Thus the bacteria surviving this selection procedure should also carry the site mutation, because of the ratio of the oligonucleotides added.

5.1.5. Isolation and Purification of Plasmid DNA.

At a number of stages in the mutagenesis protocol plasmid DNA had to be rescued from bacterial cultures. Recovery of the DNA was performed using Wizard™ Minipreps (Promega), according to the protocol supplied with the Wizard kit. The kit is based upon plasmid preparation by the alkaline lysis method (Sambrook, 1989). The plasmid DNA is purified by binding to Wizard purification resin and adding to a mini-column. The column is washed with the column wash solution provided with the kit, before elution of the purified plasmid DNA in 10mM TE buffer, pH7.5.

5.1.6. Gene Cleaning Procedure.

Gene cleaning, a protocol by which DNA fragments can be separated by gel electrophoresis and the fragments of interest recovered from the gel, was carried out as follows. The gel slices were crushed in an Eppendorf tube. To this, a volume of sodium iodide equal to twice the weight of gel was added, and the agarose dissolved by heating at 55°C. Once the gel had dissolved, 10µl of glass milk (glass beads suspended in water) was added and the sample left at room temperature for 5 minutes. DNA carries a

negative charge at neutral pH and will therefore stick to glass beads allowing the removal of contaminants held in solution. Spinning at full speed in a microfuge for 20 seconds was followed by careful removal of the liquid. Three such washes were carried out, each with 300µls of fresh sodium iodide, and the liquid discarded. After ensuring all the liquid had been removed after the final wash, the DNA was resuspended in 15µls of TE buffer, aided by heating at 55°C for 3 minutes. After spinning again at full speed in a microfuge for 20 seconds, the liquid was carefully removed and placed in a second Eppendorf tube. The resuspension of the glass beads in TE buffer was repeated twice more. Each time the liquid was added to the fresh Eppendorf. A small sample of the TE buffer suspension was run out on an agarose gel, to estimate the concentration of the DNA fragment.

5.1.7. Phosphatasing Reactions.

Phosphatasing reactions were performed to remove the phosphate groups from the 5'-ends of cut plasmid DNA that was to be used as a host for a DNA fragment. This prevents the plasmid DNA recombining (i.e. reforming the circular plasmid without insertion of a new fragment). The DNA to be inserted into the plasmid carries a 5'-phosphate group, and therefore will be able to recombine with the plasmid. Phosphatasing increases the efficiency by which a new stretch of DNA can be introduced to a cut plasmid.

The reaction was performed by adding 1µl of alkaline phosphatase per 20µl of sample solution. The mixture was then incubated at 30°C for 30 minutes. EDTA was added to a concentration of 20mM, and the solution heated to 65°C, and incubated at this temperature for 20 minutes. The DNA was then purified by gene cleaning (see 5.1.6.).

5.1.8. Mating of E. coli cells with Rb. sphaeroides.

Successful mutagenesis of the reaction centre genes was followed by a series of sub-cloning steps (Section 5.2.1.). The outcome of these procedures was the mutated fragment of the M-subunit was reinserted into the complete reaction centre operon and carried on the pRKEH10D plasmid in *E. coli.* DH5α. Introduction of the reaction centre genes into a

Rb. sphaeroides background is normally carried out by direct conjugation with *E. coli.* (Hunter and Turner, 1988). However, DH5α cannot be used for this step. For this reason the isolated pRKEH10 had first to be transformed into another *E.coli* strain, S17-1. Transformation and growth on LB/ampicillin plates were performed in the normal way. The mating protocol is described below.

The grown *E.coli* S17-1 cells were scraped off the agar plates with a sterile inoculating loop, and placed in a sterile Eppendorf tube containing 50μls of LB media. Fresh cultures of three DD13 strains (Jones et al, 1992a) of *Rb. sphaeroides* cells [identical strains except for deletions in the carotenoid biosynthesis pathway leading to the expression of either phytoene (DD13/W1), neurosporene (DD13/G1) or spheroidenone (DD13/R1)] were prepared. These were spun down and resuspended in a small volume of M22+ media. 100μls of DD13 cells were placed in a fresh tubes, and to these were added 5μls of the S17-1 cells. The suspension was mixed thoroughly before spotting out onto a LB agar plate. The plate was incubated at 34°C for 8 hours, after which the bacteria were scraped off the plate and resuspended in 200μl of M22+ media. A 1 in 10 dilution was performed and the "neat" and diluted suspensions used to inoculate two separate M22+ agar plates. The plates were supplemented with neomycin (6μg/ml) and tetracycline (1μg/ml). Single colonies that grew after incubation in the dark at 34°C for 5-7 days were screened for the presence of reaction centres using a Guided Wave Model 260 fibre optic spectrophotometer (Guided Wave Inc., El Dorado Hills, CA). Using this apparatus it was possible to obtain spectra directly from single bacterial colonies of ~1mm in diameter, or greater. Colonies grew up over 7 days, after screening liquid cultures were prepared as described in section 4.5. These liquid cultures were then used to produce glycerol stocks which were stored at -70°C.

5.1.9. Agarose Gel Electrophoresis.

Agarose gel electrophoresis was used on a number of occasions to separate different sized DNA fragments. DNA is negatively charged at neutral pH. Therefore, DNA was loaded onto a gel near to the cathode and an electric current applied to the gel, drawing the DNA towards the anode. Separation of fragments of DNA occurs because of the differential

retardation of the movement of differently sized fragments, larger fragments are impeded to a greater extent than smaller fragments (see Sambrook et al 1989). All agarose gel electrophoresis was performed using BioRad horizontal gel apparatus.

5.1.10. DNA Sequencing Reaction: Di-Deoxy. Method.

The success of the mutagenesis reaction was checked by DNA sequencing using the Sanger di-deoxy method (Sanger et al, 1977). This was performed using Sequenase [USB Corporation] according to manufacturers instructions. The Sanger method requires a synthetic oligonucleotide to bind to the single stranded DNA template to act as a primer for the synthesis of a new strand of DNA by the action of the DNA polymerase. The polymerase used is capable of introducing radio-labelled nucleotides, causing the new strand to be labelled, and also dideoxynucleotides which when incorporated terminate the growing DNA chain. The two steps, labelling and termination, are performed in two separate but sequential reactions. The addition of the radiolabelled and the dideoxynucleotides in the correct proportion to the standard deoxynucleotides, will yield a range of labelled transcripts of different lengths. The radiolabelled fragments can then be separated on a polyacrylamide gel and the DNA sequence read directly off the resulting autoradiograph.

Sequencing gels were made at a concentration of 6% acrylamide with 50% urea as a denaturing agent. The stock acrylamide solution (used in a 15% dilution) contained 40% acrylamide at a ratio of 19:1 of acrylamide to *bis*-acrylamide [BDH Ltd., Electran Grade]. This was used to make a 100ml gel mix with 30µl of TEMED and 1ml of 10% ammonium persulphate added to initiate polymerisation. The gels were poured between two glass plates using plastic spacers (0.4mm thickness) and allowed to set overnight. Sharkstooth combs were used to provide the sample wells and the gel prewarmed to ~55°C before loading the samples. Vertical gel kits [BioRad] were used to run the sequencing gels, using a Consort Bioblock E734 power pack [BioRad]. The length of time that sequencing gels were run was dependant on the distance from the primer that one was trying to sequence. Following the run the gels were fixed by immersion in 2 litres of 10% acetic acid for 15min. They were then dried in an oven at ~60°

until dry (approximately 1.5 hours). Once dried, the pattern of bands on the gel was determined by autoradiography using GRI blue-sensitive X-ray film.

5.2 Genetic Manipulations

5.2.1. Mutagenesis Reaction.

The mutagenesis of the reaction centre protein was performed by mismatch oligonucleotide mutagenesis, using the Promega pALTER® system and an expression system described in Jones et al (1992b). The p-ALTER-1 plasmid as supplied by Promega contains a multiple cloning site, into which a fragment containing residues 83-235 of the reaction centre M-subunit gene was inserted (Figure 23). The resulting plasmid construct was named pALTPC-1. It was this construct that was used to perform the mutagenesis reactions. The mutagenesis procedure is summarised in Figure 24.

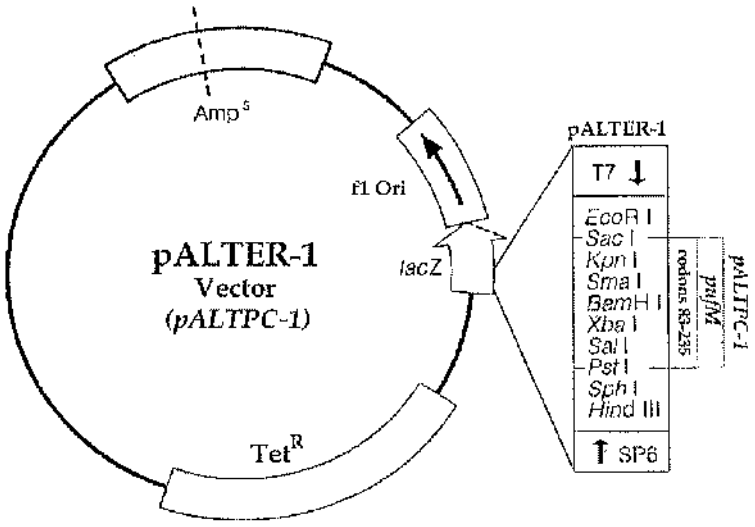

Figure 23: The pALTER-1 plasmid showing the position of the *pufM* (codons 83-235) insert which produces the pALTPC-1 mutagenesis plasmid used in this project (Promega).

The oligonucleotides used to introduce the mutations, MRCM 21-25, are described in Table 8, with the native DNA coding sequence shown for each. They were prepared for the mutagenesis procedure as described in

sections 5.1.1. to 5.1.3., by desalting and kinasing, and correcting for concentration.

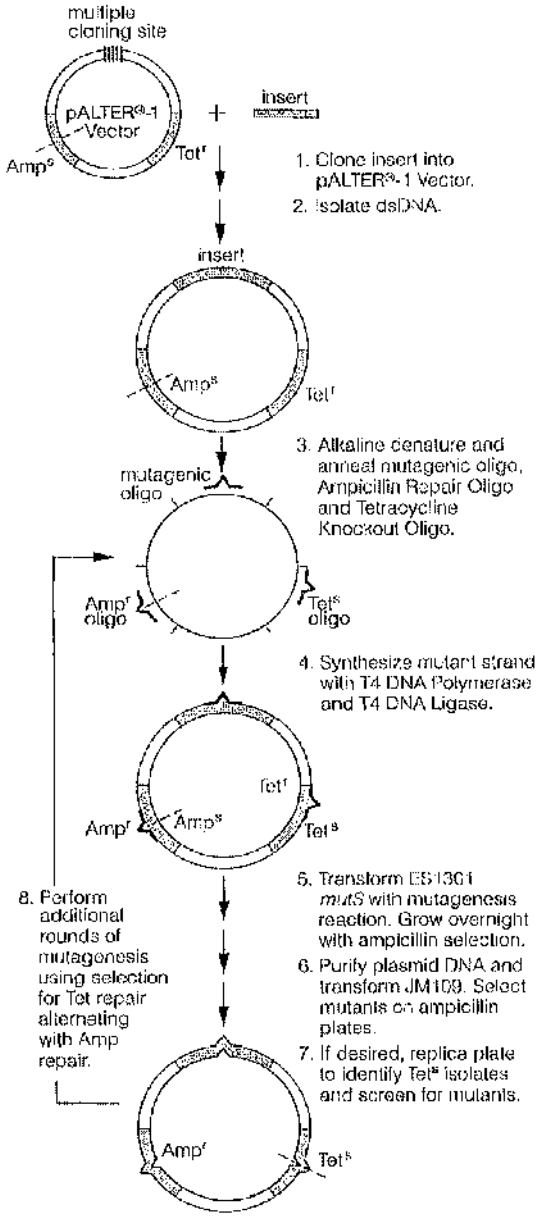

Figure 24: Schematic diagram of the Altered Sites®II System procedure using the pALTER®-1 Vector (Promega).

For each mutagenesis reaction, 1µl of denatured pALTPC-1 plasmid was resuspended in 9µl d.H_2O, 2µl of 10x annealing buffer (Appendix III) and 1µl of the kinased ALTER3 oligonucleotide suspension (1pmol/µl). ALTER3 is an oligonucleotide which repairs the faulty ampicillin resistance gene carried on the pALTPC-1 plasmid. The ampicillin

resistance gene carries a single point mutation, which destroys its function. The ALTER3 oligonucleotide restores the ampicillin resistance during the mutagenesis reaction. This oligonucleotide is annealed to the ssDNA template at the same time as the mutagenic oligonucleotide (MRCM21-25), and subsequent synthesis and ligation of the mutant strand links the two. To each reaction 8µls of the kinased mutagenic oligonucleotide (5pmol/µl) was added. The ratios of the ALTER3 and mutation inducing oligonucleotide (MRCM 21-25) were carefully controlled so that the latter was in a 40:1 excess. Therefore, any plasmid selected as having a repaired ampicillin resistance gene should, in theory, have a high probability of co-annealing, and so carry the desired mutation. The tubes were then mixed, and boiled for 3 minutes before placing on ice to anneal the oligonucleotides to the ssDNA template. Second strand synthesis was then carried out by addition of the extension/ligation mix components, as described in Table 9.

Table 8: The sequences of the mutation introducing oligonucleotides used in this project. The native sequences Are given, and positions of point changes in the DNA sequence are marked (|).

Name	Mutation.	Sequence.
Native.		GAAGCCCAGCACCATCCACAGCCAGATGGCCG
		. . . . . || . . . . .
MRCM21	TrpM157-F	GAAGCCCAGCACCATGAACAGCCAGATGGCCG
Native		CGAGAAGATGCCGTAGGGAACCGCTTC
		. . . . . | . . . . .
MRCM22	TyrM177-F	CGAGAAGATGCCGAAGGGAACCGCTTC
Native		GAACGACGCGATCAGCCACAGCCCGCCTTCCT
		. . . . . || . . . . .
MRCM23	TrpM115-F	GAACGACGCGATCAGGAACAGCCCGCCTTCCT
Native		AACATGAAGAACGACGCGATCAGCCAC
		. . . . . | . . . . .
MRCM24	SM119-A	AACATGAAGAACGCCGCGATCAGCCAC
Native		ACCGCGACGAACATGAAGAACGACGCG
		. . . . . | . . . . .
MRCM25	MM122-L	ACCGCGACGAACAGCAAGAACGACGCG

The reactions were then incubated at 37°C for 90 minutes to perform second strand synthesis and ligation. After completion of the incubation, 5µls of each of the reactions was transformed into 120µls of *E. coli.* strain

BMH 71-18 mut S. This strain of *E. coli.* is a mismatch-repair minus strain. Therefore, transformation of DNA into this strain prevents the repair of any altered strands, in turn helping to return a high frequency of mutation. The BMH 71-18 mut S *E. coli* cells were grown up overnight in LB medium supplemented with tetracycline and ampicillin, and the plasmid DNA recovered. This was transformed into DH5α, and single colonies were grown on agar plates supplemented with tetracycline and ampicillin. These colonies were picked, and 10ml LB (tet/amp) cultures of each grown. The plasmids were recovered from these, and sequencing reactions performed. Plasmids carrying the correct DNA sequences were then taken through a series of sub-cloning steps, discussed in the next section.

Table 9: The extension reaction mix components.

Solution	Volume added
Synthesis Buffer (10x)	3µl
ATP (10mM)	3µl
dNTP's (5mM)	3µl
DNA ligase (2u/µl)	1µl
T4 DNA polymerase (10u/µl)	1µl

5.2.2. Engineering of an Extra Restriction Site within Pst–Sac Fragment.

All the mutagenesis was carried out on a Pst–Sac fragment of the reaction centre *puf*M gene, carried on the pALTER 1 plasmid (pALTPC-1). It was necessary to restore this fragment to the complete *puf* operon. This was done in two steps. Firstly the mutated *Pst*I-*Sac*I fragment had to be shuttled into a pUC18 based plasmid (pUCXB-1) containing an *Xba*I-*Bam*HI restriction fragment encompassing the entire *puf*LM genes. To speed cloning of *Pst*I-*Sac*I fragments into the pUCXB-1 vector a version of this plasmid containing a *Sal*I site at the M197 position was constructed as follows. A *Pst*I-*Sac*I fragment had previously been produced which contained a Sal site at position M197 (pSE2AS, M.R. Jones, Unpublished data). This fragment was digested out of its host plasmid by digestion with *Pst*I and *Sac*I overnight, at 37°C. The digest was then run out on a preparative gel (Appendix III). The *Pst*I-*Sac*I fragment was cut out of the gel and the DNA recovered by "gene cleaning". The gene-cleaned

fragments were checked by gel electrophoresis and a fragment of the size expected of the *Pst*I-(*Sal*I)-*Sac*I fragment was observed.

The final step in this experiment was to clone this *Pst*I-(*Sal*I)-*Sac*I fragment into vector pUCXB-1 which carries the reaction centre *puf*LM genes. Vector pUCXB-1 was digested overnight with *Pst*I and *Sac*I at 37°C and the large fragment separated by gel electrophoresis followed by gene cleaning and a phosphatase reaction. Ligation of the *Pst*I-(*Sal*I)-*Sac*I fragment into the *Pst*I/*Sac*i cut vector was performed by incubating at 16°C in a vacuum flask for ~48 hours. The incubation mix contained the *Pst*I-(*Sal*I)-*Sac*I fragment, along with the *Pst*I-*Sac*I cut pUCXB-1 plasmid, T4 DNA ligase buffer, and T4 DNA ligase. The ligation mix was transformed into DH5a, single colonies picked and grown. Versions of the pUCXB-1 plasmid with the new *Sal*I site at the M197 position were identified by running the plasmid DNA out on an agarose gel, after digesting with *Sal*I-*Bam*HI. The final construct was named pUCXBS-1.

5.2.3. Cloning of the Mutant Pst-Sac Fragments into pUCXBS-1.

The mutated reaction centre genes carried on the pALTPC-1 plasmid, were digested overnight with *Pst*I and *Sac*I at 37°C. A sample of pUCXBS-1 was digested with *Pst*I and *Sac*I. The success of the digestions was checked by running samples on an agarose gel and looking for a 450b.p. fragment. The pUCXBS-1 restriction digest was then subjected to a phosphatase reaction, preventing its subsequent re-ligation with anything other than a non-phosphatased *Pst*I-*Sac*I fragment. The 450b.p. mutant fragment was gene cleaned, as was the *Pst*I-*Sac*I cut pUCXBS-1 vector. Ligation reactions were then carried out in order to insert the mutated *Pst*I-*Sac*I reaction centre fragments into the pUCXBS-1 vector. The ligation reaction was carried out as described previously. After overnight incubation, the "mutant-pUCXBS-1" vector was transformed into DH5α competent cells, following the previously described procedure. Following outgrowth in 0.6mls of LB media, the cells were spun down in a microfuge. The cell pellet was resuspended in 200µls of media, before being spread onto LB/ampicillin agar plates. Single colonies which had grown up overnight on the plates were picked and added to 10ml aliquots of LB media.

After growth, the DNA was rescued from the 10 ml cultures and the plasmids purified by running Wizard Mini-Preps (Promega). When digestion of the plasmids with *Sal*I-*Bam*HI was complete, the ligation reactions were observed to have been successful, i.e. only two bands were observed in the gel (Figure 25). Three bands would have indicated the presence of the M197 *Sal*I site in the unaltered pUXCBS-1 plasmid. This rapid selection allowed sequencing reactions to be performed only on the bacteria carrying plasmid DNA which contained a mutated *Pst*I-*Sac*I fragment generated from the pALTPC-1 plasmid and the MRCM21-25 oligonucleotides. Sequencing reactions were then carried out to check the sequence of the DNA inserted.

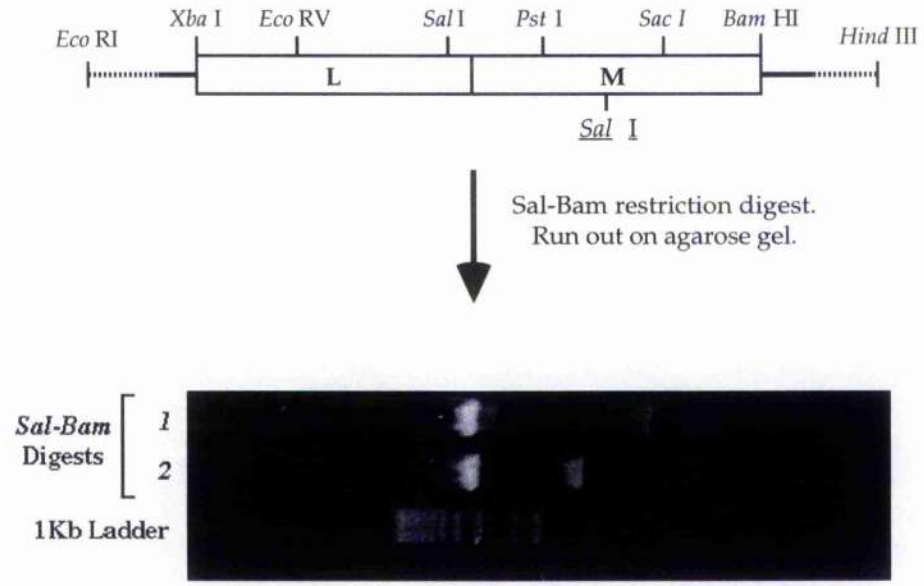

Figure 25: The use of pUCXBS-1 in rapid initial screening ligation reactions. *Sal*I-*Bam*HI Digests: 1. Original pUCXBS-1 Plasmid; 2. pUCXSB-1 plasmid with new mutant *Pst*I-*Sac*I fragment inserted. Both samples in lanes 1 and 2 were treated identically with a *Sal*I-*Bam*HI double digest being performed on each. Lane 3 is a standard 1Kb DNA ladder.

5.2.4. Final Sub-Cloning and Mating into Rb. sphaeroides background.

The mutant genes at this point had been successfully created and cloned into the *puf*LM genes. The aim of the next series of steps was to complete the manufacture of a complete *puf* operon, inserting the remaining H-subunit gene. The complete reaction centre *puf* operon fragment then had

to be transformed into a *Rb. sphaeroides* background where the mutant genes can be expressed and the effect of the mutations on the reaction centre protein investigated. The plasmid pRKEH10D contains a fragment which carries the complete set of reaction centre structural genes. The L and M genes are carried within a *Xba*I-*Bam*HI fragment. The mutant pUCXBS-1 plasmid and pRKEH10D plasmid DNA were cut with *Xba*I and *Bam*HI and the resulting fragments separated by gel electrophoresis. The relevant bands were cut out from the gel and gene-cleaned. Ligations were set up in order to insert the mutant *Xba*I-*Bam*HI fragment cut from the pUCXBS-1 plasmid into the *Xba*I-*Bam*HI cut pRKEH10D plasmid and the reaction transformed into DH5a. The success of this insertion of the mutant DNA into pRKEH10D was checked by digestion of rescued plasmid DNA with *Pst*I. The M subunit in pRKEH10D lacks the *Pst*I site, hence digestion with this enzyme and subsequent separation of the resulting fragments by gel electrophoresis shows whether the plasmid is "normal" or is carrying an inserted "mutant" strand.

After the *Pst*I digestion investigation, the remaining step in the protocol was the transformation of the plasmid into *Rb. sphaeroides* strains. Prior to this the plasmid had to be transformed into *E. coli* S17-1, the strain which is capable of mating with *Rb. sphaeroides*. This sub-cloning was performed and the subsequent mating as described in section 5.1.8. The successful expression of the reaction centre genes was gauged by investigating colonies grown on agar plates using a Guided Wave fibre optic, spectrophotometer, in addition the plasmid DNA was rescued from the *Rb. sphaeroides* strains and the DNA sequence determined.

CHAPTER 6

Methods used in Sample Preparation

6.1. Preparation of Reaction Centre Samples.

6.1.1. Preparation of Chromatophores from Bacterial Cells.

The purification of reaction centres was performed either on freshly harvested cells or on cells that had been grown previously and stored at -20°C, in MES/KCl buffer (pH 6.8). The cells were thawed at room temperature (if frozen), before being spun down at 10,000 rpm (~10,000 x g) at 4°C, in a benchtop centrifuge. The supernatant was poured off and the cell pellet resuspended in 20mM Tris/HCL buffer, pH 8.0. A hand homogeniser was used to ensure the cells were thoroughly resuspended. A small amount of DNase and magnesium chloride was added and the cells disrupted in a French Press cell (10 ton.inch^{-2}). After pressing, the sample was spun at 10,000 rpm (~10,000 x g) at 4°C, and the resulting supernatant decanted off into ultracentrifuge tubes, care being taken to leave as much of the pellet intact in the bottom of the centrifuge tube as possible. The supernatant was then spun at 50,000rpm (~150,000g) at 4°C in an ultracentrifuge for 90 minutes. The pellet formed consisted of the photosynthetic membranes, i.e. chromatophores. An attempt could now be made to extract the reaction centres from the prepared chromatophores.

6.1.2. Solubilisation of Reaction Centres from Chromatophores.

Solubilisation of the reaction centres from the membrane was carried out using a method developed from that described by Jolchine & Reiss-Husson (1974). The chromatophores were resuspended in 20mM Tris/HCl, pH 8.0. The absorption at 800nm was recorded, and the concentration of the sample adjusted until the ODcm^{-1} equalled 50. Solid sodium chloride was added to the solution, initially to a final

concentration of 150mM. However this concentration was later reduced to only 100mM without any apparent loss in the yield or stability of reaction centres. The sample was then incubated in a water bath until the temperature increased to 28-30°C, although this initial protocol was again altered with incubations performed at room temperature. The incubations were carried out in darkness, and from this point on the samples were maintained in as close to complete darkness as possible. Once the desired temperature had been reached LDAO was added dropwise until a concentration of 0.75% (v/v) was reached. The sample was incubated in a water bath at 28-30°C / room temperature for 90 minutes. The sample was on occasion, and with equal success, incubated in 150mM/100mM NaCl, 0.75% LDAO at 4°C overnight.

After incubation, the sample was spun at 50,000 rpm (~150,000 x g) at 4°C in an ultracentrifuge for 90 minutes. If the solubilisation had been successful, the reaction centres would be present in the supernatant after centrifugation. However, on most occasions this was not the case after the first incubation. When the first incubation was unsuccessful the chromatophore pellet was resuspended in 20mM Tris/HCl, pH 8.0, and the OD_{800nm} adjusted to 50. NaCl and LDAO were then added to give the same concentrations as before, and the sample incubated once more. The procedure was normally successful at the second attempt, with the reaction centres present in the supernatant after centrifugation.

6.1.3. Preparation of Ultrapure Reaction Centres for Crystallography and Spectroscopy.

Solubilisation of the reaction centres from chromatophore membranes did not yield protein of sufficient purity and/or concentration for immediate use in most analytical techniques. This is especially true when the reaction centres in question were to be subjected to crystallography or to investigation by resonance Raman spectroscopy. A very useful indicator of the purity of a reaction centre sample was first described by Okamura et al (1974). They used the ratio obtained when the absorbance of the sample at 279nm is divided by that of the absorbance at 800nm as a quick and relatively reliable measurement of purity. The absorbance at 279nm is due to the presence of aromatic ring containing amino acids in all protein present in the sample, i.e. tyrosine, tryptophan and

phenylalanine. In contrast, the absorption at 800nm is entirely due to the accessory bacteriochlorophylls of the reaction centre. A "pure" reaction centre sample, under these criteria, is one that provides a 279:800nm ratio approaching 1.2:1 (the higher the ratio, the poorer the sample). Many of the crystallography trials, described later, were carried out using samples of below 1.5:1, but, when attempts were made to obtain high quality crystals for x-ray diffraction, data collection samples with a ratio of around 1.3:1 were used. Similarly, the resonance Raman experiments required protein of especially high quality. For these experiments, only samples with a ratio of better than 1.3:1 were used for analysis.

6.1.4. Ammonium Sulphate Precipitation.

The purification of the reaction centres initially began with ammonium sulphate precipitation. This was performed following the general procedure discussed by Clayton and Wang (1971) and Englard & Seifter (1990). The procedure used consisted of two phases. Firstly, virtually all the protein in the sample, including the reaction centre protein, was precipitated upon the addition of the equivalent of 35g of ammonium sulphate to 100mls of solution. After spinning at 10,000rpm (~10,000 x g) at 4°C, in a bench-top centrifuge for 10 minutes, a levitate of protein was formed. Careful removal of the supernatant was followed by resuspension of the levitate in 20mM Tris/HCL buffer, pH 8.0, 0.1% LDAO. The levitate was resuspended in as small a volume of buffer as possible. This rapid procedure reduced the volume of sample to a more manageable size speeding the steps which follow considerably. The equivalent of 12g ammonium sulphate was then added to 50mls of sample solution. Again the sample was spun and the resulting supernatant retained. The levitate was then resuspended and set aside. The ammonium sulphate concentration was then made up to 14g in 50mls and after it had dissolved, the sample was spun again. The above procedure was repeated with further additions of the precipitate to give concentrations of 16 and 18g ammonium sulphate. The levitates from each step were resuspended and retained separately. Upon completion of these steps the final supernatant was clear of reaction centres. The resuspended reaction centre containing resuspended levitates were then analysed in a spectrophotometer to determine the level of purity of each of the samples. Samples of sufficient purity were combined and used in the next step of the purification

procedure. This precipitation procedure was replaced in the purification procedure by an initial step comprising a large scale anion exchange (DE52 cellulose) column.

6.1.5. Anion Exchange Chromatography.

The sample derived from the ammonium sulphate precipitation was then in a much more concentrated state but the level of purity remained generally poor (279nm:802nm ratio of no lower than 2.5:1). To obtain the purity required, alternative forms of chromatography were utilised. Two types of anion exchange chromatography were used, followed by a single gel filtration column. The ion exchange procedures made use of two systems. Firstly a relatively crude gravity-fed, large scale column (up to 150cm^3) of Whatman DE52™ medium was used. After this, an ion-exchange medium capable of much higher resolution was used and run on a Pharmacia FPLC™.

The DE52™ (Whatman) gravity fed step although crude, had several useful properties. Being able to readily adjust the scale of the column required for each run was an advantage because it allowed the entire reaction centre-containing sample to be loaded on a single column. The subsequent reaction centre eluant could be kept to a minimal volume. DE52 provided a rapid and useful system with which to reduce the volume of sample to a point when it became feasible to carry out the remaining work using a second system more capable of providing the high resolution desired. At the same time it provided a useful purification step.

The sample was usually dialysed overnight against 20mM Tris/HCl, 0.1% LDAO at 4°C prior to application onto the column. However, on occasion, the sample was simply diluted to reduce the salt concentration prior to loading onto the column. A glass column with a sintered glass disk at the base was washed and placed upright in a clamp stand. The preswollen DE52 medium was equilibrated in 20mM Tris/HCl, and gently shaken to obtain a slurry. This slurry was then poured into the column. A layer of 20mM Tris/HCl, 0.1% LDAO was gently pipetted onto the top of the slurry so as not to disrupt the top of the settling media. The medium was allowed to slowly pack down and at least two column volumes of 20mM Tris/HCl, 0.1% LDAO allowed to pass through before application of

the sample. Prior to loading the sample the layer of 20mM Tris/HCl, 0.1% LDAO was removed until only a small volume remained. The sample was then gently pipetted onto the top of the column. Upon completion of the loading, a further two column volumes of 20mM Tris/HCl, 0.1% LDAO was added and allowed to run through before starting to resolve the column.

The chromatographic separation consisted of three steps. Firstly certain components of the original sample ran straight through the column without binding. Secondly the column was washed with salt solution; at least the equivalent of two column volumes of 50mM NaCl, 20mM Tris/HCl, 0.1% LDAO buffer was run through, followed by a similar addition of 100mM NaCl, 20mM Tris/HCl, 0.1% LDAO buffer. These two latter washes produced eluent rich in protein, as demonstrated by a prominent peak in the absorption spectra at 279nm, but it was generally devoid of any reaction centre protein (no peaks detected in the 800nm region). Finally, the reaction centres along with the other bound components were then eluted from the column by the addition of 300mM NaCl, 20mM Tris/HCl, 0.1% LDAO buffer. The resulting eluent was collected in testubes in volumes of approximately 0.5-1.0mls. The fractions were then analysed in a spectrophotometer and the reaction centre rich fractions pooled for further purification.

The second anion exchange step was carried out using a Pharmacia FPLC system™. The chromatographic medium used was Pharmacia Q Sepharose-HP™ in a self-poured column of approximately 10 mls volume. The FPLC system allied with the Q Sepharose-HP medium provides extremely fast separation of much greater resolution than could be expected from the DE52 system described above. All buffers used in this form of chromatography were passed through a 2μm filter and degassed under vacuum prior to use. Two buffers were used; the 20mM Tris/HCl, 0.1% LDAO as before and a 1M NaCl, 20mM Tris/HCl, 0.1% LDAO buffer. The FPLC system was programmed to provide a salt gradient from 0-1M NaCl, with the proteins of interest eluting at between 20-35mM NaCl. The gradient chosen was set to provide the greatest resolution of the peaks eluting off the column, while also producing the reaction centre band in a relatively concentrated form. After this chromatographic step the reaction

centres were commonly of a purity to give a 279nm:800nm ratio of below 2:1, often as low as 1.5:1.

6.1.6. Gel Filtration Chromatography.

The final step in obtaining ultrapure reaction centres was gel filtration chromatography. This was carried out using a column packed with Sephadex 200 (prep. grade)™ gel filtration medium supplied by Pharmacia, in a column of approximately 70mls. This was run using the Pharmacia FPLC system™. The buffer used was 20mM Tris/HCl, 0.1% LDAO, again filtered and degassed under vacuum. A maximum 2mls sample could be loaded onto the column and still achieve sufficiently good resolution of the eluting protein bands, although in practice a sample volume of 1ml was used. Because of this, it was usually necessary to concentrate the sample prior to application. This was performed using an Amicon Stirred Filtration Cell™ and/or Amicon Centricons™ spun in a benchtop centrifuge at 5000g until the required volume was obtained. Once sufficiently concentrated, the sample was loaded and the column run at a maximum of 0.75ml/min, usually at 0.5mls/min. The purest of the reaction centre samples obtained commonly approached the 1.2:1 ratio regarded as being indicative of 100% "purity". However, on occasion it was found necessary to run an additional column to achieve this level. The small sample size made it possible, at this stage, to use a 1ml Resource Q™ column, again supplied by Pharmacia. This provided extremely good resolution of any remaining protein contaminants of the reaction centre sample. Raman spectroscopy was the only technique for which this purity of sample was required.

6.1.7. Concentration and Detergent Exchange of Reaction Centre Samples for Crystallography and Raman Spectroscopy.

The reaction centres were at this point of sufficient purity to allow crystallisation trials. The crystallisation conditions required that the protein was concentrated and placed into slightly different buffer conditions from those used in the purification procedures. In the early stages of the project, the LDAO detergent had to be replaced by β-octyl glucoside detergent because at that point crystallisation had only been achieved with the latter. However, in the latter stages only the

concentrations of the components of the buffer system had to be altered. Initially, these procedures were carried out by running the samples through a small DE52 column and washing with a large volume of the new buffer, before eluting with the new conditions plus 300mM NaCl. However, it was reported to be beneficial to adopt the use of Amicon Centricon centrifuge membrane concentrators to carry out these steps. It had been noted that crystals of LHII produced from protein concentrated with Centricon concentrators were regularly producing higher resolution diffraction, than those prepared from DE52 concentrated sample (McDermott, G., personal communication). The sample was loaded into a concentrator, and spun at 5000 x g at 4°C until the sample was in a highly concentrated form. At this point the centricon was filled with the replacement buffer, and the sample respun. This was carried out at least three times (usually five when detergent exchange was also being performed), ensuring complete buffer exchange.

CHAPTER 7

Biochemical Analysis of Reaction Centres.

7.1. Analysis of Pigments.

The investigation of the pigment content of the reaction centre samples provided a method by which the assembly of the protein-pigment complexes could be analysed. In particular, the effect of the point mutations within the carotenoid binding pocket on the carotenoid binding characteristics were studied. They also provided data required prior to investigation by the techniques which follow. These experiments were carried out using the highly purified form of the reaction centres generally used for crystallography or resonance Raman experiments.

7.1.1. Extraction of Pigments.

The small volumes and relatively low concentrations required for the analysis of pigments by HPLC, allowed small scale experiments to be carried out and replicated using the same protein sample. In this way, the reliability of the extraction procedure could be evaluated. The following protocol was performed in very low light intensities.

The isolation, identification and quantification of pigments from membranes and purified protein were performed using methods described by Gardiner (1992), Britton & Goodwin (1971) and Britton (1985). A small volume (~100µl) of the reaction centre sample was pipetted into a clean unused disposable glass test tube. To this approximately 5mls of 7:2 acetone/methanol solvent mix was added, and mixed thoroughly by gentle aspiration with a glass pasteur pipette. Approximately 2mls of low boiling point petroleum ether was added, and the liquids again gently aspirated with a glass pasteur pipette. A small volume of deionised water was added, causing the formation of two layers in the test tube. The

bottom layer contained the acetone/methanol in solution with the water. The top layer of pet. ether, containing the pigments, was carefully removed with a glass pipette and placed in a clean round-bottomed flask. The pigment sample was dried off in a rotary evaporator, with the flask immersed in a 25°C water bath. Once the majority of the pet. ether had evaporated off, the remainder was dried in a stream of N_2, before the pigments were taken up in HPLC grade dichloromethane (supplied by Rathburn Chemicals, Walkerburn, Scotland). The sample was filtered through a 0.2µm nylon filter into a HPLC sample vial, ready for HPLC analysis.

7.1.2. HPLC Analysis of Pigments.

HPLC analysis was performed on a Hewlett Packard HP1090A Liquid Chromatograph, attached to a Hewlett Packard HP1040 DAD Detector and driven from a Hewlett Packard Chemstation. The column used to perform the analysis was a Spherisorb ODS-2, reverse phase column of dimensions 250mm x 5mm provided by Jones Chromatography (Mid Glamorgan, Wales). All solvents used were HPLC grade and provided by Rathburn Chemicals. The pigment analyses were performed with an isocratic flow of methanol.

7.2. Protein Analysis.

The analysis of the protein subunits of the reaction centre complex was limited to Polyacrylamide Gel Electrophoresis (Laemmli, 1971; Schägger & von Jagow, 1987). Two forms of PAGE were performed, native and non-native. The recipes for the polyacrylamide gels and the treatment buffers are given in Appendix II. A Hoefer Mighty Small™ SE 250 vertical slab gel apparatus was used to perform all the experiments. Samples were prepared in the following manner. An equal volume of protein sample and treatment buffer was added to an Eppendorf tube and the solutions mixed thoroughly. A brief spin in a microfuge to collect the sample in the bottom of the tube was followed by incubating at 70°C for 45 mins (boiling of reaction centre samples causes the formation of an amorphous aggregate which will not enter the gel). After completing the incubation, the samples were again briefly spun in a microfuge before the samples

were loaded into the sample wells of a prepared gel using a Hamilton syringe. The gels were prepared as in Appendix II. Prior to the addition of the ammonium persulphate and TEMED, the acrylamide solution was degassed under vacuum. The glass and ceramic plates were washed thoroughly and rinsed once in $d.H_2O$ and finally with acetone.

The gels were run with cold tap water circulating through the cooling system within the SE 250 apparatus. 20mA constant current was applied to each gel (the SE 250 can run two gels), and the gel left to run until the blue tracking dye reached the bottom of the gel. The gels were then stained using a coomassie blue stain (see Appendix II; Wilson, 1983) for approximately 30 minutes on an orbital shaker. The stain was then removed and destain solution added. The gel was typically left to destain overnight, with at least two changes of destain solution made. Standard molecular weight markers were routinely run alongside investigated lanes.

CHAPTER 8.

Spectroscopic Analysis of Reaction Centres.

8.1. Absorption Spectroscopy.

Absorption spectroscopy was routinely carried out on a Shimadzu Corporation UV-160A scanning absorption spectrophotometer. More accurate room temperature measurements were performed on a Shimadzu UV-PC2101 scanning absorption spectrophotometer. In both cases only quartz cuvettes were used, with a 1cm pathlength. Baseline corrections using the appropriate buffer solution were performed prior to all measurements.

8.2. Circular Dichroism Spectroscopy.

Circular dichroism (CD) is the phenomenon by which a substance differentially absorbs right and left circularily polarised light. Circularily polarised light is made up of two non-superimposable, mirror image forms; i.e. it is chiral. For a molecule to discriminate between the two forms it too must be chiral. CD is often applied in investigations of protein secondary structure. The different forms of secondary structure give characteristic spectra. It can give estimates of the type of secondary structure and the percentage composition. However, in the study of photosynthetic systems, CD has been used as a method by which the chromophores can be investigated. For a review of circular dichroism see Woody, R.W. (1995).

Circular Dichroism spectroscopy was performed in two different labs. The Scottish Circular Dichroism Facility, based in Stirling University, consists of a JASCO J-600 spectropolarimeter. Initial measurements were made at room temperature, with 1cm cells. Only latterly did cryo-cooling

facilities become available. Further CD spectroscopy measurements were performed in the CNRS labs in Saclay, France. The apparatus at the CNRS in Saclay consists of a CD6 Dichrograph plus a ISA Jobin-Yvon.

Cryo-cooling was not initially available at the facility in Stirling, and only limited use was made of this facility when it did arrive. Instead the majority of the cryo-cooled CD data was obtained from investigations performed in Saclay. The cryo-cooling experiments required the use of glassing agents which perform a role basically identical to that of the cryoprotectants in cryo-cooling of crystals for X-Ray analysis. The formation of water crystals has to be prevented. This was ensured by the addition of glycerol to give a final concentration of 60% (v/v). Therefore conditions used for the reaction centre analysis where RC's with an OD of 0.5 at 360nm, in 10mM Tris/HCl, pH8.0, 0.05% LDAO and 60% glycerol. The cuvettes used were Hellma quartz with a 10mm path length. Accumulation of data was performed with a standard R928 phototube, with a fixed band width of 1nm, at increment of 0.5nm (0.5secs) per data point. Each spectra was the average of 3 scans, from which the baseline was subtracted. The baseline was obtained by running a sample of the above buffer.

8.3. Resonance Raman Spectroscopy.

The resonance Raman spectroscopy was kindly performed by Dr. A. Gall in the laboratory of Dr. B. Robert in the CNRS laboratories at Saclay, France. The experimental procedure used is described below.

The experiments were performed with a U-1000 Jobin-Yvon Raman spectrometer equipped with a charge-coupled device detector (Spectraview 2D, Jobin-Yvon). The Raman signal was recorded with a 90° geometry using grazing incidence onto the sample. All experiments were performed using a Inova 1000 Argon Laser, both at 488nm and 514.4nm. To minimise photodegradation of the carotenoids the samples were cooled to 77K in a helium gas-flow cooled cryostat. Between 5 and 25 scans were performed to produce each spectrum

8.4. Electron Paramagnetic Resonance Spectroscopy.

The ESR spectroscopy was kindly performed by Dr. D. Chynwat in the laboratory of Professor H. Frank. The experimental procedure used to perform these investigations is described below.

Samples for the electron paramagnetic resonance (EPR) studies were prepared by mixing 250 µl of sample (OD_{800} of approximately $10cm^{-1}$) with 40 µl of degassed ethylene glycol, and 40 µl of 100 mM sodium dithionite prepared in 15 mM Tris buffer, pH 8.0. All oxygen was removed from the solutions by bubbling nitrogen gas through the solution. The samples were then introduced into EPR tubes. EPR spectra were taken using a Bruker ESP300 instrument equipped with an ER 023 M signal channel, an ESP1600 1070 10 MHz digitizer, an ER 032 M field controller and an ER 041 MR bridge. Operating system version 9 (OS9/680) was used with a 1 MB base memory. An Oxford ITC4 helium temperature controller and an ESR 900 cryostat were used to achieve temperatures below 70K. A Eurotherm B-VT 2000 nitrogen temperature controller was used to achieve a temperature of 100 ± 0.5 K. A 1000 W xenon arc lamp was used as the light source. The light was filtered by 8 cm of water in a Pyrex bottle and passed through a light chopper of local design that modulated the light at 100 Hz. The modulated light was focused into the ER 4102 STO standard rectangular cavity with a 100 % light- transmitting front flange. The DC output of the EPR magnetic field modulation amplifier (signal channel ER023 M) was fed directly to an external lock-in amplifier (EG&G model 128A) referenced to the 100Hz frequency of the modulated light source. Output from the external lock-in amplifier was fed directly back to the digitizer and into the EPR computer system. The EPR conditions were as followed: field modulation frequency: 100 kHz; field modulation amplitude: 20 G; receiver gain: 1×10^4 - 1×10^5; sweep time: 335.54 s; time constant: 163.84 µs; and conversion time: 327.68 ms. Spectra were the average of 2 to 9 scans.

CHAPTER 9

Crystallography.

9.1. Growth of Crystals.

9.1.1. The Procedures used to Prepare Crystals.

Crystallisation was carried out using the sitting drop method (Fig. 26). This was performed in Cryschem plates (JBL Scientific) made up of 24 wells, each with a volume of 15µls. The protein solution was made up to the correct concentration and exchanged in the desired detergent and/or detergent concentration described above. A calculated amount of amphiphile (either heptane-1,2,3-triol, hexane-1,2,3,-triol or a defined mixture of the two) was weighed out in an Eppendorf tube. The desired volume of protein solution was added to this and the solution vortex mixed until the amphiphile was dissolved. The precipitant solution was then added. The solutions were mixed by vortexing and then spun in a microcentrifuge to sediment any precipitated protein and particles which might otherwise cause problems in the crystallisation. The tubes were then stored on ice whilst the outside wells of the crystal trays were prepared. The outside wells contained the precipitant solution plus sufficient water to produce the desired concentration in a total volume of 1ml. To each of the crystal reservoirs 15µls of protein solution was added and the trays sealed with adhesive tape. The tape was carefully smoothed down, ensuring that each cell was sealed from those surrounding. The trays were placed in a cooled incubator, ~18°C, and left undisturbed for a minimum of two weeks. After two weeks the trays were examined for the growth of crystals. Early attempts often required a longer incubation time before crystals were observed. The later experiments generally produced useful sized crystals by the end of the two week period.

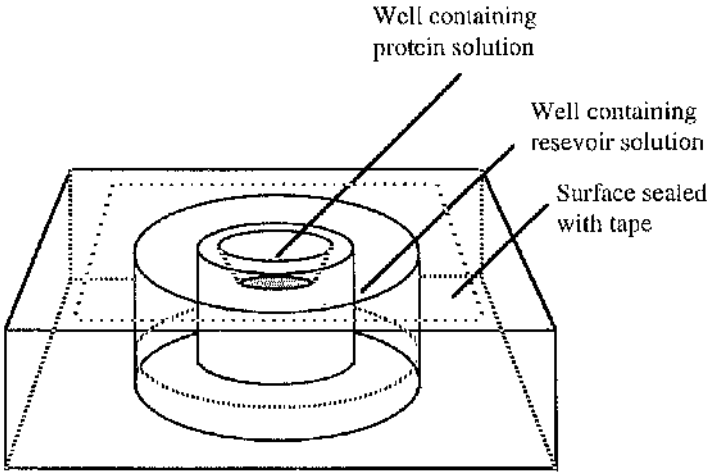

Figure 26: Growth of crystals using the sitting drop, vapour diffusion method.

9.1.2. Optimisation of Crystallisation Conditions.

A wide range of crystallisation conditions was studied. These can be split into two groups. The initial trials were based on ammonium sulphate as the precipitant, and were carried out utilising the additives hexane-1,2,3-triol, 1,4-dioxane and TEAP, under a range of concentrations, pH levels and temperatures. When the detergents LDAO and β-OG were used, both led to the growth of crystals. However with this precipitant system β-OG was by far the most successful. This system produced some success with wild type *Rb. sphaeroides* 2.4.1. reaction centres, affording diffraction to about 2.8Å. However, when applied to the mutant system, it achieved only limited success. With this form of the reaction centre the crystallisation was much slower and more inconsistent than had been the case for the 2.4.1. reaction centres. A second precipitant system, based on the use of potassium phosphate, provided much better results. Again trials were set up to investigate a range of concentrations, temperatures and pH levels.

Optimisation proceeded following an empirical trial and error formula. The early conditions were based around those previously determined in Glasgow (R.J. Cogdell, personal communication). Individual investigations were performed to study the effect of changing a number of variables - pH, protein concentration, concentration of the amphiphile, concentration of the detergent, the type of detergent (either LDAO or β-OG)

and the type of precipitant (ammonium sulphate or potassium phosphate), extra additives (1,4-dioxane and TEAP) and concentration of precipitant in the protein well and in the external reservoir. All of the above investigations were based on an identical set of control conditions, with each experiment performed by altering a single parameter. The data were collated and the most successful conditions noted. The procedure was then repeated with a new "improved" set of control conditions.

The success of the crystallisation conditions was determined by observation of a number of parameters. Initial screening was to simply identify wells containing crystals, and conditions which appeared to be reliably producing crystals. More detailed inspection was then carried out under a binocular microscope. Factors investigated included the size and shape of the crystal. In general, the larger the crystal the stronger the diffraction in X-ray experiments. However, this is a simplified view because with increased size comes the increased possibility of imperfections in the crystal packing which could pose problems in processing data collected from such a crystal. Therefore, note was also taken of the crystal shape, i.e. what basic shape (thin needles, cubes, ovals, plates, or hexagonal rods) did the crystal adopt? Were the faces of the crystal smooth? Were the crystal edges sharp? Also noted was the amount of amorphous precipitant contained in the well. Too much of this could cause difficulty when trying to mount the crystals for X-ray analysis, and suggests that a large proportion of the protein was being wasted. The ultimate test of the quality of the crystals was investigation in an X-ray beam. This was routinely performed using the in-house detectors available. It would be impractical, and relatively uninformative, to list all the conditions investigated in this work. However, Table 10. provides a summary, showing each of the compounds investigated and the range concentrations used for each.

Table 10A: The range of crystallisation conditions analysed for the reaction centre proteins‡. This table presents the data from crystallisations using ammonium sulphate as the precipitant and *Rb. sphaeroides* 2.4.1 (anaerobic) reaction centres protein. A similar system was also used for attempts at crystallisation of *Rb. sphaeroides* strains R-26 and G1C.

Ams.	[Protein] (mg/ml)	$[Ams]_{in}$ (M)	$[Ams]_{out}$ (M)	[β-OG] (%)	[LDAO] (%)	[Hpt] (%)	[TEAP] (%)	[Diox.] (%)	pH	Tot. No. Tested Conditions
Range analysed	7-9	1.0-1.4	1.4-2.4	1.5-2.0	0.1	1.5-3.5	3	1-3	9-10	202
Range most succesful.	9	1.0-1.1	1.6-1.8	2.0	-	2.5%	-	-	9.0-9.5	-

Table 10B: The range of crystallisation conditions analysed for the reaction centre proteins‡. This table presents the data from crystallisations using potassium phosphate as the precipitant and *Rb. sphaeroides* RCO2 (aerobic) reaction centre protein (wt and mutant).

Phos.	[Protein] (mg/ml)	$[Phos]_{in}$ (M)	$[Phos]_{out}$ (M)	[LDAO] (%)	[Hpt] (%)	[Hex] (%)	[TEAP] (%)	[Diox.] (%)	pH	Tot. No. Tested Conditions
Range Analysed	9-10	0.65-1.1	1.4-2.1	0.09-0.12	1.8-3.5	2	3	1-3	7.0-8.0	92
Range most useful	9-10	0.7-0.8	1.5-1.6	0.09	3.5	-	-	-	7.5	-

‡ These tables comprise details of the most commonly investigated paramters. Other parameters were also investigated including additives such as EDTA and glycerol, various other buffer systems (CAPSO, CHES & AMPSO), the concentration of Tris/HCL buffer, trials into the effects of NaCl on crystallisation and also methods by which buffer/detergent exchange and concentration of the protein was performed.

9.2. Collection of X-Ray Diffraction Data.

The collection of X-ray diffraction data was carried out using the Synchrotron Radiation source at Daresbury Laboratories England and the in-house facilities within Glasgow University. Two techniques were utilised in the attempts to gain high-quality diffraction data. For most of the work, room temperature exposures were carried out. However, later work attempted to develop a procedure for freezing the crystals for analysis. The potential advantages of freezing are discussed below (see also Rodgers, 1994, 1997 for reviews).

Initial trials of crystals were carried out using the in-house rotating anode facilities at Glasgow University. Two sets of equipment are available for protein crystal analysis in Glasgow University. A Siemens multi-wire area detector in conjunction with a Siemens rotating anode X-ray generator and a Nonius system with DIP1030 and a DIP2020 image plate detectors. The collection of full data was performed only at the Synchrotron Radiation Facility at Daresbury Laboratories, using either Station 9.5 or 9.6. with MAR 30cm image plate detectors.

9.2.1. Preparation of Crystals for Room Temperature Exposures.

All crystals for exposure at room temperature were mounted in fine (0.7-1.0mm) quartz capillaries, a method based on that first described by Bernal & Crowfoot in 1934. The mother liquor surrounding them was carefully removed with fine paper wicks. To prevent the crystal drying out in the beam, a small volume of mother liquor was then drawn up into the tube close to the position of the crystal. Both ends of the capillary were then sealed with beeswax. This procedure is summarised in Figure 27.

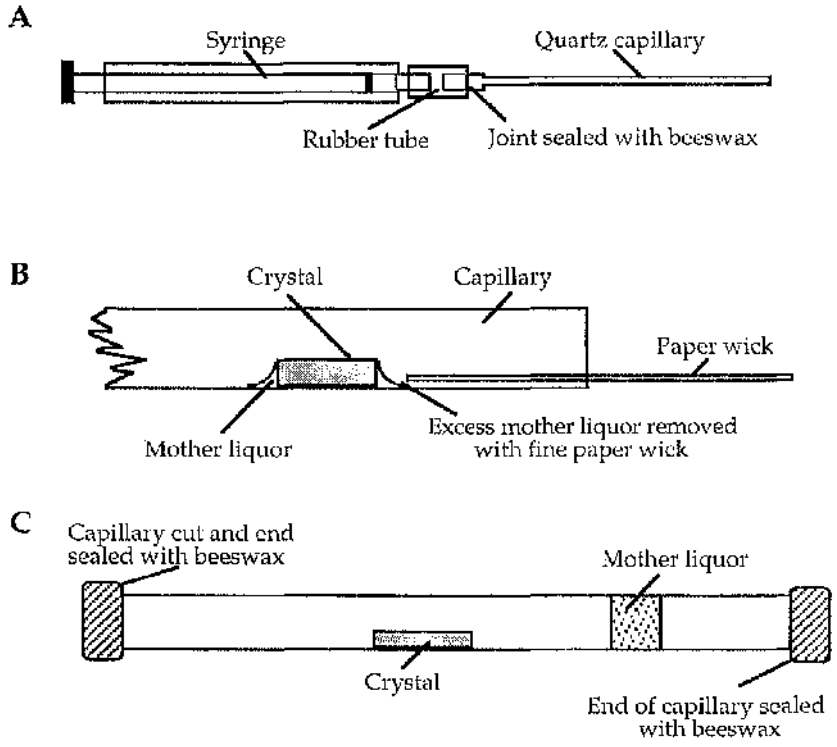

A: Quartz capillary attached to syringe via a short length of rubber tubing and joint sealed with beeswax.

B: The crystal is drawn up from the crystal tray, into the capillary. The excess mother liquor is drawn away from the crystal with a paper wick.

C: A small volume of mother liquor is drawn into the tube to a point 5-10mm short of the crystal. The end of the capillary is sealed with wax. The capillary is then removed from the syringe, this end cut before again being sealed with beeswax. The crystal is now ready to be placed in the X-ray beam.

Figure 27: Technique used to mount crystals in quartz capillary for X-Ray analysis.

9.2.2. Preparation of Cryo-cooled Crystals for X-ray Analysis.

One major problem in X-Ray diffraction analysis of crystals is the damaging effect of the radiation on the crystal. This is especially true for

fragile protein crystals. Collection of data sets at room temperature usually required the use of several crystals. The cause of the damage to the crystals remains unclear, however it is generally assumed to be the result of the radiation producing free radicals in the liquid regions of the crystal as first suggested by Strandberg (1968). Sufficient free radicals will cause specific chemical changes in the surface of the protein molecules leading to a general disordering of the crystal lattice. In this project up to 8 individual crystals were used in the collection of data for a single protein. There has been much interest in recent years in the possibility of freezing crystals, typically to around 100K. The major advantage of successful cryo-cooling experiments is that crystal lifetime in the X-ray beam is extended dramatically. This may permit the collection of a complete data set from one crystal, where previously numerous crystals would have been required. However, some other advantages have also been found. In a number of cases, the maximum resolution had increased. This was probably the result of a combination of reduction of thermal disorder within the crystal, possible beneficial effects from the cryoprotectant itself, and the longer exposure times made possible due to the increased crystal stability. The simple introduction of the cryoprotectant, without subsequent cryo-cooling, has been reported to have beneficial effects on the maximum resolution (Schick & Jurnak, 1994). Cryo-cooling of crystals has much to offer to protein crystallography, but the degree of success of the procedure is determined by the ability to flash-freeze the crystals, without causing damage to the crystal. This can cause great problems as discussed by Rodgers (1994, 1997).

9.2.3. Experiments to Determine Ideal Cryoprotectant Solution.

The major problem in cryo-cooling experiments arises because of the need to cool the crystal quickly, but without causing any damage to its structure. In practise this requires the use of cryoprotectant solutions combined with flash-freezing of the crystal by either plunging into liquid nitrogen, or placing in a stream of cold nitrogen gas from a cryostat. The primary role of the cryoprotectant solution is to prevent ice-formation. The cryoprotectants do not prevent freezing, but rather prevent or slow down nucleation so that a solid glass is formed before ice-formation can occur. The formation of ice crystals would lead to the destruction of the

crystal. A number of compounds have been described as useful cryoprotectants (Table 11), with glycerol being by far the most common.

Table 11: List of compounds successfully used in cryo-cooling experiments with protein crystals.

Compound	Concentration (%)	References
Glycerol	20- 50% (v/v)	Petsko (1975)
		Guo, et al (1992)
		Lee, et al (1994)
		Mitchell, et al (1994)
Ethylene Glycol	10-30 (v/v)	Feymann, et al (1990)
		Rini, et al (1992)
Polyethylene glycol 400	9% (v/v)	Lee, et al(1995)
		Ellenberger, et al (1992)
Glucose	25% (w/v)	Rodgers (1997)
Sucrose	2M	S. Prince (personal communication)
		Haas & Rossmann (1970)
R-R, 2,3 Butane-diol	8% (v/v)	Rodgers (1997)
	'Neat'	Hope (1988)
		Young, et al (1993)

The preparation of crystals for cryo-cooled analysis in an X-ray beam is markedly different from that of room temperature experiments. Teng (1990) described a method in which the crystals are maintained in a thin film of cryoprotectant solution held within a fine wire-loop. Teng described loops made from 25-75μm thick copper or gold-plated tungsten. A method similar to this was utilised in the investigations reported here, with one major alteration. The material used to manufacture the loop was individual fine nylon threads isolated from dental floss. This material being much cheaper and easier to obtain whilst maintaining the required strength with minimal diameter, but most importantly because the fibres are of an amorphous structure, no diffraction will be observed from the fibre itself. The method of construction of these loops, with sizes ranging from 0.4-1.5mm is shown in Figure 28. The size of a loop was defined as the distance from the top of the glass capillary to the tip of the loop. This distance was measured with the aid of a microscope lens with an eyepiece graticule. In later experiments a system produced by Hampton

Research (U.S.A.) was purchased. This system is essentially identical to the "home-made" apparatus. However, it was also possible to pre-cool, store and transport crystals held within the mounting loop. This dramatically decreases the turnover time required between investigation of each crystal, a valuable property with scarce synchrotron beam-time.

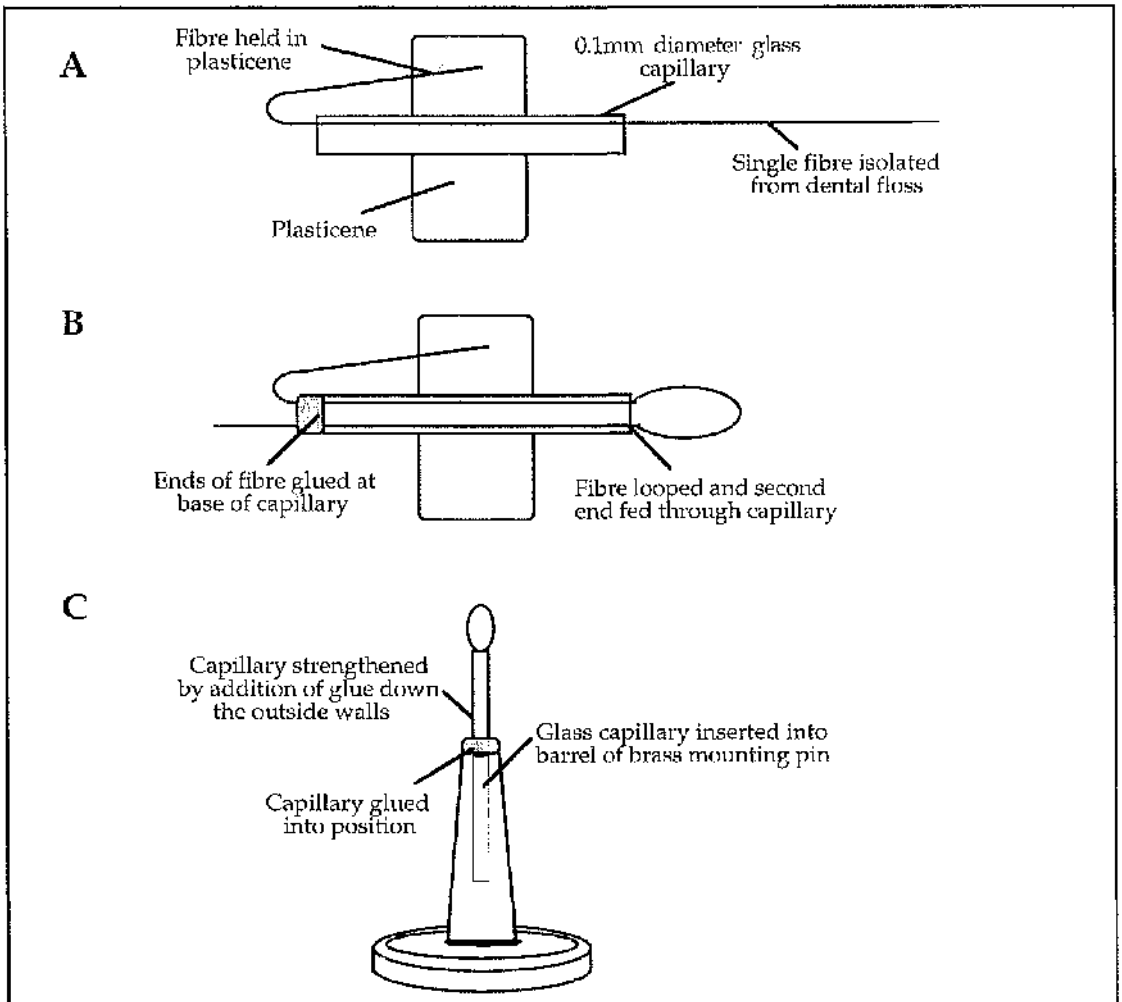

A: A short length (~10mm) of 0.1mm diameter glass capillary tubing is cut, and placed in plasticene under a dissecting microscope. A single nylon fibre isolated from dental floss is pushed through the capillary and the end held in the plasticene.

B: The fibre is looped and the second end fed through the capillary. The two ends of the fibre are then glued firm to the capillary. Glue is also carefully added to secure the bottom of the loop to the glass.

C: The capillary is glued into position within a brass mounting pin. Extra glue is placed down the walls of the capillary to provide extra strength.

Figure 28: The procedure used to manufacture mounting loops for cryo-cooled X-ray analysis of crystals.

Experiments were carried out using a wide range of potential cryoprotectant solutions. The preparation of crystals for these investigations required a number of steps. First, the goniometer head was positioned on the X-ray detector. The chosen mounting pin was then located on the goniometer head, and the loop centred such that it would lie within the beam. The cryostat nozzle was then set so as to be as close to the position of the crystal as possible, whilst care was taken to ensure that it remained outwith the path of the X-ray beam. The loop was then removed and the crystal mounted.

Crystals were prepared for cryo-cooling experiments in one of two ways. Initial experiments involved soaking the crystals briefly in the cryoprotectant solution, before placing in the X-ray beam. Mounting the crystal in this way was also a multi-step process. The chosen crystal was isolated within the well, and carefully lifted in the mounting loop. The crystal was then placed into a well in a cryschem plate, into which the cryoprotectant solution to be investigated had been placed. After the crystal had been soaked in the solution for the desired period of time, it was again carefully lifted in the mounting loop, and quickly transferred to the X-ray detector. The loop was located on the goniometer head, placing the crystal into the cold nitrogen stream.

The second method for introducing the cryoprotectant solution was by button dialysis. This method was used to equilibrate the crystal with the cryoprotectant very slowly, over 1-2 days. The chosen crystal was placed inside a micro-dialysis button with 10-15µls of mother liquor. A putative cryoprotectant solution was prepared with potassium phosphate to a final concentration equal to that of the mother liquor. A low molecular weight dialysis membrane (typically 3.5Mwt. cutoff) was prepared (Appendix III), and secured over the top of the dialysis button with a rubber O-ring, taking care not to trap air bubbles. A clean vial was filled with 1ml of the cryoprotectant solution and the microdialysis button placed into this solution, ensuring the dialysis membrane was in contact with the cryoprotectant solution. After dialysis the crystal was mounted in the cryo-loop and positioned in the cryostat stream as above.

A visible check was then made on the state of the crystal, and on whether a clear glass had been formed. If the solution surrounding the

crystal had a cloudy appearance it almost certainly meant that ice-crystal formation had occurred, and that the crystal was probably damaged. If the state of the crystal and surrounding solution was acceptable, X-ray investigation began.

9.2.5. Collection of Data.

All crystallographic data collection was carried out using the oscillation technique. Prior to the start of data collection, each new crystal was placed in the beam and at least one test image collected. The instrument was set up with parameters to reflect the expected quality of the crystal. Typical test conditions for the collection of a test image of a crystal using Station 9.5 at Daresbury are given in Table 12.

Table 12: Typical values used to produce test images of a fresh crystal on Station 9.5 at Daresbury.

Parameter	Typical Initial Value
Wavelength	0.9Å
Crystal-Detector distance	350mm (resolution at the outside edge ~2.2Å)
Time of exposure	400secs
Oscillation range	1°

The test image was analysed, and a number of points considered for the production of a data collection strategy. Firstly, the possibility of changing the crystal-detector distance was considered. The detector to crystal distance determines the maximum resolution which can be detected, the closer the detector, the higher the resolution of spots at the outer edge. However, this is not the only criterion that had to be considered. If the detector is to close to the crystal, the spots on the image can fall too close to one another. This has the effect of making the images difficult to process, and require the rejection of otherwise acceptable spots. Secondly, the time of exposure of each image had to be determined. Increasing the time can lead to the production of higher resolution (weaker diffraction) spots on the image. However, in doing this there is the concomitant problem of producing overloaded spots, i.e. spots which have reached the saturation level of the detector, and increased radiation damage. These overloaded spots when processed will not release any useful data on their intensities. This possibility had to be avoided if possible, but to collect the high

resolution data long exposure times were required. If required, two sets of exposures with two different exposure times and different distances from the detector could be performed. The combination of these two sets of data provided both the high resolution data (requiring short crystal-detector distance and long exposure times) and low resolution data (where the crystal-detector distance was longer, and exposure times relatively short).

The third parameter was the oscillation range. Typically for proteins, where the data is collected by film or image plate, an oscillation range of around 1° is used. Sometimes the range is set higher although again the problem of overlapping spots becomes prohibitive. One major indication useful in determining the oscillation range is its effect on the signal to noise ratio. The longer the oscillation the smaller the ratio. Finally, it was important to take into account the structure of the crystal itself. The space group of the crystal defines the minimum range over which data must be collected to collect a "full" data set. Due to the symmetry of the crystal it is not necessary to collect a full 360°. The reaction centre crystals were of the space group $P3_121$. This form of crystal requires that a minimum of 30° of data is required to obtain a complete data set. In practice it is important to collect more than this. In this case 30° should provide a single measurement of every unique reflection. This is not a desirable situation: when multiple measurements of the same reflection are obtained, the quality of the data will increase. It would be preferable to collect 60° or even 90° of data.

The ideal data collection would perhaps consist of two passes, one to collect low resolution data and the other to collect the high resolution. The images would be of "thin" frames, in order to create images with good signal - to - noise ratios. However, in practice this is unlikely to be possible. The reasons for this are numerous, but two factors are dominant. Protein crystals are not infinitely stable in the X-ray beam, and the resolution of diffraction slowly decreases over time. This can be overcome by using a number of crystals to collect the data, an approach which makes the subsequent processing more difficult, but not prohibitively so. The stability problem may be overcome in the future, with the increased use of cryo-cooling systems to stabilise the crystal. However, the biggest single obstacle is the difficulty in securing sufficient time on a detector system, to carry out such a lengthy experiment. This is especially true when using

synchrotron radiation. The various theories and considerations behind the development of a data collection strategy have been recently discussed by Dauter (1997)

A typical set of parameters used in the collection of data in this project is given below in Table 13. This particular set of parameters was used to collect the data set of the RM197 single mutant crystals.

Table 13: Collection parameters used to collect data from the RM197 single mutant crystals. *The Data was collected on station 9.6 at Daresbury, where the software driving the data collection on this station does not rely on timed exposures, but rather on photon counting / dose measurement. Settings here do not relate directly to time. The actual time of exposure was typically ~5 minutes.

	Crystal			Total
Parameter	1	2	3	n/a
Wavelength (Å)	0.87	0.87	0.87	n/a
Apparent Max. resolution (Å)	2.4	2.6	2.5	n/a
Crystal to detector distance (mm)	400	400	400	(gives a max. resolution to the outside edge of ~2.4Å)
Oscillation range	0.75	0.75	0.75	n/a
Exposure setting*	2400	2400	2400	n/a
No. frames collected	15	22	33	70
Resolution decayed to (Å)	2.7	2.8	3.0	n/a
Total no. of degrees collected	11.25	16.25	24.75	52.5
Data Completion statistics	Statistics refer to the overall completeness of the data to maximum resolution (2.55Å). The figure in brackets gives the completeness in the highest resolution shell.			89.4% (64.4%)

9.3. Processing of Diffraction Data, Generation of Structures and Refinement procedures.

9.3.1. Indexing and Integration of Diffraction Data.

Indexing the positions and integration of the intensities of the diffraction spots were carried out using the package DENZO (Otwinowski, 1993; Otwinowski & Minor, 1997). Indexing refers to the procedure of assigning *hkl* indices to each spot, while integration is the process by which the intensities of the spots are determined. Integration in DENZO is performed by profile fitting. In this method a curve is fitted to the data and the area under the curve estimated as the intensity. This method allows a correction to be made to the intensity to reduce the influence of the background signal. In practice, the diffraction image is split into a number of sectors, and the average profile in each of these sectors determined. The averaged profile will vary depending upon the position on the detector. This profile is then best-fit to the counts in the area where the spot is predicted to be. The area under this best-fit curve is used to determine the intensity of the spot. The number of counts is not directly translated into the intensity. The reliability of the output from this package is presented in the form of Chi-square values, and the averaged spot profile from each sector is produced by DENZO for inspection. Alteration of the various input parameters was carried out, within acceptable limits, until satisfactory statistical data were generated.

9.3.2. Scaling Data.

Scaling of the data sets was performed using the package SCALEPACK (Otwinowski, 1993; Otwinowski & Minor, 1997). This process creates a combined data set from two or more individual sets. Successful scaling involves identifying symmetry related reflections in the different data packs and placing them together. In addition the data have to be corrected for factors such as crystal decay over time. This weighting of the data leads to the scaling of observations, such as symmetry equivalents, to give a unique set. SCALEPACK also allows for alteration of other factors such as definition of the level of mosaicity and alteration of the dimensions of the unit cells between different crystals. Like DENZO, SCALEPACK generates

detailed statistical analyses of the data which allows the error model to be weighted to obtain the best scaling statistics for each data set.

The final output from the combination of the DENZO and SCALEPACK investigations gives the first indication as to the quality of the data set. The major statistical indicator at this point is the R_{merge}. This statistic compares the agreement between multiple measurements of the same reflection on different images and the symmetry related reflections. In an ideal case the intensities of these related reflections would be identical. In practice an error is found. For example, the average R_{merge} for the seven published reaction centre structures is 12%. Diederichs & Karplus (1997) and Weiss & Hilgenfeld (1997) have both recently suggested that Rmerge is seriously flawed. The problem lies with R_{merge} being dependent on the redundancy of the data, highly redundant data will inescapably have higher R_{merge} values, despite being the preferred situation for data collection. However, this statistic remains widely used in the crystallographic community. R_{merge} is calculated as follows:

$$R_{merge} = \Sigma_h\Sigma_i | \langle I(h)\rangle - I(h)_i | \Sigma_h\Sigma_i I(h)_i \qquad \textit{Equation 17.}$$

where I(h) is the intensity of reflection h, Σ_h is the sum over all reflections and Σ_i is the sum over all i measurements of reflection h.

9.3.3. Molecular Replacement.

All the structures generated in this project derived the phase information from earlier reaction centre models using molecular replacement. Diffraction data contains information only about the amplitude. There is no information regarding the phase. To obtain the electron density map all the information to solve the following equation is required.

$$\rho(x,y,z) = {}^{1}/_{V} \sum_{h}\sum_{k}\sum_{l} F_{hkl} \exp^{-2\pi i (hx+ky+lz)} \qquad \textit{Equation 18.}$$

The amplitudes of the F_{hkl} can be computed from $|F_{hkl}|^2 = I$, the intensity observed from diffraction. The above equation is an approximation, additional correction factors must also be included, the so-called Lorentz corrections. The Lorentz corrections allow for differences in the time over which a particular point in reciprocal space remains on the surface of the Ewald sphere. This is necessary because the time will vary depending upon where the spot is in relation to the origin of the reciprocal lattice (Figure 29). If the particular point lies close to the origin (Y), it can be imagined that could remain in a diffracting position for longer than a second point lying some distance from the origin (X).

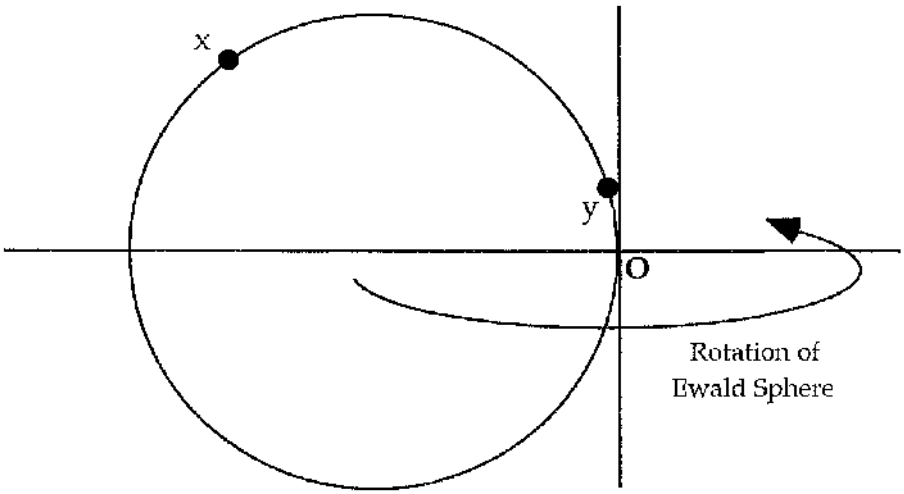

Figure 29 : Two reciprocal lattice points on the Ewald Sphere. As the sphere rotates around the origin point Y will remain in a diffracting position for longer than point X. The Lorentz correction calculations allow for this phenomenon.

Thus 'I' can be calculated from the collected diffraction data. However the phase information is lost. One method to overcome this problem is molecular replacement using previously determined atomic resolution structures for reaction centres The phases of atomic structure factors, and therefore the molecular structure factors, depends upon the location of atoms in the unit cell. To be capable of extracting phase information from an old model structure for molecular replacement, the structure of the old model must be superimposed on the structure of the new protein in its unit cell. However, all that can be determined from the new data is the

unit cell dimensions and symmetry, no information exists on where to place the old model within this unit cell constraint. Whilst theoretically it would be possible to perform a search of all possible positions, in practise this is impossible. Instead, the search procedure is simplified by the use of Patterson maps.

Patterson maps are calculated from the diffraction data, the amplitude of each term in the Patterson is the square of one structure factor, which in turn is proportional to the measured intensity of the reflection. The Patterson function equation is given in Equation 19 below.

$$P(u,v,w) = {}^{1}\!/_{V} \sum_{h}\sum_{k}\sum_{l} \Delta F^{2}_{hkl} \cdot e^{-2\pi i(hu + kv + lw)} \qquad \textit{Equation 19.}$$

The Patterson maps itself does not contain any phase information, it is after all calculated simply from the diffraction data. While the ultimate aim is to produce a map of $\rho(x,y,z)$, showing peaks of electron density from which the positions of atoms can be determined, the Patterson map of $P(u,v,w)$, displays peaks at locations which correspond to vectors between atoms. However, it is possible to calculate Patterson maps from both diffraction data and, importantly, from known structures. The advantage to Pattersons is that the position of the molecule in the unit cell has no effect on the final Patterson map, while rotation of the molecule will alter the arrangement of the Patterson atoms in the Patterson unit cell. Hence it is possible to use Patterson maps to perform searches to determine the best orientation of the old model in the unit cell of the new protein. In this manner it is possible via a trial and error approach to determine the best orientation using Pattersons, before using this single orientation to determine the best position within the unit cell using the determined structure factors. Hence, the structure factors were constructed from the amplitudes derived from the diffraction data, and phase information gleaned from the 2.65Å structure of the *Rb. sphaeroides* reaction centre (Ermler et al, 1994). Molecular replacement was performed using AMoRe (Navaza, 1994).

9.3.4. Computational Refinement Procedures.

Refinement of the model required the use of a series of programs from three software suites. Visualisation and manual manipulation of the structures were performed using the package O (Jones, 1991). The refinement was performed on Silicon Graphics Indigo workstations. Typically, a series of refinement procedures was carried out using X-PLOR 3.1. (Brünger, 1992). The output of these procedures was checked and manual manipulations of the co-ordinates performed using O, before reading back into X-PLOR. The maps and co-ordinates read into O were produced from X-PLOR files using programs from the CCP4 suite (CCP4, 1994), and vice-versa.

$$E_{total} = \omega_{xray}E_{xray} + E_{chem} \qquad \textit{Equation 20.}$$

X-PLOR combines energy terms defined by the structure (Equation 20) to form an energy function which it then attempts to minimise. In Equation 20 E_{chem} describes information about chemical interactions within the complex. It includes information regarding the atomic positions, information describing covalent (bond lengths, bond angles, torsion angles, chiral centres and the planarity of aromatic rings) and non-covalent (Van der Waals, hydrogen bonding and electrostatic) interactions. E_{xray} describes the difference between observed and calculated diffraction data, with ω_{xray} a weight balancing the forces arising from each term. Minimisation is performed by a variety of techniques all within the scope of the X-PLOR suite. The X-PLOR refinement programs used were rigid body refinement, simulated annealing, positional refinement and B-factor refinements (overall refinement and individual). The topology files and parameter files used in X-PLOR were kindly supplied by U. Ermler, G. Fritzsch and C.R.D. Lancaster (Max-Planc Institut für Biophysik, Frankfurt, Germany). In addition several data manipulation programs from the CCP4 program suite were used to generate files required for application of the refinement procedures.

For the analysis of mutant reaction centres, the co-ordinates of the amino acid residue concerned were replaced by those of an alanine residue

and run through the first round of refinement. This introduces the smallest possible amino acid side-chain, but still retains the restraints on main-chain conformation. A glycine residue would provide a smaller side chain, but would also allow unusual conformations of the main-chain. After the first rounds of refinement had been carried out, the mutant side-chain was built into the extra density found in the particular site in the $2F_O$-F_C maps, and highlighted by the use of F_O-F_C maps. This should remove bias of the new model towards the old model.

The two Fourier maps mentioned above, the $2F_O$-F_C and the F_O-F_C maps, are the two most widely used forms of map used in protein crystallography. A simple F_O map can be calculated, which is the observed amplitudes with the most current phases. However, this map is subject to bias towards the initial model, and hence is not particularly useful for identifying incorrect portions of the structure. Of more interest is the F_O-F_C or difference map. This map is especially useful for identifying where corrections are required in the current model. In this form of map there are peaks where the density is not accounted for by the model used to calculate the F_C, and holes, or regions of negative density where there is insufficient density to satisfy the model as it stands. Isolated peaks of positive or negative density can arise from movement of atoms, changes in B-values, or a change in occupancy. However, a pair of negative and positive density peaks indicates a shift of the model co-ordinates is required, from the negative region to the positive. This map, while powerful, is difficult to interpret in isolation. It is normally used in conjunction with a $2F_O$-F_C map. This latter form of map is that which is frequently displayed as the electron-density map. It is the easiest form of map to interpret, although it suffers from similar problems as the F_O map, being susceptible to bias from the starting model, the quality of the $2F_O$-F_C map is dependant upon the quality of the phases. The $2F_O$-F_C and the F_O-F_C were the two models most heavily used in the refinement procedure. One other form of map was used, the omit map. The omit map is performed by omitting a region of the model from the Fourier calculations. Therefore, all the phase information for the production of the maps comes from regions distant from the omitted portion. Care must be taken to ensure proper scaling of Fo to Fc, as the omission of a region will decrease the sum of Fc. The resulting map should relieve the effects

of initial model bias, potentially uncovering previously hidden or clearing incomplete regions of density.

Rigid-body refinement was the starting point for the refinement procedures. This procedure refines the positions of fixed groups of atoms to the observed amplitudes, and refines individually over six parameters, three rotations and three translations. The co-ordinate file produced from rigid-body refinement was then submitted to a limited round of positional refinement. Positional refinement carries out conformation searches of the structure, attempting to fit the Fobs (Fo) parameters to the Fcalcs. (Fc), whilst placing the residues in the lowest possible energy conformation. This limited positional refinement (20-25 rounds) was performed simply to relieve any strains or bad contacts within the co-ordinates prior to the simulated annealing procedure.

One of the major obstacles in crystallographic refinement is the existence of multiple energy minima. The problem lies with procedures such as positional refinement having a limited radius of convergence. This means that they don't posses the ability to shift the co-ordinates sufficiently to overcome the problem of localised energy minima. To overcome this problem the technique referred to as simulated annealing is used. Simulated annealing, often called "slow-cooling", has a much wider radius of convergence, and is therefore more suited to the multiple minima characteristics of macromolecular crystallographic refinement. Positional refinement can be likened to a gradient, the energy can only decrease. Hence small energy minima can trap the system: it is incapable of performing a small increase in energy, even though a deeper minima may result. The nature of simulated annealing is to allow just such an increase in energy to occur, hence escape from the "gradient trap" is made possible. Energy is introduced to the system via a "temperature" term which defines the likelihood of overcoming an energy barrier. Simulated annealing progresses by starting with a high radius of convergence as defined by high temperatures, typically 3000-4000K, which decreases in size with "cooling" down to ~300K over a period of a few picoseconds. As the temperature descends so the movement possible for the co-ordinates decreases "settling" the co-ordinates into a energy minima.

The final computational cycle in the refinement was the analysis of the isotropic temperature, or B-factors. The B-factors give a measure of the thermal motion of the atom concerned. Initial B-factor refinements were performed treating the complete structure as a single group. Only once the refinement statistics showed an R-factor of less than 25%, and the resolution of the model of beyond 2.8Å were individual B-refinements carried out for each of the atoms. The distribution of the B-factors was carefully noted. Atoms which are bound to each other have effects on the others' motion. If one atom is undergoing strong displacement in the structure, then neighbouring atoms would be expected to be undergoing similar levels of movement. It is important to ensure that the B-factor distribution follows this kind of pattern, i.e. those residues buried within the core of the protein are expected to have much lower B-factors than those residues exposed on the surface of the protein. The relative behaviour of the two R-factors, Rnorm and Rfree, was carefully monitored to ensure overfitting was not taking place. All of the X-PLOR programs discussed were run with the inclusion of the bulk solvent correction given in X-PLOR. The correction works by defining the solvent region in the unit cell of the crystal, assigning an average electron density to it, and Fourier-transforming this region.

Electron density maps were calculated using the CCP4 suite programs SFALL, FFT and MAPMASK. SFALL was used to calculate the phase information required for map calculation from the model co-ordinates. FFT, standing for Fast Fourier Transform, generated the electron density maps, performing analyses on the co-ordinates and transforms to obtain the structure factors required, with MAPMASK used to generate the complete electron density map. The map output from FFT, was only of a single asymmetric unit. This final program extends the range of the Fourier map.

9.3.5. Interactive Refinement Procedures

Map fitting, i.e. studying the maps produced and attempting to build in the co-ordinates interactively, was carried out using the package O. Several computer programs were used to aid this procedure, identifying regions of the map which required greater attention (see Dodson, et al 1996 for review of available programs). The programs used were PROCHECK

(Laskowski et al, 1993), WHATCHECK (Vriend & Sander, 1993) and also OOPS (Kleywegt & Jones, 1996). The latter program carried the great advantage of being able to run within O. Data from WHATCHECK could also be read into OOPS for interactive investigation. This offered the advantage that, with the use of a macro, each suspect area could be investigated in turn, with the statistics and particular problem displayed in the O command line. This greatly increased the speed and quality of the investigations. Factors investigated during the interactive rebuilding stage included the quality of fit to the density maps, the geometry of the main chain and of the side chains, and the interaction of groups with neighbouring residues. Tools provided in O for the rebuilding of the protein are discussed in Zou & Jones (1996).

The map fitting made use of several forms of density maps. The most commonly used were the F_O-F_C and $2F_O$-F_C maps. The F_O-F_C, or difference Fourier map, displays peaks where the density encountered can not be accounted for in the model used to calculate the F_C. These can be either positive peaks, where the model does not possess a group capable of filling that region of density, or negative, where the density is too limited to carry the co-ordinate model. This form of map provides a great deal of information in terms of identifying regions of the model that require remodelling. However, it is difficult to interpret. The $2F_O$-F_C map shows combined information from the F_O, the Fourier synthesis map, and also the difference map. The $2F_O$-F_C map is commonly given as the electron density map of the protein. The map produced is much easier to interpret than the F_O-F_C. However, this map is especially susceptible to inaccurate phase information, the map will always tend to mirror the model used to calculate the phases. Therefore, refinement of the protein model map must use at least the F_O-F_C and $2F_O$-F_C maps in combination, and preferably with another form of map, the omit map. Only using the combined information provided by these maps can the validity of the map be ensured.

The omit map is simply a map calculated from a model from which some regions of the model have been removed. The phases are calculated from the remainder of the model. Thus, any particularly dubious regions can be left out of the calculation, allowing the production of more accurate phase information from the remainder of the model, which may lead to

the "appearance" of an alternative conformation for the model in the new maps. Calculation of the omit map requires that the F_O to F_C scaling be carried out with care. The removal of a portion of the model will cause a reduction in the Fc. It is therefore important to use a scale calculated from the entire model. In addition, it is suggested that only 10% of the model be omitted at any one time (Kleywegt & Jones, 1997), because otherwise the phase information available will offer an inadequate base for calculation. In addition, the choice of omitted region is also of importance. Simple omission of one or two residues from the model, will not sufficiently clear the phase bias represented by the old model. Therefore, a significant chunk of the protein must be omitted, centred around the selected residues, removing all the biased phasing information from the area around the region of interest. The new omit maps should in theory provide a clearer indication of the "true" structure of the complex in the omitted region being calculated from phase information from distant, presumably more reliably modelled, regions. The model can then be carefully built interactively back into the correct conformation.

9.3.6. Building of Hetero-Molecules into the Model.

The introduction of water molecules and detergent molecules to the structure was only attempted once a relatively high quality model had been established. The statistics produced by the various programs were used to help define when this procedure could begin. Typically, once the R-factor (see below) had dropped to below 25%, the first round of fitting was carried out. Initial fitting made use of two programs from the CCP4 suite (1994), viz. PEAKMAX and WATPEAK. PEAKMAX searches through the density maps, and notes the co-ordinates of all peaks of density over a certain threshold. WATPEAK combines the identified peaks from PEAKMAX with atomic co-ordinates, and attempts to identify likely candidates for water molecules by analysing the distance from the peak to the nearest atom. If the peak is too close to the atom or too far to interact with it, the peak is rejected.

The surviving density peaks were then investigated interactively using O. Each peak was analysed with F_O-F_C and $2F_O$-F_C maps, and any potential hydrogen bonding groups identified. Water molecules were only added when there existed a peak of roughly spherical density in both maps, and

where hydrogen bonding groups were available at acceptable distances from the peak. Detergent molecules were added strictly by interactive building, but the selection procedure followed similar lines. The amphipathic nature of the detergent was used as an additional criterion for selection. Addition was only made if the hydrophobic and hydrophilic regions could be sensibly accommodated in the respective putative binding pockets.

The progress of the refinement was followed by analysis of the statistics produced. The major statistical indicator used was the R-factor. The movement of the model to the "correct" structure will lead to the convergence of the calculated structure amplitudes $|F_{calc}|$ with the observed values $|F_{obs}|$. The state of this relationship is followed by calculating the R-factor (Equation 21).

$$R = \frac{\sum | |F_{obs}| - |F_{calc}| |}{\sum |F_{obs}|} \qquad \textit{Equation 21}$$

Values for R-factors typically lie around 0.4 at the beginning of a refinement, and structures with a resolution of around 2.5Å, should fall to 0.2 or lower upon completion. The progression of refinement was observed using a utility program which makes a plot of the R-factor and free R-factors output in the log files. An example of this is given in Figure 30. However, the R-factor was used only as a general indicator of quality; other parameters were monitored. The geometry of the structure was investigated throughout the successive refinements. Values of interest were the rms (root-mean-square) deviations of bond lengths and bond angles, with typical values for a refined structure lying around 0.02Å for bond lengths and 4° for bond angles. The programs PROCHECK (Laskowski et al, 1993) and WHATCHECK (Vriend & Sander, 1993) perform many analyses of the stereochemistry of the structure. They analyse the stereochemical parameters of the model with the parameters held in a data base of solved structures. These programs were used routinely to identify any regions requiring remodelling or improvements.

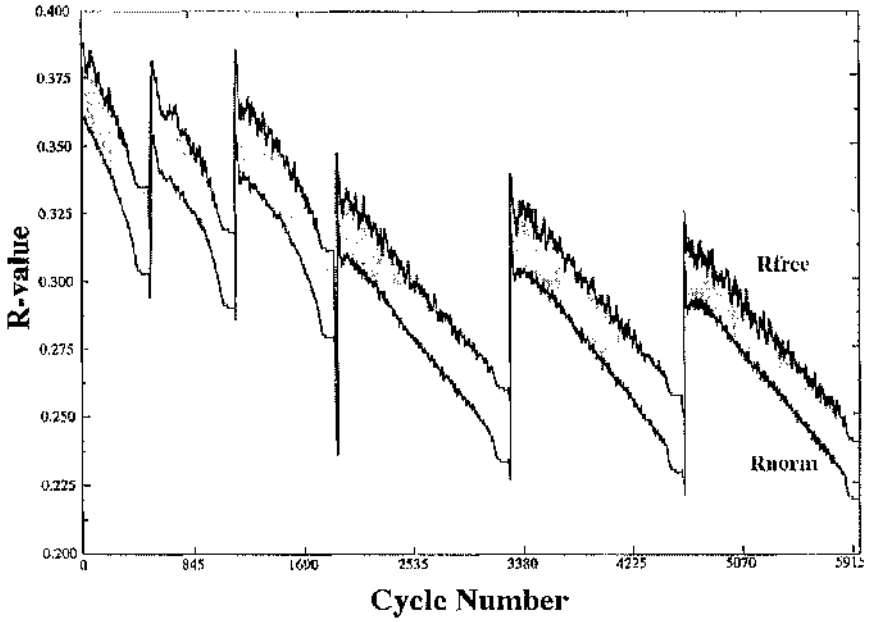

Figure 30: Plot of R-factors and Free R-factors against the calculation cycle number for the refinement of the FM115/RM197 model. Each sharp peak marks the "re-entry" of the model into computational refinement after a period of interactive modelling. R-factors typically increase after rebuilding, but should always decrease quickly to lower values. The increase is due in part to inaccuracies in the interactive modelling procedures, however, the spike is realistically due to the effects of "heating" the protein to 3-4000K as part of the slow-cooling. The two statistics Rfree and Rnorm should mirror one another throughout the refinement.

C. Results.

CHAPTER 10

Site-Directed Mutagenesis & Preliminary Investigations.

10.1. Site-Directed Mutagenesis

The point mutants engineered in the reaction centre complex are listed in Table 14. The mutants were produced in two batches. The first batch(A) was produced during a month spent working in Sheffield University in the laboratory of Dr M.R. Jones. The final batches (B) were kindly supplied by Dr M.R. Jones & J.P. Ridge.

Table 14: The reaction centre complexes investigated in this project. Also shown are the point mutations carried and the pigments on the characteristics of which the mutated residues were postulated to have an influence.

Batch	Mutations Carried	To investigate effect on character of:
A	Ser M119 to Ala	Carotenoid
	Trp M157 to Phe	Carotenoid
B	Trp M115 to Phe	Carotenoid
	Phe M197 to Arg	Special pair
	Met M122 to Leu	Carotenoid
	Phe M197 to Arg	Special pair
	Tyr M177 to Phe	Carotenoid
	Phe M197 to Arg	Special pair
	Trp M115 to Phe	Carotenoid
	Met M122 to Leu	Carotenoid
	Tyr M177 to Phe	Carotenoid
	Phe M197 to Arg	Special Pair

The information gathered about the two mutants in batch A, biochemical and spectroscopic, appeared to show that mutations in the region of the carotenoid were unlikely to have any effect on the special

pair and its immediate environment. The production of mutant strains in which the mutation in the carotenoid binding pocket was joined by an extra mutation in the special pair region permitted the maximum use of stretched X-ray crystallographic facilities to be made. In short, two structures could be solved in a single investigation. It was, however, essential that the single mutants were also available for full analysis using the other techniques. The conservative nature of the carotenoid binding pocket mutants was expected to leave the mutant structure essentially unaltered, while the Phe-Arg change at M197 would produce a much more interesting result. The crystal structure of the single Arg-M197 mutant was also determined due to the high level of interest which already surrounded the intriguing absorption spectrum obtained from this strain (Jones. M.R. & Spiedel, D., personal communication).

10.2. Growth Experiments.

The growth of the RCO2 strain of *Rb. sphaeroides*, the expression vector for the mutated reaction centres, was investigated. Two separate experiments were performed. The first examined the growth of the bacterium in two types of media; c-Succinate and M22+ (Appendix I). A second set of experiments was performed to investigate the growth of these bacteria on a range of carbon sources. The ultimate aim of this section was to reduce both the production time and the volume of media required to generate sufficient reaction centre material for the later investigations.

10.2.1. Comparison of M22+ and c-Succinate.

c-Succinate was the medium used for photosynthetic growth of *Rb. sphaeroides*. However, M22+ had been proposed as the best medium for semi-aerobic growth of the RCO2 bacteria (Jones, M.R. personal communication). A simple growth experiment was set up to compare the growth of RCO2 in combinations of c-Succinate medium and M22+ medium of different ratios. Growth was measured by measuring the OD at 803nm (a measure of the production of RC's) and at 650nm (to measure the cell density). The results, shown in Figure 31, were very clear: M22+ media provided the best growth medium, providing higher cell yields,

with OD_{650} of ~1.8 with M22+ only, compared with 1.2 for c-Succinate only. The advantages of growth on M22+ was observed at both measured wavelengths, although the actual ratio of 800 : 650 was very similar in both cases irrespective of the medium used. Therefore, M22+ medium was adopted as the medium of choice for semi-aerobically grown bacteria.

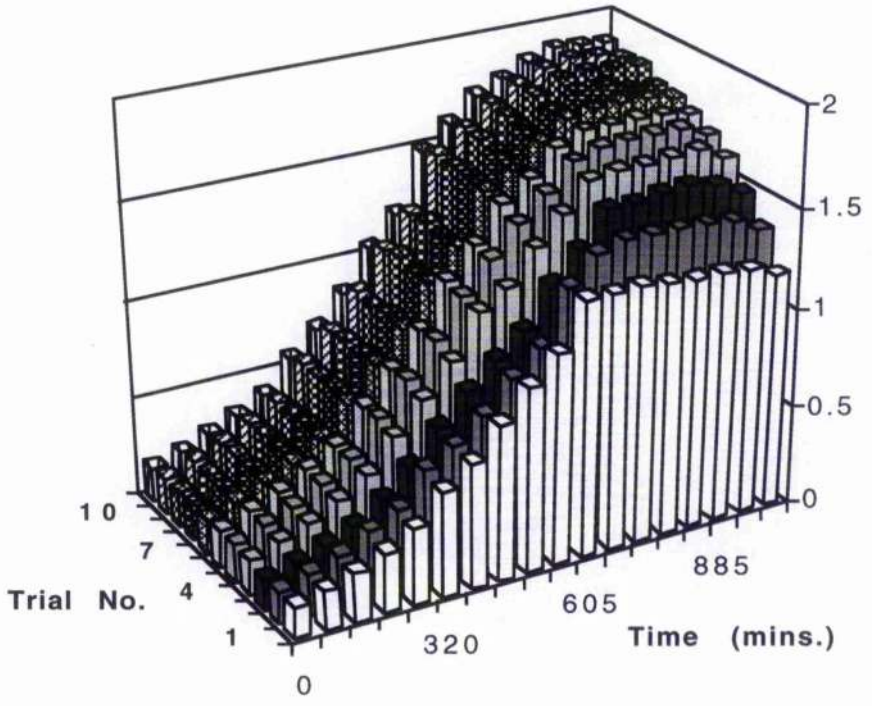

A.

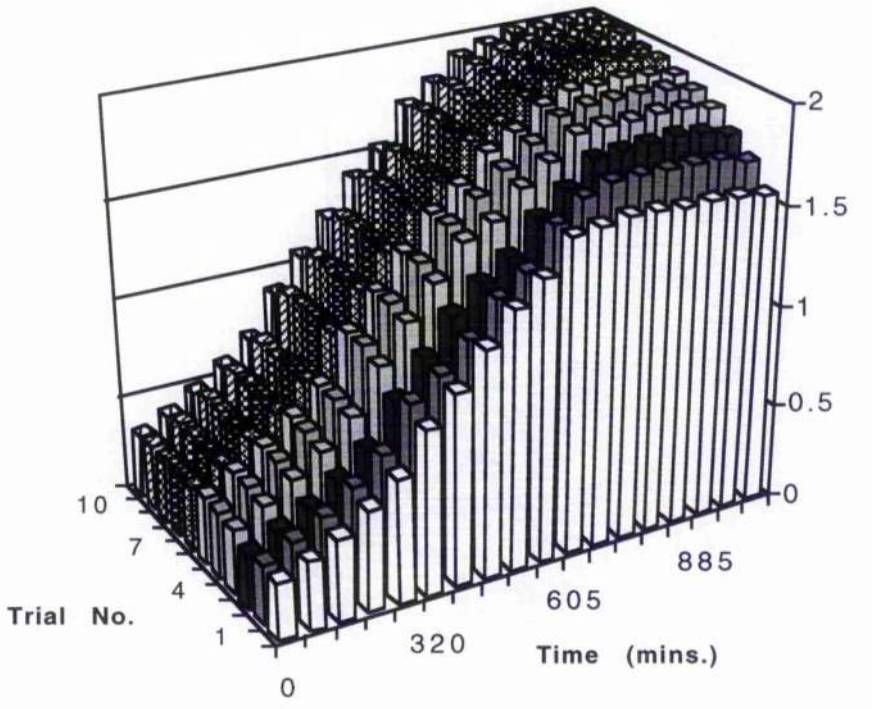

B.

Figure 31: The growth curves for RCO2 strains of *Rb. sphaeroides* when grown in varying ratios of c-Succinate and M22+ base media. **A.** Measurements at 803nm report on the synthesis of photosynthetic apparatus; **B.** measurements at 650nm report on the overall cell density. The trials are numbered 1 (100% c-Succinate) to 11 (100% M22+). Trials 2 to 10 are of increasing M22+ to c-Succinate ratios.

10.2.2. Growth on Different Carbon Sources.

The ability of *Rb. sphaeroides* strain RCO2 to grow on different carbon sources was investigated. Growth of this strain was initially performed on M22+ medium supplemented with sodium lactate. Growth on a range of C-sources was measured with regards to both overall cell density and the production of photosynthetic apparatus. The C-sources investigated were fructose, glucose, lactate and pyruvate. All the C-supplements were added to the growth medium in amounts calculated to provide identical carbon content, and not simply in equal molar concentrations and /or double the C-content. The growth curves produced from these experiments demonstrated the relative abilities of the RCO2 bacterium to grow on different c-sources. The results obtained from these experiments showed a slight increase in the yields obtained when fructose was used as the carbon source. Monitoring the cell density at 650nm the levels observed were ~1.6 with growth on fructose, and ~1.3 on all the remaining sources tested. The improvement was observed at both monitored wavelengths, although comparison of both sets of data again showed no alteration in the ratio of 800:650. However, growth was observed to be at slightly faster rates with fructose as the carbon source, as compared to other sources. The differences are small, however, when the aim is to grow sufficient quantities of cells for a reaction centre purification protocol, any increase in growth rate or cell yield is valuable. One additional parameter tested in this investigation was whether increasing the concentration of the carbon source led to any alteration in the cell yield/growth rate. No difference was detected in any of these investigations. To summarise the results of the experiments performed to improve the growth conditions for RCO2 strains, the basal media of choice was M22+, with fructose at a concentration of 1.5mM the carbon source.

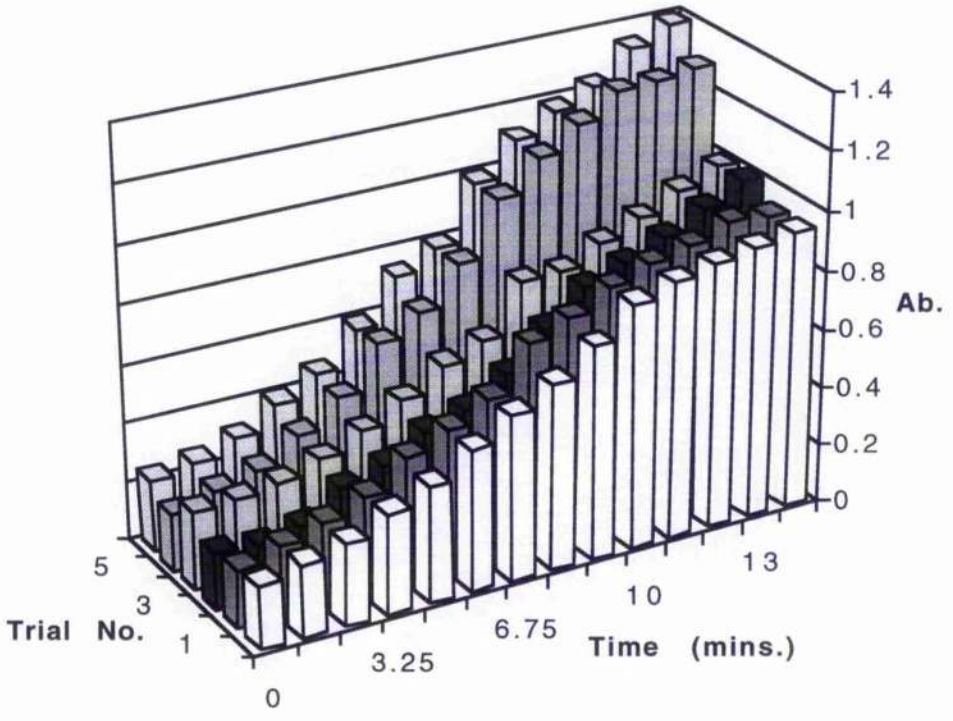

A.

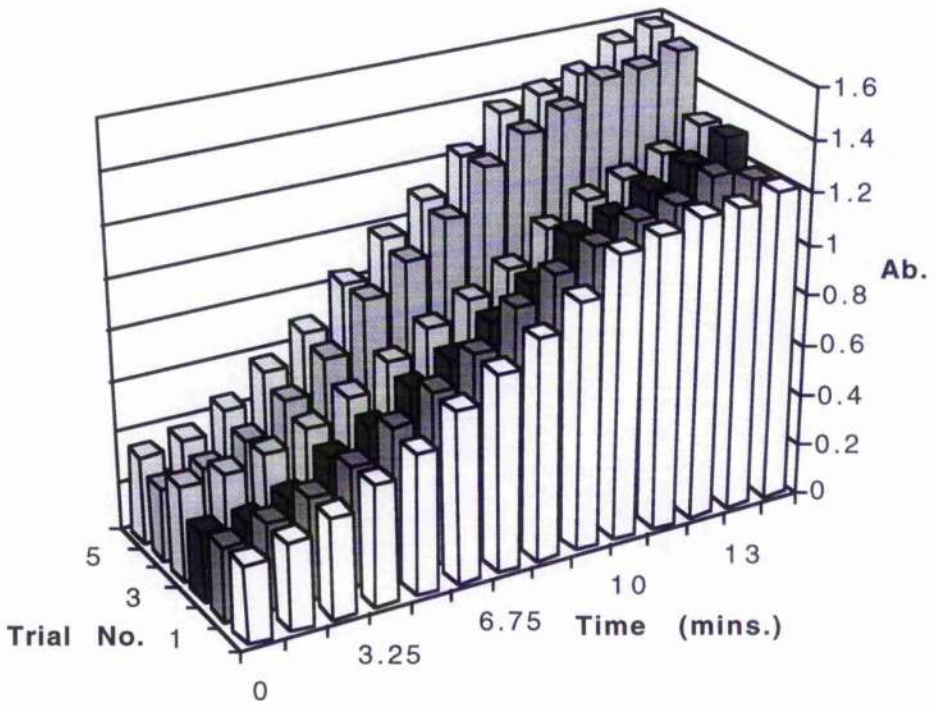

B.

Figure 32: The growth of RCO2 *Rb. sphaeroides* on different C-sources. **A.** Production of photosynthetic apparatus (800nm); **B.** measurement of cell density (650nm). Both graphs show from front to back: **1.** Glucose (1C), **2.** glucose (2C), **3.** lactate (1C), **4.** pyruvate (1C), **5.** fructose (1C) and **6.** fructose (2C).

10.3. Absorption spectroscopy.

Absorption spectroscopy provided a quick and straight-forward method by which the condition of the RC complexes could be probed. Comparison of membrane samples from the mutant strains and the WT RCO2 strain showed that the mutations had no effect on the ability of the bacteria to form stable complexes within the membrane. However, some alteration of the P band in those strains carrying the FM197-R mutation was evident. When spectra were taken for the isolated and purified complexes this alteration in the FM197-R strains became clear, although no significant alterations were observed in the remainder of the spectra. Finally, spectra were obtained for crystals of reaction centres, although only two samples were tested this way (WT and YM177-F & FM197-R), showing that the crystal form maintained similar spectral behaviour to the isolated complex, although they possibly were closer in character to that of the membrane bound complex.

10.3.1. Chromatophores.

The spectra of chromatophore membranes of some of the strains investigated during this project are presented in Figure 33. The membrane spectra are limited to the NIR region as the effects of scatter and components of the membrane other than the photosynthetic apparatus make the region below 650nm uninterpretable. However, the NIR region does display very clearly the peaks of the reaction centre produced by the absorbance of, in the wild type complex, the special pair (~865m), the accessory bacteriochlorophylls (~803nm) and the bacteriopheophytin (~770nm). Figure 33 presents the absorption spectra obtained from investigation of 5 different RCO2 strains. Three "wild-type" spectra, where the reaction centre is expressed in different carotenoid backgrounds, red, containing spheroidenone as the majority carotenoid; green, neurosporene; and white, phytoene and phytofluene. Also shown are two of the mutant strains (AM119 and FM115/RM197, both in the spheroidenone background), showing a clear alteration of the spectra in the RM197 containing set of mutants.

The spectra were obtained by scanning membrane samples resuspended in Tris/HCl, pH8.0, with ~0.5% LDAO detergent added and 10mM sodium ascorbate. The added detergent helps to overcome some of the light scattering problems. The spectra of the WT green membranes was obtained without the addition of detergent, consequently the spectra is not so well resolved. The sodium ascorbate ensures the special pair remain reduced, the spectrum shown of the WT red strain was obtained without the addition of ascorbate, and the spectra obtained shows an oxidised P band. The WT red and WT green samples, when analysed with the addition of both LDAO, and ascorbate both show very similar spectra. WT white membranes gave a slightly altered P band position, apparently red shifted to ~869nm. Time unfortunately did not permit a more detailed analysis of the "white" system, the significance of this shift therefore remains unresolved. However, this shift is possibly an indicator that the "white" carotenoids, phytoene and phytofluene are not bound within the reaction centre. Results from analysis of the mutant complexes showed that all the RM197 mutants showed an identical blue-shift of the P band of ~15nm. In addition, a slight change in the shape of the 803nm band is observed, with the formation of an apparent shoulder in the band to the red of the normal peak (at approximately 812nm). Investigation of the single mutants in the carotenoid binding pocket showed all the strains to have WT character. Although it should be remembered that in this particular set of experiments the information is limited to only the BChl and BPheo constituents of the reaction centre.

Table 15: The position of absorption peaks observed for the chromatophores of the strains analysed. There is some difficulty in determining whether the small shifts in band position are "real effects" or are simply inconsistencies introduced by the light scattering problem.

Sample Group	BPheo Absorption	Monomeric BChl Absorption	Special Pair Absorption Band
WT Red	~757nm	~803nm	~865nm
WT Green	~756nm	~802nm	~866nm
WT White	~758nm	~803nm	~869nm
RM197 containing Strains	~754nm	~802nm (shoulder at ~812nm)	~850nm
Red Single Carotenoid Mutant Strains	~756nm	~802nm	~864nm

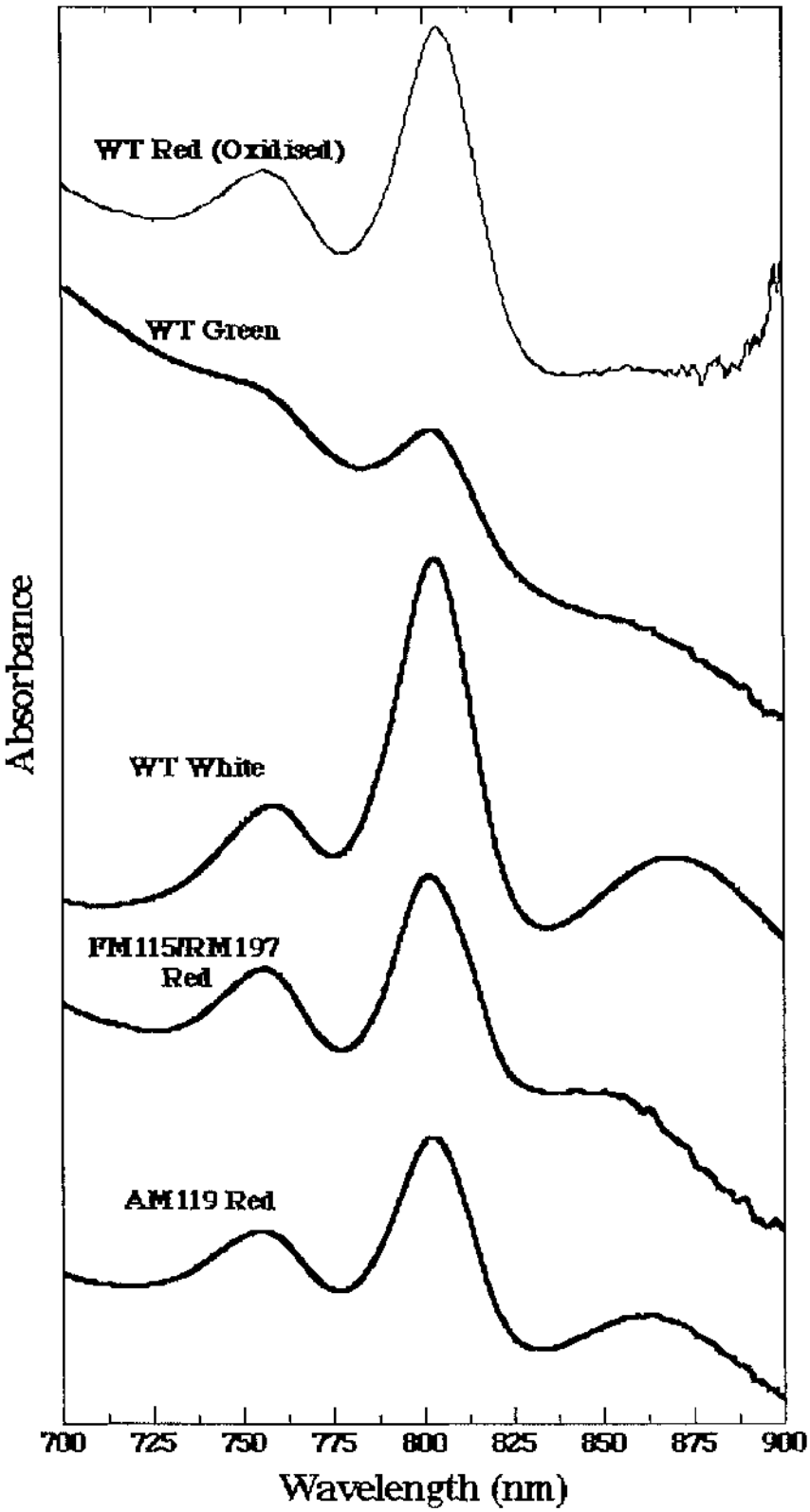

Figure 33: The absorption spectra obtained from analysis of chromatophore membranes from the RCO2 strains, 1cm pathlength. Samples in 20mM Tris/HCl, pH 8.0, 0.5% LDAO, 10mM ascorbate.

To summarise, the results of this investigation led to the splitting of the mutant complexes into two groups. The first group, containing all the single carotenoid mutants, exhibited spectra identical to the WT. However, the second group, all the FM197-R carrying strains, exhibited altered characteristics around the special pair band (normally at ~865nm), manifesting as a blue shift of approximately 15nm in the *in vivo* spectra.

10.3.2. Purified Complexes.

The absorption spectra of the range of purified mutant complexes exhibited results which backed the separation into two groups made from the chromatophore spectra. Figure 34 presents a selection of spectra obtained for isolated complexes with the summarised data presented in Table 16. No alterations of the carotenoid spectra (~430nm to ~500nm) were obtained in any of the strains, however again a blue-shift of the special pair band (normally ~865nm, now ~848nm) of ~18nm was observed in all mutants strains carrying the FM197-R mutation. This effect is clearer in the isolated complex as compared with the chromatophore spectra presented in the previous section, with the effects of light scatter removed from the spectra. As expected, from previous reports (Clayton, 1978; Debus et al 1985; Wang et al, 1994; Müh et al, 1996) there is an additional ~2nm blue-shift of the special pair band upon removal of the reaction centre from the membrane. Therefore, the larger blue-shift in the isolated complex as compared to when in the membrane, was not unexpected. Therefore, it is clear that the mutation of the phenylalanine residue at position M197 to arginine, had resulted in a major alteration in the characteristics of the special pair.

Table 16: The positions of the absorption peaks obtained from analysis of isolated and purified reaction centre complexes.

Sample Group	Special Pair BChl Qy band	Monomeric BChl Qy band	BPheo Qy	BChl Qx band	BPheo Qx band	Soret Band
WT red	865±0.5nm	803±0.5nm	757±0.5nm	598±0.5nm	530±0.5nm	366±0.5nm
Single Carotenoid Mutant (Red)	866nm±1nm	802±0.5nm	757±1nm	596±0.5nm	530±0.5nm	366±0.5nm
RM197 Containing Strains (Red)	848±0.5nm	801±0.5nm	757±0.5nm	596±0.5nm	532±0.5nm	366±0.5nm

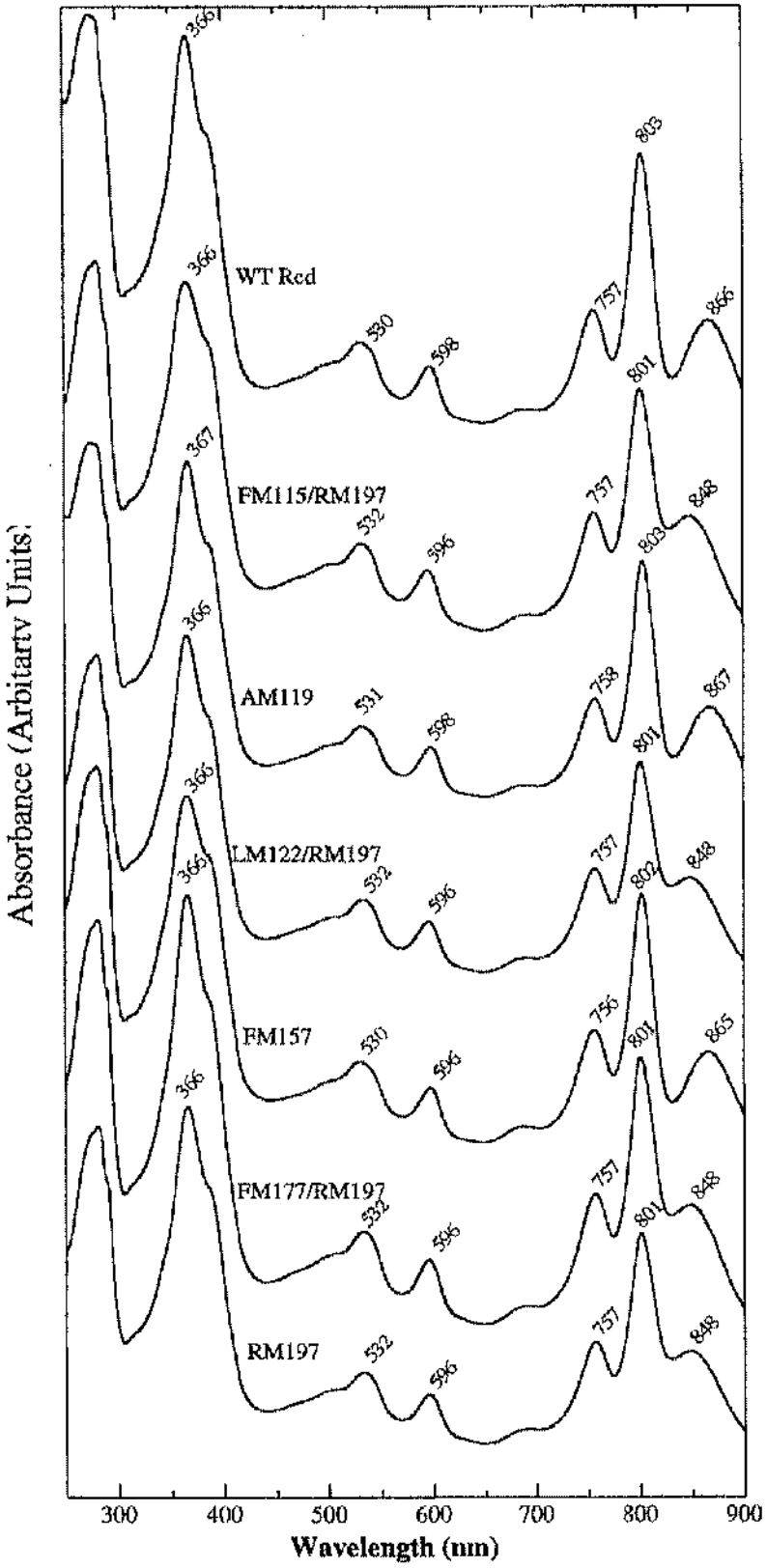

Figure 34: The absorption spectra of purified reaction centres from selected bacterial strains. Samples in 20mM Tris/HCl, 0.01% LDAO, 10mM ascorbate, 1cm pathlength.

10.3.3. Absorption Spectra from Crystals.

One frequently asked question in crystallography is how the crystal structure of a protein relates to the structure of the protein as it would be found *in vivo*. The null light-harvesting complex expression system allowed the spectral characteristics of the membrane bound RC to be probed, and with the availability of a Guided Wave (model 260) Fibre Optic Spectrophotometer, it was possible to obtained spectra through to intact crystals. The spectra was limited to the range 650nm - 900nm, because of the poor quality of the spectra at lower wavelengths (due to absorbance by other membrane bound components and increasing noise due to scatter at lower wavelengths). However, this region was used to probe the behaviour of the RC as it passed from membrane to crystal form. The spectra obtained are presented in Figure 35. The RC only expression system is unique in allowing this kind of investigation into the properties of the reaction centre as it passes through the various stages involved in the production of crystals. The effect of detergent solubilisation, purification and crystallisation on the optical properties of the reaction centre complex could, therefore, be monitored. The extraction of the reaction centres from the membrane and subsequent purification had a small effect on the near-infrared absorption spectrum, with a 4nm red-shift of the BPheo Qy band and a ~2nm blue shift of the special pair Qy band. No effect was observed on the spectral characteristics upon crystallisation of the purified complex. It would seem that the structural and functional integrity of the reaction centre is essentially preserved upon extraction from the membrane, although alterations in the P and BPheo Qy bands suggest that these pigments do sense the change in environment.

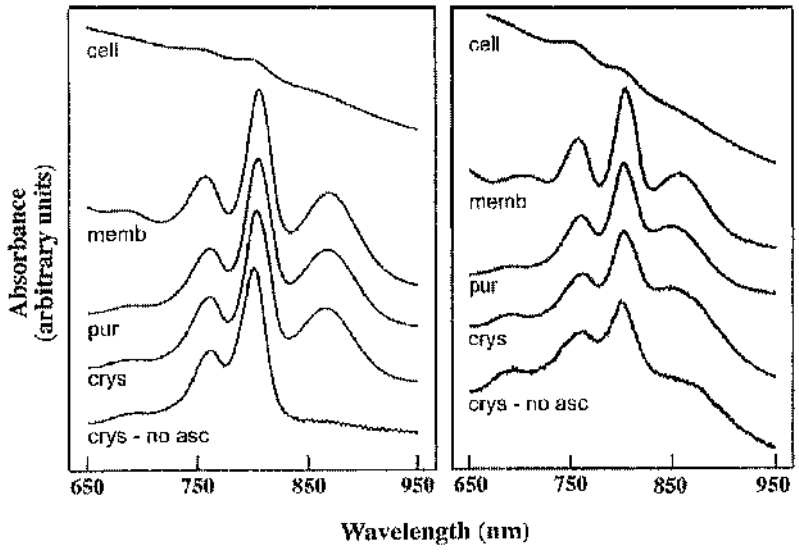

Figure 35: Absorption spectra obtained from investigation of samples as they progress through the purification and crystallisation protocol, A. WT red; B. RM197.

10.4. HPLC Analysis of Pigments.

Isolation, identification and quantification of the pigments was not performed for every mutant strain. The FM197 mutation carried in three of the carotenoid binding site mutants appeared, in each case, to have no effect on the binding characteristics of either the BChl or the carotenoid. For this reason, pigment analysis was not performed on the single FM197-R strain, nor was it performed on the single WM115-F, MM122-L or YM177-F mutants. While the completion of this work would be more ideal than leaving it at this stage, the time which remained at this point in the project made this of low priority. Thus this was sidelined to allow the completion of the ESR experiments, and the crystallographic investigations which were providing a great deal of data.

The results obtained are presented in Table 17 and example chromatograms for WT red and WM157 red are shown in Figure 36. In all cases the ratio of BChl to the carotenoid was found to be the same as that of the wild-type. The use of the extinction coefficients for BChl A_{360} = 53.9 mmol/cm^{-1} (Clayton, 1966) and spheroidenone of A_{486} = 124 mmol/cm^{-1} (Evans, 1989) led to the determination of a ratio of approximately 4:1 in each case. The chromatograms obtained tended to show families of peaks, rather than one single peak for each component. The major reason for this was the injection of relatively large amounts of sample tending to

cause spreading of the peaks. The column used was more suited towards simple identification of pigments, requiring only small amounts of sample. However, to obtain reliable, quantitative, results it was found that increasing the amount of sample was beneficial. Analysis of the chromatogram in conjunction with the spectra obtained at each time point allowed the individual peaks to be collected into single groups. In addition to this, although all the pigment extractions and subsequent steps prior to injection into the HPLC were performed in the lowest possible light intensities, there was almost certainly some photodegradation and photoisomerisation of pigments prior to examination. For example, the spheroidenone samples from isolated and highly purified reaction centres should all show the characteristic *cis* band at ~380nm. However, the majority of spheroidenone detected did not show this band, and therefore had presumably isomerised into the all-*trans* form. In addition to problems with ambient light, it was not possible to control the temperature at which each experiment was performed.

The use of the HPLC did provide strong evidence that spheroidenone was the major carotenoid bound within the reaction centres of RCO2 (semi-aerobically grown) bacteria. There was no indication of other carotenoids being present in the samples, however, it is not possible to discount this possibility, and from previous investigations (Cogdell & Frank, 1993), there was almost certainly a small amount of spheroidene present. Allowing for the limitations imposed by the conditions in which these experiments had to be performed, the obtained results do show a consistently observed figure of 4 BChl pigment molecules per spheroidenone carotenoid in each of the RCO2 strains isolated reaction centre preparations. This was taken as an indication of normal insertion of the carotenoid into the binding pocket, and that the mutant reaction centres were assembling normally.

a)

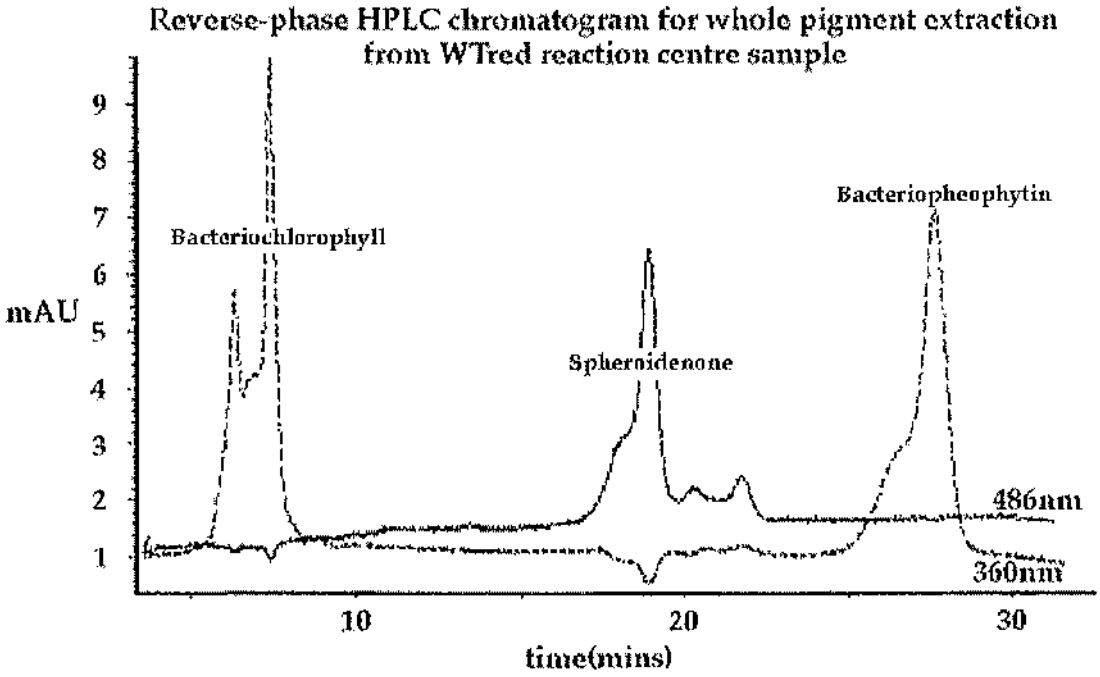

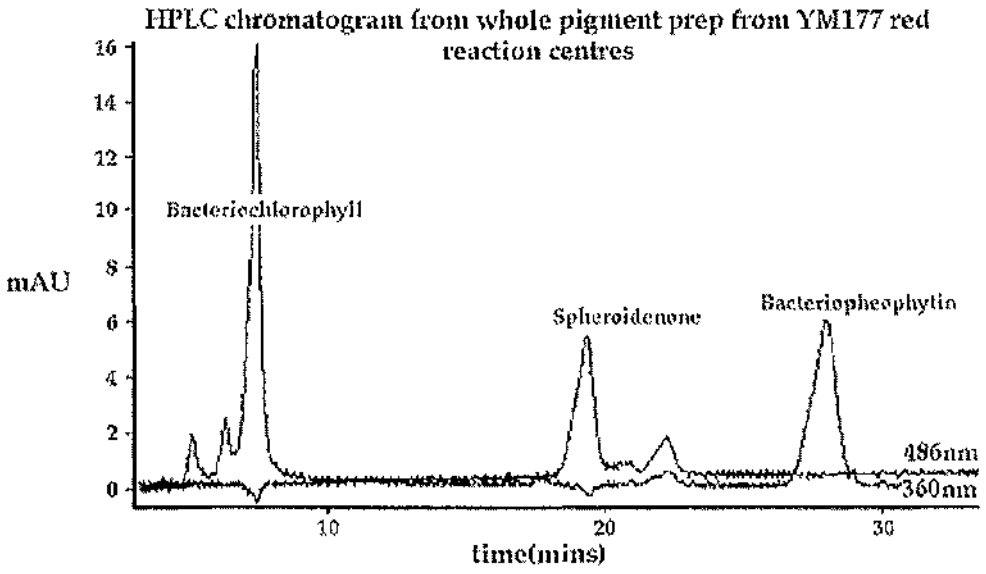

b)

Figure 36: Example chromatograms taken from the HPLC analysis of purified reaction centres. Samples were injected in 10-20µls of dichloromethane, and separation performed with an isocratic flow of methanol. All solvents used were of HPLC grade, obtained from Rathburn Chemicals, Scotland. (a) Chromatogram obtained from investigation of WT red; (b) chromatogram obtained from investigation of FM177/RM197-F red.

Table 17: The results of the pigment analysis experiments. *These results are taken from the results of double mutants with the FM197-R mutation. This result is the average figure gleaned from the three investigations involving the FM197-R mutation. †Correction made using the extinction coefficient for spheroidenone (124 mmol/cm^{-1}) from Evans, 1989). ¥Correction made using the extinction coefficient for BChl 53.9 mmol/cm-1 (Clayton, 1966). Two extractions were performed for each sample, with 5 HPLC injections made with each.

	A 360nm	A 486nm	correct. BChl.¥	corrected Spo.†	Determined ratio.
WT	2814.36	1656.41	52.2	13.3	3.9:1± 0.3
WM115-F*	3271.73	1974.37	60.7	15.9	3.8:1 ± 0.3
SM119-A	4047.89	2472.61	75.1	19.9	3.8:1 ± 0.3
MM122-L	3535.08	2076.23	65.6	16.7	3.9:1 ± 0.3
WM157-F	7502.31	4270.54	139.2	34.4	4.0:1± 0.3
YM177-F*	1781.26	1081.71	33.0	8.7	3.8:1± 0.3

CHAPTER 11

Specialised Spectroscopic Investigations.

Absorption spectroscopy provided the first information regarding the characteristics of the mutant complexes. The reaction centres appeared to have been successfully formed and integrated within the chromatophore membrane. The structure of the P absorption band was altered quite significantly in the FM197-R mutants, but the carotenoid bands in all the strains appeared to be as in the wild-type complex. Three, more sophisticated forms of spectroscopy were employed. The first two, circular dichroism (CD) and resonance raman spectroscopy, probe the structure of the pigment molecules bound within the reaction centre and their interaction with the immediate environment. The final spectroscopic method used was EPR (electron paramagnetic resonance spectroscopy, alternatively known as electron spin resonance spectroscopy). EPR was used to probe the ability of the reaction centre to funnel triplet state energy from P to the carotenoid molecule, the triplet states providing the single (paramagnetic) electron.

11.1. Circular Dichroism Spectroscopy.

The cryo-cooled CD spectra obtained for each of the samples are shown in Figure 36. The CD spectra of spheroidenone bound within reaction centres is quite different from that of spheroidene. As in the absorption spectra, spheroidenone does not give rise to the three peaks produced by spheroidene, a consequence of the additional carbonyl group which spheroidenone carries. The spectra between 400nm and 650nm of the wild-type complex shows four major features. Firstly there is a large negative "peak" centred at ~645nm, followed by a positive peak centred at approximately 610nm. These peaks are of course not due to the carotenoid pigment, but rather to the Qx band of the reaction centre BChl pigments. Monomeric BChl molecules show weak CD character, however, when in dimers or in aggregates, the signal is intensified due to the excitonic

coupling. The signal in the reaction centre, as mentioned above, contains a positive and a negative component, with the negative component of slightly greater magnitude due to contributions by the monomeric BChls (Scheer, 1991). This phenomenon is observed for both the BChl Qx and the Qy transitions. The region of the spectrum attributed to the spheroidenone pigment comprises a very broad, positive peak, centred at approximately 520nm. Lastly, there is a further negative "peak" beyond ~440nm to the edge of the spectra at 400nm.

Four spectra are shown in Figure 37, in addition to the wild-type spectra. Two single mutants are shown, AM119 and RM197, along with the FM115/RM197 and FM177/RM197 double mutants. The spectra for the FM157 and LM122 mutant complexes were identical to that of AM119. No differences were observed in the pattern in the carotenoid absorbing region in any of the spectra, suggesting the carotenoids in the mutant complexes were assuming an essentially wild-type conformation. However, when comparing the peak sizes in the mutants, it was observed that the maximum peak height of the spheroidenone band was approximately equal to that of the positive BChl peak at ~610nm in all of the carotenoid binding site mutants. This was not found to be the case in the WT spectra, and interestingly the single RM197 mutant, which appeared much closer to the WT pattern.

Alterations in the spectra were also obtained for the bands associated with P. Each of the mutant samples carrying the RM197 mutation showed shifts in the Q_X region with the negative peak position moving from 640nm to 628nm. A slight blue-shift of the positive band was also observed, shifting from 603nm to 605nm. These are consistent with the shifts described for these bands in the absorption spectra of these mutants. In summary the carotenoid binding site mutations would appear to have had an effect on the CD characteristics of the reaction centre complex. The ratio of the peak heights in the carotenoid binding site mutants has been altered with respect to the wild-type complex, and the complex where the P binding site has been altered. Given the conservative nature of the point mutations introduced, a large alteration in the carotenoid configuration sufficient to produce an greatly altered CD spectrum would have been unexpected. It would appear that some change in the carotenoid environment has occurred with respect to the behaviour of the complex in

CD investigations. However, it is very difficult/impossible to define what effect the mutations have had to cause such spectral alterations from CD spectroscopy alone.

[Following Page]

Figure 37: The CD spectra obtained from cryo-cooled investigations of: WT red; FM115/RM197 and AM119, RM197 and FM177/RM197 reaction centre preparations. All of the reaction centres were from the spheroidenone producing strains. Samples were prepared in 60% glycerol, 10mM Tris/HCl, pH8.0, 0.05% LDAO, with an OD_{360} of 0.5. Spectra are an average of three separate scans, with a baseline for the buffer subtracted.

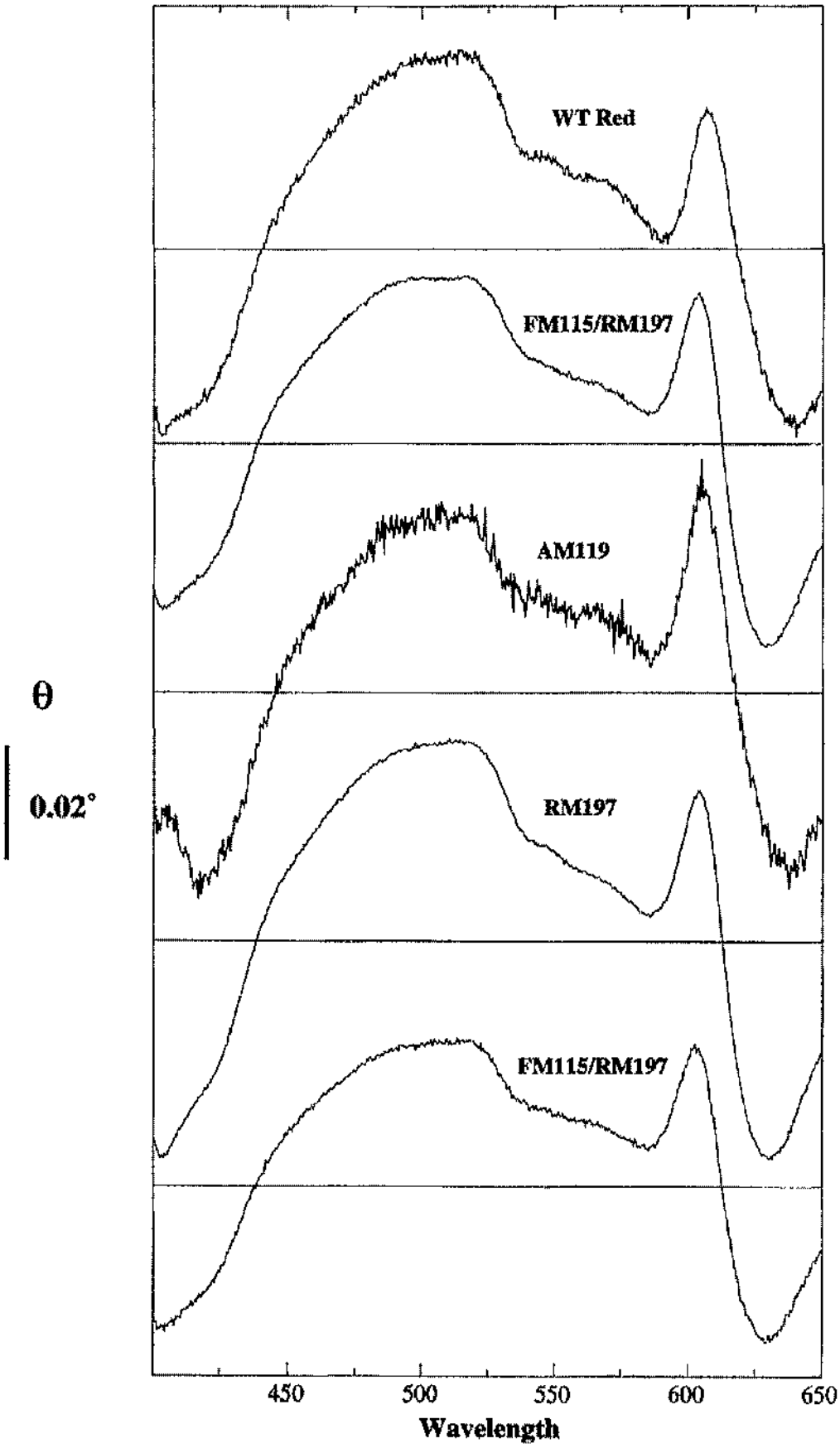
WT Red
FM115/RM197
AM119
RM197
FM115/RM197
θ
0.02°
450
500
550
600
650
Wavelength

11.2. Raman spectroscopy.

Raman spectroscopy provided the most sensitive method of probing the configuration of the carotenoid molecules bound within the reaction centre complex. As discussed in Section 3.3 of the Introduction, resonance raman provides a method of investigating the molecular configuration and interaction of the environment with the carotenoid molecule. The spectra obtained from the investigation of the complexes are presented in the following pages (Figure 38). A resonance raman study of spheroidenone containing reaction centres has not been previously undertaken. Therefore, the assignment of the lines in the spectra is based upon those made from investigation of spheroidene containing reaction centre complexes. The major lines, such as the ~1240cm^{-1} line, the strongest indicator for the 15-*cis* configuration, were observed in these investigations, and it was deemed unlikely that there would be any major alteration in the position of these lines in the spheroidenone spectra (Gall, A, personal communication, 1997).

The wild-type complex resonance raman spectra was found to be essentially identical to that of wild-type spheroidene containing reaction centres (See Introduction Section 3.3). The position and relative intensities of the various lines indicates that the major components of the spheroidenone RC are the same as the spheroidene RC complex. Thus the WT red complex was determined to have spheroidenone bound in the complex in an identical configuration to that of spheroidene. The results of the CD investigations, discussed above, suggested that there were no major alterations of the carotenoid configuration in any of the mutants. The spectra obtained from the resonance raman investigations supported this finding, with no large alterations found in any of the mutant spectra versus the wild-type (Figure 38: a). All the strains were interpreted as having the normal twisted, 15-cis conformation due to their peaks at ~1240cm^{-1} and ~960cm^{-1} (Figure 38: b and c).

The configurations of the carotenoids are, therefore, similar. However, there was evidence to suggest that they are not identical. Close inspection of the two bands at ~1158-~1170 cm^{-1} (Figure 38: c) revealed some alteration

of the resonance raman spectra between strains. The bands in this region (ν_2) have been assigned to C-C stretching coupled with C-H in-plane deformation. In the WT strain the second of the two peaks shows slightly higher intensity than the first. The spectra obtained for LM122 closely follows that of the WT. However, the remaining strains (AM119 was not analysed) all showed patterns which show slight alteration from the WT pattern. In the case of FM115, the peaks are again relatively close in intensity, but the first peak is of slightly greater intensity than the second. The strains FM157 and especially FM177 gave spectra in this region in which the second peak is much lower in intensity than the first. In addition to these observations, it was also noted that the separation of the same two peaks in the different strains, and the positions of the peaks were also varying. Observation of these two peaks identified FM177 as showing the greatest shift away from the wild-type pattern. However, the peak lying between ~1180 cm^{-1} and 1200 cm^{-1} gives a different view, with the strain FM157 showing greater movement away from the wild-type spectra.

Table 18: The positions (cm^{-1}) of the peaks in the RR spectra obtained for each examined sample (SM119-A was not investigated). The RR lines v1-v3 are marked along with the ~1238cm^{-1} line, the strongest indicator of the cis conformation of the carotenoid. The results of investigation with two excitation wavelengths are shown, 514.4nm and 488nm.

	WT red	FM115		LM122		FM157		FM177	
	514.4	488	514.4	488	514.4	488	514.4	488	514.4
v4	950.4	952.8	953.6	952.3	950.8	950.5	953.4	948.9	947.6
v3	1002.6	1004	1004.2	1003.9	1003.5	1002.1	1005.1	1002	1001.7
v2	1158.7	1159.7	1158.0	1159.7	1159.2	1158.8	1160.7	1158	1158.0
v2	1169.3	1170.8	1169.1	1170.7	1170.2	1169.1	1170.9	1168.6	1168.4
	1193.5	1192.4	1192.3	1194.2	1193.2	1193.6	1195.5	1192.6	1192.5
cis	1238.1	1238.5	1238.3	1238.6	1238.8	1237.4	1239.5	1237.6	1237.6
	1284.3	1284.5	1284.1	1285.7	1285.2	1284.7	1285.9	1282.8	1282.9

Investigations were performed at two different wavelengths, 488nm and 514.4nm. The above discussion referred to the 514.4nm excitation wavelength experiments. The 488nm analyses produced identical results (Figure 38: d). The pattern of peaks discussed in the 514.4nm data was also found in the 488nm data.

[Following four pages]

Figure 38: The spectra obtained from resonance raman spectroscopic investigations of the purified reaction centres. Excitation wavelength 514.4nm: A. Scan from 920 to 1440cm^{-1}; B. scan from 900 to 1050cm^{-1}; C. scan from 1125 to 1250cm^{-1}. Excitation wavelength 488nm: D. scan from 900 to 1500cm^{-1}.

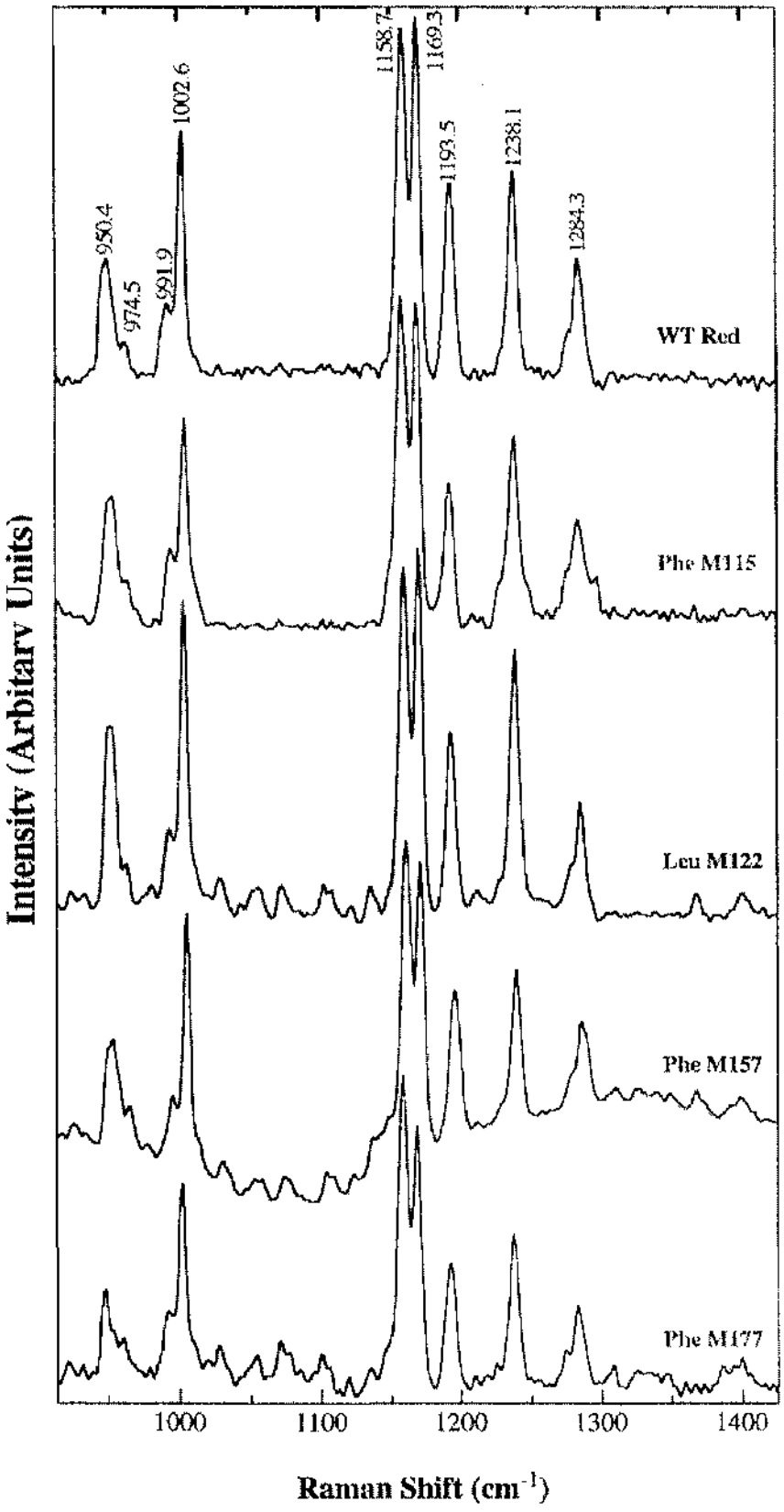

A. Excitation Wavelength 514.4nm

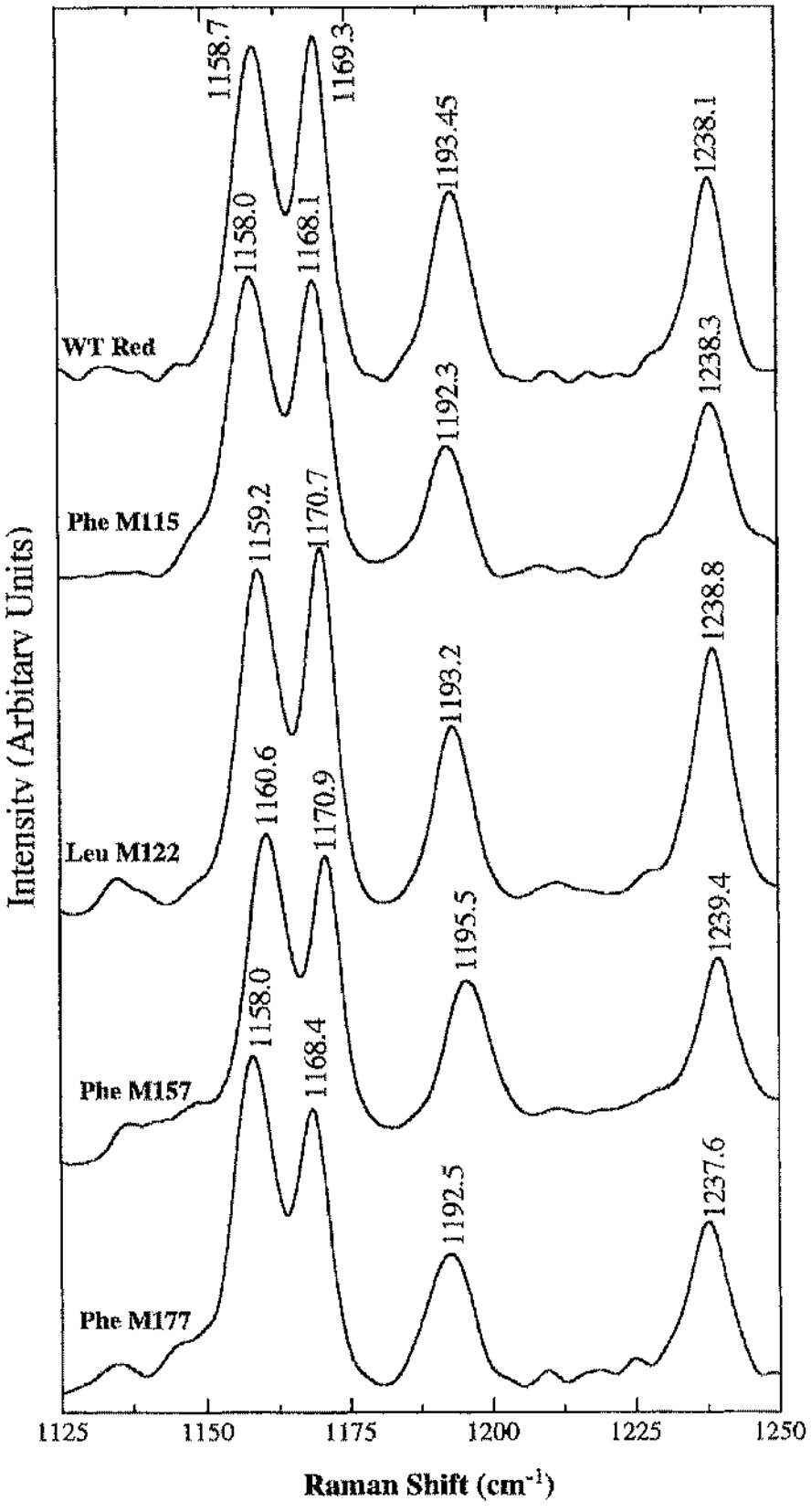

C. Excitation Wavelength 514.4nm

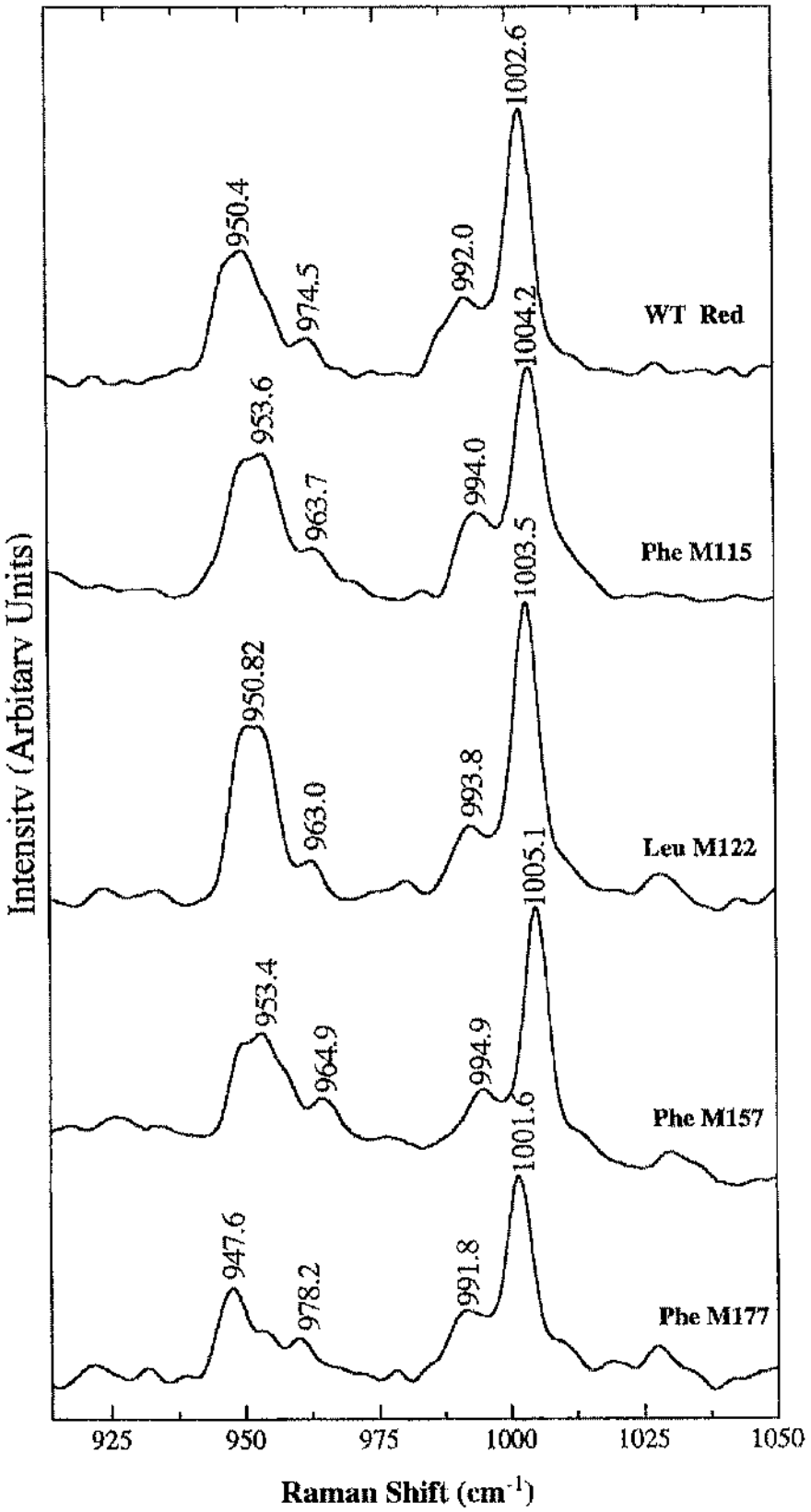

B. Excitation Wavelength (514.4nm)

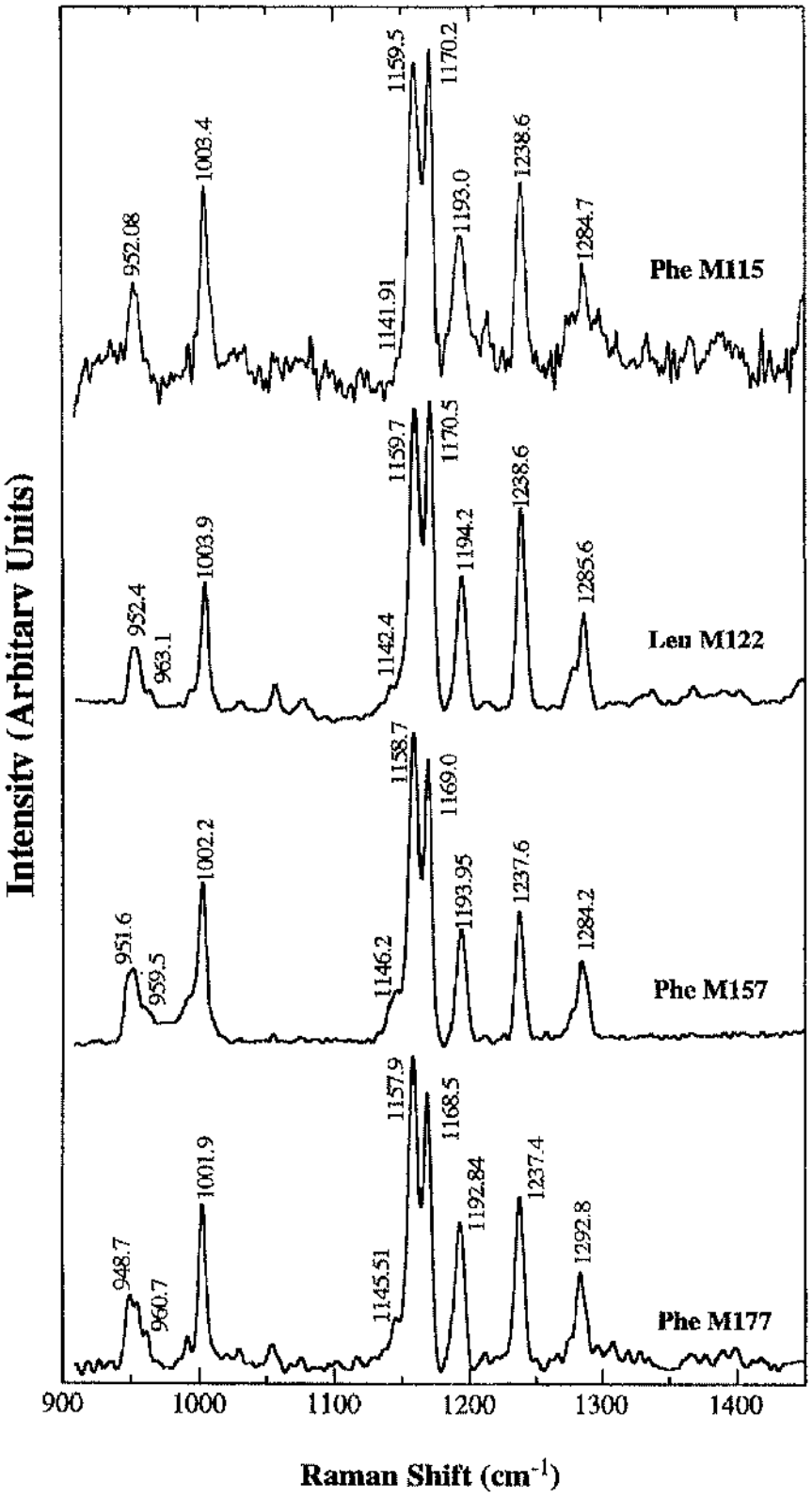

D. Excitation Wavelength 488nm

11.3. ESR spectroscopy.

The spectroscopic investigations discussed above, all perform analysis of the structure of the carotenoid and its interactions with its environment. They do not provide any information as to the effect any changes might have on the function of the carotenoid in the reaction centre. ESR was used to probe the ability of the carotenoid to transfer the triplet state energy induced on the special pair to the carotenoid. Sample spectra obtained are shown in Figure 39 (over seven pages), beginning with the WT red spectra (a) and the single carotenoid mutant spectra (b, c & d) followed by the single RM197 mutant (e) and two double mutant strains (f & g). The |D| and |E| zero field splitting parameters determined are shown in Table 19 below.

The wild type spectra presented in Figure 39 a), shows the expected results from ESR analysis of *Rb. sphaeroides* reaction centres. Investigation of *Rb. sphaeroides* R26.1 reaction centres by ESR generates a spectrum which has been assigned to that of the BChl triplet state. This spectrum is identical to that of the WT red at 10K (bottom spectrum). The BChl triplet is observed because transfer of triplet energy from the BChl to the carotenoid does not occur at these temperatures. The decrease in triplet energy transfer can be seen to begin at temperatures around 35K (centre spectrum), where a combination of the BChl triplet signal and the carotenoid triplet signal can be observed. The carotenoid signal includes troughs at approximately 3010 and 3650cm^{-1}, which are absent in the BChl signal, and also the width and position of the major peaks in the signal, at ~3150 and ~3550cm^{-1} differ between the two states. Hence the assignment of a mixed triplet state population at 35K. At 110K, however, the BChl signal is entirely absent. The transfer of triplet energy to the carotenoid is proceeding as efficiently as to make the BChl state too transient to be detected.

Table 19: The zero field splitting parameters obtained for the membrane bound reaction centres.

	|D| (±0.0003) cm^{-1}		|E| (±0.0003) cm^{-1}	
Sample Strain	10K	100K	10K	100K
WT red	0.01879	0.02926	0.00321	0.00452
FM115	n/d	0.02766	n/d	0.00484
AM119	0.01886	0.02815	0.00321	0.00476
L.M122	0.01889	0.02761	0.00305	0.00430
FM157	0.01891	0.02832	0.00322	0.00441
FM177	0.01870	0.02842	0.00312	0.00430
RM197	0.01949	0.02711	n/d	0.00476

Both the carotenoid binding site mutants and the RM197 strains show primary donor peaks at 10K and carotenoid peaks at 100K. At 35K both groups show evidence of both carotenoid triplet and BChl triplet signals. However, at 10K the RM197 carrying strain showed significantly larger values for |D| than found in the wild-type (and carotenoid binding site strains). The "normal" value for *Rb. sphaeroides* reaction centres is ~0.01888cm^{-1}, the observed value for this strain was 0.01949cm^{-1}. An alteration of this extent could be caused by a number of factors, either the structure of the P has been changed, or the extent of triplet delocalisation in the primary donor has been altered, or there has been a change in the extent of charge transfer character in the primary donor brought about by a slight change in the structure of P. The evidence, along with the altered absorption spectra and CD spectra, reinforced the hypothesis that the introduction of arginine in place of phenylalanine at M197 has caused the formation of some form of new interaction between the protein and BChl P_M. Upon completion of the spectroscopic analysis, the nature of this interaction remained unresolved. However, structural information was gathered for the RM197 mutants via X-ray crystallography, and the unexpected nature of the "interaction" determined (Section 13.3).

In addition to alteration of the zero-field splitting parameters, the introduction of arginine at M197 causes the transfer of the triplet state to continue at temperatures lower than observed in the wild-type. Analysis of any of the spectra from RM197 containing strains shows some features of the carotenoid triplet state at 10K, a temperature at which the signal should be exclusively that of the BChl triplet. The clearest indication of

the carotenoid signal in the 10K spectra are the large, negative (emissive) peaks (~3100 Gauss) prior to the major absorption peak. This effect is presumably due to an enhancement in the ability of the carotenoid to accept the triplet state.

[Following Seven Pages]

Figure 39: The ESR spectra obtained from the investigation of chromatophores obtained from WT red and mutant strains of *Rb. sphaeroides* RCO2. The strains can be quickly split into two groups. The essentially wild type single carotenoid binding site mutants, and the strains which are carrying the RM197-R mutation.

Both the reaction centre car^{T*} and the RC Bchl ^{T*} ESR signals have polarisation patterns that show they were formed by a radical pair mechanism. The difference in the polarisation pattern seen between the car^{T*} and the Bchl ^{T*} siganls have been documented before (Frank, 1992). They can arise either because of changes due to the differential decay rates of the individual triplet sub-levels during the lifetime of the car ^{T*} population, or because of differential mapping of the triplet states on the molecular frame of the RC carT related to the BChlT.

WT Red Reaction Centre ESR Spectra

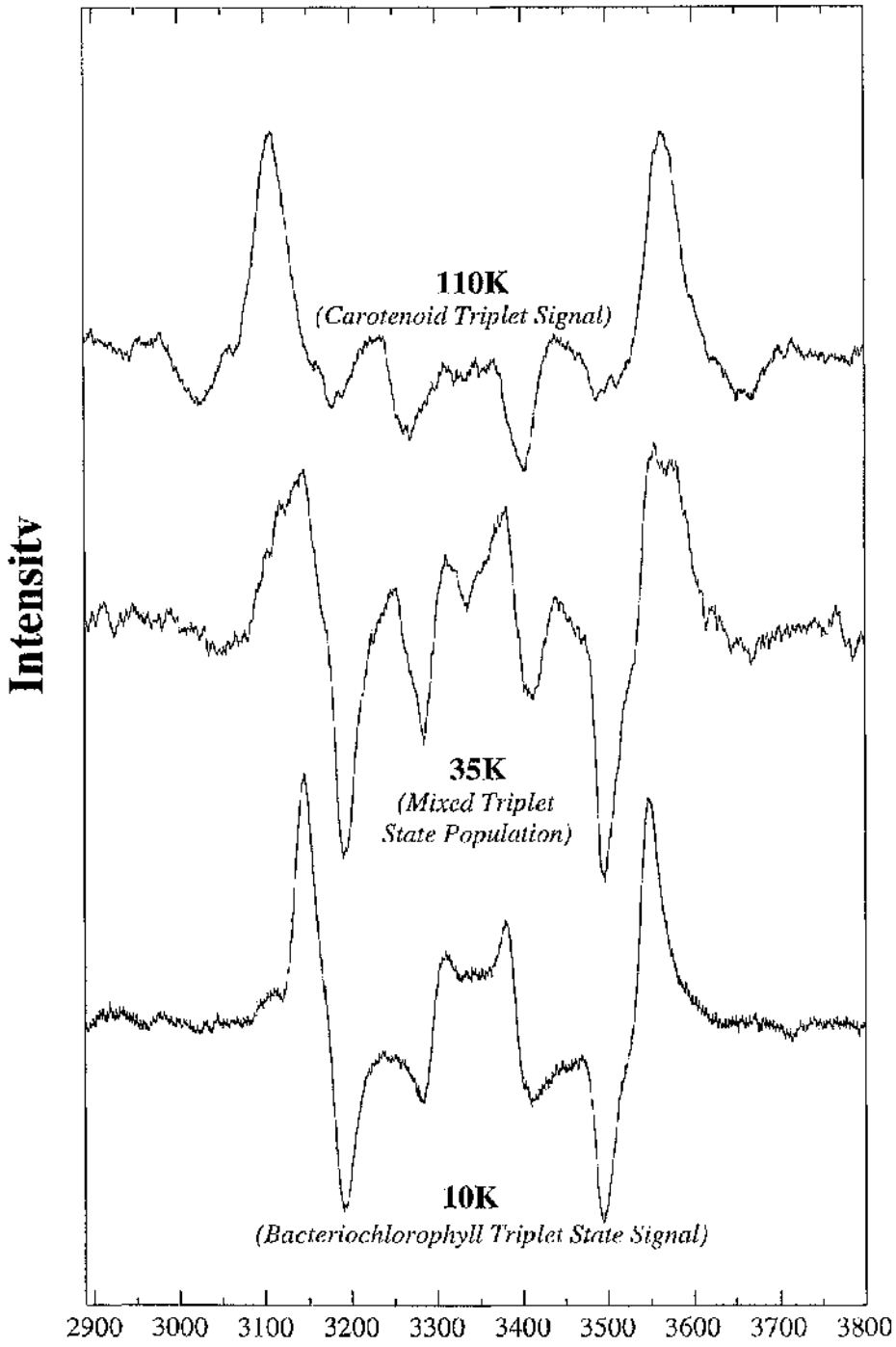

Ala M119 Reaction Centre ESR Spectra

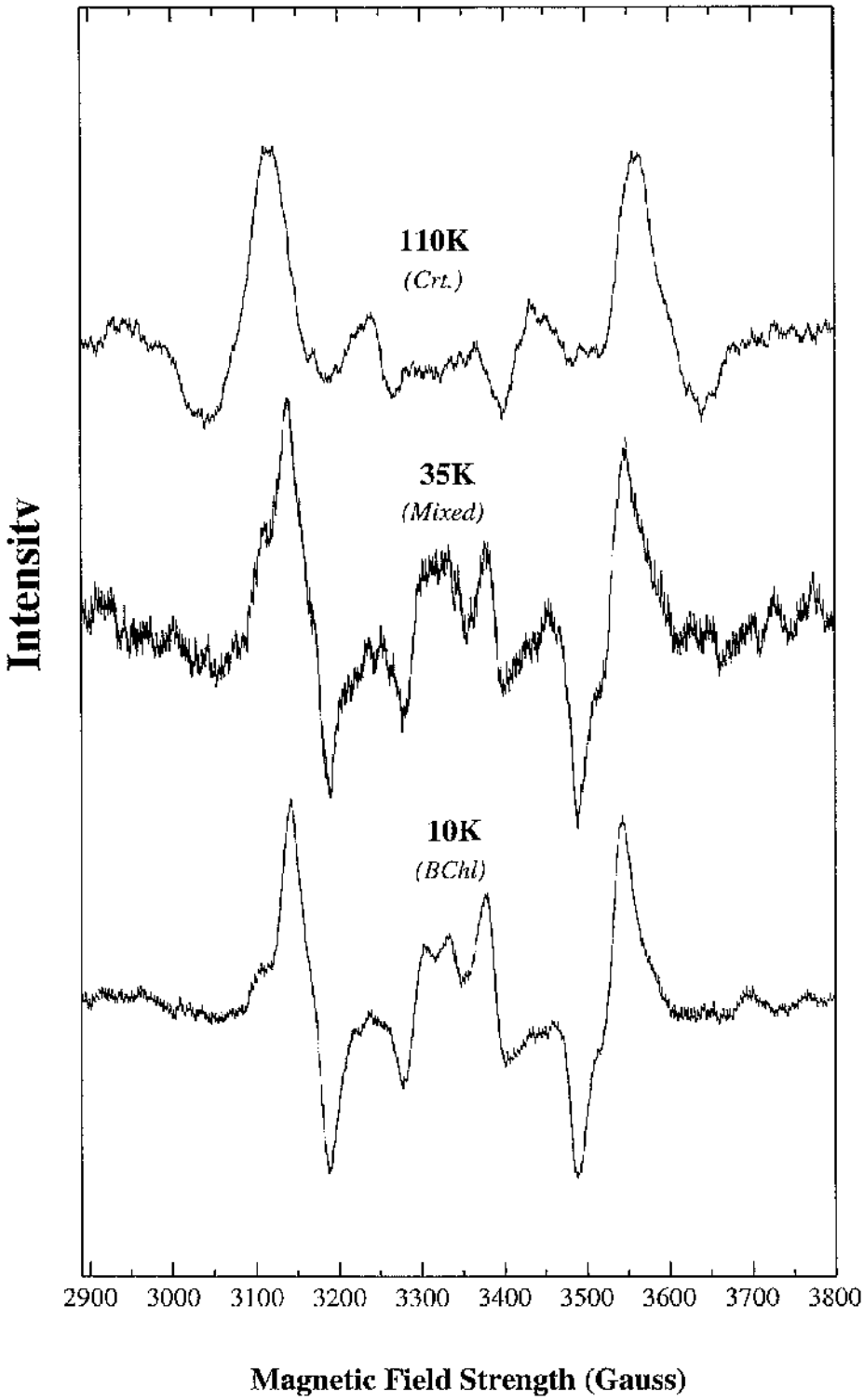

Trp M157 Red Reaction Centre ESR Spectra

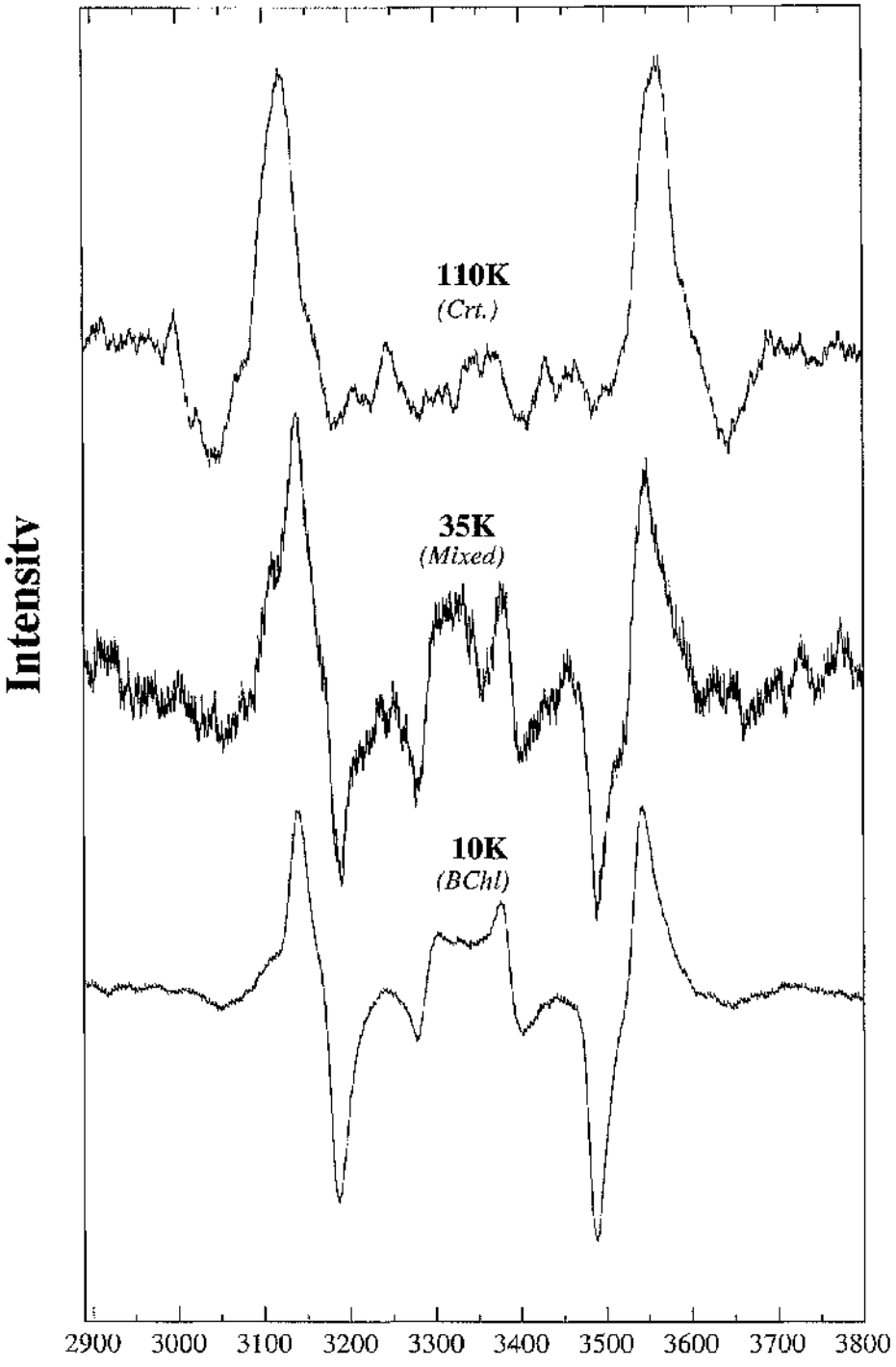

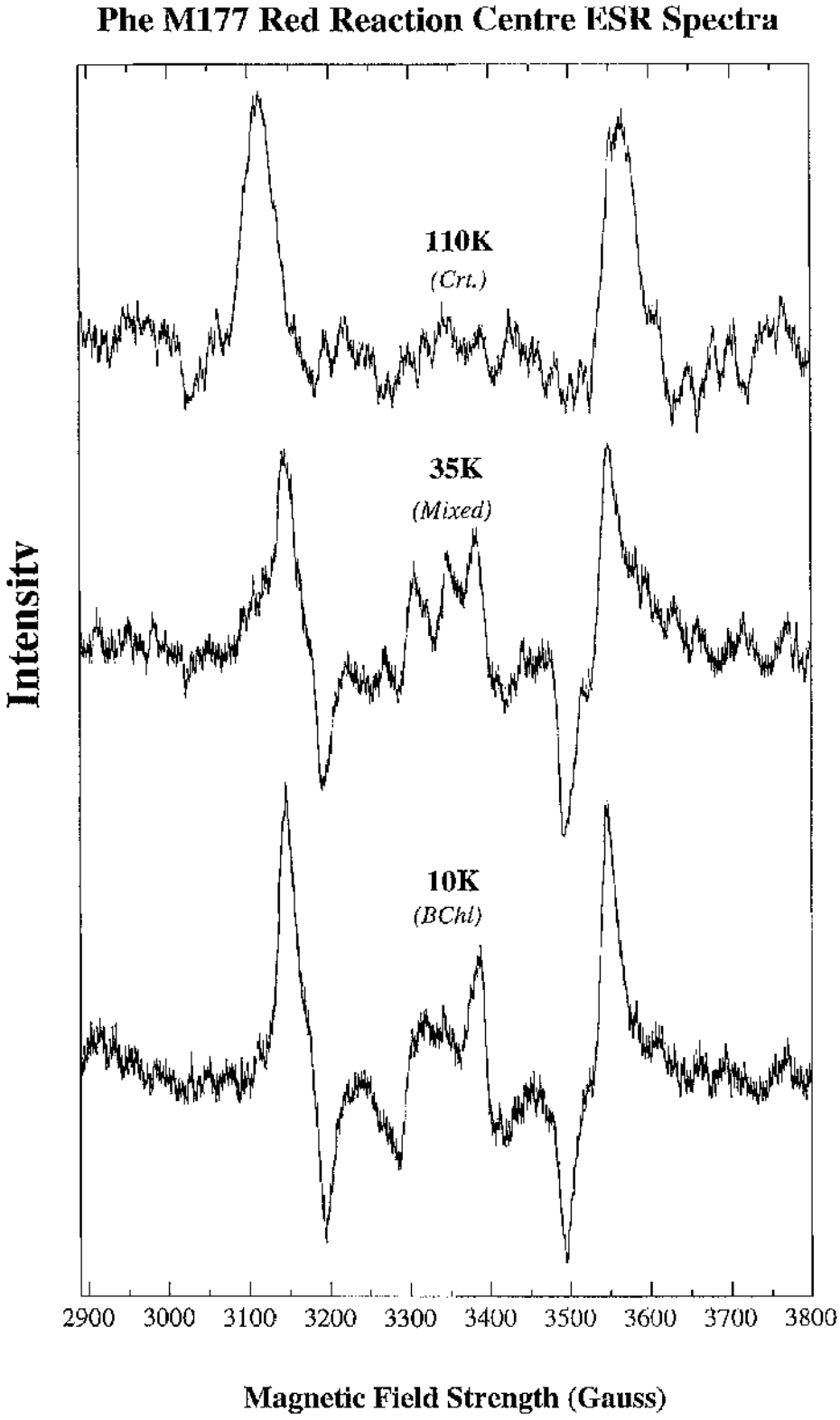
Phe M177 Red Reaction Centre ESR Spectra
110K
(Crt.)
35K
(Mixed)
10K
(BChl)
Intensity
2900
3000
3100
3200
3300
3400
3500
3600
3700
3800
Magnetic Field Strength (Gauss)

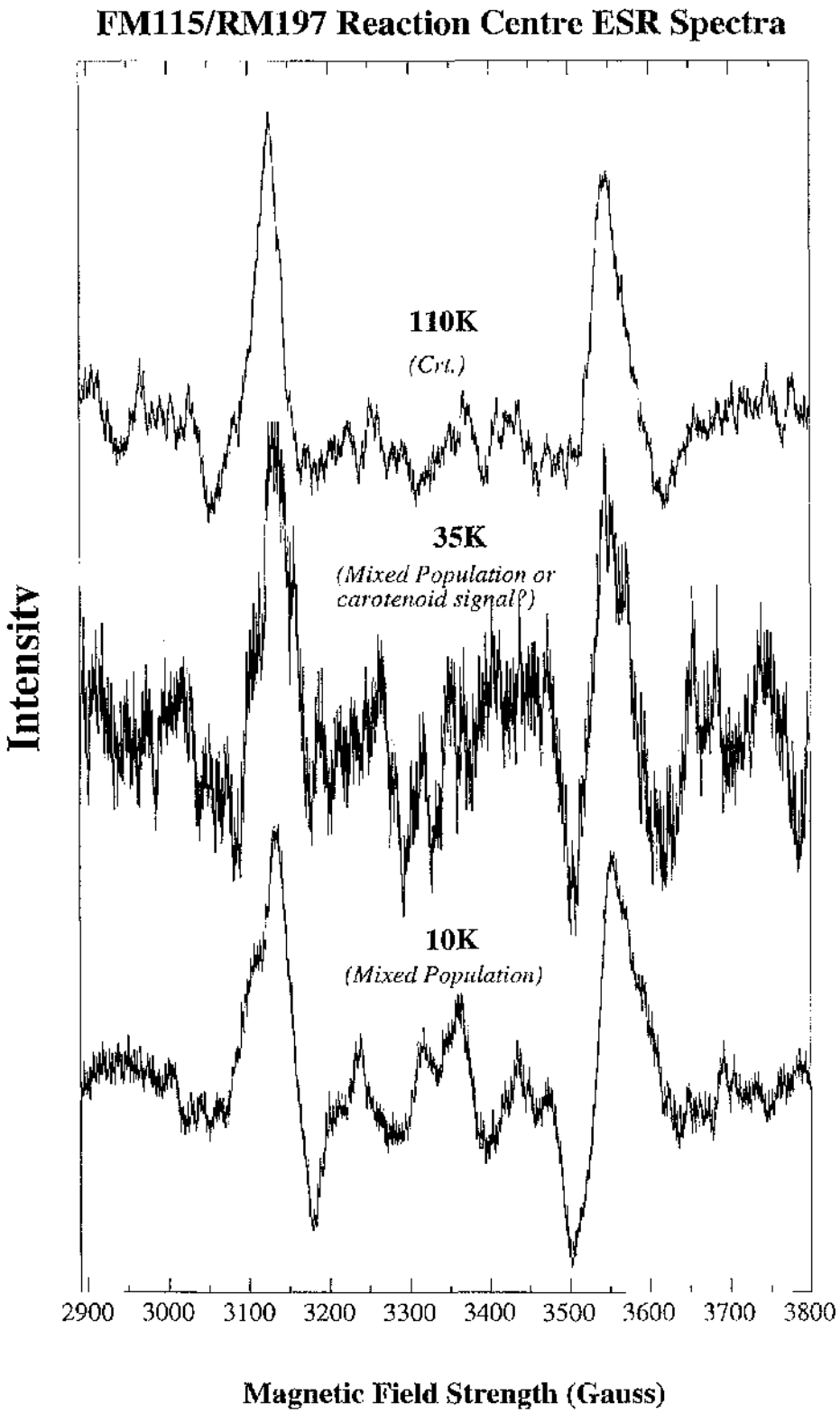
FM115/RM197 Reaction Centre ESR Spectra
110K
(Cyt.)
35K
(Mixed Population or carotenoid signal?)
10K
(Mixed Population)
Intensity
2900
3000
3100
3200
3300
3400
3500
3600
3700
3800
Magnetic Field Strength (Gauss)

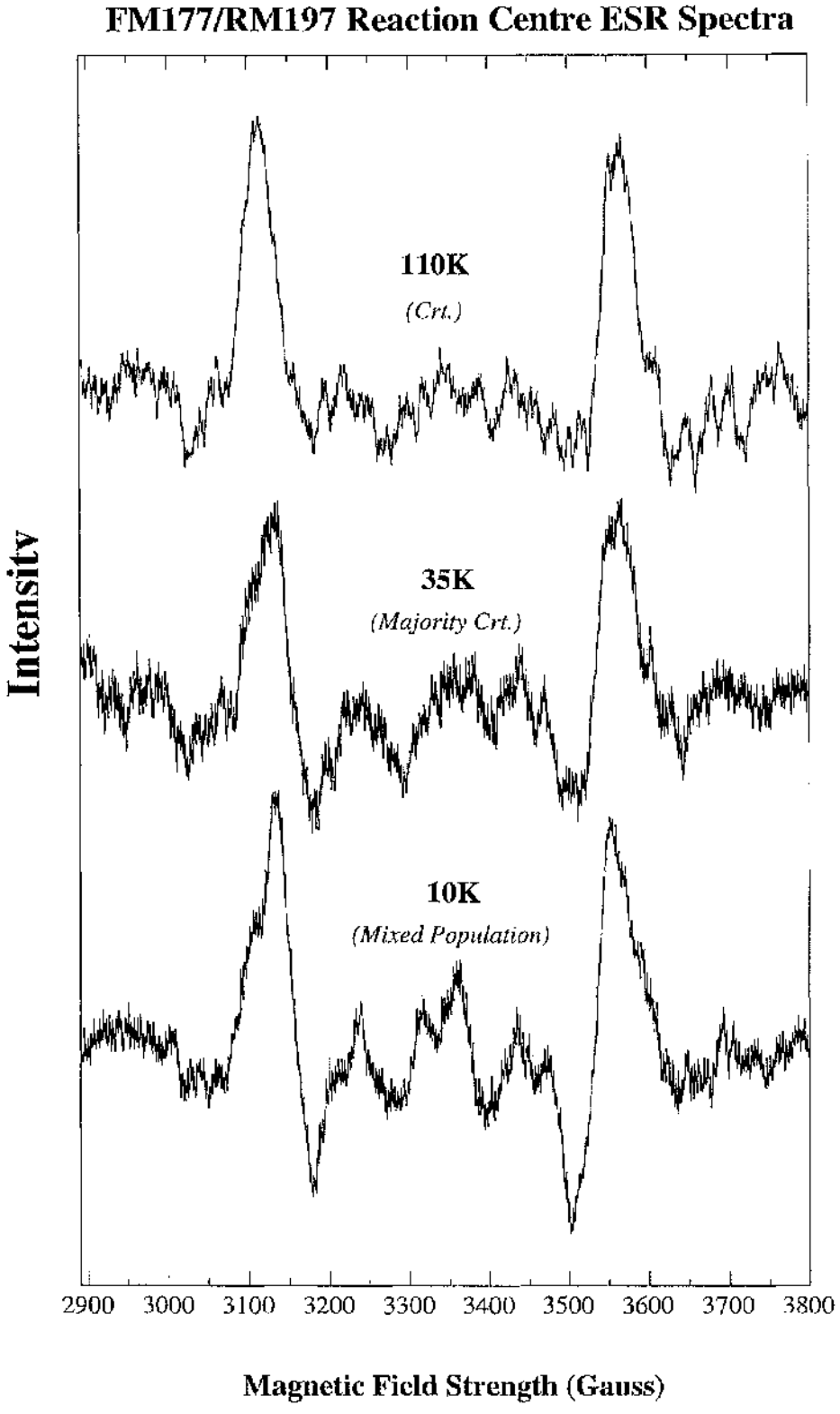
FM177/RM197 Reaction Centre ESR Spectra
110K
(Crt.)
35K
(Majority Crt.)
10K
(Mixed Population)
Intensity
2900
3000
3100
3200
3300
3400
3500
3600
3700
3800
Magnetic Field Strength (Gauss)

Arg M197 Reaction Centre ESR Spectra

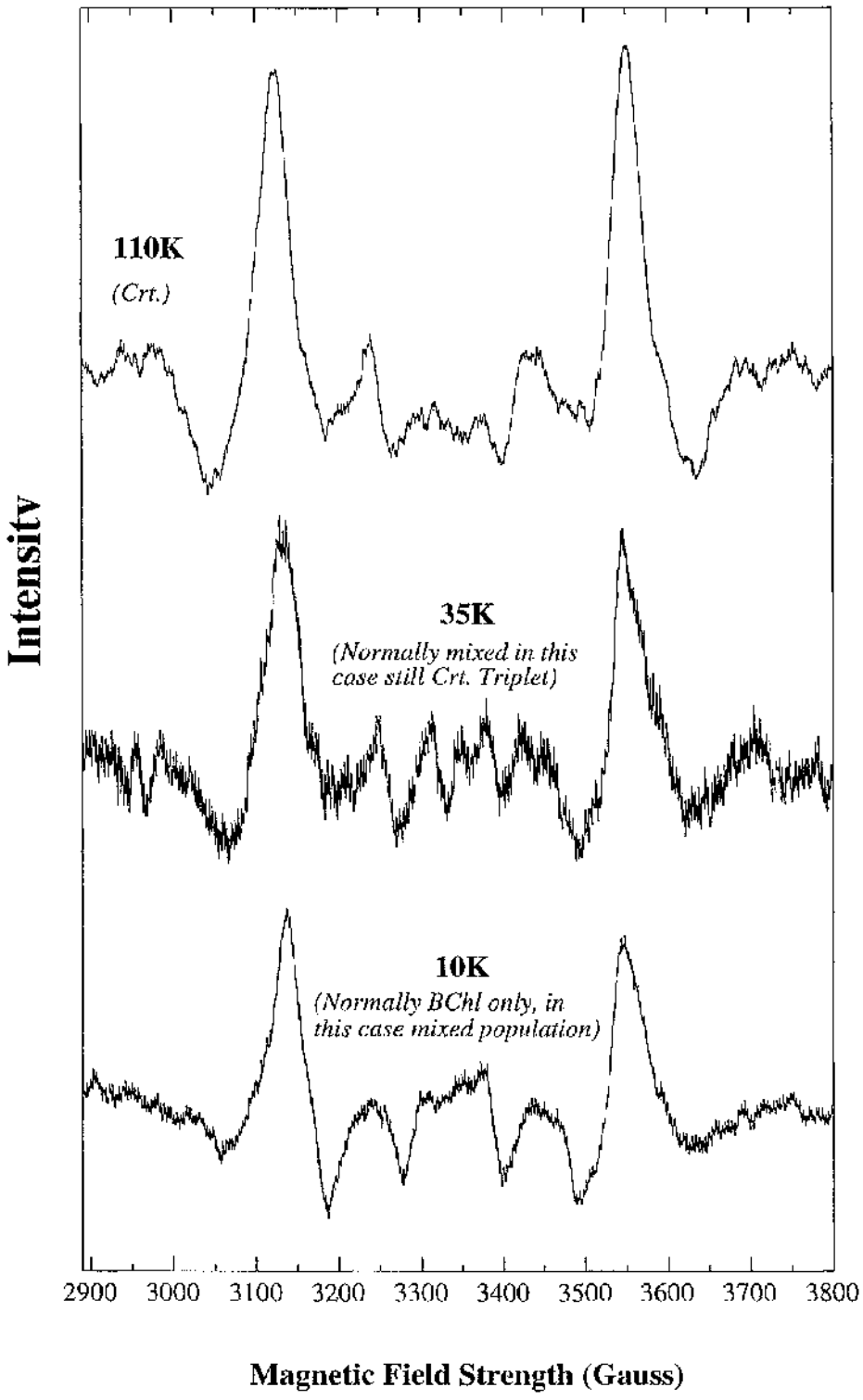

CHAPTER 12.

Crystallography: Preliminary Investigations.

This section will discuss the various investigations undertaken which have ultimately led to the successful elucidation of five different reaction centre structures. Before beginning the structural determinations it was necessary to determine crystallisation conditions which would give quality crystals in sufficient numbers to allow the collection of high quality, high resolution data. In addition the possibility of cryo-cooling the reaction centre crystals for use in X-ray analysis was investigated.

12.1. Crystallisation trials.

The optimisation of the crystallisation conditions spanned a period of over 2 years by which time the maximum resolution had dropped from the initial "Glasgow best" of 3.2Å to observed diffraction approaching 2.0Å. Unfortunately, the crystals were highly susceptible to radiation damage in the X-ray beam and although the diffraction was observed to ~2.0Å, the best data set had to be cut back to a resolution of only 2.3Å. This still remains a great improvement, a fact which is made clear when the quality of maps from a 3.1Å data set and the 2.3Å data set are compared (Figure 40). One of the main aims for future work in Glasgow is to produce conditions in which the crystals will be stable in the X-ray beam. This work has started, and some promising early results are reported in this thesis.

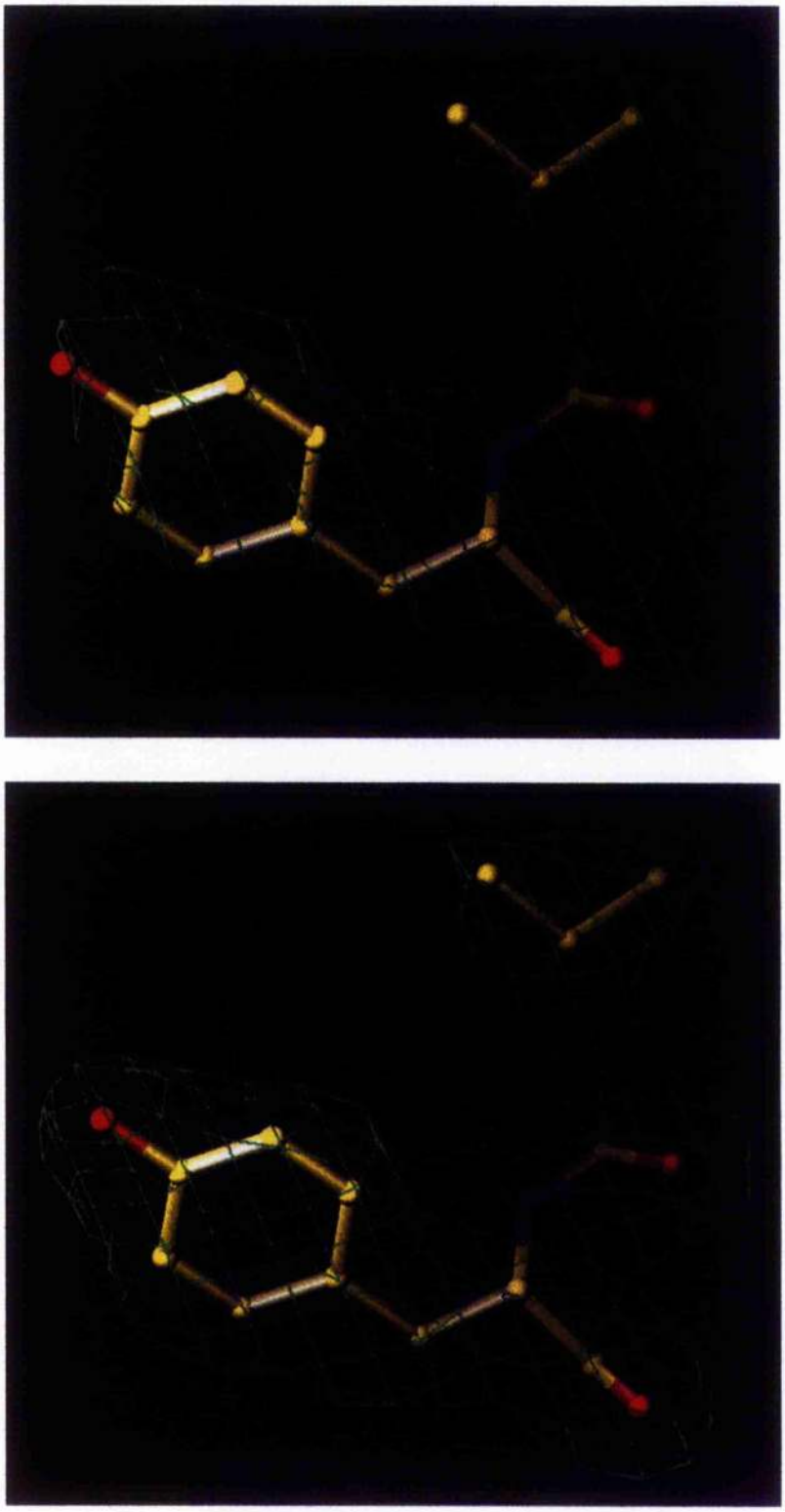

Figure 40: Comparison of the 2Fo-Fc maps taken from the same region of the reaction centre complex from two different models: (a) the WM157-F model (3.1Å) and (b) the WM115-F(2.3Å).

A wide range of different conditions were used in the attempt to get suitable crystals for X-ray analysis. These are summarised in Table 20. Initial experiments were performed on reaction centre complexes from anaerobically grown *Rb. sphaeroides* 2.4.1. The crystals which produced the highest resolution diffraction were obtained using the sitting drop vapour diffusion method. 15µl drops of ~9mg/ml protein in 20mM Tris/HCl , ~1.0M ammonium sulphate (pH of 9.5), 2.5% heptane-1,2,3-triol, 2.0% βog detergent were pipetted into a well of a cryschem plate. The outside wells contained ammonium sulphate solution in a range of concentrations varying from 1.6M to 2.1M. Large, well-shaped hexagonal crystals normally formed within two-three weeks with incubation at 18°C. Crystal dimensions were typically 1.5 x 0.6 x 0.6mm. Diffraction was observed for these crystals to a resolution of up to 2.8Å (Daresbury, Beamline 9.6).

Table 20A: The range of crystallisation conditions analysed for the reaction centre proteins‡. This table presents the data from crystallisations using ammonium sulphate as the precipitant and *Rb. sphaeroides* 2.4.1 (anaerobic) reaction centres protein. A similar system was also used for attempts at crystallisation of *Rb. sphaeroides* strains R-26 and G1C.

Ams.	[Protein] (mg/ml)	$[Ams]_{in}$ (M)	$[Ams]_{out}$ (M)	[β-OG] (%)	[LDAO] (%)	[Hpt] (%)	[TEAP] (%)	[Diox.] (%)	pH	Tot. No. Tested Conditions
Range analysed	7-9	1.0-1.4	1.4-2.4	1.5-2.0	0.1	1.5-3.5	3	1-3	9-10	202
Range most succesful.	9	1.0-1.1	1.6-1.8	2.0	-	2.5%	-	-	9.0-9.5	-

Table 20B: The range of crystallisation conditions analysed for the reaction centre proteins‡. This table presents the data from crystallisations using potassium phosphate as the precipitant and *Rb. sphaeroides* RCO2 (aerobic) reaction centre protein (wt and mutant).

Phos.	[Protein] (mg/ml)	$[Phos]_{in}$ (M)	$[Phos]_{out}$ (M)	[LDAO] (%)	[Hpt] (%)	[Hex] (%)	[TEAP] (%)	[Diox.] (%)	pH	Tot. No. Tested Conditions
Range Analysed	9-10	0.65-1.1	1.4-2.1	0.09-0.12	1.8-3.5	2	3	1-3	7.0-8.0	92
Range most useful	9-10	0.7-0.8	1.5-1.6	0.09	3.5	-	-	-	7.5	-

‡ These tables comprise details of the most commonly investigated paramters. Other parameters were also investigated including additives such as EDTA and glycerol, various other buffer systems (CAPSO, CHES & AMPSO), the concentration of Tris/HCL buffer, trials into the effects of NaCl on crystallisation and also methods by which buffer/detergent exchange and concentration of the protein was performed.

Crystals of the RCO2 strain reaction centres were produced using the same technique. However the conditions required were quite different. 15µl drops of 9mg/ml protein in 10mM Tris/HCl, ~0.7M potassium phosphate (pH of 7.5), 3.5% heptane-1,2,3-triol, 0.09% LDAO detergent were pipetted into the sample wells of Cryschem plates. The outside reservoirs contained a range potassium phosphate solutions between 1.3M and 1.7M. Crystals normally formed within two weeks, although occasionally within one week, with incubation at 18°C. Crystal dimensions typically ranged from 0.3 x 0.3 x 0.3mm to 1 x 0.3 x 0.3mm, although occasionally much larger crystals up to 2mm in length were obtained.

Diffraction of X-rays from these crystals ranged from ~3.0Å to approaching 2.0Å. Sample X-ray diffraction patterns are shown in Appendix IV. The first image shown in the appendix is of an image which was collected at room temperature on a 30cm MAR image plate at Daresbury, station 9.5, and was generated by exposure of a FM115/RM197 red crystal. The outer resolution limit is 2.2Å, the zoomed image shows the diffraction to the outer edge of the plate: with longer exposure times greater resolution may have been obtained. The remaining images are of cryo-cooling trial exposures performed at Glasgow on the DIP 2000. Data sets were collected from all of the RCO2 mutant strains, with the exception of the MM122-L mutation, plus additional data sets were collected for the "wild-type" reaction centre and for the single RM197 reaction centre. The crystals produced were all trigonal and belonged to the space group $P3_121$ and had approximate unit cell dimensions of a=b=142Å, c= 188Å, $\alpha=\beta=90°$ and $\gamma=120°$. The collection and processing statistics generated for each of the collected data sets are presented in Table 21, and photographs of typical crystals are shown in Figure 41.

Table 21: The data collection statistics, and the statistics generated from DENZO and SCALEPACK for all of the crystallographic data sets collected in the course of the project.

	WT red	WM115-F	SM119-A	WM157-F	YM177-F	FM197-R
Max resolution of diffraction. (Å)	2.4	2.25	3.0	2.5	2.45	2.4
Max resolution of data set. (Å)	2.6	2.3	3.1	3.1	2.55	2.55
Completeness	95% (98%)	95% (71%)	88% (94%)	84% (90%)	76% (83%)	94% (97%)
No. of unique reflections.	64069	90885	35223	33688	54163	67571
Rmerge.	7% (40%)	11% (53%)	8% (29%)	7% (31%)	13% (36%)	9% (39%)
No. of reflections, I > σ.	59649	84549	33532	32135	52077	64366

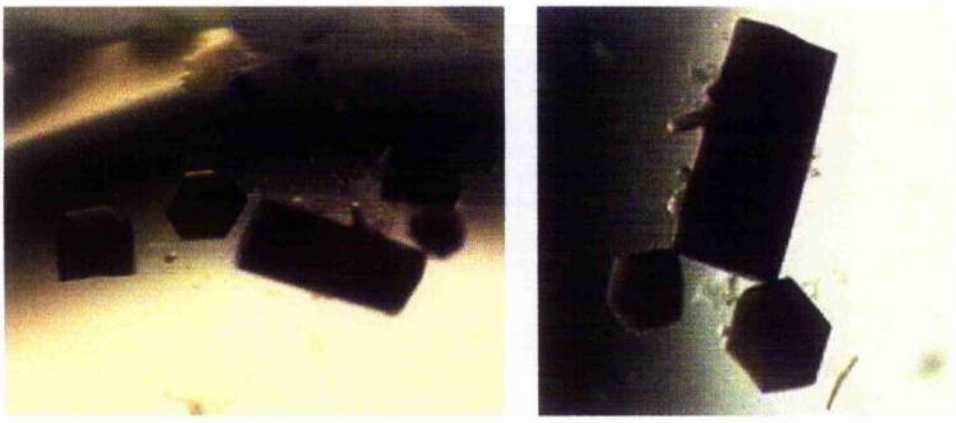

Figure 41: Photographs of typical crystals produced from reaction centres from RCO2 strains of *Rb. sphaeroides*. The dimensions are approximately 1.5 mm x 0.6 mm x 0.6 mm.

Table 21, above, gives two values for the maximum resolution; the maximum resolution of diffraction and the maximum resolution of the data set. Crystals, as mentioned in section 9.2.2, are susceptible to damage in the X-ray beam. As diffraction data collection continues, so the maximum extent of diffraction from the crystal decreases because of the increased damage to the crystal. The RC crystals proved to be susceptible to this damage, and therefore although initial diffraction from crystals, for example the WT red, was to beyond 2.4Å after only 10 frames diffraction to this extent was lost. This has the effect of making the processing and scaling statistics for the higher resolution shells very poor. The quality of the data sets drops at the outer shells because firstly the redundancy drops, i.e. the number of observations for the same reflection drops, and secondly

scaling of the images becomes increasingly problematical as, for example, the outer spots decrease in intensity. Therefore, the data used for subsequent refinement of the reaction centre structures normally had to be cut off at a lower resolution than the absolute diffraction limit.

12.2. Cryo-cooling trials.

The trials were split into two groups. Early trials, based upon simply soaking the crystals briefly in the cryo-protectant solution before quickly mounting in the cryostat stream, proved to be relatively unsuccessful. Initial attempts were based around the use of glycerol as the cryo-protectant. The solutions were prepared in buffer containing a similar concentration of KPi as was in the outer well of the crystal plate from which the crystals were taken. The crystals were isolated from the well using a cryo-loop and soaked for 10secs - 1min in the cryo-protectant solution. The crystals were then quickly taken back up in the loop and placed into the cryostat stream (100K). This method was superseded by button dialysis, in which the cryo-protectant is slowly dialysed into the mother liquor surrounding the crystal. It was hoped that by slowing the rate of equilibration of buffers the "shock" to the crystal would be reduced, and therefore the crystal would remain undamaged by the process.

Table 22: The range of cryo-protectant solutions used in the experiments. *0.06% corresponds to the approximate concentration of LDAO in the crystallisation well after addition of all components. [† Work not presented in this thesis has allowed the collection of a data set of another mutant strain to ~2.75Å (Daresbury, Beamline 7.2). Unfortunately time did not permit the collection of sufficient data to collect high completeness. The mosaicity of the crystal was also observed to have been significantly increased, and the unit cell dimensions had decreased from 142Å to 138Å in two dimensions and 187Å to 186Å in the third.].

Putative Cryo-protectant Compound	Conc.	LDAO % (v/v)	β-OG %(v/v)	Heptane-triol	Mosaicity	Resolution Best Result Å
Room Temp.	n/a	n/a	n/a	n/a	≤0.1	~3.0
Glycerol	30-50%	0.09-0.06*	1.6%	0, 3.5%	0.2-0.3	~3.2
Butane-diol (r/r)	8-11%	0.06	1.6%	3.5%	0.2-0.3	~3.0
Ethylene Glycol	30%	0.06	-	3.5%	~0.8	~2.75†
Xylitol	11%	0.06	-	3.5%	n/a	n/a
Erythritol	22%	0.06	-	3.5%	n/a	n/a
Sucrose	2M	0.09	-	-	n/a	n/a
Fructose	20%-40%	0.09	-	-	n/a	n/a
Glucose	30%	0.09	-	0, 3.5%	n/d	~8.0

The "quick-soak" technique did not provide high resolution diffraction in any of the trials. The best achieved was provided by a soak in 30% glycerol, in "equilibrated" mother liquor (i.e. mother liquor of the same concentration as would be found in the well from which the crystal was taken), and in 0.09% LDAO detergent. The soak lasted for approximately 30 seconds, and the crystal was transferred to the cryostream within 2-3 seconds from removal from the cryo-protectant. This particular trial was performed on Daresbury synchrotron station 9.5, and provided diffraction to at best, 3.5Å. However, the same batch of crystals were diffracting beyond 2.25Å when routine room temperature exposures were performed.

The button dialysis technique provided greater success. Presumably this was due to the slower exchange of the initial mother liquor within the crystal with cryo-protectant. Koepke et al (1996) discuss the problems they faced handling crystals of LH II from *Rps. molischianum*. The crystals had

to be maintained in a saturated heptane-1,2,3-triol solution at all times. Up to this point, all the cryo-cooling trials had been performed using cryo-protectant solutions which did not contain the amphiphile. Trials performed by dialysis against cryo-protectant solutions, in which heptane-1,2,3-triol was absent, did not provide results significantly better than those of the "quick-soak" protocol. However, diffraction was observed from a soak against 30% glycerol, "equilibrated" mother liquor, 0.09% LDAO buffer which had been saturated with heptanetriol, to approximately 3.5Å. Trials of soaked crystals prepared by button dialysis were performed on the in-house Siemens area detector. The level of diffraction of the above soaked crystal compares favourably with the diffraction normally observed from room temperature experiments on this detector system.

Further experiments were performed, in which the concentrations of detergent and amphiphile were carefully calculated to generate the same ratio as would be found in the crystallisation well. If the amphiphile was responsible for increasing the quality of the diffraction from the frozen crystals, then it was hypothesised that the ratio of amphiphile to detergent could be crucial. The crystals for these trials were all selected from the same crystallisation tray. Room temperature exposures were performed following two separate protocols. Firstly, crystals were taken straight from the tray and mounted in the normal manner. Secondly, crystals were dialysed overnight against the mother liquor used in the cryo-cooling experiments, but to which no putative cryo-protectant had been added. These two experiments gave very similar limits of diffraction of approximately 3.2Å (Siemens area detector). Thus soaking overnight in the artificial mother liquor did not appear to be responsible for any decay which might be occurring in the crystal.

Cryo-cooling experiments were then performed, again using crystals from the same batch. Two dialysis experiments were set up, with dialysis against buffers containing 0.06% LDAO, 3.5% heptanetriol, 1.2M KPi, pH7.5 (pH and [Kpi] corresponds to that used in the crystallisation) and either 30% glycerol, or 30% ethylene glycol. These crystals both generated diffraction images with a maximum resolution of approximately 3.2Å, i.e. of the same quality as the room temperature experiments. "Quick-soak" experiments using identical buffer systems failed to provide diffraction to beyond 8Å, and this protocol was therefore dropped in favour of dialysis.

Several other putative cryo-protectants were then investigated, two more sugars, erythritol and xylitol, and a specific isomer of butanediol, R,R-2,3 Butanediol. The results obtained from experiments with erythritol and xylitol followed the previous lack of success with other sugar forms. However, butanediol showed much more promise. A single experiment with dialysis of a crystal against 8% butanediol, 3.5% Hpt, 1.4M Kpi produced a diffraction pattern to approximately 3.2Å on the Nonius DIP 2020 at Glasgow. The level of mosaicity was increased (~0.6), but not as far as had been previously observed with ethylene glycol (~0.8). Experiments conducted at the same time as this may have identified methods by which the mosaicity of the crystal can be reduced.

The mosaicity gives a measure of the level of disorder in the crystal. Typical room temperature data sets showed a mosaicity figure of around or below 0.1. Mosaicity manifests itself in the diffraction pattern, with the number of spots on the image increasing. This caused great problems for the collection of reaction centre data, where the large size of the unit cell had already required careful planning of the data collection strategy to limit the number of overlapping spots on the image. The increased mosaicity, it was hypothesised, was most probably caused at one of two points in the protocol. Firstly, dialysis instead of "quick-soaking" had already been observed to lead to an improved final product, i.e. the diffraction pattern. It was thought that slowing the introduction of the cryo-protectant might improve things still further. To this end, serial dialysis was investigated, where the crystal was dialysed against four solutions, stepping up the concentrations of the cryo-protectant in each.

Secondly, the method by which the crystals are frozen was considered. Until this point, flash freezing was performed by placing the crystal into the cryostream *in situ* on the goniometer. In doing so, the crystal is cooled at a relatively uneven rate. One potential remedy for this problem is to freeze the crystal by plunging in liquid nitrogen prior to mounting in the X-ray beam. This second procedure was adopted, with transfer from the liquid nitrogen to cryostream of the crystal performed with Cryotongs (Hampton Research, U.S.A.). The tongs maintain the crystal at liquid nitrogen temperatures for sufficient time to install the crystal on the goniometer. In addition, Michel (1991) had noted that reaction centre

crystals grown in LDAO, showed lower levels of mosaicity in diffraction experiments, if they had been dialysed against β-OG prior to mounting in the X-ray beam. The combination of serial dialysis and inclusion of β-OG in place of LDAO in the dialysis, and the pre-freezing of the crystal in liquid nitrogen led to a drop in the mosaicity of ~0.4 from ~0.7 to ~0.3 (30% Glycerol was the cryo-protectant). More recent experiments using butanediol achieved diffraction to ~3.0Å with a mosaicity value of ~0.2. Therefore, it is hoped that the results presented in this sub-section will allow ideal conditions to be determined in the relatively near future.

CHAPTER 13

Crystallographic Structure Determinations.

13.1. Wild Type Structure for *Rb. sphaeroides* RCO2.

A model for the WT red reaction centre structure was elucidated to a resolution of 2.6Å. This, until very recently, compared with the highest resolution published of a *Rb. sphaeroides* reaction centre at 2.65Å. However, two new models have been reported by Stowell et al (1997) with resolutions of 2.2Å and 2.6Å. The detail available on these new structures is limited, and the co-ordinates have yet to be released. For this reason, the following discussions of comparison of the WT red and mutant structures with previous *Rb. sphaeroides* reaction centres will not include the models of Stowell et al (1997). The discussions begin with a description of the WT red structure, including a detailed comparison with the 2.65Å structure of Ermler et al (1994). The two models were compared, and apart from a few regions, the models were found to be in close agreement. However, a residue which may be involved in the strong selection of methoxy/hydroxy carotenoids by *Rb. sphaeroides* reaction centres was identified and an alternative configuration for one of the 2-acetyl groups from one of the BChls of the special pair has been proposed.

13.1.1. Quality of the Model.

The WT red model is to a resolution of 2.6Å with diffraction initially observed to ~2.4Å. The data was collected from exposure of a single crystal at Station 9.5 at Daresbury. To minimise the effects of radiation damage the crystal was translated three times during the data collection. The model presented is fully refined, with 108 waters and four LDAO molecules built in. The refinement of the structure was based on 64069

unique reflections between 11 and 2.6Å, with reflections with $I<1\sigma$ rejected. The calculation of the R-free was based on 5% of the reflections, selected randomly. The behaviour of R-free was monitored throughout the procedure to guard against overfitting of parameters. Individual atomic temperature factors were refined isotropically. The refinement statistics and measurements of the quality of the geometry of the model are presented in Table 23.

Table 23: The crystallographic/refinement statistics and measurements of the quality of the geometry of the WT model of *Rb. sphaeroides* RCO2. $R_{merge} = \Sigma_h\Sigma_i|<I(h)>-I(h)_i|\Sigma_h\Sigma_i|I(h)_i$, where I(h) is the intensity of reflection h, Σ_h is the sum over all reflections and Σ_i is the sum over all i measurements of reflection h. The R-factor is defined by $\Sigma||Fo|-|Fc||/\Sigma|Fo|$; Free-R was calculated with 5% of the reflections, selected randomly (Brünger, 1992). The Ramachandran plot was produced using Procheck version 3.0. (Laskowski, 1993), and the co-ordinate error was estimated from a Luzzati plot (Luzzati, 1952), both plots are presented in Appendix IV (see also below).

Data Collection Statistics	
Resolution Range	11-2.6Å
Rmerge	7.0%
Number of Unique Reflections	78013
Completeness of Data	90.6%
Refinement Statistics	
Number of selected reflections $F > \sigma F$	57980
R Factor	18.3%
Free-R Factor	20.4%
Average B-Factor:	
Overall	44.6Å^2
Main Chain	51.0Å^2
Side Chain	51.1Å^2
Geometry	
RMSD from Ideality:	
Bonds	0.012Å
Angles	1.68°
Impropers	2.17°
Ramachandran Plot:	
Most favoured areas	90.7%
Additional allowed areas	9.0%
Generously allowed areas	0.3%
Disallowed areas	0.0%
Co-ordinate Error	0.3Å
Model	
No. of Protein Residues	823
No. of Pigment Molecules	4 BChl, 2 BPheo, 2Ubi, 1 Spo, 1 Fe
No. of Waters	108
No. of Detergents	4

Appendix IV presents two forms of plot, the Ramachandran plot of each of the crystal models (models of four carotenoid mutants plus models of the RM197 mutant follow) and Luzzati plots for those models which have been fully refined. The Ramachandran plot represents the torsional angles ϕ and Ψ on either side of the α-carbon of each individual residue. Model studies have shown that these angles are greatly restricted by steric repulsion, and therefore all of these angles should fall into the "allowed" conformational angles. The plot itself, plots ϕ versus Ψ for each residue, against a background in which the regions in which allowed $\phi\psi$ pairs are found are marked as a contour. The Luzzati plot is used to estimate the precision in a refined crystallographic model. The uncertainty depends upon the R-factors derived from the final model at various resolution shells. The plot is of the R-factor versus the mid-point value of $1/d(Å^{-1})$ for each individual resolution shell. Lines, depicting theoretical estimates of the average uncertainty in the positions of atoms in the refined model, are drawn. The curve produced from the refined model should roughly fit one of the theoretical curves, in turn providing an estimate for the average uncertainty for the atom positions.

A portion of the $2F_O$-F_C electron density map, contoured at the 1σ level and covering the porphyrin ring structures of the four Bacteriochlorophyll molecules of the reaction centre is shown in Figure 40. The special pair rings are shown edge on as would be seen if the reaction centre pigments were observed from the periplasmic side of the membrane. The density map for the model was generally excellent. However the map was poor in some isolated regions of the complex. The ends of the protein subunit chains all showed high levels of disorder. A similar problem was described for the 2.65Å structure, with residues 251-260 of the H-subunit and 303-307 of the M-subunit effectively missing from the density map.

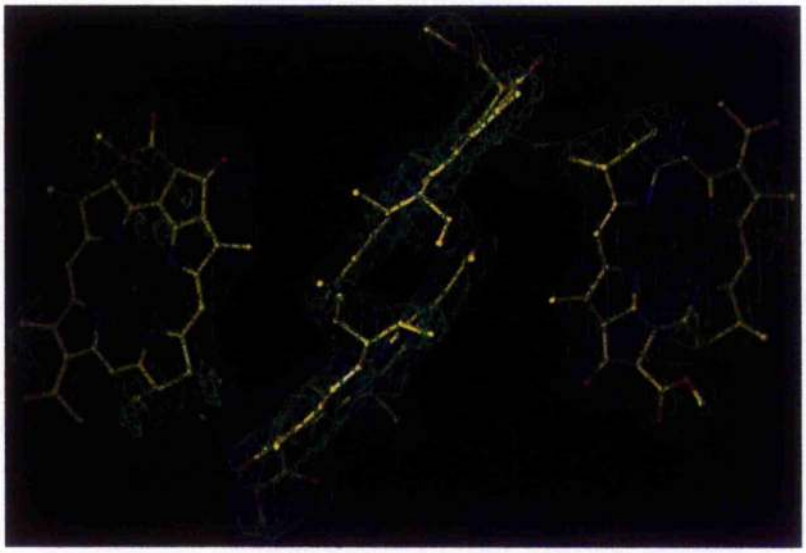

Figure 42: The 2Fo-Fc electron density map for WT red at 2.6Å resolution showing density for the special pair and accessory BChl rings. The map is contoured at the 1σ level.

13.1.2. Similarity with Previous Models: The Protein Subunits.

The co-ordinates of the RCO2 model were analysed to estimate the level of identity with the model described by Ermler et al (1994). The program LSQKAB (CCP4, 1994) was used to superimpose the C-alphas of the two models, giving a rms displacement of 0.352Å. Figure 43 shows the variance of each residue in the two structures for all three subunits. The level of structural conservation is greatest within the main body of the complex. The transmembrane regions (marked by black bar in Figure 43) show the lowest levels of variance, whilst regions exposed on the surface of the protein and especially the C-terminal end of the H-chain show the highest levels. The overall structure of the protein subunits is, therefore, very similar to the previous models. This would be expected given that the two proteins are highly homologous, and that the crystal form is the same. Perhaps of more interest, given the marginally higher resolution for this structure, is the detailed interactions of the protein residues with the range of pigment molecules held within this protein cage.

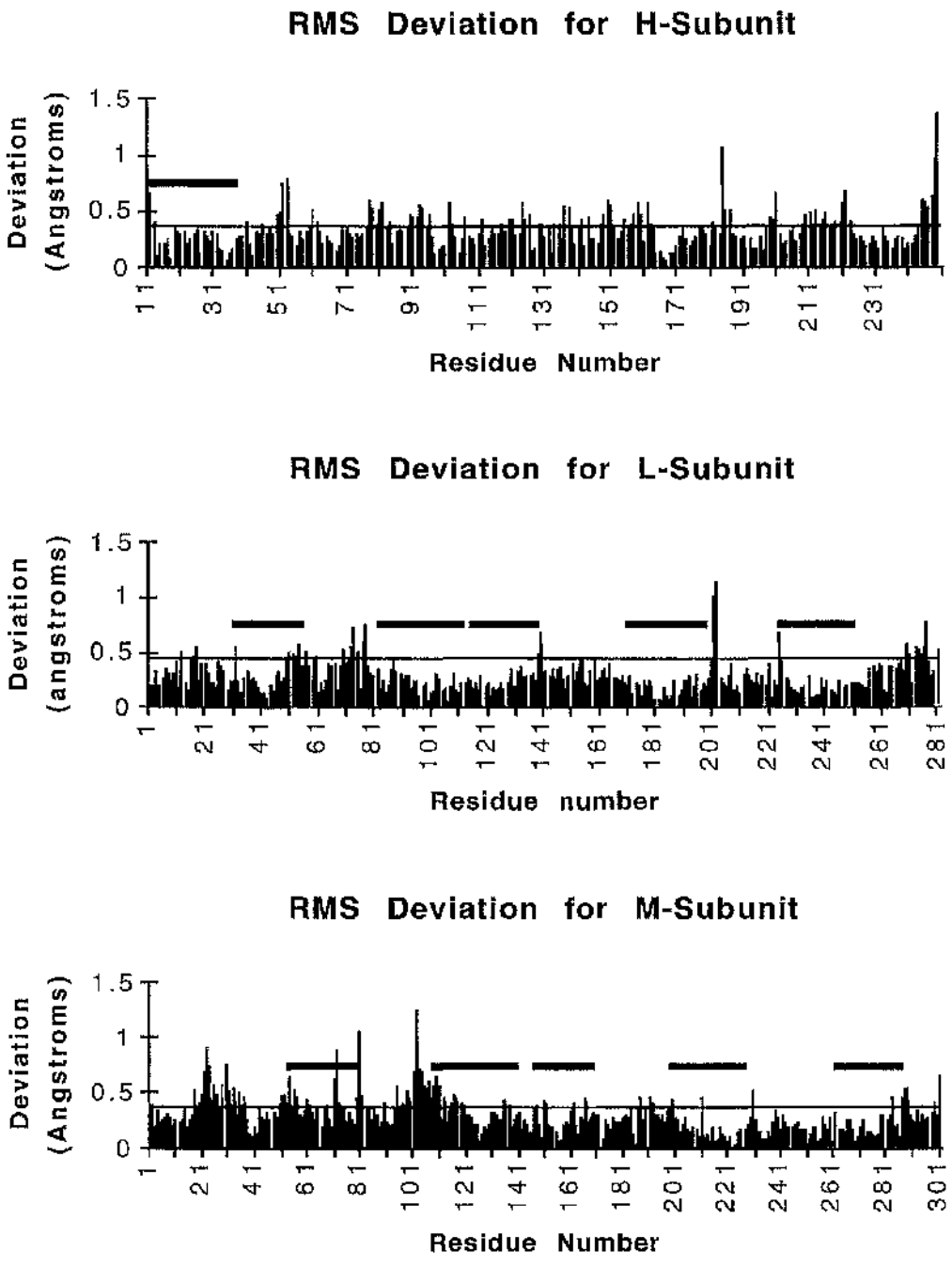

Figure 43: Charts showing the distance between the C-alpha backbone co-ordinates from Ermler et al (1994) versus the RCO2 WT red structure. Solid bars represent the transmembrane regions of the subunits, the continuous line shows the average rms deviation at 0.352Å.

Detailed analysis of the individual amino acid side chains identified very few residues with significant alteration between the two compared

structures. One potentially very interesting difference is the side chain orientation of tryptophan M75. This residue lies in close proximity to the methoxy group at the end of the carotenoid. As mentioned in Section 2.4.5. of the Introduction, reaction centres from *Rb. sphaeroides* show strong binding preference for methoxy/hydroxy carotenoids. To date, an particular amino acid side-chain has not been proposed to perform the selection procedure. The structure of the reaction centres previously published did not produce any likely candidates for this. However, in the WT red model, and in all other models produced in this thesis, Trp M75 clearly assumes an orientation not modelled in any of the other structures (Figure 44). The resulting model places the N atom of the indole ring of the tryptophan side chain in a position which could potentially lead it to perform as the "selector" for methoxy/hydroxy carotenoids. The distance separating the oxygen atom on the carotenoid and the nitrogen atom held in the Trp side chain is approximately 3.2Å Further research, in which the Trp at M75 is being replaced with a Phe residue is currently being performed (M.R. Jones & Ridge, J.P., personal communication)

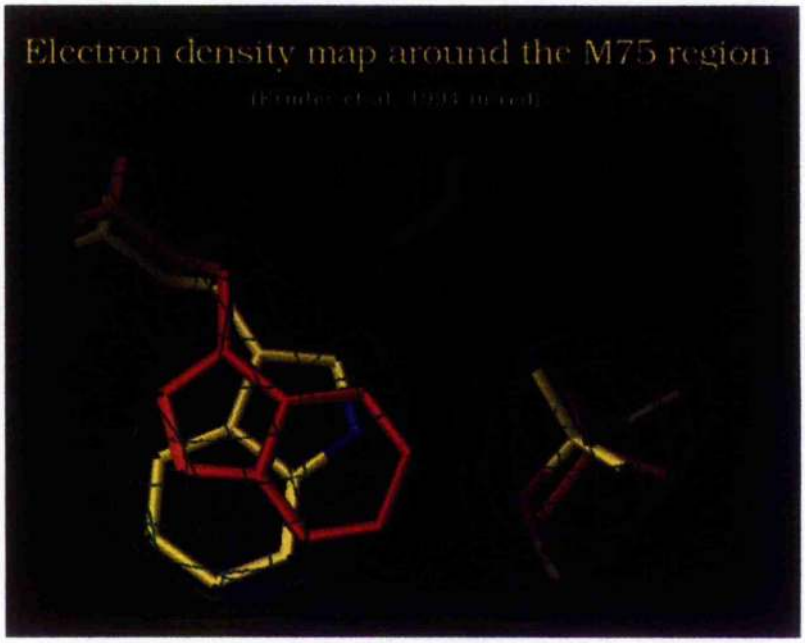

Figure 44: Tryptophan M75 as found in all the RCO2 reaction centre models. This position and orientation of the side-chain places the N-atom of the indole ring in a position where it could interact with the methoxy/hydroxy groups of carotenoids in the reaction centre. The 2Fo-Fc map, and RCO2 model co-ordinates are from the FM115/RM197 model. The map is contoured at the 1σ level.

13.1.3. *Similarity with Previous Models: The Cofactors.*

This section will deal with the binding of the various co-factors within the reaction centre. The high level of conservation of the arrangement of the cofactors in the two strains makes a detailed comparison unnecessary. Thus, the report will concentrate on the regions which do show some differences between the structures for detailed investigation, and confine the explanation of the highly homologous regions to only brief remarks. Table 24 reports on the distances obtained from the WT red model for some of the more heavily investigated interactions in the reaction centre. Also given is the mean value for these distances as determined from the six PDB files available for *Rb. sphaeroides* reaction centres in the Brookhaven Data Bank, plus WT red, along with the calculated deviation in these values.

Table 24: This table presents a small selection distances between groups whioch have been the centre of recent publications. The distance as measured in the WT red structure is presented, as is the mean distance from all the reaction centre models whose PDB files are available.

From	To	WT Red Model Distances Å	†Mean. Dist. Å	Overall Deviation Å	References to investigations probing the importance of these residues by site-directed mutagenesis.
HisL173 NE2	D_A Mg^{2+}	2.67	2.52	0.5	McDowell et al (1991)
HisM202 NE2*	$D_B Mg^{2+}$	2.65	2.31	0.7	Huber et al (1996)
His L168 NE2	D_A OBB	3.01	3.11	1.08	Murchison et al (1993) Rautter et al (1995) Mattioli (1994)
‡EL104 OE2	H_B OBD	2.79	2.76	0.3	Bylina et al (1988) Kirmaier et al (1995a) Kirmaier et al (1995b)
YM210 OH	D_B CMB	3.55	3.51	0.75	Finkele et al (1990) Hamm et al (1993)
YM210 OH	B_A CHD	3.85	3.78	1.15	Nagarajan et al (1990) Nagarajan et al (1993) Shochat et al (1994)
YM210 CD2	H_A CBB	3.22	3.34	0.17	Beekman et al (1994) Vos et al (1996)

The arrangement of the pigments (only the head groups of BChl, BPheo and Ubi), molecules in the Ermler et al model and the RCO2 model were superimposed (Figure 45) along with the other six published reaction centre models. The agreement in the structure of these groups in the all of the models was very high. Some alterations were detected in the conformation of the ends of the carotenoid molecule, but in general the head groups of the pigments closely resembled each other. However, the hydrocarbon chains of the BChl, BPheo and Ubi molecules did show some marked differences. The position of Q_B in the models is, however, more variable. Interestingly, the structures produced from X-ray studies on the trigonal form of reaction centre crystal, have both produced models, where

the Q_B is inserted significantly further into the reaction centre, than in any of the other models. This position was assigned to all of the structures determined in this thesis. Reasons for the variability in the determined structures for this region of the complex include: i) differences in the levels of light exposure of the protein/crystals; ii) the generally low occupancy of the Q_B site, and the relatively low resolution of the structure; iii) Variation in the purification and crystallisation protocols, especially in the use of detergents, which have been show to influence the binding of ubiquinone in the Q_B pocket; iv) the effect of electrons created during the X-ray data collection itself maybe leading to reduction of the Q_B molecule, with room temperature exposures the reduced quinone molecule would be free to move within the pocket.

The recent publication by Stowell et al (1997) documents structural investigations which occur when the reaction centre has been either dark adapted or light-adapted. In the two models the position of Q_B has been found to differ. The dark adapted model, appears to show two alternative positions, with a lower occupancy position lying ~4.5Å closer to the cytoplasm than the other. This low occupancy position is also assumed by the quinone in the light-adapted state, although it differs in that the quinone head is postulated to have undergone a 180° rotation from the dark adapted conformation. The models presented in this thesis all show greater similarity to the dark-adapted model, with evidence also for the alternative "deeper" position. However, an important point with respect to Q_B is the low level of occupancy found. The average B-factor for the protein surrounding the Q_B molecule determined for the reaction centre models discussed in this thesis, were all in the mid to high thirties. However, the B-factors determined for Q_B in each model was much higher, generally around 3 times as high. Analysing the B-factors in this way, it can be crudely determined that the quinone inserted to the Q_B binding pocket is only present in approximately 30% of the reaction centre complexes in the crystal. This has the effect of making the electron density maps more difficult to interpret.

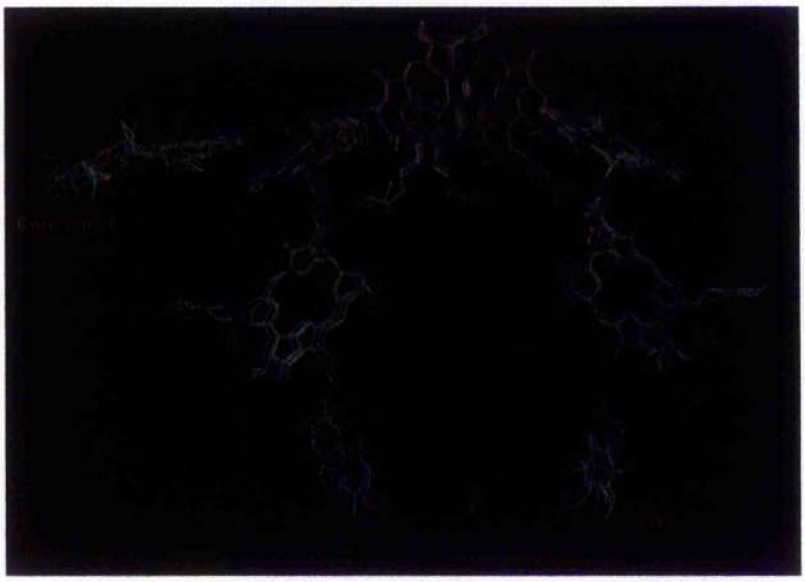

Figure 45: WT red pigments (green) superimposed upon the pigment molecules in the previously published models. Superimposition was performed using the program LSQKAB (CCP4, 1994)

Aside from Q_B, which is after all the constituent of the reaction centre which can leave the complex, the pigments were found to all assume essentially an identical position/ orientation in the two reaction centres. Closer inspection did, however, lead to the unearthing of one interesting alteration in the assignment of the 2-acetyl group of BChl P_L. His L168, has been shown to H-bond to P_L (e.g. Mattioli et al, 1994), onto the 2-acetyl group, the X-ray data suggests the His interacts via the NE group. The structural assignment made for the 2-acetyl group on the BChl differs significantly compared that of Ermler et al (Figure 46). While the 2-acetyl group had been previously thought to be twisted out of the plane of the BChl macrocycle, the data presented here, repeatedly (i.e. in all six models) shows the group to be assuming a configuration such that it lies in the same plane as the BChl ring. Figure 46 below shows the position of the WT red and FM115/RM197 co-ordinate model compared to that of Ermler et al, with electron density map of the highest resolution structure (FM115/RM197). It should be stressed that all of the maps indicated an identical assignment, however, the highest resolution map does make it clearer than the others. This configuration would seem to be more likely, the twisting to the extent as depicted in the older structure, with its ~90° twist out of the plane of the BChl macrocycle, would probably cause breakage of the conjugate system. If this was the case, no alteration would be expected upon breakage of the H-bond. Studies by site-directed

mutagenesis allied to raman spectroscopy, have shown this not to be the case (Mattioli et al, 1994; Williams et al, 1992).

Figure 46: The region surrounding His L168 and P_L. (labelled BChl 202) The configuration assigned for the acetyl carbonyl group of the BChl by Ermler et al (1994) is significantly different from the assignment made for the RCO2 strains in this thesis. Strains shown are WT red [red], FM115/RM197 [cpk] and the Ermler et al model [orchid]. The 2Fo-Fc map is from the FM115/RM197 model and is contoured at the 1σ level.

The reaction centre from *Rb. sphaeroides* RCO2 has an essentially identical structure to those proposed previously for other *Rb. sphaeroides* strains. The disagreements found were most likely due to alternate interpretation of the density maps, variation in map quality etc. However, the structure of a reaction centre produced in a null light-harvesting complex background, had not been produced previously. It was important to ensure that the lack of LH complexes in the membrane did not have a structural impact on the reaction centre itself. It was also deemed important to perform the preliminary optimisation of not only the crystallisation protocol, but also the cell growth and reaction centre purification protocols with the stable wild-type complex. The effect of the various mutations on the structure and behaviour/stability of the isolated complex were at this point unknown. The successful completion of these

sections allowed interest to move onto attempts at determining the atomic structures of the mutant complexes.

13.2. Carotenoid Mutants.

The models of all the mutant reaction centres showed structures essentially identical to that of WT red discussed above, with only very localised structural alterations. For this reason detailed descriptions of each of the individual mutants are not presented here. Instead the focus will be on the localised effects each had on their immediate environment. The intention from the outset had been to engineer a number of structurally conservative site-directed mutations, which would have minimal impact on the structure of the reaction centre protein, whilst altering the character of the amino acid side chain. The results of the crystallographic analysis showed this to have been remarkably (although at the same time a little frustratingly!) successful. Four crystal structures were produced containing mutations in the carotenoid binding pocket, and none of these showed any significant alterations in the models when compared with the WT red structure. The models are discussed in the order of decreasing maximum resolution, with those containing the Phe M197-Arg mutation discussed here as single carotenoid binding pocket mutants.

13.2.1. TrpM115-Phe (Phe M197-Arg) Model: 2.3Å Resolution.

The FM115/RM197 model is to a resolution of 2.3Å, the highest resolution data collected, with diffraction initially to ~2.2Å. The data was collected from exposure of eight crystals on Station 9.5 at Daresbury. The model presented is not fully refined, although 207 waters have been built in, along with seven LDAO molecules and two phosphate groups. The refinement statistics for the model are given below in Table 25. The effects of the mutation of the carotenoid binding pocket were minimal, although points of interest were found which will be discussed later. The remainder of the model is identical to the WT red structure, therefore a detailed discussion of the complete complex will not be made.

Table 25: The refinement statistics and measurements of the quality of the geometry of the FM115/RM197 model. $R_{merge} = \Sigma_h\Sigma_i|<I(h)>-I(h)_i|\Sigma_h\Sigma_i I(h)_i$, where I(h) is the intensity of reflection h, Σ_h is the sum over all reflections and Σ_i is the sum over all i measurements of reflection h. The R-factor is defined by $\Sigma||Fo|-|Fc||/\Sigma|Fo|$; Free-R was calculated with 5% of the reflections, selected randomly (Brünger, 1992). The Ramachandran plot was produced using Procheck version 3.0. (Laskowski, 1993), and the co-ordinate error was estimated from a Luzzati plot (Luzzati, 1952), both plots are presented in Appendix IV.

Data Collection Statistics	
Resolution Range	26.4 - 2.3Å
Rmerge	11%
Number of Unique Reflections	90885
Completeness of data	94%
Refinement Statistics	
Number of selected reflections	90808
Free-R Factor	21.5
R Factor	20.7
Average B-Factor:	
Overall	34.2Å^2
Main Chain	44.9Å^2
Side Chain	45.2Å^2
Geometry	
RMSD from Ideality:	
Bonds	0.008Å
Angles	1.638°
Impropers	2.141°
Ramachandran Plot:	
Most favoured areas	92.5%
Additional allowed areas	7.2%
Generously allowed areas	0.3%
Disallowed areas	0.0%
Co-ordinate Error	0.35Å
Model	
No. of Protein Residues	823
No. of Pigment Molecules	4 BChl, 2 BPheo, 2Ubi, 1 Spo, 1 Fe
No. of Waters	207
No. of Detergents	7
No. of Phosphates	2

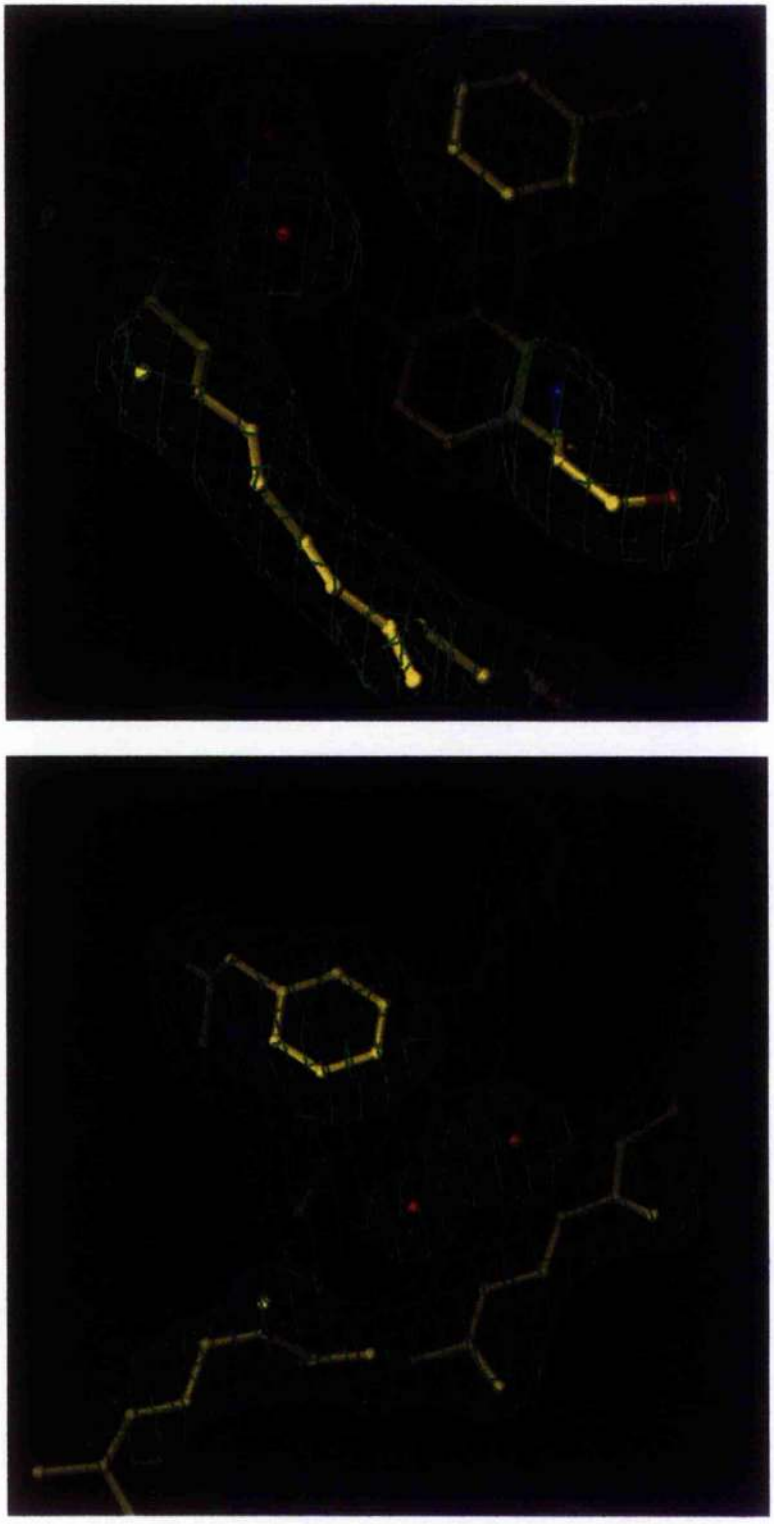

Figure 47: The area surrounding M115. The alteration of tryptophan to phenylalanine resulted in no major alterations in the configuration of the carotenoid or of the protein surrounding the mutation site. However, two molecules of water are suggested to have entered the void left by the removal of the larger Trp side-chain. 2Fo-Fc map is contoured at the 1σ level.

Figure 47 shows two views of the carotenoid and amino-acid residues in the area of the Trp to Phe mutation at M115, while Figure 48 below, shows the model produced for FM115 superimposed on the WT red structure. The position of the two amino acids SM119 and YM177 can be seen to be identical in both models (allowing for a slight translation between models). In addition, there appears to have been no alteration in the structure of the carotenoid itself. The mutated residue has also shown a remarkable level of conservation in the position it has assumed. The benzene ring of the Phe residue can be seen to be almost perfectly positioned where previously the indole-ring of the Trp residue was located. However, there has been some response to the mutation. The replacement of a Trp side chain with a much smaller side-chain has left a void in the interior of the protein. This void has been filled by two water molecules (2.85Å apart), forming a small water chain, H-bonding to the protein via the carbonyl group of Val M175 (~2.85Å) and the carbonyl of Gly M161 (~2.8Å).

This phenomenon of water entering proteins to fill voids created by site-directed mutagenesis is not without precedence. An investigation by Goldsmith et al (1996) in which the residue that provides the axial ligand to P_M, His M202 was replaced by a Gly residue found that the BChl dimer remained intact. Experiments in which the same residue was replaced with Leu or Phe, had led to the incorporation of BPheo into the P_M position, creating a BChl:BPheo heterodimer (Bylina & Youvan, 1988). However, in the glycine mutant, where the new residue side-chain could not be providing the axial ligand, it has been suggested that water is filling the void left by mutation of the side chain, and it is this water which is acting as the axial ligand to P_M. The data presented here from crystallographic investigation of mutant complexes (See also the discussion into the effects of the RM197 mutation, section 13.3.) shows that it is indeed possible for water molecules to fill voids left upon mutation of amino acids in the interior of protein complexes.

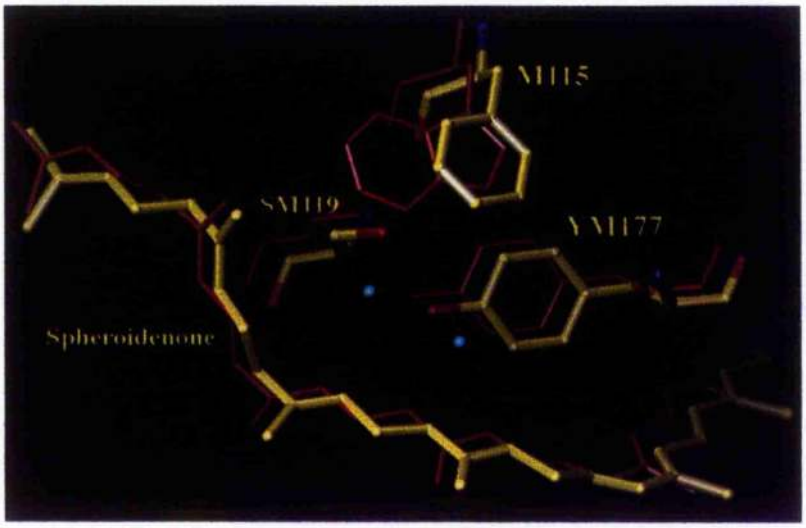

Figure 48: Comparison of the FM115 model (cpk) and the model of WT red (red).

13.2.2. Tyr M177-Phe (Phe M197-Arg) Model: 2.55Å Resolution.

The RM197 model is to a resolution of 2.55Å with diffraction initially to ~2.4Å. The data was collected from exposure of two crystals on Station 9.6 at Daresbury. The model presented is fully refined, with a hundred waters built in, along with three LDAO molecules and a phosphate group. The model of the TyrM177-Phe (double) reaction centre structure was to a lower resolution than the previous model, in this case only to 2.55Å. The quality of the model was significantly lower than that of the FM115/RM197 model. The crystallographic statistics are presented below in Table 26. Despite the lower resolution the maps were in general of sufficiently high quality to make refinement of the structure relatively straight-forward. Again the structure is essentially identical to the wild-type structure so no detailed description of this model will be presented. Within the carotenoid binding pocket, the effect of the TyrM177 to Phe mutation on the structure of the complex is negligible, at least to the resolution of the investigation. The benzene ring of the new Phe residue is located in an identical position and conformation as the Tyr at M177 in the WT structure (Figure 48).

Table 26: This table shows refinement statistics and measurements of the quality of the geometry of the FM177/RM197 model. $R_{merge} = \Sigma_h\Sigma_i|<I(h)>-I(h)_i|\Sigma_h\Sigma_i I(h)_i$, where I(h) is the intensity of reflection h, Σ_h is the sum over all reflections and Σ_i is the sum over all i measurements of reflection h. The R-factor is defined by $\Sigma||Fo|-|Fc||/\Sigma|Fo|$; Free-R was calculated with 10% of the reflections, selected randomly (Brünger, 1992). The Ramachandran plot was produced using Procheck version 3.0. (Laskowski, 1993), and the co-ordinate error was estimated from a Luzzati plot (Luzzati, 1952), both plots are presented in Appendix IV.

Data Collection Statistics	
Resolution Range	11-2.55Å
Rmerge	12.9%
Number of Unique Reflections	54163
Completeness of data	76.5%
Refinement Statistics	
Number of selected reflections	54129
R Factor	19.4
Free-R Factor	21.7
Average B-Factor:	
Overall	34.3Å^2
Main Chain	39.4Å^2
Side Chain	39.8Å^2
Geometry	
RMSD from Ideality:	
Bonds	0.008Å
Angles	1.415°
Impropers	1.993°
Ramachandran Plot:	
Most favoured areas	91.0%
Additional allowed areas	8.7%
Generously allowed areas	0.3%
Disallowed areas	0.0%
Co-ordinate Error	0.35Å
Model	
No. of Protein Residues	823
No. of Pigment Molecules	4 BChl, 2 BPheo, 2Ubi, 1 Spo, 1 Fe
No. of Waters	100
No. of Detergents	3
No. of Phosphates	1

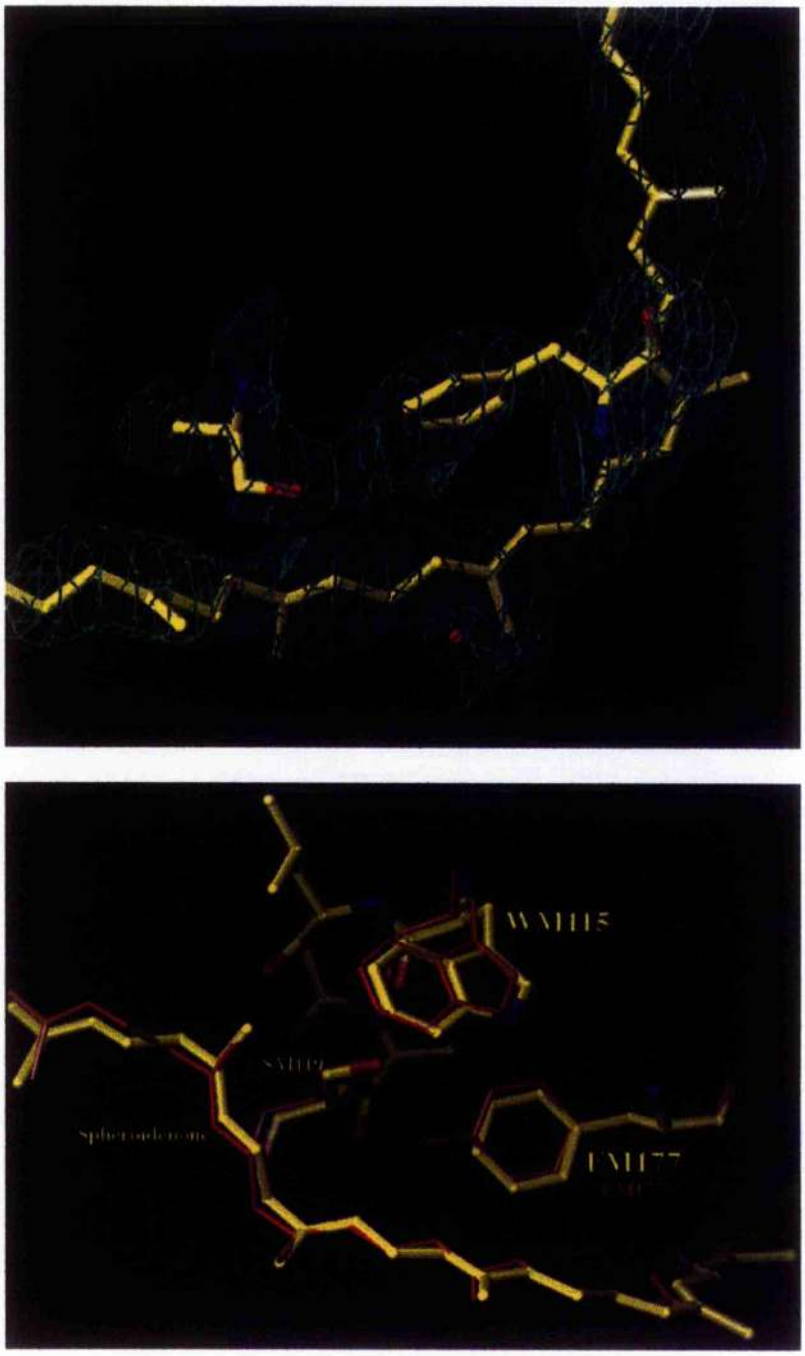

Figure 49: A. Section of the FM177 model (RM197) with the 2Fo-Fc electron density map contoured at the 1σ level. Minimal alteration in the structure was found. The single water molecule present is also found in the WT red structure. **B.** Comparison of the FM177/RM197 model (cpk) and the model of WT red (red).

13.2.3. Ser M119-Ala Model: to 3.1Å & the Trp M157-Phe Model: to 3.2Å.

The two remaining mutant structures are of significantly lower resolution then the FM115/RM197 and FM177/RM197 models. The crystallographic statistics are presented in Table 27. The data was collected from exposure of single crystals on Station 9.6 at Daresbury. The models presented are not fully refined, a limited number of waters have been built in to the AM119 model, along with two LDAO molecules. The fully refined model is unlikely to contain many more, due to the low resolution, peaks of density likely to be waters/detergents are difficult to identify with sufficient confidence.

Table 27: This table shows refinement statistics and measurements of the quality of the geometry of the models of AM119 and FM157. $R_{merge} = \Sigma_h\Sigma_i|<I(h)>-I(h)_i|\Sigma_h\Sigma_i|(h)_i|$, where I(h) is the intensity of reflection h, Σ_h is the sum over all reflections and Σ_i is the sum over all i measurements of reflection h. The R-factor is defined by $\Sigma||Fo|-|Fc||/\Sigma|Fo|$; Free-R was calculated with 10% of the reflections, selected randomly (Brünger, 1992). The Ramachandran plot (See Appendix IV) was produced using Procheck version 3.0. (Laskowski, 1993).

Data Collection Statistics	Ser M119-Ala	Trp M157-Phe
Resolution Range	19.6 - 3.1 Å	19.7 - 3.1Å
Rmerge	7.7	7.1
Number of Unique Reflections	35223	33688
Completeness of Data	87.6%	84%
Refinement Statistics		
Number of selected reflections	35218	33678
R Factor	23.8	25.5
Free-R Factor	28.4	30.6
Overall B-Factor	46.3	50.7
Geometry		
RMSD from Ideality		
Bonds	0.011Å	0.01Å
Angles	1.635°	1.645°
Impropers	2.192°	2.261°
Ramachandran Plot		
Most favoured areas	89.0%	87.6%
Additional allowed areas	10.7%	11.9%
Generously allowed areas	0.1%	0.4%
Disallowed areas	0.1%	0.0%
Model		
No. of Protein Residues	823	823
No. of Pigment Molecules	4 BChl, 2 BPheo, 2Ubi, 1 Spo, 1 Fe	4 BChl, 2 BPheo, 2Ubi, 1 Spo, 1 Fe
No. of Waters	8	0
No. of Detergents	2	0

In both of these models, B-refinement was performed for the complex as a single entity, it was not split into individual residues. This was a direct consequence of the lower resolution. It should be noted that neither of these models are completely refined. Only a few rounds of refinement have been performed, with only a limited number of hetero-atoms (water and detergent) built into the AM119 model (Refinement is currently being completed). However, again as a consequence of the resolution, the number of hetero atoms built into the completed models will be well below that of the two high-resolution structures discussed above. These two models are of a similar resolution to the highest resolution structure reported by Chirino et al (1994). The level of information that is afforded by models of this quality, is inherently low. Trying to solve this problem, was one of the motivations for the work described in this thesis.

The maps, in general were of poor quality. The limitation of the resolution made assignment of amino-acid side chain configuration very difficult. Figure 40, presented in section 12.1. compared the maps obtained from 2.3Å data and the FM157 model at 3.2Å. The difference between the two models in the definition around the side chain, and especially in the carbonyl groups along the protein backbone, illustrates the difficulty in building models from such low resolution data. Given the limitations discussed above, it is clearly difficult to determine whether a structure has indeed been altered, unless the effect of the mutation is major. The introduction of altered amino-acid side-chains was designed to be conservative with regards to the size of the residue. Again, as in the previous two models, this appears to have produced mutant models of identical structure to the wild-type. The maps for the areas surrounding the mutation sites are shown, along with diagrams comparing the wild-type and mutant co-ordinate models. Figure 50 presents views of the AM119 model, and Figure 51 presents the FM157 model.

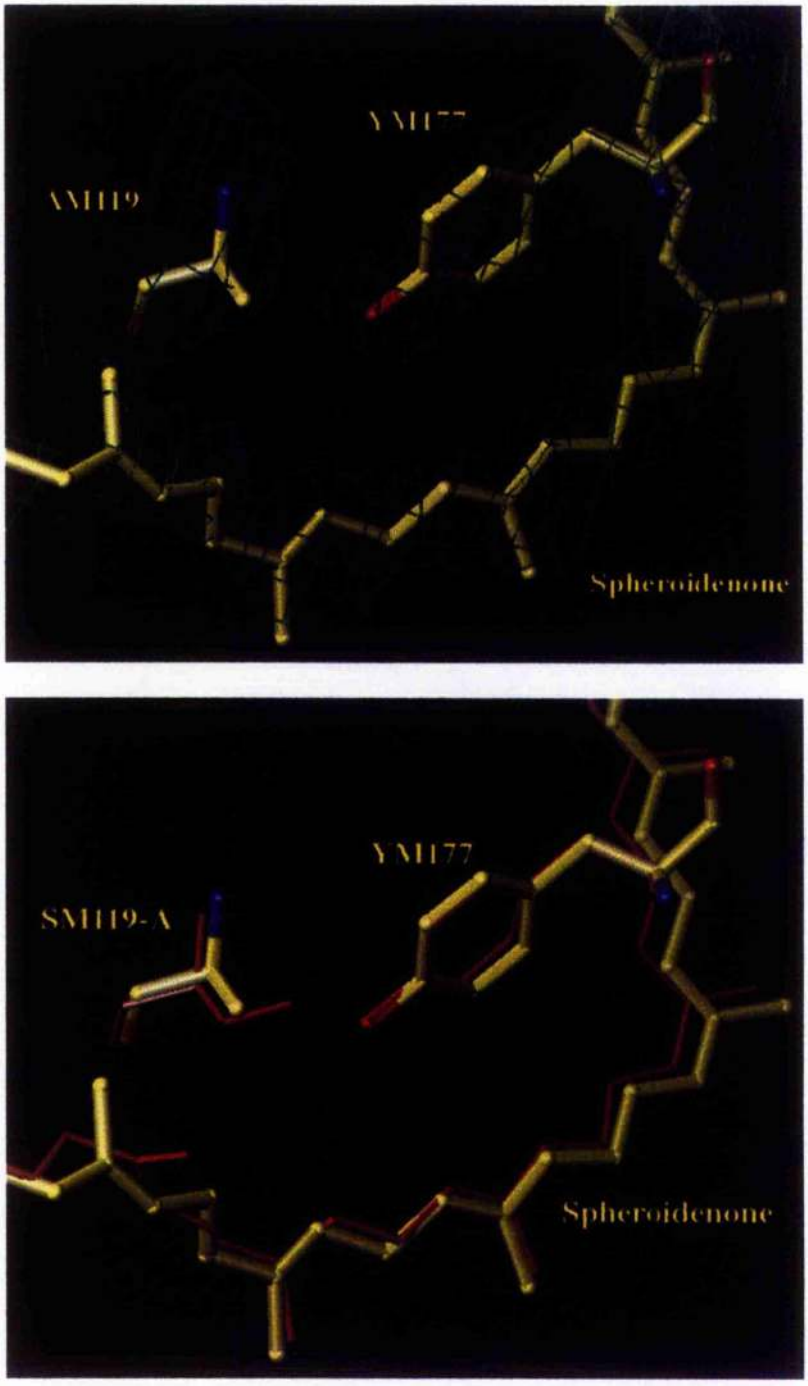

Figure 50: a) The model produced for the AM119 reaction centre with the 2Fo-Fc electron density map contoured at the 1σ level; **b)** The WT red (red) model superimposed on the AM119 model. The structural alterations are confined solely to the altered side-chain.

[Following Page]

Figure 51: a) FM157 model and 2Fo-Fc electron density map contoured at the 1σ level. **b)** WTred (red) model shown superimposed on the FM157 model. Some alteration can be observed for MM122, Tyr M177 remains apparently unaltered.

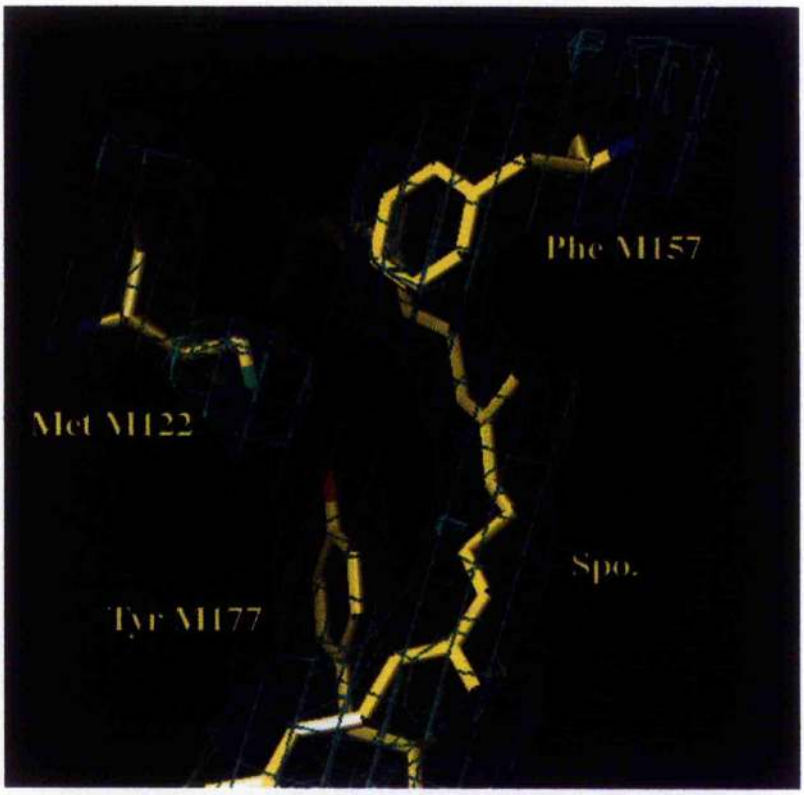
Phe M157
Met M122
Spo.
Tyr M177

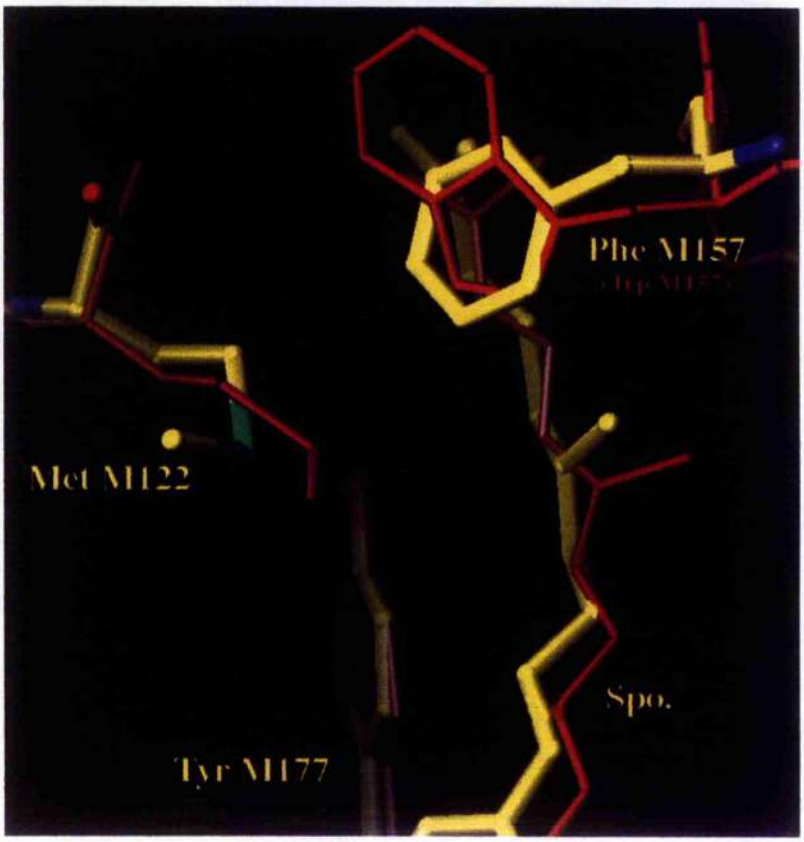
Phe M157
Met M122
Spo.
Tyr M177

13.2.4. General Points from the Carotenoid Binding Site Mutant Structures.

The remaining structures to be discussed relate to the effects of a mutation in the proximity of the special pair. Therefore, at this point a discussion into the findings of the crystallographic investigations with regards to the carotenoid and its binding site is required. Given the extremely hydrophobic character of the carotenoid binding pocket, the alteration of the few polar residues was expected to yield some alteration in the carotenoid binding characteristics of the reaction centre or the character and function of the carotenoid itself. However, in the crystallographic data presented above, no alteration has been observed. The carotenoid had been found to be bound in identical ratios as found in the wild-type reaction centre, i.e. 1:1, from HPLC investigations. Crystallography has now also shown that the carotenoids are bound in an identical manner to that found in the wild-type (Figure 52). Indeed, the only alterations detected in all of the investigations performed has been from resonance raman spectroscopy. Unfortunately, there is no previous data regarding resonance raman data of spheroidenone bound within reaction centres, hence the assignment of small alterations of band intensity and position is not as yet possible. It is hoped that the crystallographic data presented here might be able to aid the future interpretation of the resonance raman spectra for reaction centre bound spheroidenone.

The effect of the mutations around the carotenoid binding pocket are minimal. The stability of the protein:pigment complex appears to be sufficient to withstand the effects of a single amino acid substitution. The example of the FM115 mutant complex showed that there is perhaps surprising levels of structural rigidity. Rather than collapsing the protein complex in towards the carotenoid, or movement/alteration of the carotenoid position/configuration, the response to the formation of void space in the complex interior was the insertion of two water molecules. In this way, the remainder of the pocket is held in essentially an identical structure to the wild-type. This contrasts sharply with the results found in some other systems. In an extreme example, PLP, one of the major protein components in the myelin sheath surrounding nerve fibres in the CNS and also an integral membrane protein, is extremely sensitive to alteration. This protein has been found to be 100% conserved from rats to

humans, and alteration of a single amino acid, almost always results in death of the organism (e.g. Jung, 1996). PLP and the reaction centre seem to be extreme cases. In other investigations of the reaction centre, such as that reported by Goldsmith et al (1996), where mutations lying close to the special pair had been altered, and also those structures reported by Chirino et al (1994), the reaction centre complex has shown remarkable ability to accommodate quite different amino-acid residues with minimal structural impact.

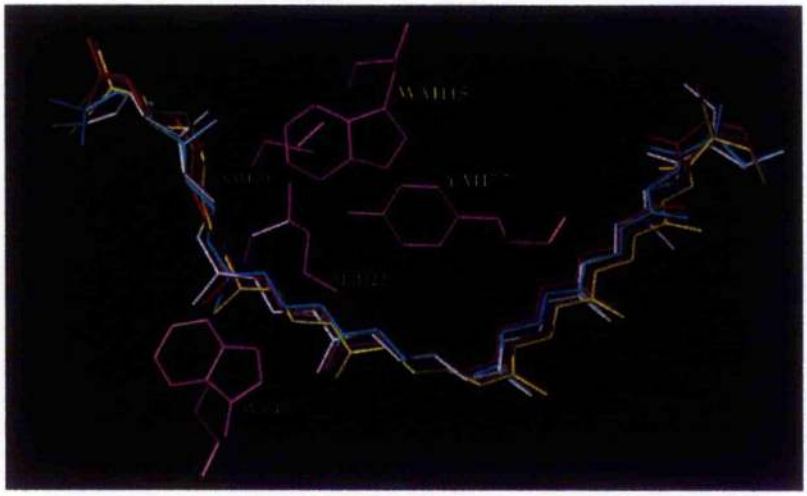

Figure 52: The structures of the carotenoids found in five of the models produced in this thesis: WT red [red]; FM115/RM197 [yellow]; AM119 [white]; FM157 [cyan]; and FM177/RM197 [salmon]. The positions of the "pre-mutated" residues, as found in the WT red structure are also shown.

Given that the alteration of the selected polar residues has had no effect on the characteristics/function of the carotenoid, and the structure of the carotenoid has not undergone any apparent structural alterations, the role of these residues in the pocket remains unclear. That polar groups have no effect on the carotenoid characteristics, is backed by the results of the Trp M115-Phe alteration. The crystal structure of this strain shows two water molecules inserted into the void created by the introduction of a smaller amino-acid side-chain. In effect, rather than removing a polar group from the pocket, an extra group has been introduced. Therefore, the investigations have analysed both the effect of increased and decreased dielectric constant of the pocket.

The carotenoid in the reaction centre, as mentioned previously, assumes an unusual twisted 15-15'-*cis* conformation. The role of these

residues may lie in the mechanism by which this conformation is forced onto the carotenoid. The residues form a ring around the carotenoid molecule, closer to the "non-methoxy" end (Figure 52). If Trp M75 is, as suggested in Section 13.1.2., binding to the methoxy group of the spheroidenone molecule, then one can imagine a system where TrpM75 and the ring of polar residues might act together to bend the carotenoid into the twisted 15-15'-*cis* conformation as the complex assembles. The fact that no effect has been seen through introduction of single mutants, need not disprove this hypothesis. The loss of one group may not be sufficient to destroy the "twisting capability" of the protein completely.

13.3. The FM197-R Models.

The discussions contained within this section could be based on any of the three crystallographic models that have been produced for the RM197 containing reaction centres. The structures obtained were identical in all cases, a satisfying observation in its own right. This section will, however, begin with a brief discussion of the single RM197 strain, before going on to describe the alterations of the structure in more detail, with inclusion of the other models, one of which was at a higher resolution than the single mutant model.

The RM197 model is to a resolution of 2.4Å with diffraction initially to ~2.2Å. The data was collected from exposure of three crystals on Station 9.6 at Daresbury. The model presented is not fully refined, although over a hundred waters have been built in, along with six LDAO molecules and a phosphate group. The maps were of significantly better quality than were initially expected, given the resolution limit. The major reason for this is most likely the high completeness of the diffraction data, 93.6% for RM197 (compared to only 76.5% for the FM177/RM197 data). The resolution of the data is, therefore, by no means the only point to be considered when analysing crystallographic data. The model is essentially identical to that of WT red, as is the case in all the previously described mutant models, with differences confined to the region surrounding the mutation site. However, the effect of this particular mutation was dramatic and completely unexpected.

Table 28: This table shows the refinement statistics and measurements of the quality of the geometry of the RM197 model. $R_{merge} = \Sigma_h\Sigma_i|<I(h)>-I(h)_i|\Sigma_h\Sigma_i|I(h)_i|$, where I(h) is the intensity of reflection h, Σ_h is the sum over all reflections and Σ_i is the sum over all i measurements of reflection h. The R-factor is defined by $\Sigma||Fo|-|Fc||/\Sigma|Fo|$; Free-R was calculated with 5% of the reflections, selected randomly (Brünger, 1992). The Ramachandran plot was produced using Procheck version 3.0. (Laskowski, 1993), and the co-ordinate error was estimated from a Luzzati plot (Luzzati, 1952), both plots are presented in Appendix IV.

Data Collection Statistics	
Resolution Range	16.4-2.4
Rmerge	9.1%
Number of Unique Reflections	67571
Completeness of Data	93.6%
Refinement Statistics	
Number of selected reflections	67561
R Factor	20.2
Free-R Factor	22.2
Average B-Factor	
Overall	34.3
Main Chain	39.4
Side Chain	39.8
Geometry	
RMSD from Ideality	
Bonds	0.07Å
Angles	1.498°
Impropers	3.343°
Ramachandran Plot	
Most favoured areas	92.1%
Additional allowed areas	7.2%
Generously allowed areas	0.7%
Disallowed areas	0.0%
Co-ordinate Error	0.35Å
Model	
No. of Protein Residues	823
No. of Pigment Molecules	4 BChl, 2 BPheo, 2Ubi, 1 Spo, 1 Fe
No. of Waters	101
No. of Detergents	6
No. of Phosphates	1

Three separate crystallographic models of reaction centres containing this mutation were produced: a single mutant along with two double mutants (with WM115-F and YM177-F). All of the models produced almost identical structures, with the variation in structure confined to the pattern of water molecules built into the refined structure. In the highest resolution structure, which is also the structure with the most complete diffraction data set (94%), a network of four water molecules was built into the model (Figure 53). This network could not be satisfactorily built into the other two models, although in each case there was some evidence for the existence of an identical network. The insertion of waters into the

structure reflects a void created within the protein as a consequence of the mutation at M197. The replacement of the Phe residue by an Arg residue had resulted in a major, although again essentially localised, structural reorganisation. An alteration in the structure and configuration of a side-chain to this extent might be expected to have a major impact on the surrounding protein. However, the mutation lies at a "fortuitous" position within the protein complex.

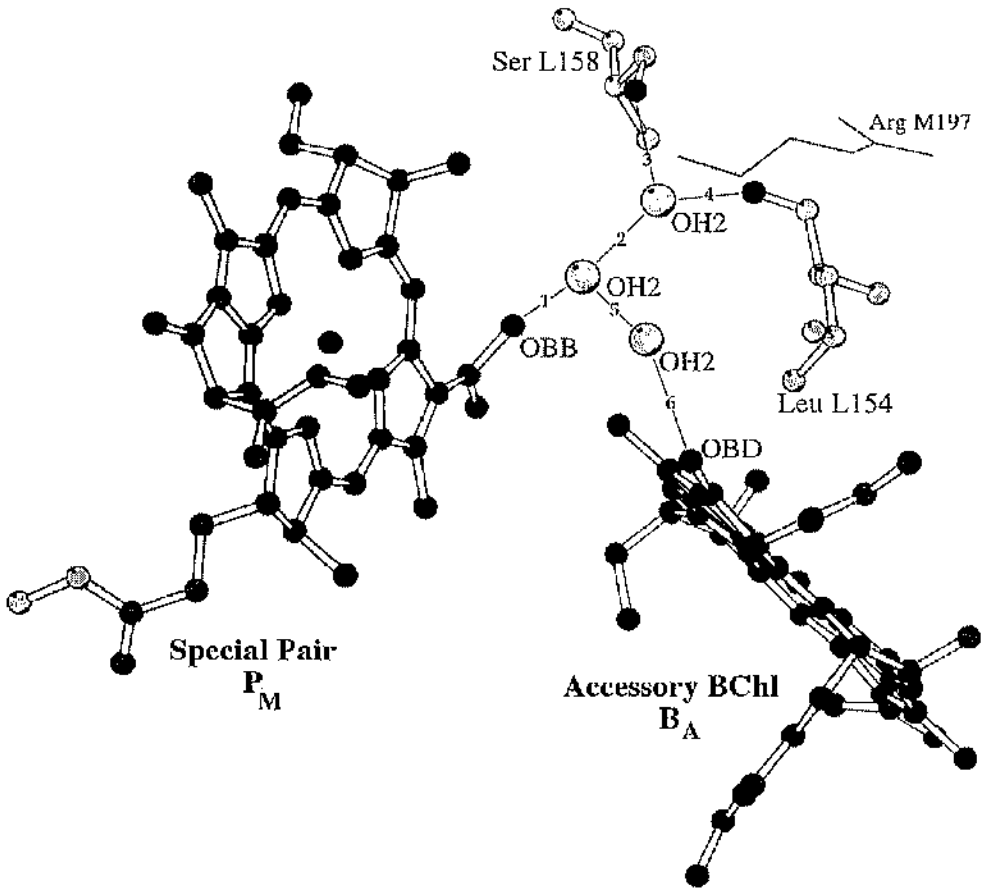

Figure 53: The network of water molecules introduced close to P_M upon mutation of Phe M197 to Arg. The distances between the interacting groups are given in angstroms. Diagram produced using Molscript (Kraulis, 1991).

The amino acid at position M197 is in very close proximity to the BChl special pair. Interestingly, the M197 residue is also positioned at the interface between the L and M polypeptide subunits. The alteration of Phe M197 to Arg has had minimal structural impact because the extended arginine side chain has rotated away from the wild-type position of the Phe residue, to point up between the L and M polypeptides. The arginine extends towards the periplasm, where it probably forms a salt-bridge interaction with an aspartic acid residue (Asp L155). This has not demanded any major structural alterations. In the wild-type structure, Phe M197 can be clearly identified from the periplasmic surface of the protein, even in space-fill representation (Figure 54). There appears to be a small cleft in the protein surface extending down to M197. An identical situation is found at the symmetry related site above the other BChl of the special pair. The role of this cleft in the function of the reaction centre is unclear. Perhaps it is in some way involved with the interaction between the soluble cytochrome and the reaction centre. However, what is clear is that the arginine residue uses this cleft as an "escape route" passing up between the L and M subunits.

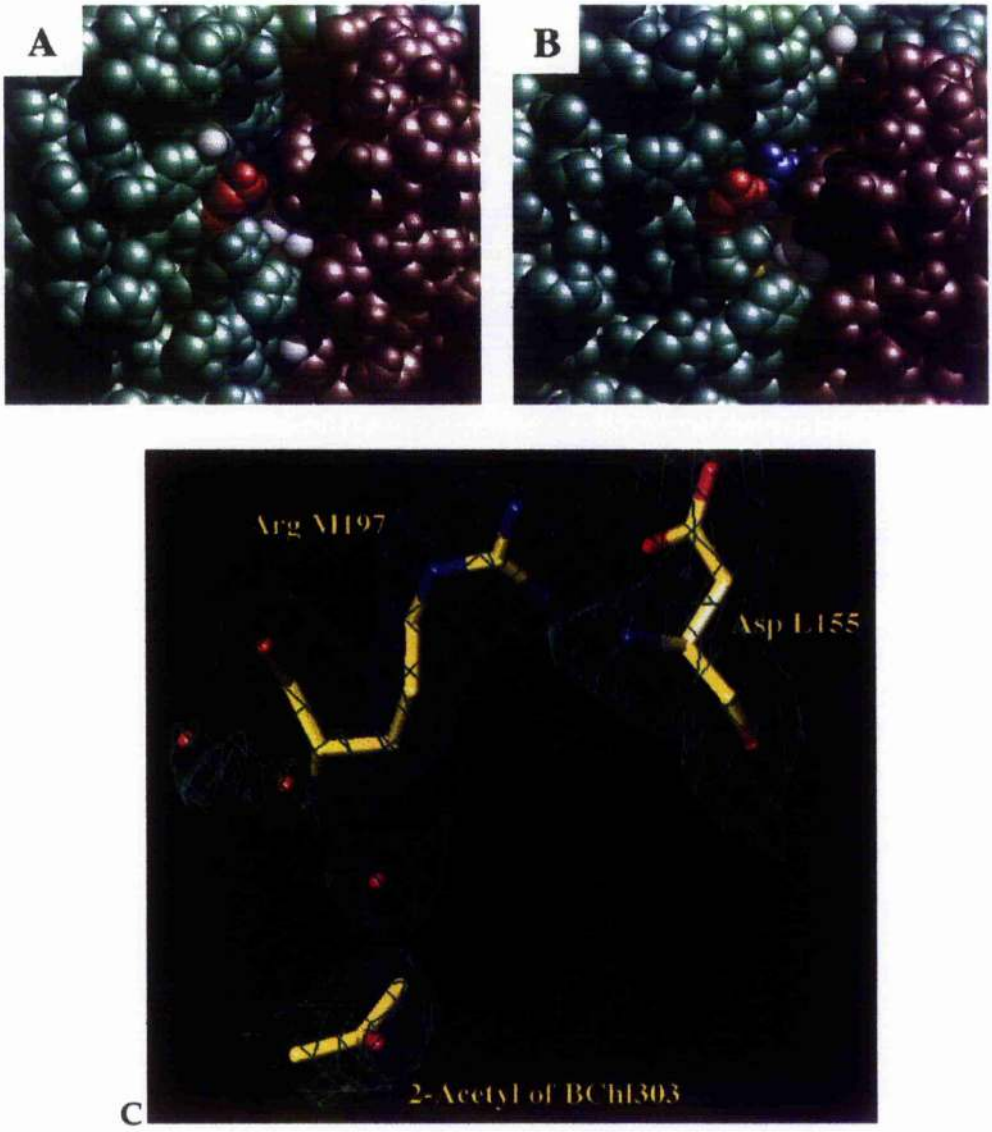

Figure 54: **A.** Phe M197 (blue) can be observed at the base of a cleft on the periplasmic surface of the wild-type reaction centre model. The cleft lies along the interface between the L (green) and M (wine) subunits. **B.** The mutation of M197 to arginine results in the twisting of the M197 side chain, so that it escapes up through the cleft to interact with an aspartic acid residue, Asp L155 (red). Water molecules are coloured white. **C**. The interaction of Arg M197 with Asp L155 as assigned in the FM115/RM197 crystal structure model. All three models with Arg M197 showed identical structures. The 2-acetyl group of P_L (labelled BChl303) was placed as assigned by Ermler et al (1994).

All three crystallographic models produced for the Arg M197 mutants showed identical conformations for the arginine residue. Electron density maps for this region taken from the highest resolution model are shown in Figures 54 & 55. It is hypothesised that Asp L155 and Arg M197 interact

between the OD and NH groups over a distance of approximately 2.65Å, well within the 2.5-4.9Å range of inter-residue distances cited for possible salt-bridge interactions in the reaction centre (Chang et al, 1991). The removal of the Phe side chain from the core of the protein left a void in the complex into which water molecules appear to have become inserted. The precise pattern of the water network is not identical in the three structures. One water, which is suggested to interact with the 2-acetyl carbonyl group of P_L (one of the special pair BChl's), is maintained in an identical position in each model with clear peaks of density observed in each. However, although an additional three waters have been inserted into the 2.3Å structure, the density in the two remaining models (2.4Å and 2.55Å) was not sufficiently clear as to allow the insertion of an identical network. It should be stressed that there was evidence in the 2.4Å and 2.55Å models to support the interpretation made in the high resolution model with respect to the waters, but the peaks of density were not sufficiently strong to merit the building of further waters into these particular models.

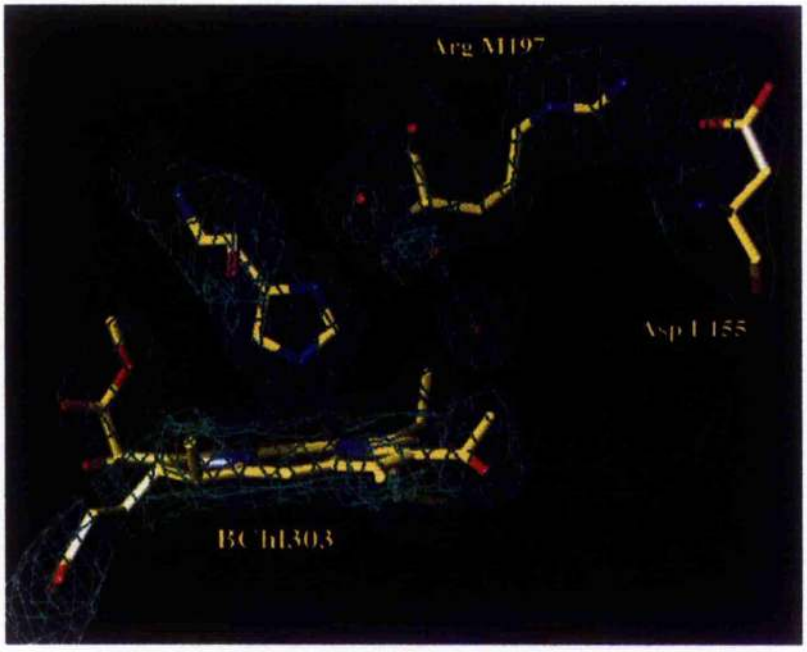

Figure 55: The structure observed in the RM197 mutants around the mutation site. The 2-Acetyl of P_M is placed as was assigned in the work of Ermler et al (1994). It is believed that this acetyl group is in fact rotated such that the carbonyl is H-bonded to the water molecule. Three waters have been built into the model , as in the FM115/RM197 model (See also Figure 53 above), a fourth density peak (out of shot) may also be due to a water molecule, but the density is to poor to make the assignment reliable.

The H-bonding between one of the waters and the 2-acetyl carbonyl group of P_M could be assumed to be the interaction which has caused the alteration in the absorption spectra. The original theories put forward to explain the observed alterations had assumed H-bonding between the arginine and the 2-acetyl carbonyl group. The model structures demonstrate this is not the case. However, the precise mechanism which underlies the spectral shift is not clear. Wachtveitl et al (1993) reported that the insertion of a tyrosine residue in place of the phenylalanine at position M197, led to a 10nm red shift of the P band in 77K photobleaching electronic absorption difference spectra of chromatophores. Upon isolation of reaction centres from the membrane, the P-band absorption typically becomes blue-shifted by up to 15nm (Wang et al, 1994). Absorption spectra of the isolated tyrosine M197 complexes were observed to show a red-shift of only 1-2nm compared to the WT. FT raman spectroscopy of the tyrosine M197 mutant determined that a new H-bond had been formed to the 2-acetyl group of P_M, hence the red-shift of the P absorption band (Wachtveitl et al, 1993). However, the formation of the water to 2-acetyl carbonyl of P_L H-bond has apparently caused a ~7nm blue-shift in the special pair absorbance peak when compared to the WT.

In addition to the insertion of the water molecules, one small, but significant, additional structural alteration is the rotation of the P_L 2-acetyl carbonyl group (Figure 55). Although the rotation is apparently small (~20°), an identical configuration is found in all three mutant models. However, there is difficulty assigning the precise orientation of this group. X-ray crystallography cannot determine which terminal group is the carbonyl, and which is the methyl. The rotation of this group may be ~20° or it may be ~160°, it depends upon what the orientation is with respect to the carbonyl in the mutant and wild-type structures. The mutant is probably easier to define. For the water molecules to be observed in crystal structures by X-ray crystallography, they must be fixed. The only group capable of fixing the water in the position observed is the carbonyl carried on the 2-acetyl group. Therefore, it would seem that the 2-acetyl must be rotated in such a way as to position the carbonyl to interact with the fixed water molecule. Unfortunately, no such assignment is possible for the wild-type structure. However, this rotation is an important finding. Perhaps the size of the rotation might be sufficiently small to bring its

significance into question, given the co-ordinate error built into the models. However, it is proposed here that the elucidation of identical structures in all three models, strongly suggests that the rotation is real, and not a result of the level of model precision. In addition, the quality of the maps, and especially the 2.3Å map of FM115/RM197 (Figure 55), is adequate to make this assignment with a reasonable level of confidence.

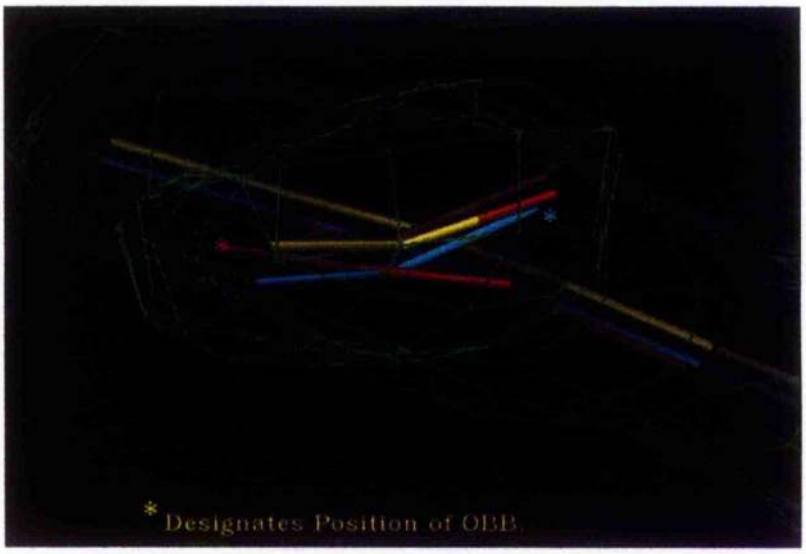

Figure 56: This figure shows the rotation of the group carrying the acetyl carbonyl on P_L. All three mutant structure are observed to have essentially identical configurations with a rotation away from that in the wild type of either 20 or 160°. The 2Fo-Fc map, contoured at the 1σ level, is from the FM115/RM197 model. The models are coloured: WT red [red], FM115/RM197 [cpk], FM177/RM197 [bronze], RM197 [cyan].

The observed 7nm blue shift in the P-band of the Arg M197 mutants cannot be explained by the simple formation of an H-bond. However, an H-bond has been formed and the resulting spectra might have been expected to show a red-shift of the P-band, by ~1-2nm as detected by Wachtveitl et al (1993). The explanation of the altered spectra may, therefore, lie with the rotation of the P_L 2-acetyl carbonyl. This group is normally part of the conjugated system of the BChl. However, if the 2-acetyl carbonyl group is sufficiently rotated away from the plane of the BChl porphyrin ring, then this conjugation will weaken. The hypothesis from this would be that this may have occurred. Of course, the state of conjugation is a major factor in determining the spectral characteristics of pigments, and henceforth the loss/weakening of a π bond from the BChl

system may be sufficient to blue-shift the absorption peak of P by 7nm. The effect of the additional H-bond on the 2-acetyl carbonyl would be expected to be minimal, with this group now separated from the conjugated system.

However, the above hypothesis ignores other possible mechanisms by which the observed spectroscopic data can be explained. Indeed, calculations performed by Parson and Warshel (1987) predicted that rotation of the 2-acetyl group from fully in plane to fully out of plane of the BChl macrocycle would lead to a ~50nm red shift in the absorbance of the P band in *Rps. viridis* reaction centres. The results described here would at first glance appear to contradict this. In the same paper, the authors describe calculations whereby a 0.1Å separation of the two BChls comprising the special pair would lead to a 20nm blue-shift in the observed absorption spectrum. A movement of 0.1Å is beyond the resolution of the crystallographic models discussed here, therefore it is not possible to determine whether alteration of the gap separating the two BChls of the special pair has occurred. However, Gudowska-Nowak et al (1990), presented computational models based on the BChl pigments of the bacteriochlorophyll *a* antenna protein complex from *Prosthecochloris aestuarii*, whereby a rotation of the acetyl group could lead to a blue-shift in the optical spectrum. In addition to all of the above, it should also be noted that the dielectric constant of the media surrounding the special pair has changed, with the insertion of up to four water molecules. Clearly, further work is required before a complete picture of the how the mutation and resulting structure described cause the observed effects on the character of the special pair.

D. Discussion

CHAPTER 14

Discussion and Conclusions.

14.1. Innovations in Technique.

This research has in large made use of pre-existing techniques. Certainly the spectroscopic investigations were performed using standard techniques. However, innovation was required at several points. Preliminary investigations were needed to firstly determine the most useful method by which large amounts of bacterial cells could be produced and secondly a relatively rapid, and yet non-wasteful reaction centre purification procedure. Investigation of growth conditions examined the most beneficial carbon source for growth of the RCO2 strains, and also a trial of two base media, c-Succinate and M22+. The conditions adopted were quite different from the initial conditions. Lactic acid as the carbon source was dropped in favour of fructose, and the base media was changed from c-Succinate to M22+. The size of the cultures was significantly scaled-up, with the successful use of "fermenters" to grow aerobic 20 litre cultures of RCO2 strains. The new purification protocol was based on the use of an FPLC system. This introduces both reliability and increased accuracy over the precipitation and gravity fed anion exchange columns used initially. The wastage of reaction centre protein was also reduced, the ability rapidly to determine and apply the most advantageous salt gradient to anion-exchange columns and the increased resolution of the separations reducing the amount of protein lost.

The application of crystallographic techniques in the research required much preparatory investigation prior to collection of the high resolution diffraction data described in Chapter 13. Initial trials with anaerobic *Rb. sphaeroides* 2.4.1. had met with some success with ammonium sulphate as the precipitant in β-OG detergent with a data set collected to ~2.8Å resolution. However, these conditions met with only limited success

when applied to the semi-aerobically grown RCO2 strains of *Rb. sphaeroides*. New conditions based on potassium phosphate as the precipitant and LDAO as the detergent were developed from those initially described by Buchanan et al (1993). This approach was ultimately much more successful than the ammonium sulphate system, with observed diffraction approaching 2.0Å. The reasons why different crystallisation conditions for reaction centres from 2.4.1. and the RCO2 strains of *Rb. sphaeroides* are needed are unclear, but one possibility is the altered lipid content in the semi-aerobically and anaerobically grown bacteria. Additional studies with the aim of identifying conditions in which the reaction centre crystals can be successfully cryo-cooled have also met with some success. However, the ultimate success of these conditions can only be evaluated by exposure of cooled crystals at a synchrotron source.

14.2. New Findings

The previous section identified areas where the experimental protocol had been developed and improved from that initially adopted. In this section the cumulated results of the different experiments are discussed. Before beginning the discussion, on a more general note, it should be emphasised that the crystal structures of six different *Rb. sphaeroides* reaction centre complexes have been produced. This compares with just seven structures currently available through the Brookhaven structural database of *Rb. sphaeroides* reaction centres. Admittedly, not all of the models generated in this work are of sufficient quality to demand submission. However, it does serve to highlight the success of the system developed for the purification and crystallisation of the reaction centre complexes.

[Following Page]

Table 29: Summary of the observations made from each individual investigation, and the accumulation of information and ideas as the project progressed.

Technique	Isolated observations	Accumulated observations
Absorption Spectroscopy	• Reaction centres present in membranes, and stable when isolated from membranes. • 7nm blue shift in P band in a sub-set of mutants. • Carotenoid absorption bands appear normal.	• Assembly of reaction mutant reaction centres appears normal. • Shift in the P-Band absorption in all RM197 mutants. • Carotenoid absorption bands normal in all strains.
Pigment Analysis	• Pigment ratios normal	• Shift in P-band not due to altered pigment ratios • Reaction centres appear to be assembling normally.
CD Spectroscopy	• Carotenoid region of spectra normal. • Shifts in the spectra in the P bands in sub-set of mutants.	• RM197 mutants show altered CD as well as absorption spectra. in the P band. Not possible to ascertain cause at this point. • Single carotenoid mutants with "WT" phenotype.
Raman Spectroscopy	• Small alterations in the carotenoid raman spectra. • However, strong evidence for a twisted 15'-cis conformation	• No information regarding the effect of RM197 on P from this study. • Indication of minor alterations in the carotenoid structure / carotenoid environment. However, no prior knowledge of the RR. spectra of spheroidenone limits interpretation of the data.
ESR Spectroscopy	• Alteration of the |D| value in RM197 mutants, suggesting a change in the structure of P, or that the extent of triplet delocalisation on P has been altered. • RM197 mutants found to perform triplet energy transfer from P to crt. at lower temps than the WT. • The mutations in the carotenoid binding pocket have no effect on the ESR spectra.	• P in RM197 mutants has been altered. Absorption peak is at higher energy, simplistically taken along with the ESR results the energy of the BChl triplet may also have increased. Thus the enhancement of the ability to transfer the triplet state to the carotenoid. • Surprisingly, the mutations in the carotenoid binding pocket appear to have no effect on the properties of the carotenoid itself.

Technique	Isolated observations	Accumulated observations
X-ray Crystallography	• The carotenoid binding pocket mutants show only localised structural alterations. • In three cases this alteration is limited to just the amino acid side-chain. • The fourth model (WM115-F) shows water molecules have filled the void left by the insertion of a smaller amino acid side chain. • Three models of the RM197 mutants show unexpected reorganisation of the M197 sidechain. • The arginine was determined to be pointing up towards the periplasmic surface of the protein. • Void left by removal of M197 from protein interior has been filled by at least 2 probably 3 water molecules. • The 2-acetyl of P_M is hypothesised to be H-bonding to one water molecule, which in turn appears to be part of a water chain. • The 2-acetyl group of P_M is also undergone a rotation away from the plane of the BChl ring.	• Carotenoid had been previously determined to have only minor alterations in its configuration and interactions with the protein environment. As expected, the models showed no alteration in the structure of the carotenoid molecules. • One point of interest is the introduction of water into the WM115 structure, filling the void left in the protein interior by replacement of Trp with Phe. This phenomenon is repeated for the RM197 mutants (See below) • All the spectroscopic investigations pointed towards a significant alteration in the structure of P in the RM197 mutants. • "Fortuitous" positioning of M197, allows the arginine side chain to escape the protein interior. • As was found in the WM115 model, the introduction of a cavity in the interior of the protein has permitted water molecules to enter. • The introduction of water, has probably led to the altered characteristics, however, the precise mechanism remains unclear. Three factors could be involved : The introduction of a new H-bond to P; the rotation of the 2-acetyl group of P_M further away from the BChl plane; and the alteration of the polarity of the medium surrounding P.

14.2.1. The Selection of Carotenoids Binding within the Reaction Centre

The results of the analyses of the carotenoid binding site mutants would suggest that the five residues mutated have limited influence on the structure and function of the carotenoid. This finding is somewhat surprising, given that the nature of the carotenoid binding pocket is predominantly hydrophobic. The positioning of the five polar residues in close proximity to the carotenoid suggested that they have some influence on the properties of the carotenoids molecule. However, the evidence gathered would seem to show this hypothesis to be incorrect. Despite this, during the progress of the research a number of potentially important observations have been made with regard to the selective nature of the reaction centre for carotenoids, and the possible implications for function.

The mechanism used by the reaction centres to select and bind only certain carotenoids has remained unknown for many years. This selection was first shown by Cogdell et al (1975) in *Rb. sphaeroides*, with similar findings produced for *R. rubrum* by Boucher et al (1977). The reaction centres of *Rb. sphaeroides* generally show a strong preference for the binding of methoxy (or hydroxy) carotenoids; e.g. spheroidene, spheroidenone and also spirilloxanthin, or hydroxy forms such as hydroxyspheroidene and hydroxyneurosporene. Carotenoids containing methoxy and hydroxy functional groups are known as xanthophylls. The strain G1C is an exception to the rule, in that it binds the carotenoid neurosporene, which does not carry a methoxy/hydroxy group. The crystal structures of the *Rb. sphaeroides* reaction centres (all but the 2RCR and 4RCR models, which are models of the carotenoidless strain R-26) show that the carotenoid is bound in an identical orientation, with methoxy group always present in the same end of the binding pocket (See Figure 52 for the RCO2 structures). Given that the remainder of the xanthophyll structure is essentially identical to neurosporene, an extremely hydrophobic hydrocarbon chain, the methoxy/hydroxy group must itself be the group responsible for selection.

Published crystal structures have failed to produce any likely candidates for amino acid residues capable of binding to the carotenoid methoxy/hydroxy group. However, in the structures presented in this work, a tryptophan residue (M75) seems to be ideally positioned to

perform this role. The initial electron density map produced in the Trp M75 region is shown in Figure 57. The skeleton is present as given by the co-ordinates of Ermler et al (1994). It is very clear, from the $2F_O$-F_C electron density map, and especially when the positive and negative F_O-F_C maps are overlaid, that the orientation of this tryptophan is incorrect when investigated with the new data. This observation was confirmed through comparison with all the structures analysed in these investigations. Therefore, the hypothesis is put forward that this residue, tryptophan M75, is responsible for observed selection of methoxy/hydroxy carotenoids, in all but the strain G1C of *Rb. sphaeroides*. An obvious question leads from this. What allows neurosporene to be bound within the G1C reaction centre? Unfortunately the amino acid sequences of the G1C reaction centre protein subunits have not been determined. However, site-directed mutagenesis of TrpM75 to a phenylalanine residue, is now being performed (M. Jones & J. Ridge, personal communication), the impact of this mutation on the ability of the reaction centre to bind/select carotenoids is awaited with interest.

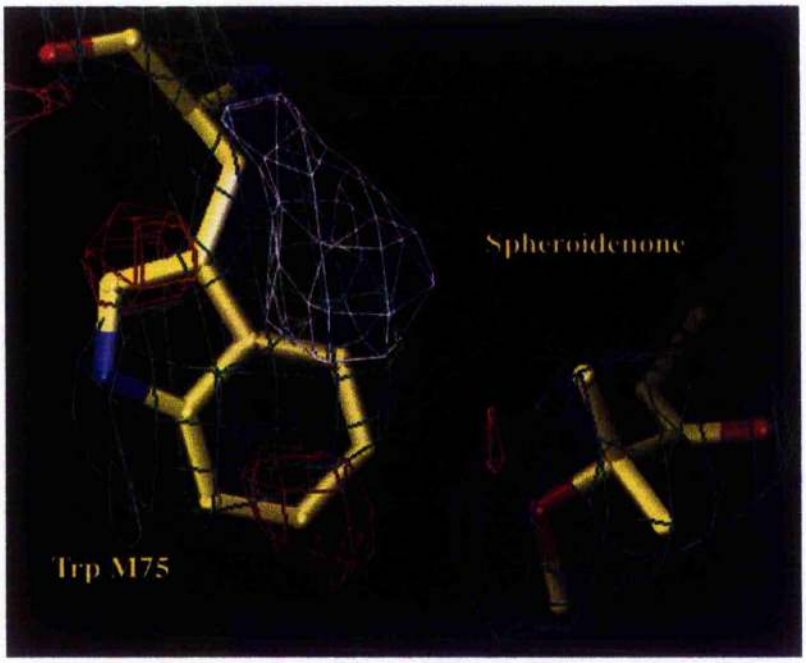

Figure 57: The 2Fo-Fc (sea-green), contoured at the 1σ level, and Fo-Fc (negative map in red, positive map in green) maps, contoured at the 3σ level, for the region surrounding Tryptophan M75, and the end of the spheroidenone molecule. The orientation of the tryptophan would appear to be incorrect as it is shown. Manipulation of the residue into an orientation matching the evidence from the maps, places the NE1 group within potential H-bonding distance of the methoxy group of the carotenoid (See Figure 44, Section 13.1.2.).

The character of the reaction centre carotenoids requires that there be more than just selection for xanthophylls. As discussed in Chapter 2 (Section 2.4.4.), the ability of carotenoids to quench bacteriochlorophyll triplet states is found only when the number of conjugated C=C double bonds in the system is at least nine. Carotenoids with a conjugated system shorter than this, must be in some way selected against by the reaction centre. Chadwick and Frank (1986) performed a survey of carotenoid binding within reaction centres of *Rb. sphaeroides*. In a series of reconstitution experiments the ability of a range of carotenoids with different functional groups and lengths of conjugation to bind within reaction centres isolated from *Rb. sphaeroides* R-26 was tested. Several of the investigated carotenoids are shown in Figure 58.

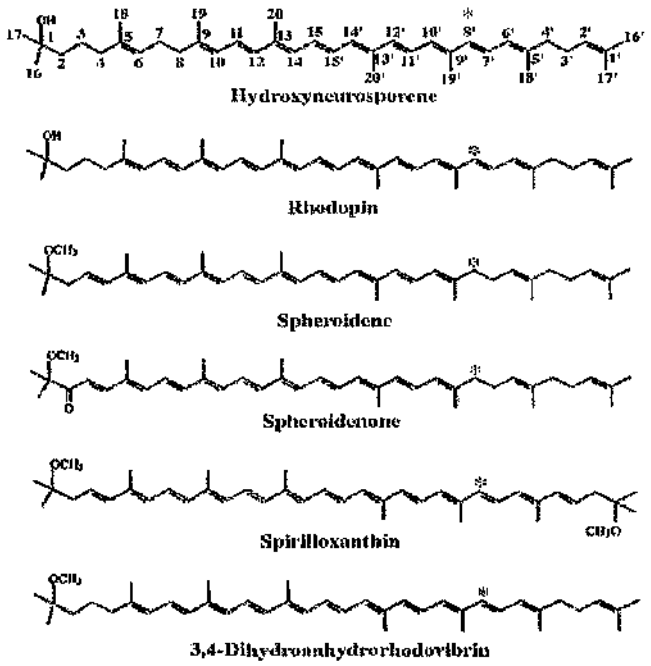

Figure 58: The structures of several of the carotenoids discussed by Chadwick & Frank (1986) in their survey of carotenoid binding within *Rb. sphaeroides* reaction centres. The mark (*) demotes the 8' position referred to in the text below.

The results showed, as expected, that the binding was only observed for xanthophylls: no carotene-type carotenoids were observed to bind. However, not all xanthophylls could become inserted into the reaction centre. One of these xanthophylls, zeaxanthin, carries bulky cyclohexane rings at each end on which the hydroxy groups are held. This implies that the binding of zeazanthin is prevented simply by steric effects. Rhodopin does not carry any such bulky terminal groups. In fact rhodopin is of a very similar structure to hydroxyneurosporene. The properties exhibited by rhodopin in this experiment were explained by the greatly increased solubility of this carotenoid in the aqueous detergent phase. Perhaps this was essentially excluding the carotenoid from accessing the reaction centre complex itself.

Several points remain to be explained with regard to the binding of carotenoids within the reaction centre. The need for a conjugated system consisting of at least 9 C=C bonds is possibly satisfied outside the reaction

centre; the ratio of carotenoids in the cell itself is heavily biased towards chains of this length, or longer. However, when grown in aerobic conditions, the ratio of spheroidenone:spheroidene bound within the reaction centre is higher than the ratio observed in the cell as a whole (Frank & Cogdell, 1993). There would appear, then, to be some process actively selecting particular carotenoids for binding within the reaction centre, beyond that of xanthophyll selection.

One other point of interest is the structure of the carotenoid binding pocket at the opposite end from the methoxy/hydroxy group. The carotenoid is heavily twisted in this region, with group of hydrophobic residues forming a tight ring around the molecule (Figure 59). This twisted region lies just after the ring of polar residues identified and investigated as part of this thesis.

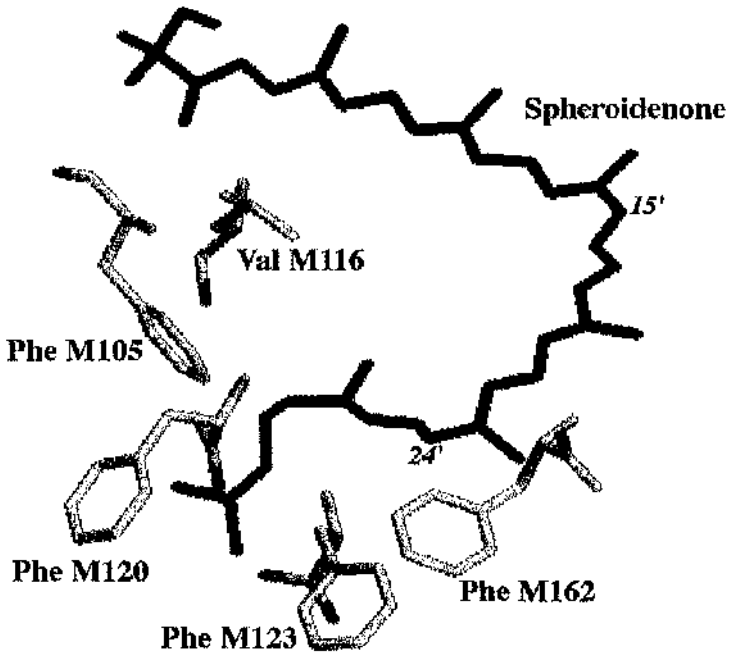

Figure 59: One end of the spheroidenone molecule in the reaction centre model. The spheroidenone molecule is quite heavily twisted after 8'. The end of the carotenoid molecule is surrounded by a cluster of hydrophobic residues; Phe M105, Val M116, Phe M120, Phe M123 and Phe M162.

The deformation of the carotenoid in this region is possibly responsible for the ESR characteristics reported by Chadwick and Frank (1986) for

different lengths of C=C conjugation. The ESR spectra described for spheroidenone, spirilloxanthin and 3,4-dihydroanhydrorhodovibrin showed triplet state ESR zero-field splitting parameters which do not appear to follow the expected trends for varying lengths of conjugated π-orbital system. The zero-field splitting factor |D| is known to correlate with the level of π orbital conjugation (Yarmus et al, 1972), the value of |D| decreasing as the level of conjugation increases. The values determined by Chadwick & Frank are given in Table 30. The values obtained for the reaction centre carotenoid triplet state zero-field splitting parameters should therefore decrease as carotenoids of longer conjugated systems are incorporated. The results showed a stable value for carotenoids with 9 and 10 conjugated C=C bonds

Concomitant with the twisting of the carotenoid molecule will be twisting of the conjugated π orbital system, possibly to such an extent that it weakens /breaks at around 8'. Thus, spirilloxanthin and 3,4-dihydroanhydrorhodovibrin would appear in ESR investigation to posses a much shorter conjugated bond system than might be expected. The "conjugated system" of both these carotenoids extends into the twisted region of the reaction centre carotenoid.

Table 30. The |D| and |E| values obtained by Chadwick & Frank (1986) when they analysed *Rb. sphaeroides* R-26 reaction centres which had been reconstituted with each of the above carotenoids.

Carotenoid	|D|	|E|	No. of conjugated C=C bonds.
Hydroxyneurosporene	0.0284±0.0006	0.0041±0.0003	9
Methoxyneurosporene	0.0286±0.0006	0.0044±0.0003	9
Spheroidene	0.0286±0.0006	0.0044±0.0003	10
Hydroxyspheroidene	0.0286±0.0006	0.0044±0.0003	10
Spheroidenone	0.0271±0.0005	0.0042±0.0003	11
3,4-Dihydroanhydrorhodovibrin	0.0201±0.0003	0.0037±0.0002	11
Spirilloxanthin	0.0201±0.0003	0.0037±0.0003	13

The formation of two rings of amino acids, one of polar residues, immediately followed by another of hydrophobic residues is interesting. It is tempting to hypothesis some link between this formation and the ability

of the reaction centre to force the carotenoid into adopting an unusual configuration. As was briefly discussed in section 13.2.4. of the Results, it is possible to imagine these two rings acting in conjunction with tryptophan M75 to hold and twist the carotenoid into the 15,15'-*cis* configuration. From the results of resonance Raman spectroscopy of the single carotenoid binding pocket mutant complexes, the removal of one polar residue is not enough to effect the twisting process, although small alterations in the spectra suggest some structural differences between strains. Might more than one mutation be sufficient to bring about a detectable alteration? Perhaps removal of the anchoring role of Trp M75 will effectively destroy this ability of the reaction centre, removing the "leverage" for the twisting action.

14.2.2. The Effect of the PheM197 to Arg Mutation.

The effect of the FM197-R mutation on the absorption spectra of reaction centres was observed prior to any analysis performed as part of this thesis. As such, the interest was already high in this strain. The aim was to produce high quality structural data via X-ray crystallography, and also to study the effects of an altered special pair on the relationship between P and the carotenoid. The results presented in Chapters 10, 11 and 13, have produced a large amount of information, and the level of analysis ongoing on this mutation goes beyond what is presented here. One of the major difficulties in detailed characterisation of reaction centre mutants has been the lack of detailed structural models against which assignments made by spectroscopic analysis can be measured. The models produced for this mutant have shown a structure that had not been- and it is doubtful if it ever would have been- proposed from the published spectroscopic data or from data that continues to be produced. However, the X-ray models by themselves do not tell the complete story. The effects presented earlier for absorbance spectroscopy, ESR and CD investigations remain to be fully explained.

The models of the M197 region show three alterations. Firstly, there is, of course, the withdrawal of the M197 side chain from the region close to the BChl molecule. Secondly, there is the insertion of the water molecules into the concomitant void. Lastly, there is the apparent alteration in the configuration of the BChl itself, with the 2-acetyl carbonyl of P_M twisting

out of the plane of the chlorin macrocycle. A number of possible explanations for the observed effect on the absorption spectra have been proposed. Firstly, there is the introduction of an extra H-bond to P. Previous studies (Lin et al, 1994; Mattioli et al, 1995), in which an H-bond has been proposed from a His residue introduced in place of the Phe, did not observe any alteration of the absorption spectra of P. The simple addition of an H-bond does not appear to explain the observations.

Secondly, perhaps the formation of this bond has a further effect, in that it appears to have caused a rotation of the group carrying the acetyl carbonyl away from the macrocycle plane. The rotation of the acetyl carbonyl may have weakened the extent of conjugation that exists between this group an the chlorin macrocycle. The effects of rotation of the 2-acetyl group from the plane of the chlorin macrocycle have been computed by two groups, producing apparently contradictory results. Gudowska-Nowak et al (1990), presented computational models based on the BChl pigments of the bacteriochlorophyll *a* antenna protein complex from *Prosthecochloris aestuarii,* whereby a rotation of the acetyl group could lead to a blue-shift in the optical spectrum. The observed blue shift of the P-band in the RM197 strains could, therefore, be explained by the observed rotation. However, in earlier work, Parson and Warshel (1987) predicted that rotation of the 2-acetyl group from fully in plane to fully out of plane of the BChl macrocycle would lead to a ~50nm red shift in the absorbance of the P band in *Rps. viridis* reaction centres. The rotation in the RM197 strains is not as extreme as a 90° rotation out of the plane, but from the above publication it would be assumed any torsion of the 2-aectyl out of the plane of the ring would lead to a red-shift in the absorption band.

Thirdly, the introduction of water molecules into the area surrounding the BChl will have had an effect on the dielectric constant of that region, a factor which Gudowska-Nowak et al (1990) also examined and suggest that this could indeed explain the observed blue-shift. Finally, the calculations of Parson and Warshel (1987) predicted a separation of just 0.1Å between the two BChls comprising P, would be sufficient to cause as much as a 20nm blue-shift in the P absorption band. A movement of this size is unresolvable by X-ray crystallography, at least at the resolution currently available.

In practice it is unlikely that any one of these proposed mechanisms will be solely responsible for the character of the complex. It is much more likely that a combination of a number or all of the above is responsible. With the high-resolution crystal structure now available, there is considerable interest in expanding the work on this particular mutant. It is unusual to be able to reinforce spectroscopic assignments and calculations based on them, with detailed structural information. This is now possible. The carotenoid mutant structures are remarkable if only for there "unremarkableness". It is perhaps unfortunate that no functional changes were observed for any of these mutants. However, further mutant structures are already becoming available, with "screening" performed by initial spectroscopic analysis.

14.3. Conclusions.

The influence that the reaction centre carotenoid binding pocket has on the carotenoid pigment remains unclear. Removal or addition (addition of water molecules in the FM115 structure) of polar groups has no apparent effect on the characteristics of the carotenoid within the complex. Some success has resulted from the possible identification of the method by which xanthopyhlls are selected by the complex. The most satisfying observation made in these investigations has been the determination of the crystal structure of the Phe M197-Arg strains. For possibly the first time in reaction centre research it is now possible to attempt to relate the observations made by various spectroscopic investigations into a mutant complex to a high resolution structural model. Despite this, it remains unclear as to what exactly is causing the observed spectroscopic alterations in this mutant. The existence of a high resolution structure does however, provide a strong basis for future hypotheses and calculations. With the increased automation of crystallographic refinement and the ability reliably to produce crystals of the reaction centre complex, it is hoped that the structure of some of the more widely-known reaction centre mutants, such as Trp M210 will become available in the not to distant future.

Appendices

Appendix I: Growth Media

Solid Agar.

	400mls
Yeast Extract	1·2g
Casamino Acids	0·8g
Agar	6g

Method: Made up to volume with dH_2O. The solution was then heated in a microwave until the agar had dissolved. The solution was either poured into clean universal bottles to make stabs and autoclaved, or autoclaved in a flask before being used to pour agar plates

Concentrated Base for Succinate Media.

	1 litre
Nitriloacetic Acid	10g
Magnesium Sulphate	14·45g
Calcium Chloride, $2H_2O$	3·4g
Ammonium Molybdate	0·00925g
Ferrous Sulphate, $7H_2O$	0·099g
Nicotinic Acid	0·05g
Aneurine Hydrochloride	0·025g
Biotin	0·0005g
Metos 44	50mls

Method: To the above solids, half the final volume of dH_2O was added and the pH adjusted to 6.8 using 5N KOH. The solution was then made up to the final volume with $d.H_2O$.

C-Succinate Media.

	1 litre
Conc. Base	20mls
1M Di-potassium hydrogen orthophosphate	10mls
1M Potassium Di-hydrogen Orthophosphate	10mls
10% Ammonium Sulphate(w/v)	5mls
1M Sodium Succinate	10mls
Growth Factors	1ml
Casamino Acids	1g

Method: To the above d.H2O was added and the solution stirred until all solids had dissolved. The media was then autoclaved.

Growth Factors.

	1 Litre
Biotin	0.02g
Sodium Hydrogen Carbonate	0.5g
d.H2O is added at this point and the two ingredients dissolved before the remaining constituents are added.	
Nicotinic acid	1g
Aneurine Hydrochloride	0.5g
4 Aminobenzoic acid	1g
The last three constituents were then added to the dH2O solution prepared earlier, and the solution then boiled to dissolve the ingredients.	

Metos 44.

	1 litre
EDTA	2·5g
Manganous Sulphate, 4H2O	10·95g
Zinc Sulphate, 4H2O	1·54g
Copper Sulphate, 5H2O	0·392g
Cobaltous Nitrate, 6H2O	0·248g
Ferrous Sulphate, 7H2O	5·5g
Disodium Tetraborate, 10H_2O	0.177g
The required amount of d.H_2O was added and the constituents dissolved. Finally concentrated sulphuric acid was added, 2 drops to 100mls or 20 drops to 1 litre.	

M22+ Medium (10x concentrate)

	500mls
Potassium Di-hydrogen Orthophosphate	15.3g
Di-Potassium Hydrogen Orthophosphate	15g
Sodium Lactate	12.5g
Sodium Chloride	2.5g
Ammonium Sulphate	2.5g
Solution C (see below)	100mls
Sodium Succinate	21.7g
Sodium Glutamate	1.35g
Aspartic Acid	0.2g
Method: All of the ingredients were dissolved in ~400mls of d.H_2O and the pH corrected to 7.5 with the addition of KOH pellets. The volume was then made up to 500mls and the concentrate autoclaved.	

Solution C.

	4 litres
Nitriloacetic Acid	40g
Magnesium Chloride	96g
Calcium Chloride	13.36g
EDTA	500mg
Zinc Chloride	1.044g
Ferric Chloride	1g
Manganous Chloride	360mg
Ammonium Molybdate	37mg
Cupric Chloride	31mg
Coboltous Nitrate	49.6mg
Boric Acid	22.8mg

Method: The solids were weighed out and placed in a 5 litre beaker. ~3500mls of d.H_2O were added and the solution stirred. The pH was adjusted to between 6.8 and 6.9 by the addition of KOH pellets. As the pH reached this level, the solution became clear and was placed into clean plastic bottles for storage at -20°C.

1000x Vitamin Solution.

	100mls
Nicotinic Acid	100mg
Thiamine	50mg
pABA (para-amino benzoic acid)	10mg
Biotin	1mg

Method: The above solids were disssolved in d.H_2O and filter sterilized into sterile Eppendorf tubes/Falcon tubes. The tubes were stored at -20°C.

LB Medium.

	1 Litre
Bacto-tryptone [DIFCO]	10g
Bacto-Yeast Extract [DIFCO]	5g
NaCl	10g

Method: The above solids were added to 950mls of d.H_2O and stirred until dissolved. The pH was adjusted to 7.0 with 5N NaOH and the volume adjusted to 1litre with d.H_2O. Finally the medium was sterilised by autoclaving.

Antibiotic Solutions.

	Stock Solution Concentration
Ampicillin	50mg/ml in d.H_2O
Neomycin	10mg/ml in d.H_2O
Streptomycin	10mg/ml in d.H_2O
Tetracycline	5mg/ml in ethanol

Ampicillin, neomycin and streptomycin solutions were filter sterilised into sterile Eppendorf/Falcon tubes. All solutions were stored at -20°C.

Appendix II: Gel Electrophoresis.

Acrylamide for Electrophoresis Gels.

	250mls
30% acrylamide	75g
0.8% Methylene-bis-acrylamide	2g

Electrolyte for Electrophoresis.

	1 litre
Tris (0.025M)	3g
SDS (0.1%)	1g
Glycine (0.19M)	14·56g

Electrolyte was always made up fresh as required.

Destain.

	2·5 litres
Methanol	250 mls
Glacial Acetic Acid	250mls
Distilled water	2 litres

Gel Stain.

	1·2 litres
dH_2O	500mls
Methanol	500mls
Glacial Acetic Acid	200mls
Coomassie Blue	1·2g

Running Gel Buffer.

36.3G tris (0.5M) was added to 150mls $d.H_2O$ and dissolved. The pH was adjusted to 8.8 by the addition of conc. HCl, and the solution made up to 200mls with $d.H_2O$.

Stacking Gel Buffer.

3.0g tris (0.5M) was added to 40mls of $d.H_2O$ and dissolved. The pH was adjusted to 6.8 by the addition of conc. HCl, and the solution made up to 50mls with $d.H_2O$.

2 x Treatment Buffer.

	10 mls
4 x Stacking gel buffer	2.5 mls
10% SDS	4.0 mls
Glycerol	2.0 mls
Bromophenol Blue	2.0 mg
Dithiothreitol	0.31g

Make the above up to 10·0 mls with d.H_2O and store in 0.5ml aliquots at -20°C for up to 6 months.

SDS-PAGE Gel Recipes.

i) Resolving Gels:

Final Gel Concentration(20mls; 2 0·75 mm thick Mini-gels)			
	7.5%	10%	15%
Monomer solution	2.5mls	3.3mls	5mls
4x Running Gel Buffer	2.5mls	2.5mls	2.5mls
10% SDS	0.1mls	0.1mls	0.1mls
ddH_2O	4.9mls	4.0mls	2.4mls
Ammonium Persulphate	50µl	50µl	50µl
TEMED	3.3µl	3.3µl	3.3µl

Method: The monomer solution, running buffer and d.H_2O were pipetted into a clean round-bottom quickfit flask, and mixed by swirling. The flask was covered with cling-film, before degassing the solution by the application of a vacuum from a water pump. After degassing, the remainder of the solutions were added (the ammonium persulphate was always made up fresh).

ii) Stacking Gels.

	1 x 0·75mm Gel
Monomer Solution	0·44mls
4 x Stacking gel buffer	0·83mls
10% SDS	33µl
ddH_2O	2·03mls
Ammonium Persulphate	16·7µl
TEMED	1·7µl

The method followed was identical to that described for the resolving gels above.

Appendix III: Miscellaneous.

Preparation of Dialysis Tubing.

Dialysis tubing/membrane was prepared in batches, and stored at 4°C in 20% ethanol solution. The membrane was prepared by firstly boiling for 10mins in 2% (w/v) sodium bicarbonate, 1mM EDTA solution. After boiling the membrane was rinsed thouroughly in d.H_2O, before boiling for a further 10 mins in 1mM EDTA solution. The tubing was then allowed to cool before addition to the 20% ethanol for storage. Prior to use the membrane was carefully rinsed with d.H_2O.

MES/KCl Buffer.

	1 litre
20mM MES	3.9g
0.1M KCl	7.4g

10x Annealing Buffer

Tris/HCl, pH 7.5	200mM
$MgCl_2$	100mM
NaCl	500mM

Preparative Gels

TAE Buffer: 50x concentrate.

	1 litre
Tris	242g
Glacial Acetic Acid	57.1mls
EDTA	40mls of 0.5M (pH 8.0)

Preparative gel:

	100mls
TAE Buffer (50x stock)	2mls
Agarose (Low Melting Point) [BRL]	1g
Ethidium Bromide (10mg/ml stock)	4µl
d.H_2O	97.9mls

Appendix IV:

Sample Diffraction Images & Crystallographic Plots.

Luzzati plot for the WT Red Model (2.6Å)

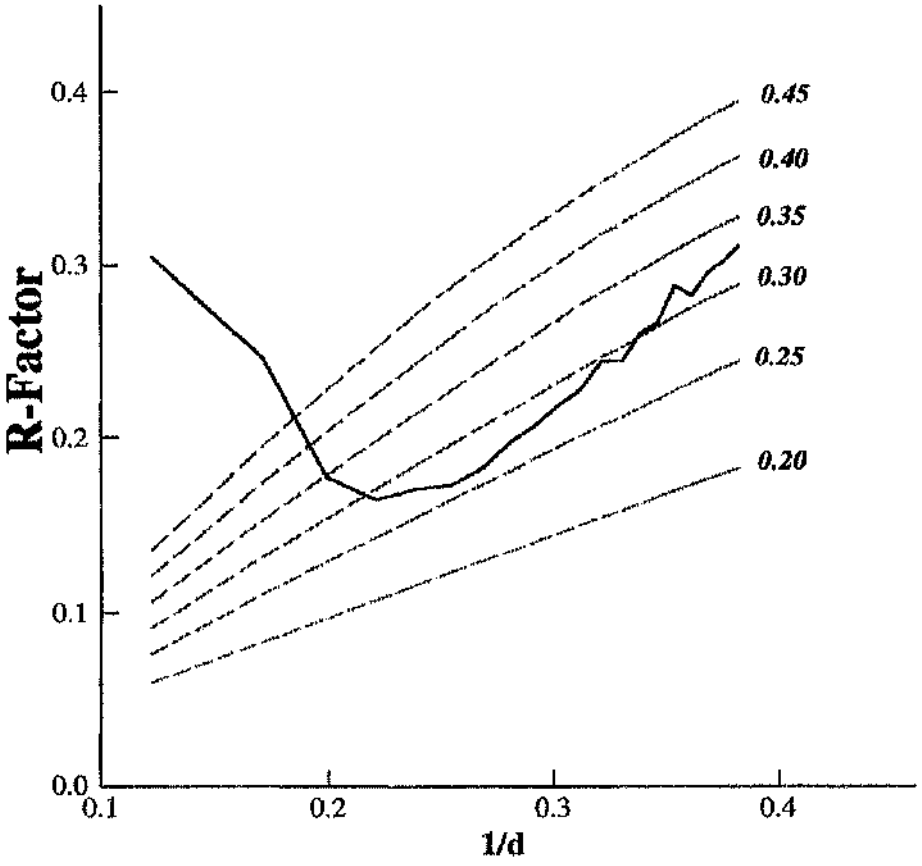

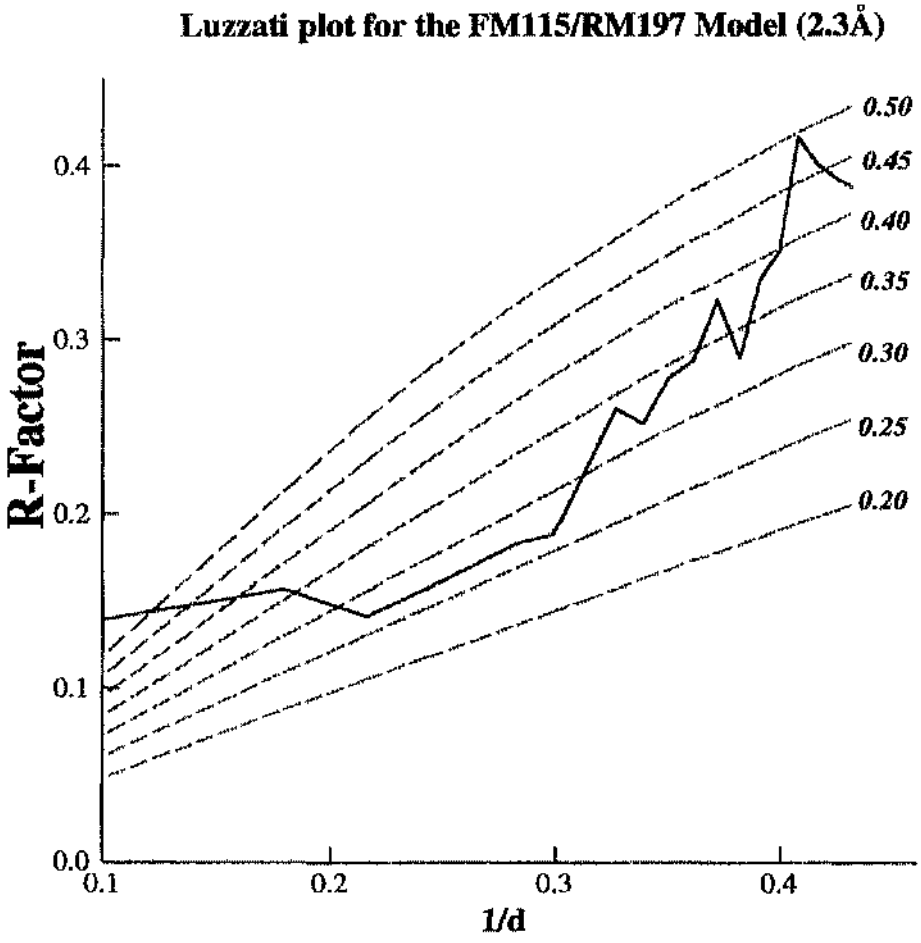
Luzzati plot for the FM115/RM197 Model (2.3Å)
R-Factor
0.0
0.1
0.2
0.3
0.4
0.1
0.2
0.3
0.4
1/d
0.50
0.45
0.40
0.35
0.30
0.25
0.20

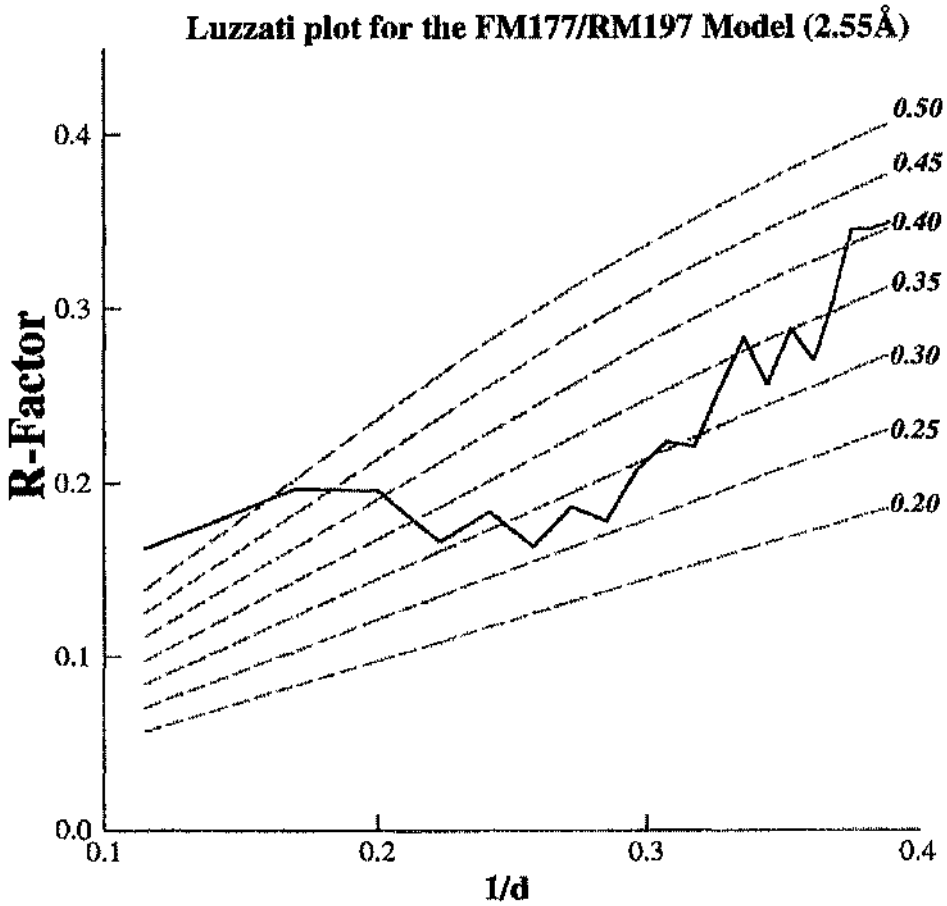
Luzzati plot for the FM177/RM197 Model (2.55Å)
R-Factor
1/d
0.0
0.1
0.2
0.3
0.4
0.50
0.45
0.40
0.35
0.30
0.25
0.20

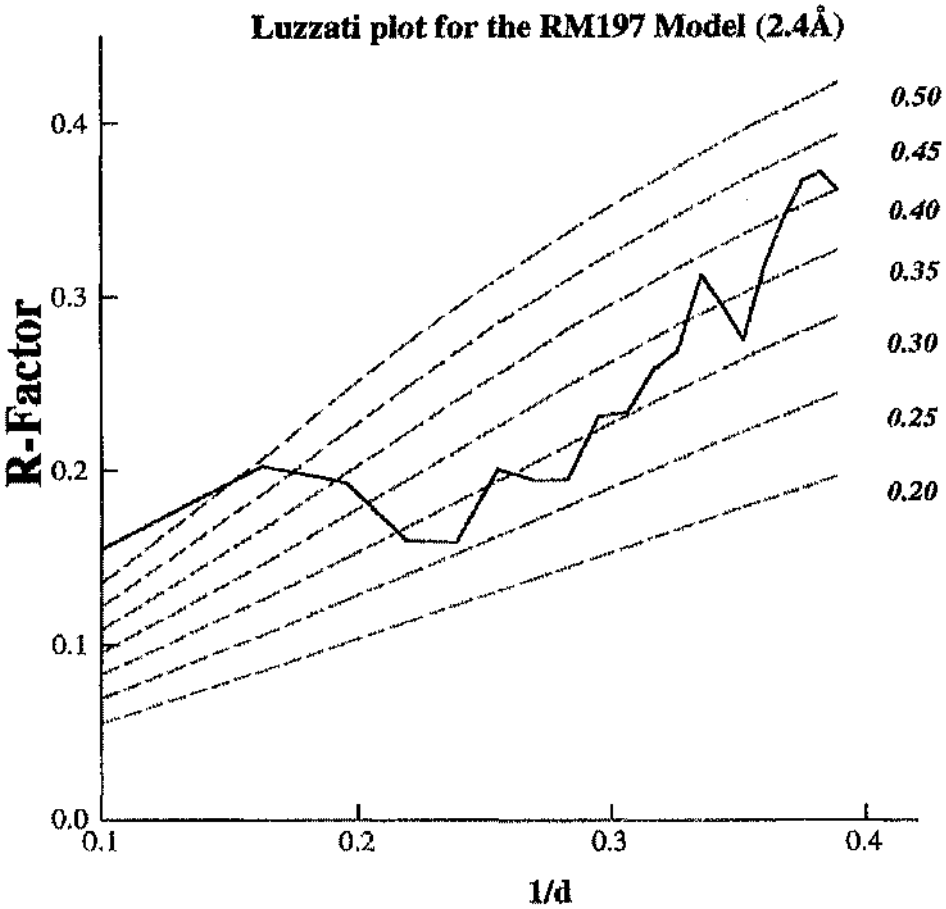
Luzzati plot for the RM197 Model (2.4Å)
R-Factor
0.0
0.1
0.2
0.3
0.4
0.1
0.2
0.3
0.4
1/d
0.50
0.45
0.40
0.35
0.30
0.25
0.20

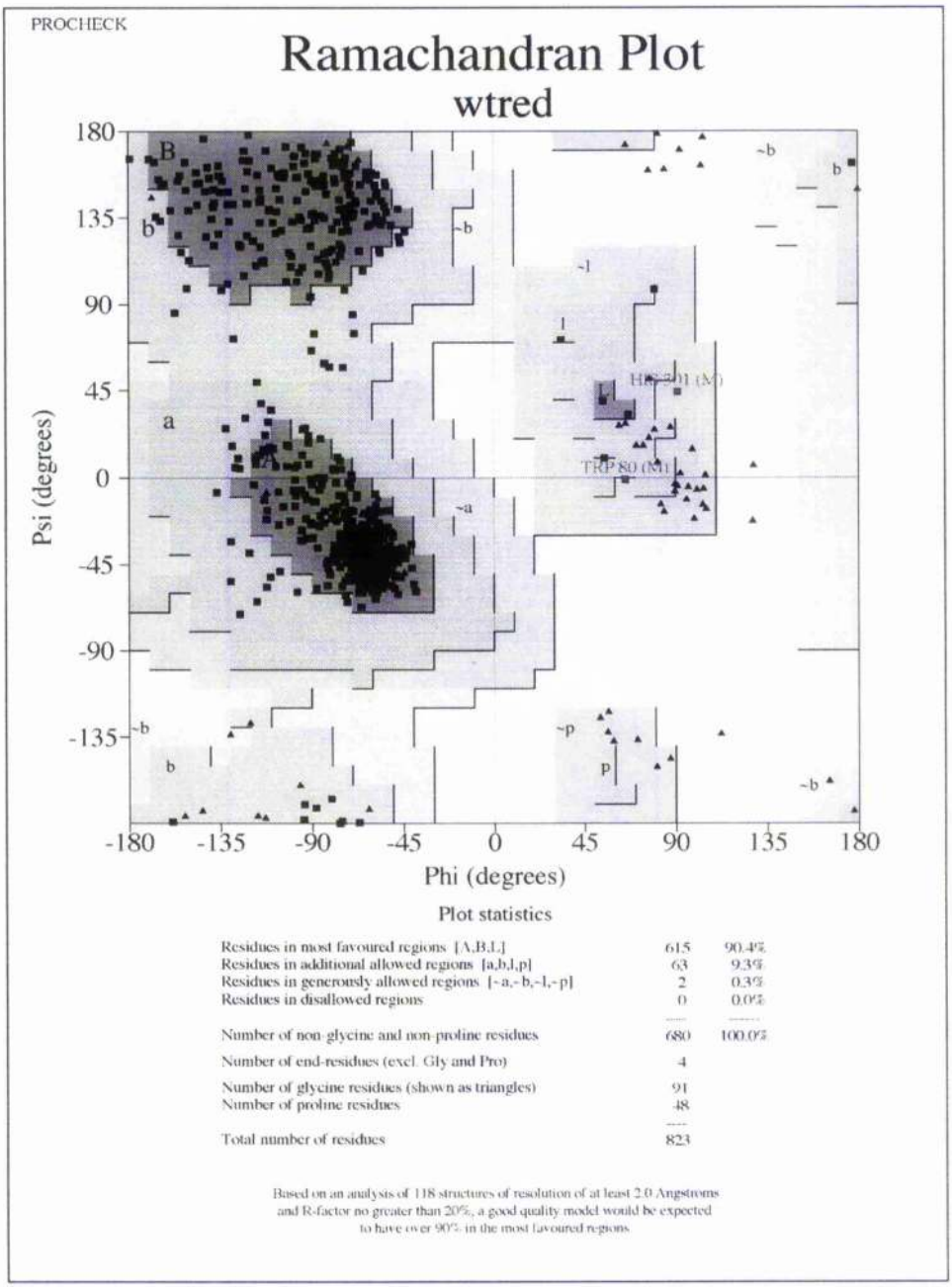

Plot statistics

Residues in most favoured regions [A,B,L]	615	90.4%
Residues in additional allowed regions [a,b,l,p]	63	9.3%
Residues in generously allowed regions [~a,~b,~l,~p]	2	0.3%
Residues in disallowed regions	0	0.0%
Number of non-glycine and non-proline residues	680	100.0%
Number of end-residues (excl. Gly and Pro)	4	
Number of glycine residues (shown as triangles)	91	
Number of proline residues	48	
Total number of residues	823	

Based on an analysis of 118 structures of resolution of at least 2.0 Angstroms and R-factor no greater than 20%, a good quality model would be expected to have over 90% in the most favoured regions.

PROCHECK

Ramachandran Plot

wm115

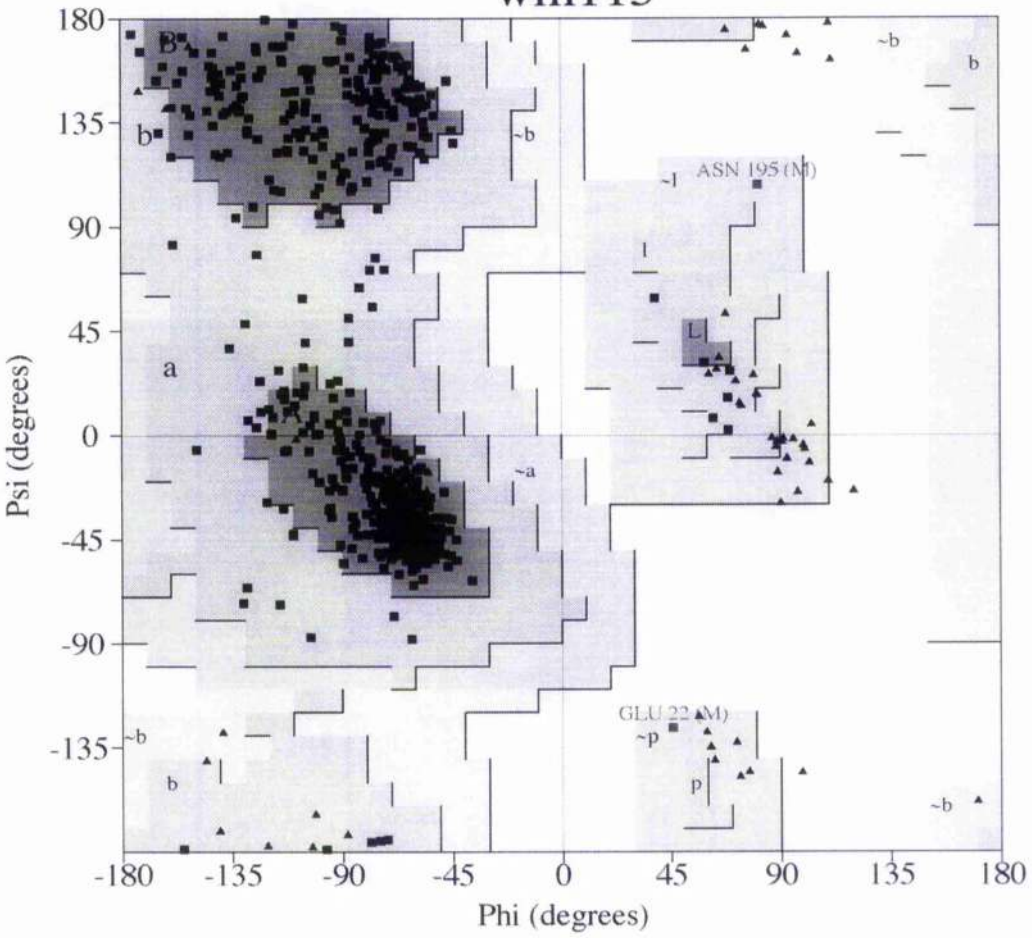

Plot statistics

Residues in most favoured regions [A,B,L]	629	92.5%
Residues in additional allowed regions [a,b,l,p]	49	7.2%
Residues in generously allowed regions [~a,~b,~l,~p]	2	0.3%
Residues in disallowed regions	0	0.0%
Number of non-glycine and non-proline residues	680	100.0%
Number of end-residues (excl. Gly and Pro)	4	
Number of glycine residues (shown as triangles)	91	
Number of proline residues	48	
Total number of residues	823	

Based on an analysis of 118 structures of resolution of at least 2.0 Angstroms and R-factor no greater than 20%, a good quality model would be expected to have over 90% in the most favoured regions.

PROCHECK

Ramachandran Plot

sm119

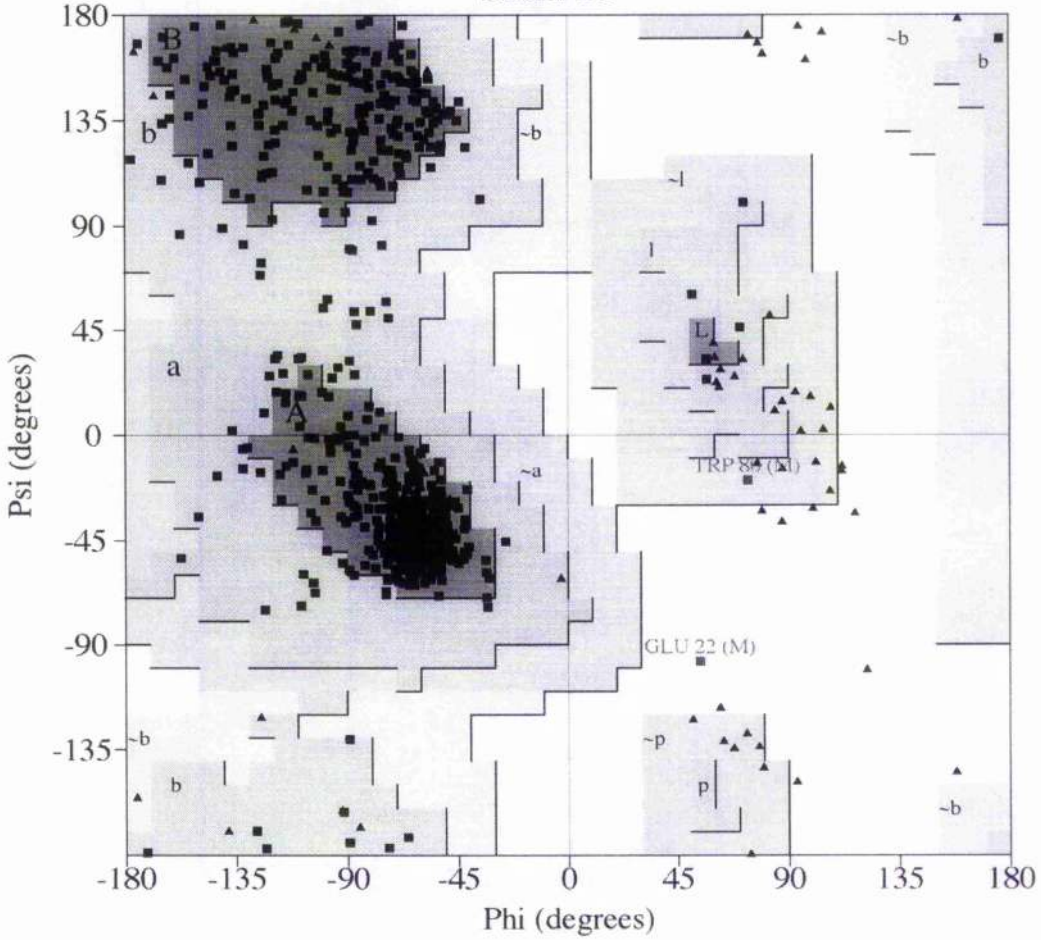

Plot statistics

Residues in most favoured regions [A,B,L]	605	89.0%
Residues in additional allowed regions [a,b,l,p]	73	10.7%
Residues in generously allowed regions [~a,~b,~l,~p]	1	0.1%
Residues in disallowed regions	1	0.1%
Number of non-glycine and non-proline residues	680	100.0%
Number of end-residues (excl. Gly and Pro)	4	
Number of glycine residues (shown as triangles)	91	
Number of proline residues	48	
Total number of residues	823	

Based on an analysis of 118 structures of resolution of at least 2.0 Angstroms and R-factor no greater than 20%, a good quality model would be expected to have over 90% in the most favoured regions.

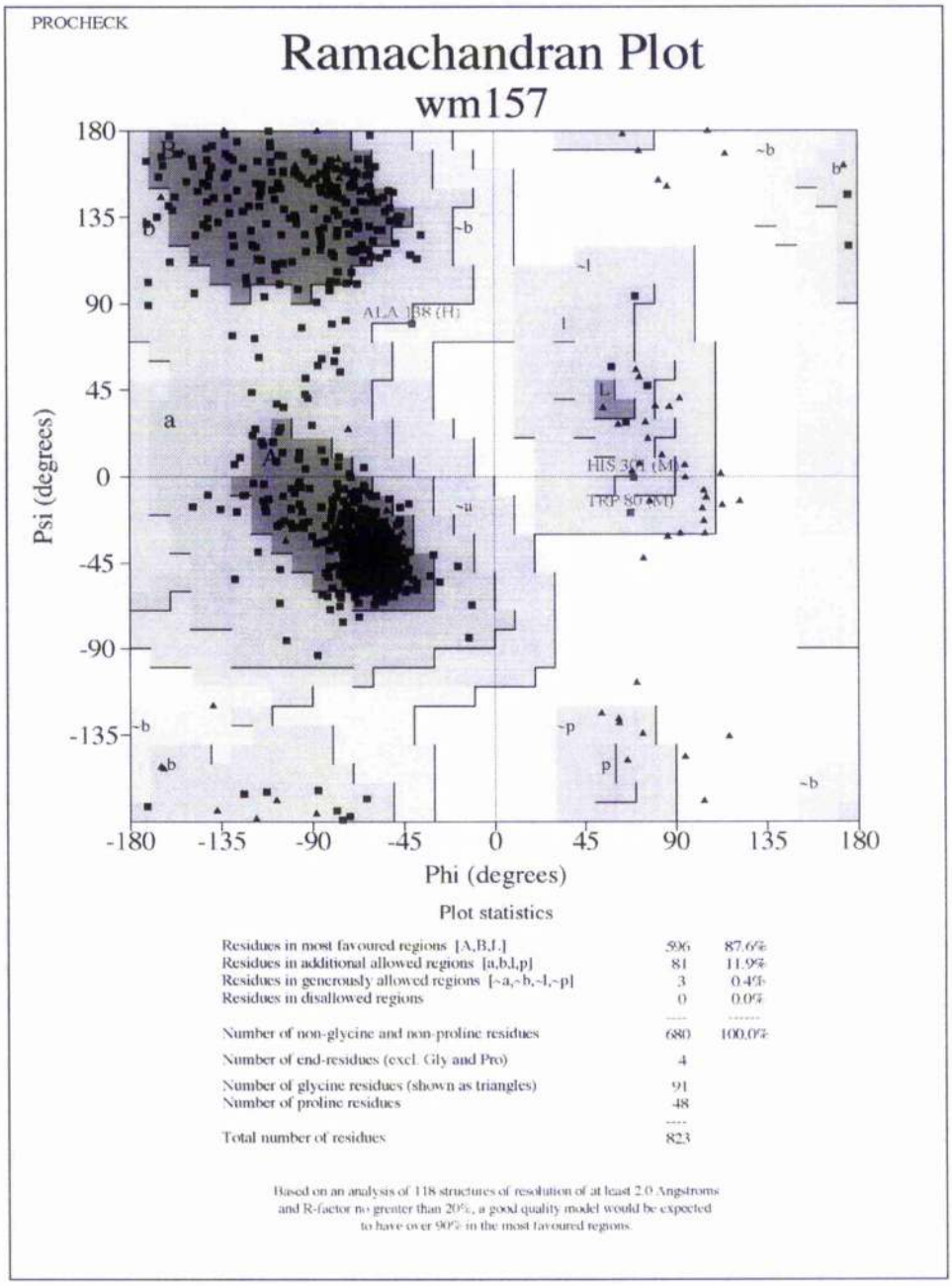
PROCHECK
Ramachandran Plot
wm157
Psi (degrees)
Phi (degrees)
180
135
90
45
0
-45
-90
-135
-180
-135
-90
-45
0
45
90
135
180
ALA 138 (H)
HIS 309 (M)
TRP 80 (A)
Plot statistics
Residues in most favoured regions [A,B,L] 596 87.6%
Residues in additional allowed regions [a,b,l,p] 81 11.9%
Residues in generously allowed regions [~a,~b,~l,~p] 3 0.4%
Residues in disallowed regions 0 0.0%
Number of non-glycine and non-proline residues 680 100.0%
Number of end-residues (excl. Gly and Pro) 4
Number of glycine residues (shown as triangles) 91
Number of proline residues 48
Total number of residues 823
Based on an analysis of 118 structures of resolution of at least 2.0 Angstroms and R-factor no greater than 20%, a good quality model would be expected to have over 90% in the most favoured regions.

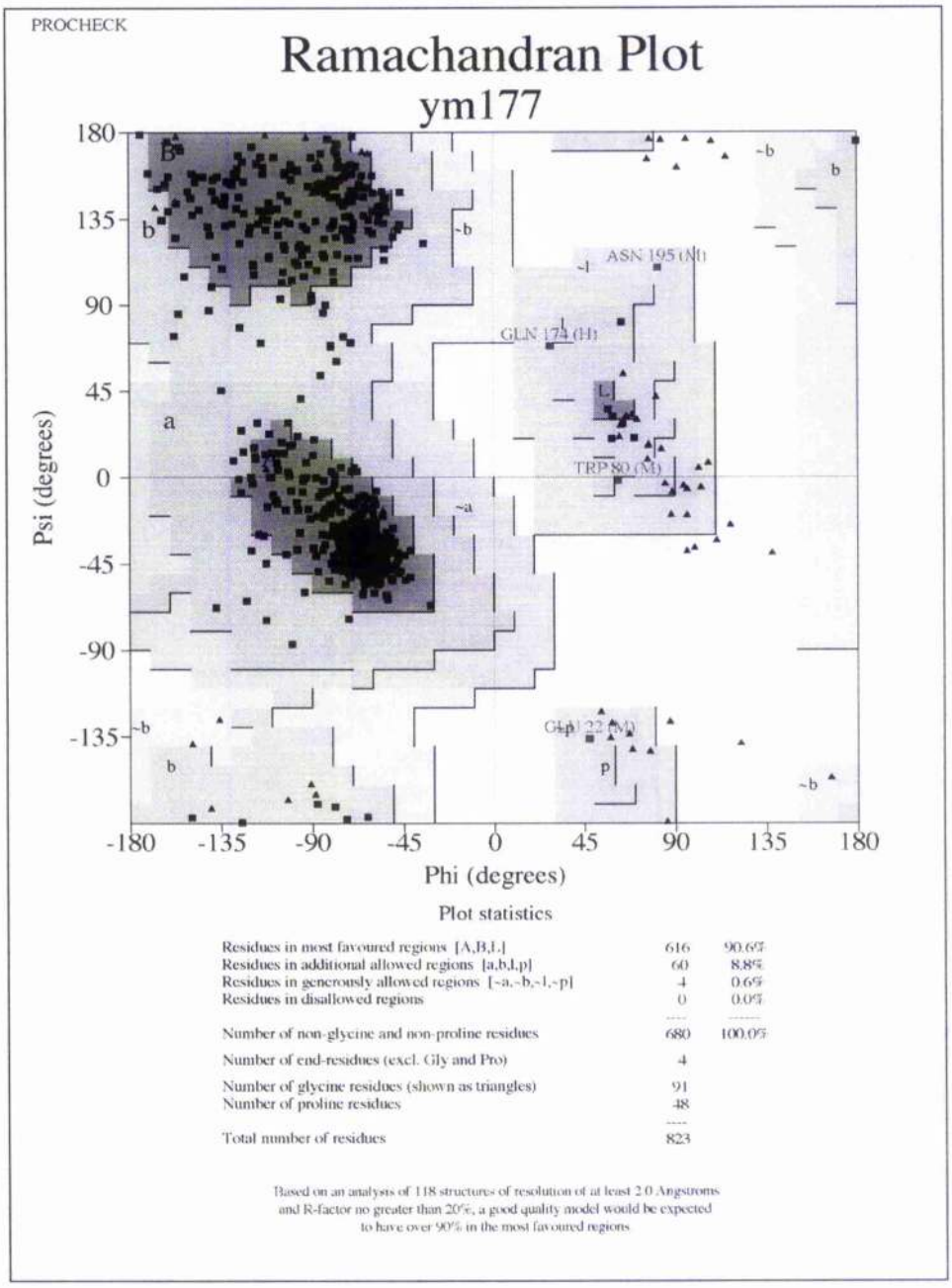

Plot statistics

Residues in most favoured regions [A,B,L]	616	90.6%
Residues in additional allowed regions [a,b,l,p]	60	8.8%
Residues in generously allowed regions [~a,~b,~l,~p]	4	0.6%
Residues in disallowed regions	0	0.0%
Number of non-glycine and non-proline residues	680	100.0%
Number of end-residues (excl. Gly and Pro)	4	
Number of glycine residues (shown as triangles)	91	
Number of proline residues	48	
Total number of residues	823	

Based on an analysis of 118 structures of resolution of at least 2.0 Angstroms and R-factor no greater than 20%, a good quality model would be expected to have over 90% in the most favoured regions

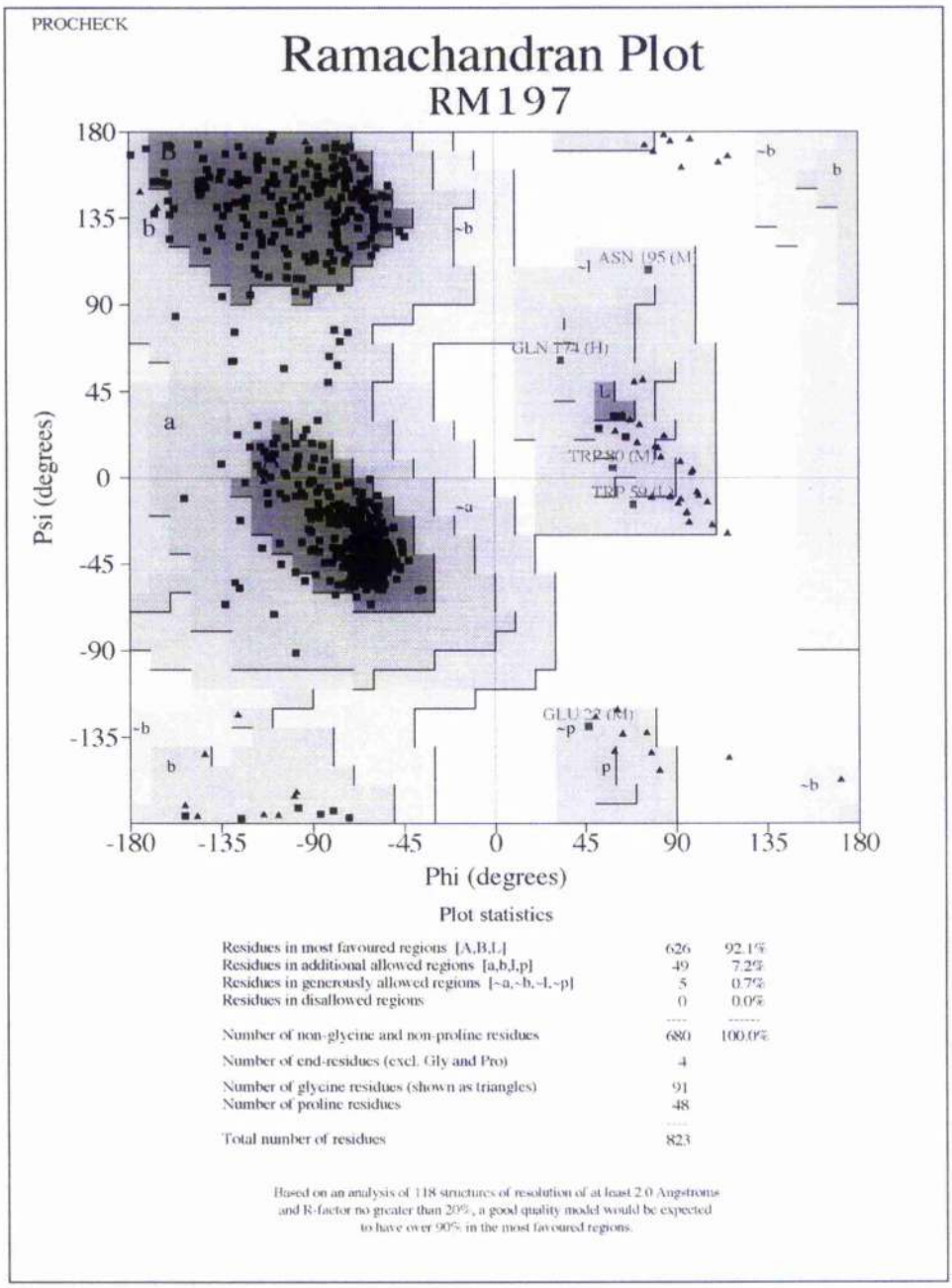

Plot statistics

Residues in most favoured regions [A,B,L]	626	92.1%
Residues in additional allowed regions [a,b,l,p]	49	7.2%
Residues in generously allowed regions [~a,~b,~l,~p]	5	0.7%
Residues in disallowed regions	0	0.0%
Number of non-glycine and non-proline residues	680	100.0%
Number of end-residues (excl. Gly and Pro)	4	
Number of glycine residues (shown as triangles)	91	
Number of proline residues	48	
Total number of residues	823	

Based on an analysis of 118 structures of resolution of at least 2.0 Angstroms and R-factor no greater than 20%, a good quality model would be expected to have over 90% in the most favoured regions.

FM115/RM197 Red
Daresbury Station 9.5

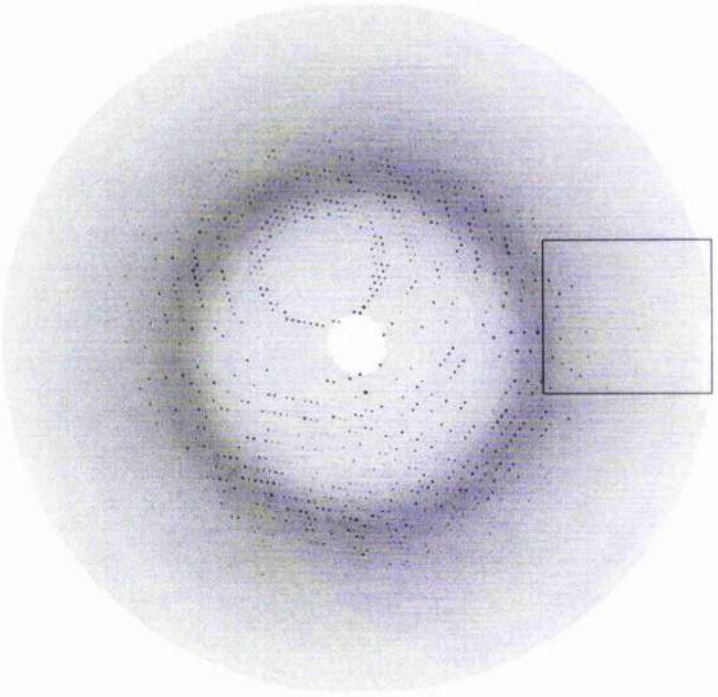

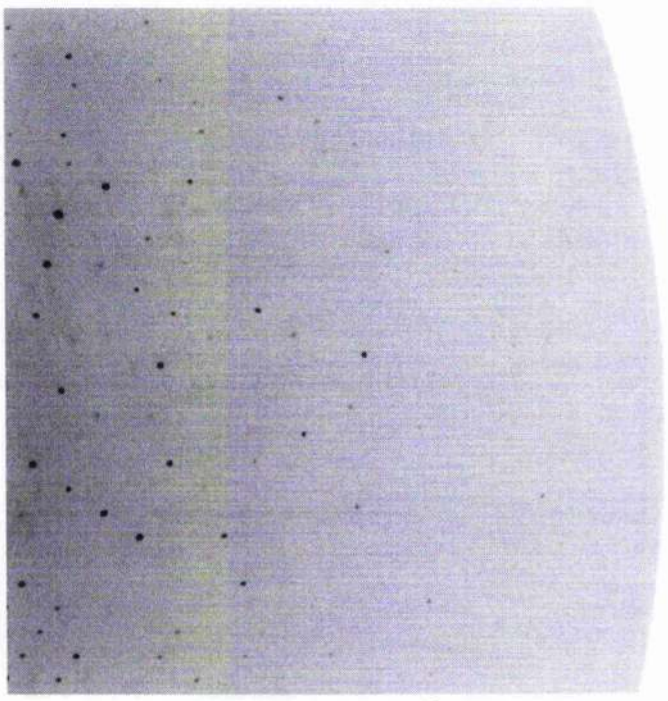

Outer Edge 2.2Å,
10min Exposure

Cryo-Trials: Sample Images

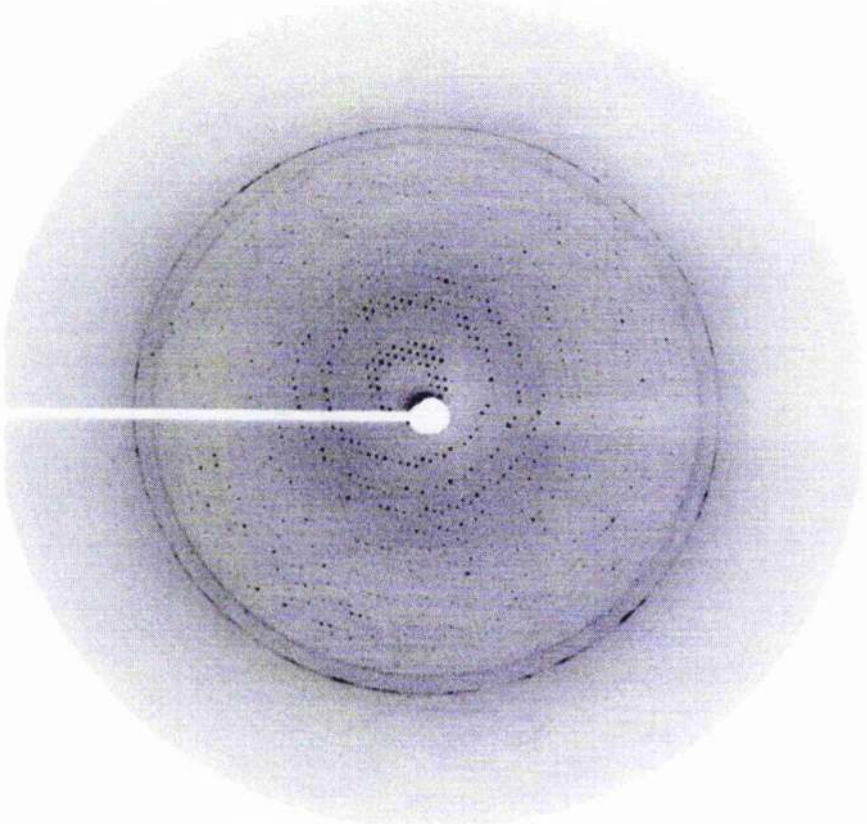

10% B.D. with b-OG detergent.
Collected on DIP 2010, Outside edge ~2.7Å
Max. Diffraction ~3.2Å, Mosaicity ~0.2

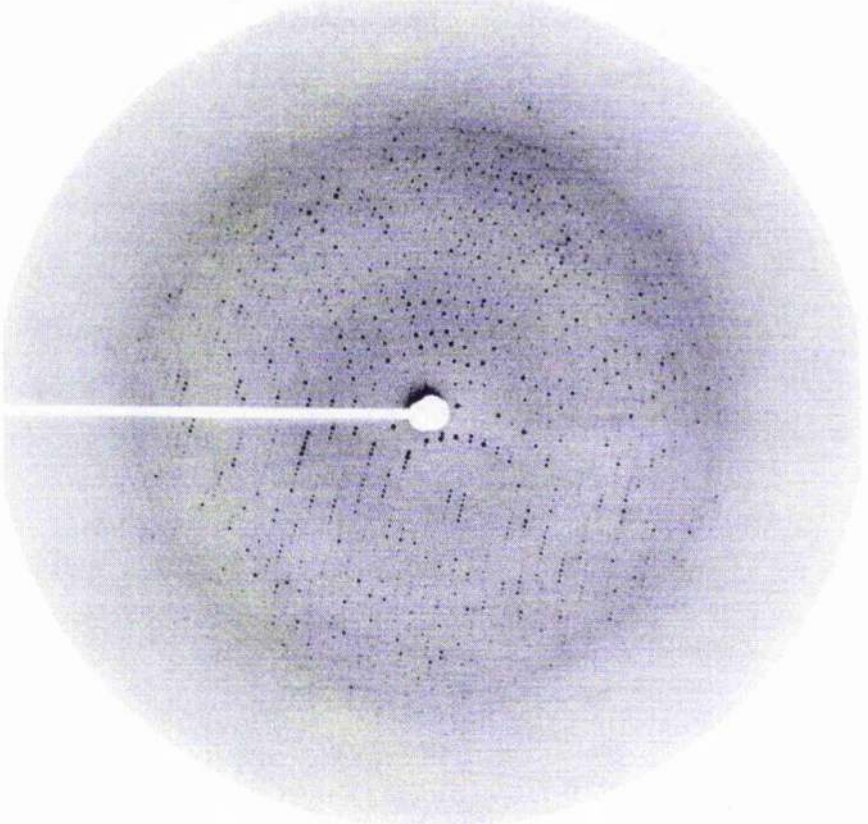

10% B.D. with LDAO detergent.
Collected on DIP 2010, Outside edge ~2.7Å
Max. Diffraction ~3.0Å, Mosaicity ~0.2

References.

Aagaard, J. & Sistrom, W.R. (1972)
Control of Synthesis of Reaction Centre Bacteriochlorophylls in Photosynthetic Bacteria.
Photochem. Photobiol. **15** : 209-225.

Adir, N., Axelrod, H.L., Beroza, R.A., Isaacson, R.A., Rongey, S.H., Okamura, M.Y. & Feher, G. (1996)
Co-Crystallisation and Characterisation of the Photosynthetic Reaction Center-Cytochrome c_2 Complex from *Rhodobacter sphaeroides*.
Biochemistry **35** : 2535-2457.

Agalidis, I., Lutz, M. & Reiss-Hussen, F. (1980)
Binding of Carotenoids in Reactions Centers from *Rhodopseudomonas sphaeroides R*-26
Biochim.Biophys. Acta. **589** : 264-274.

Allen, J.P., Feher, G., Yeates, T.O., Rees, D.C., Deisenhofer, J., Michel, H. & Huber, R. (1986)
Structural Homology of Reaction Centers from *Rhodopseudomonas sphaeroides* and *Rhodopseudomonas viridis* as determined by X-ray diffraction.
Proc. Natl. Acad. Sci. U.S.A. **83** : 8589-8593.

Allen, J.P., Feher, G., Yeates, T.O., Komiya, H. & Rees, D.C. (1987a)
Structure of the Reaction Center from *Rhodobacter sphaeroides* R-26: The Protein Subunits.
Proc. Natl. Acad. Sci. U.S.A. **84** : 6162-6166.

Allen, J.P., Feher, G. Yeates, T.O., Komiya, H., Rees, D.C. (1987b)
Structure of the Reaction Center from *Rhodobacter Sphaeroides* R-26 - The Cofactors
Proc. Natl. Acad. Sci. **84** : 5730-5734

Allen, J.P., Feher, G., Yeates, T.O., Komiya, H. & Rees, D.C. (1988)
Structure of the Reaction Center from *Rhodobacter sphaeroides* R-26 : Protein Cofactor (Quinones and Fe^{2+}) Interactions.
Proc. Natl. Acad. Sci. U.S.A. **85** : 8487-8491.

Allen, J.P., Lous E.J., Feher, G., Chirino, A. & Komiya, H. (1989)
In Curr. Research in Photosynth. - Proc. 8th Internat. Conf. on Photosynth. (Bedtscheffsky, M. and Kluer).

Allen, J.P. & Feher, G. (1991)
Crystallisation of Reaction Centers from *Rhodobacter sphaeroides*.
In Crystallisation of Membrane Proteins (Ed. Michel, H.) CRC Press Inc. Boca Raton. pp137-154.

Allen, J.P., Artz, K., Lin, X., Williams, J.C., Ivancich, A., Albouy, D., Mattioli, T.A., Fetsch, A., Kuhn, M. & Lubitz, W. (1996)
Effects of Hydrogen Bonding to a Bacteriochlorophyll-Bacteriopheophytin Dimer in Reaction Centres from *Rhodobacter sphaeroides*.
Biochemistry **35** (21) : 6612-6619.

Andersson, P. O., Gillbro, T., Ferguson, L. & Cogdell, R.J. (1991)
Absorption Spectral Shifts of Carotenoids Related to Medium Polarizability.
Photochem. & Photobiol. **54** (3) : 353 - 360.

Andersson, P.O., Gillbro, T., Asato, A.E., Liu, R.S.H. (1992)
Dual Singlet-State Emission in a Series of Mini-Carotenes
J. Lumin. **51** : 11-20

Angerhofer, A. F., Bornhäuser, F., Gall, A. & Cogdell, R. J. (1995)
Optical and Optically Detected Magnetic Resonance Investigation on Purple Photosynthetic Bacterial Antenna Complexes.
Chem. Phys. **194** : 259-274.

Arakawa, T. & Timasheff, S. N. (1985)
Theory of Protein Solubility.
Methods in Enzymology **114** : 49-77.

Arlt, T., Schmidt, S., Kaiser, W., Lauterwasser, C., Meyer, M, Scheer, H. & Zinth, W., (1993)
The Accessory Bacteriochlorophyll: A Real Electron Carrier in Primary Photosynthesis.
Proc. Natl. Acad. Sci. **90** : 11757-11761

Armstrong, G.A. (1995)
Genetic Analysis and Regulation of Carotenoid Biosynthesis: Structure and Function of the *crt* Genes and Gene Products.
In: Anoxygenic Photosynthetic Bacteria, Blankenship, E.D., Madigan, M.T. & Bauer, C.E. (Eds.) , Kluwer Academic Publishers, The Netherlands, pp1135-1157.

Armstrong, G.A. & Hearst, J.E. (1996)
Genetics and Molecular Biology of Carotenoid Pigment Biosynthesis.
FASEB J. **10** : 228-237.

Arnoux, B., Ducruix, A., Reiss-Hussen, F., Lutz, M., Norris, J., Schiffer, M. & Chang, C.H. (1989)
Structure of Spheroidene in the Photosynthetic Reaction Center from Y-*Rhodobacter sphaeroides*.
FEBS Letts. **258** (1) : 47-50.

Arnoux, B., Gaucher, J.F., Ducruix, A & Reiss-Husson, F. (1995)
Structure of the Photochemical-Reaction Center of a Spheroidene- Containing Purple Bacterium, *Rhodobacter Sphaeroides*-Y, at 3 Angstrom Resolution.
Acta Cryst. **D51** : .368-379

Awramik, S.M. (1992)
The Oldest Records of Photosynthesis.
Photosynth. Res. **33** : 75-89.

Barber, J. (1987)
Photosynthetic Reaction Centres: A Common Link.
TIBS **12** : 321-326.

Bauer, C.E. (1995)
Regulation of Photosynthesis Gene Expression.
In: Anoxygenic Photosynthetic Bacteria, Blankenship, E.D., Madigan, M.T. & Bauer, C.E. (Eds.) , Kluwer Academic Publishers, The Netherlands, pp1221-1234.

Bauscher, M., Leonhard, M., Moss, D.A. & Mäntele, W. (1993)
Binding and Interaction of the Primary and the Secondary-Electron Acceptor Quinones in Bacterial Photosynthesis : An Infrared Spectroelectrochemical Study of *Rhodobacter sphaeroides* Reaction Centers.
Biochim. Biophys. Acta. **1183** : 59 - 71.

Beekman, L.M.P., Mourik, F. van, Jones, M.R., Visser, H.M., Hunter, C.N. & Grondelle. R. van (1994)

Trapping Kinetics in Mutants of the Photosynthetic Purple Bacterium *Rhodobacter sphaeroides* - Influence of the Charge Separation Rate and Consequences for the Rate-Limiting Step in the Light-Harvesting Process.
Biochemistry **33** : 3143-3147.

Bernal, J.D. & Crowfoot, D. (1934)
X-Ray Photographs of Crystalline Pepsin.
Nature **133** : 794-795.

Bendich, A. & Olsen, J.A. (1989)
Biological Action of Carotenoids.
FASEB J. 3 : 1927-1932.

Bensassoon, R., Land, E.J. & Muadinas, B. (1976)
Triplet States of Carotenoids from Photosynthetic Bacteria Studied by Nanosecond Ultraviolet and Electron Pulse Radiation.
Photochem. & Photobiol. **23** : 189-193.

Blankenship, R.E. (1992)
Origin and Early Evolution of Photosynthesis.
Photosynthesis Research **33** : 91-111.

Boatman, E.S. (1964)
Observations on the Fine Structure of Spheroplasts of *Rhodospirillum rubrum*.
J. Cell. Biol. **20** 297-311.

Boistelle, R. & Astier, J. P. (1988)
Crystallisation Mechanisms in Solution.
J. Cryst. Growth. **90** : 14-30.

Borland, C.F., McGarvey, D.J. & Truscott, T.G. (1987)
Photophysical Studies of Bacteriochlorophyll *a* and Bacteriopheophytin *a* : Singlet Oxygen Generation.
J. Photochem. & Photobiol. **B1** : 93 - 101.

Boucher, F., van der Rest, M. & Gingras, G. (1977)
Structure and Function of Carotenoids in the Photoreaction Centre from *Rhodospirillum rubrum*.
Biochim. Biophys. Acta. **461**: 339-357.

Bragg, W.L. (1913)
Proc. Cambridge Phil. Soc. **17** : 43. *(unavailable)*

Breton, J., Martin, J.L., Migus, A., Antonetti, A. & Orszag, A. (1986)
Femtosecond Spectroscopy of Excitation-Energy Transfer and Initial Charge Separation in the Reaction Center of the Photosynthetic Bacterium *Rhodopseudomonas viridis*.
Proc. Natl. Acad. Sci. (U.S.A.) **83** (14) : 5121-5125.

Breton, J., Martin, J.L., Petrich, J., Migus, A. & Antonetti, A. (1986)
The Absence of a Spectroscopically Resolved Intermediate State $P^{+}B^{-}$ in Bacterial Photosynthesis
FEBS Letts. **209** (1) : 37-43.

Britton, G. & Goodwin, T.W. (1971)
Biosynthesis of Carotenoids
Methods in Enzymology **XVIIIC** : 654-681.

Britton, G. (1985)
General Carotenoid Methods.
Methods in Enzymology **111** : 113-149.

Britton, G. (1993)
Biosynthesis of Carotenoids
In "Carotenoids in Photosynthesis", Young, A. & Britton, G. (Eds.) Chapman & Hall, London, UK.

Brünger, A.T., Kuriyan, J & Karplus, M. (1987)
Crystallographic *R* Factor Refinement by Molecular Dynamics.
Science **235** : 458-460

Brünger, A.T. (1992)
X-PLOR, Version 3.1: A System for X-Ray Crystallography and NMR.
Yale University Press, New Haven, CT.

Brünger, A.T. (1992)
Free-R Value : A Novel Statistical Quantity for Assessing the accuracy of Crystal-Structures.
Nature **355** : 472-475.

Brünger, A.T. (1997)
The Free-R Value: A More Objective Statistic for Crystallography.
Methods in Enzymology In Press.

Brünger, A.T., Adams, P.D. & Rice, L.M. (1997)
New Applications of Simulated Annealing in X-Ray Crystallography and Solution NMR.
Structure **5** : 325-336.

Brünger, A.T. & Rice, L.M. (1997)
Crystallographic Refinement by Simulated Annealing: Methods and Applications.
Methods in Enzymology In Press.

Buchanan, S., Michel, H. & Gerwent, K. (1992)
Light-Induced Charge Separation in *Rhodopseudomonas viridis* Reaction Centers Monitored by Fourier-Transform Infrared Difference Spectroscopy: The Quinone Vibrations.
Biochemistry **31** :1314 - 1322.

Buchanan, S.K., Fritzsch, G., Ermler, U. & Michel, H. (1993)
New Crystal Form of the Photosynthetic Reaction Centre from *Rhodobacter sphaeroides* of Improved Diffraction Quality.
J. Mol. Biol. **230** : 1311 - 1314.

Bylina, E.J. & Youvan, D.C. (1988)
Directed Mutagenesis Affecting Spectroscopic and Electron Transfer Properties of the Electron Donor in the Photosynthetic Reaction Centre.
Proc. Natl. Acad. Sci. U.S.A. **85** : 7226-7230.

Bylina, E.J., Kirmaier, C., McDowell, L., Holten, D. & Youvan, D.C. (1988)
Influence of an Amino-Acid Residue on the Optical-Properties and Electron-Transfer Dynamics of a Photosynthetic Reaction Center Complex.
Nature **336** : 182-184.

Bylina, E.J., Kolaczkowski, S.V., Norris, J.R. & Youvan, D.C. (1990)
EPR Characterization of Genetically Modified Reaction Centers of *Rhodobacter capsulatus*.
Biochemistry **29** : 6203-6210.

Carter, C. W. Jr., Baldwin, E. T. & Frick, L. (1988)
Statistical Design of Experiments for Protein Crystal Growth and the Use of a Precrystallisation Assay.
J. Cryst. Growth. **90** : 60-73.

CCP4: Collaborative Computational Project, Number 4 (1994)
The CCP4 suite: Programs for Protein Crystallography.
Acta. Cryst. **D50** : 760-763.

Chadwick, B.W. & Frank, H.A. (1986)
Electron-Spin Resonance Studies of Carotenoids Incorporated into Reaction Centers of *Rhodobacter sphaeroides* R26.1
Biochim. Biophys. Acta. **851** : 257-266.

Chang, C.H., El-Kabbani, O., Tiede, D., Norris, J. & Schiffer, M. (1991)
Structure of Membrane-Bound Protein Photosynthetic Reaction Center from *Rhodobacter sphaeroides*.
Biochemistry **30** : 5352-5360.

Chirino, A.J., Lous, E.J., Huber, M., Allen, J.P., Schenck, C.C., Paddock, M.L., Feher, G. & Rees, D.C. (1994)
Crystallographic Analyses of Site-Directed Mutants of the Photosynthetic Reaction Centre from *Rhodobacter sphaeroides*.
Biochemistry **33** : 4584 - 4593.

Chynwat, V. & Frank, H.A. (1995)
The Application of the Energy Gap Law to the S_1 Energies and Dynamics of Carotenoids.
Chem. Phys. **194** : 237-244.

Claes, H. (1960)
Interaction Between Chlorophyll and Carotenes with Different Chromophoric Groups.
Biochim. Biophys. Res. Commun. **3** : 585-590.

Clayton, R.K. (1966)
Spectroscopic Analysis of Bacteriochlorophylls *in vitro* and *in vivo*.
Photochem. Photobiol. **5** : 669.

Clayton, R.K. & Wang, R.T. (1971)
Photochemical Reaction Centers from *Rhodopseudomonas sphaeroides*.
Methods in Enzymology **XXIII** : 696-704.

Clayton, R.K. (1978)
Effects of Dehydration on Reaction Centers from *Rhodopseudomonas sphaeroides*.
Biochim. Biophys. Acta **504** : 255-264.

Cogdell, R.J., Monger, T.G. & Parson, W.W. (1975)
Carotenoid Triplet States in Reaction Centres from *Rhodopseudomonas sphaeroides* and *Rhodospirillum rubrum*.
Biochim. Biophys. Acta. **408** :189-199.

Cogdell, R.J., Parson, W.W. & Kerr, M.A. (1976)
The Type, Amount, Location, and Energy Transfer Properties of the Carotenoid in Reaction Centers from *Rhodopseudomonas sphaeroides*.
Biochim. Biophys. Acta. **430** : 83-93.

Cogdell, R.J., Celis, S., Celis, H. & Crofts, A.R. (1977)
Reaction Centre Carotenoid Band Shifts.
FEBS Letts. **80** (1) : 190-194.

Cogdell, R.J., Hipkins, M.F., MacDonald, W. & Truscott, T.G. (1981)
Energy-Transfer Between the Carotenoid and the Bacteriochlorophyll Within the B-800-850 Light-Harvesting Pigment-Protein Complex of *Rhodopseudomonas sphaeroides*.
Biochim. Biophys. Acta. **634** (1) : 191-202.

Cogdell, R.J. (1985)
Carotenoids in Photosynthesis.
Pure & Appl. Chem. **57** (5) : 723-728

Cogdell, R.J. & Scheer, H. (1985)
Circular Dichroism of Light-Harvesting Complexes from Purple Photosynthetic Bacteria.
Photochem. & Photobiol. **42** (6) : 669 - 678.

Cogdell, R.J., Woolley, K.J., MacKenzie, R.C., Lindsay, J.G., Michel, H, Dobler, J. & Zinth, W. (1985)
Crystallisation of the B800-850 complex from *Rhodopseuodomonas acidophila* Strain 7750.
In Springer Series in *Chem. Phys.* **42** :85.

Cogdell, R. J. & Frank, H. A. (1987)
How Carotenoids Function in Photosynthetic Bacteria.
Biochimica. Biophys. Acta. **895** : 63 - 79.

Cogdell, R.J., Woolley, K.J., Ferguson, L.A. & Dawkins, D. (1991)
In Crystallisation of Membrane Proteins (Ed. Michel, H.) CRC Press Inc. Boca Raton. pp125-136.

Cogdell, R.J. & Frank, H.A. (1996)
Carotenoids in Photosynthesis.
Photochem. Photobiol. **63** : 257-264.

Cogdell, R.J., Fyfe, P.K., Barrett, S.J., Prince, S.M., Freer, A.A., Isaacs, N.W., McGlynn, P. & Hunter, C.N. (1996)
The Purple Bacterial Photosynthetic Unit.
Photosynthesis Research **48**, p55-63

Cohen-Bazire, G., Sistrom, W.R. & Stanier, R.Y. (1956)
Kinetic Studies of Pigment Synthesis by Non-Sulfur Purple Bacteria.
J. Cell. Comp. Physiol. **49** : 25-68.

Cohen-Bazire, G. & Kunisawa, R. (1963)
The Fine Structure of *Rhodospirillum rubrum*.
J. Cell. Biol. **16** : 401-419.

Coleman, W.J. & Youvan, D.C. (1990)
Spectroscopic Analysis of Genetically Modified Photosynthetic Reaction centers.
Annu. Rev. Biophys. Biophys. Chem. **19** : 333-367.

Cowan, S.W., Schirmer, T., Rummel, G., Steiert, M., Ghosh, R., Pauptit, R.A., Jansonius, J.N. & Rosenbusch, J.P. (1992)
Crystal Structures Explain Functional Properties of two *E. coli* Porins.
Nature **358** : 727-733.

Creighton, S. Hwang, J.-K., Warshel, A., Parson, W.W. & Norris, J.R. (1988)
Simulating the Dynamics of the Primary Charge Separation Process in Bacterial Photosynthesis.
Biochemistry **27** : 774-781.

Crielaard, W., Visschers, R.W., Fowler, G.J.S., Grondelle van R., Hellingwerf, K.J. & Hunter, C.N. (1994)
Probing the B800 Bacteriochlorophyll Binding Site of the Accessory Light-Harvesting Complex from *Rhodobacter sphaeroides* using Site-Directed Mutants. 1. Mutagenesis, Effects on Binding, Function and Electrochromic Behaviour of its Carotenoids.
Biochim. Biophys. Acta. **1183** (3): 473-482.

Crofts, A.R., Prince, R.C., Holmes, N.G. & Crowther, D. (1974)
Electrogenic Electron Transport and the Carotenoid Change in Photosynthetic Bacteria.
In: Proceedings of the Third International Congress on Photosynthesis, M. Avaron (Ed.), Elsevier, Amsterdam p1131.

Crofts, A.R. & Wraight, C.A. (1983)
The Electrochemical Domain of Photosynthesis.
Biochim. Biophys. Acta. **726** : 149-185.

Crounse, J.B., Feldman, R.P. & Clayton, R.K. (1963)
Accumulation of Polyene Precursors of Neurosporene in Mutant Strains of *Rhodopseudomonas sphaeroides*.
Nature **198** : 1227-1228.

Cullis, A., Muirhead, H., Perutz, M.Z., Rossmann, M.G. & North, A.C.T. (1962)
The Structure of Haemoglobin. IX A Three-Dimensional Fourier Synthesis at 5.5Å Resolution: Description of the Structure.
Proc. Royal. Soc. **A265** : 161-187.

D'Amico, K.L., Manos, C. & Christensen, R.L. (1980)
Electronic Energy Levels in a Homologus Series of Unsubstituted Linear Polyenes.
J. Am. Chem. Soc. **102** : 1777-1782.

Dauter, Z. (1997)
Data Collection Strategy.
Methods in Enzymology **276** : 326-344.

Debus, R.J., Feher, G. & Okamura, M.Y. (1985)
LM Complex of Reaction Centers from *Rhodopseudomonas sphaeroides* R-26 - Characterization and Reconstitution with the H-Subunit
Biochemistry **24** : 2488-2500.

Debus, R.J., Feher, G. & Okamura, M.Y. (1986)
Iron Depleted Reaction Centres from *Rhodopseudomonas sphaeroides* R-26.1 : Characterization and Reconstitution with Fe^{2+}, Mn^{2+}, Co^{2+}, Ni^{2+}, Cu^{2+} and Zn^{2+}.
Biochemistry, **25** : 2276-2287.

DeCoster, B., Christensen, R.L., Gebhard, R., Lugtenburg, J., Farhoosh, R. & Frank, H.A. (1992)
Low-Lying Electronic States of Carotenoids.
Biochim. Biophys. Acta. **1102** (1) : 107-114.

Deisenhofer, J., Epp, O., Miki, K., Huber, R. & Michel, H. (1984)
X-ray Structure Analysis of a Membrane Protein Complex: Electron Density Map at 3Å Resolution and a Model of the Chromophores of the Photosynthetic Reaction Center from *Rhodopseudomonas viridis*.
J. Mol. Biol. **180** : 385-398.

Deisenhofer, J., Epp, O., Miki, K., Huber, R. & Michel, H. (1985)
Structure of the Protein Subunits in the Photosynthetic Reaction Centre from *Rhodopseudomonas viridis* at 3Å Resolution.
Nature **318** : 618-624

Deisenhofer, J., Michel, H. & Huber, R. (1985)
The Structural Basis of Photosynthetic Light Reactions in Bacteria.
Trends in Biochemical Sciences **10** (6) : 243-248.

Deisenhofer, J. & Michel, H. (1991)
Structures of Bacterial Photosynthetic Reaction Centres.
Annu. Rev. Cell Biol. 7 : 1-23.

Deisenhofer, J., Epp, O., Sinning, I. & Michel, H. (1995)
Crystallographic Refinement at 2.3Å Resolution and Refined Model of the Photosynthetic Reaction-Center from *Rhodopseudomonas viridis*.
J. Mol. Biol. **246** (3) : 429-457.

Degroot, H.J.M, Gebhard, R., Vanderhoef, I., Hoff, A.J., Lugtenburg, J., Violette, C.A. & Frank, H.A. (1992)
C-13 Magic Angle Spinning NMR Evidence for a 15,15'-*cis* Configuration of the Spheroidene in the *Rhodobacter sphaeroides* Photosynthetic Reaction Center
Biochemistry 31 (49) : 12446-12450

DeLucas, L. J., Suddath, F. L., Snyder, R., Naumann, R., Broom, M. B., Pusey, M., Yost, V., Herren, B., Carter, D., Nelson, B., Meehan, E. J., McPherson, A. & Bugg, C. E. (1986)
Preliminary Investigations of Protein Crystal Growth Using the Space Shuttle.
J. Cryst. Growth. 76 : 681-693.

DeMattei, R. C., Feigelson, R. S. & Weber, P. C. (1992)
Factors Affecting the Morphology of Isocitrate Lyase Crystals.
J. Cryst. Growth. **122** : 152-160.

Diederichs K. & Karplus, M (1997)
Improved R-Factors for Diffraction Data Analysis in Macromolecular Crystallography.
Nature Structural Biology 4 : 269-275.

Dodson, E., Kleywegt, G.J. & Wilson, K. (1996)
Report of a Workshop on the Use of Statistical Validators in Protein X-Ray Crystallography.
Acta. Cryst. **D52** : 228-234.

Dracheva, S.M., Drachev, L.A., Konstantinov, A.A., Semenov, A.Y. & Skuvalev, V.P. (1988)
Electrogenic Steps in the Redox Reactions Catalysed by the Photosynthetic Reaction Centre Complex from *Rhodopseudomonas viridis*.
Eur. J. Biochem. **171** : 253-264.

Drenth, J. & Haas, C. (1992)
Protein Crystals and their Stability.
J. Cryst. Growth. **122** : 107-109.

Drews, G. & Giesbrecht, P. (1963)
Die Thylakoidstrukturen von *Rhodopseuodomonas* spec.
Arch. Mikrobiol. **52** : 242-250.

Drews, G., Feick, R., Schumacher, A. & Firsow, N.N. (1977)
Isolation and Characterisation of Light-Harvesting Bacteriochlorophyll Protein Complexes from *Rhodopseudomonas capsulata.*
Ann. Microbiol. (Paris) **134B** : 151-158.

Drews, G. & Imhoff, J.F. (1991)
Phototrophic Purple Bacteria.
In. Variations in Autotrophic Life, Shively, J.M. & Barton, L.L. (Eds.), Academic Press, London, pp51-97.

Drews, G. & Golecki, J.R. (1995)
Structure, Molecular Organisation, and Biosynthesis of Membranes of Purple Bacteria.
In: Anoxygenic Photosynthetic Bacteria, Blankenship, E.D., Madigan, M.T. & Bauer, C.E. (Eds.) , Kluwer Academic Publishers, The Netherlands, p231-233

Dressler, K., Umlauf, E., Schmidt, S., Hamm, P. Zinth, W. & Buchanan, S. (1991)
Detailed Studies of the Subpicosecond Kinetics in the Primary Electron Transfer of Reaction Centres of *Rhodopseudomonas viridis.*
Chem. Phys. Lett. **183** : 270-276.

Dutton, P.L. (1986)
Energy Transduction in Anoxygenic Photosynthesis.
In "Photosynthesis III" Stehlin, L.A. & Arntzen, C.J. (Eds.), Encyclopedia of Plant Physiology Vol. 19, Springer-Verlag, Netherlands, p197-237.

El-Kabbani, O, Chang, C.H., Tiede, D., Norris, J. & Schiffer, M. (1991)
Comparison of Reaction Centers from *Rhodobacter sphaeroides* and *Rhodopseudomonas viridis*: Overall Architecture and Protein-Pigment Interactions.
Biochemistry **30** (22): 5361-5369.

Ellenberger, T.E., Brandl, C.J., Struhl, K. & Harrison, S.C. (1992)
The GCN4 Basic Region Leucine Zipper Binds DNA as a Dimer of Uninterrupted α-Helices: Crystal Structure of the Protein-DNA Complex.
Cell **71** : 1223-1237.

Emerson, R. & Arnold, W.A. (1932)
The Photochemical Reaction in Photosynthesis.
J. Gen. Physiol. **16** : 191-205.

Englard, S. & Seifter, S. (1990)
Precipitation Techniques.
Methods in Enzymology **182** : 285-300.

Ermler, U., Fritzsch, G., Buchanan, S.K. & Michel, H. (1994)
Structure of the Photosynthetic Reaction Centre from *Rhodobacter sphaeroides* at 2.65Å Resolution: Cofactors and Protein-Cofactor Interactions.
Structure **2** : 925-936.

Evans, M.B. (1989)
The Structure and Function of the Light-Harvesting Antenna Complexes from Purple Photosynthetic Bacteria.
University of Glasgow, Department of Botany, PhD. Thesis.

Farchaus, J.W., Wachtweitl, J., Mathis, P. & Oesterhelt, D. (1993)
Tyrosine-162 of the Photosynthetic Reaction Center Plays a Critical Role in the Cytochrome-$C_{(2)}$ Mediated Rereduction of the Photooxidised Bacteriochlorophyll Dimer in *Rhodobacter sphaeroides*: 1. Site-Directed Mutagenesis and Initial Characterization.
Biochemistry **32** (40): 10885-10893.

Feher, G. (1971)
Some Chemical and Physical Properties of a Bacterial Reaction Center Particle and its Primary Photochemical Reactants.
Photochem. & Photobiol. **14** : 373-387.

Feher, G. & Kam, Z. (1985)
Nucleation and Growth of Protein Crystals: General Principles and Assays.
Methods in Enzymology. **114** : 77-111.

Feher, G., Allen, J.P., Okamura, M.Y. & Rees, D.C. (1989)
Structure and Function of Bacterial Reaction Centres.
Nature **339** : 111-116.

Feymann, D., Down, J., Carrington, M., Roditi, I., Turner, M & Wiley, D. (1990)
2.9Å Resolution Structure of the N-Terminal Domain of a Varient Surface Glycoprotein from *Trypanosoma bruceii*.
J. Mol. Biol. **216** (1) : 141-160.

Finkele, U., Lauterwasser, C., Zinth, W., Gray, K.A. & Oesterhelt, D. (1990)
Role of Tyrosine M210 in the Initial Charge Separation of Reaction Centers of *Rhodobacter sphaeroides*.
Biochemistry **29** : 8517-8521.

Firsow, N.N. & Drews, G. (1977)
Differentiation of the Intracytoplasmic Membrane of *Rhodopseudomonas palustris* by Variation of the Oxygen Partial Pressure and Light Intensity.
Arch. Microbiol. **115** : 299-306.

Flemming, G.R., Martin, J.-L. & Breton, J. (1988)
Rates of Primary Electron Transfer in Photosynthetic Reaction Centres and their Mechanistic Implications.
Nature **333** : 190-192.

Foote, C.S. (1968)
Mechanisms of Photosensitized Oxidation.
Science **162** : 963-970.

Foote, C.S. & Denny, R.W. (1968)
Chemistry of Singlet Oxygen. VII. Quenching by β-Carotene.
J. Am. Chem. Soc. **90** : 6233-6235.

Foote, C.S., Chang, Y.C. & Denny, R.W. (1970)
Chemistry of Singlet Oxygen. X. Carotenoid Quenching Parallels Biological Protection.
J. Am. Chem. Soc. **92** : 5216-5218.

Frank, H.A., Bolt, J.D., de Costa, B. & Sauer, K. (1980)
Electron Paramagnetic Resonance Detection of Carotenoid Triplet States.
J. Am. Chem. Soc. **102** : 4893-4898.

Frank, H. A., Machnicki, J. & Felber, M. (1982)
Carotenoid Triplet States in Photosynthetic Bacteria.
Photochem. & Photobiol. **35** (5) : 713-718.

Frank, H. A., Machnicki, J. & Friesner, R. (1983)
Energy Transfer Between the Primary Donor Bacteriochlorophyll and Carotenoids in *Rhodopseudomonas sphaeroides.*
Photochem. & Photobiol. **38**(4) : 451-455.

Frank, H. A., Chadwick, B. W., Toiremi, S., Kolaczowski, S. & Bowman, M. K. (1986)
Singlet and Triplet Absorption Spectra of Carotenoids Bound in the Reaction Centers of *Rhodopseudomonas sphaeroides* R-26.
FEBS Lett. **203** (2) : 157-163.

Frank, H.A., Chadwick, B.W., Oh, J.J., Gust, D, Moore, T.A., Liddel, P.A., Moore, A.L., Makings, L.R. & Cogdell, R.J. (1987)
Triplet-Triplet Energy Transfer in B800-850 Light-Harvesting Complexes of Photosynthetic Bacteria and Synthetic Carotenoporphyrin Molecules Investigated by Electron Spin Resonance.
Biochim. Biophys. Acta. **892** : 253-263

Frank, H. A. & Violette, C. A. (1989)
Monomeric Bacteriochlorophyll is Required for the Triplet Energy Transfer Between the Primary Donor and the Carotenoid in Photosynthetic Bacteria.
Biochim. Biophys. Acta. **976** : 222-232.

Frank, H. A. (1992)
Electron Paramagnetic Resonance Studies of Carotenoids.
Methods in Enzymology **213** : 305-321.

Frank, H.A., Farhoosh, R., Gebhard, R., Lugtenburg, J., Gosztola, D. & Wasielewski, M.R. (1993)
The Dynamics of the S_1 Excited-States of Carotenoids
Chem. Phys. Letts. **207** : 88-92.

Frank, H. A. & Cogdell, R. J. (1996)
Carotenoids in Photosynthesis.
Photochem. & Photobiol. **63** (3) : 257-264.

Fromme, P. (1996)
Structure and Function of Photosystem I.
Current Opinion in Structural Biology **6** : 473-484.

Fromme, P., Witt, H. T., Schubert W. D., Klukas, O., Saenger, W. & Krauß, N. (1996)
Structure of Photosystem I at 4.5Å: A Short Review Including Evolutionary Aspects.
Biochim. Biophys. Acta. **1275** : 76-83.

Fyfe, P.K. & Cogdell, R.J. (1996)
Purple Bacterial Antenna Complexes.
Current Opinion in Structural Biology **6** : 467-472.

Fyfe, P.K., McAuley-Hecht, K.E., Jones, M.R. & Cogdell, R.J. (1997)
Purple Bacterial Reaction Centres.
In Biomembrane Structure, Haris P. & Chapman, D. (Eds.), IOS Publishers, The Netherlands.

Gabbelini, N., Bowyer, J.R., Hurt, E., Melandri, B.A. & Hauska, G. (1982)
A Cytochrome bc_1 Complex with Ubiquinol-Cytochrome c_2 Oxidoreductase Activity from *Rhodopseudomonas sphaeroides* GA.
Eur. J. Biochem. **126** : 105-111.

Gall, A. (1994)
Purification, Characterisation and Crystallisation from a Range of Rhodospirillinae Pigment-Protein Complexes.
University of Glasgow, Department of Botany, PhD. Thesis.

Garavito, R.M., Jenkins, J., Jansonius, J.N., Karlsson, R. & Rosenbusch, J.P. (1983)
X-Ray Diffraction Analysis of Matrix Porin, an Integral Membrane Protein from *E. coli* Outer Membrane.
J. Mol. Biol. **164** : 313-327.

Garavito, R. M., Markovic-Housley, Z. & Jenkins, J. A. (1986)
The Growth and Characterization of Membrane Protein Crystals.
J. Cryst. Growth. **76** : 701-709.

Garavito, R.M. & Rosenbusch, J.P. (1986)
Isolation and Crystallisation of Bacterial Porin.
Methods in Enzymology **125** : 309-328

Gardiner, A.T. (1992)
Peripheral Antenna Complexes from *Rhodopseudomonas acidophila*: Structure, Function and Genetic Manipulation.
University of Glasgow, Department of Botany, PhD. Thesis.

Gaucher, J-F., Ries-Kautt, M., Reiss-Husson, F & Ducruix, A. (1997)
Solubility Diagram of the *Rhodobacter sphaeroides* Reaction Centre as a Function of PEG Concentration.
FEBS Lett. **401** : 113-116.

Goldsmith, J.O., King, B. & Boxer, S.G. (1996)
Mg Co-ordination by Amino Acid Side-Chains is not Required for Assembly and Function of the Special Pair in Bacterial Photosynthetic Reaction Centres.
Biochemistry **35** : 2421-2428

Griffiths, M., Sistrom, W.R., Cohen-Bazaire, G. & Stanier, R.Y. (1955)
Function of Carotenoids in Photosynthesis.
Nature **176** : 1211-1214.

Griffiths, M. & Stanier, R.Y. (1956)
Some Mutational Changes in the Photosynthetic Pigment System of *Rhodopseudomonas sphaeroides*.
J. Gen. Microbiol. **14** : 698-715.

Grondelle, van R., Kramer, H.J.M. & Rijgersberg, C.P. (1982)
Energy Transfer in the B800-850 Carotenoid Light-Harvesting Complex of Various Mutants of *Rhodopseudomonas sphaeroides* and of *Rhodopseudomonas capsulatus*.
Biochim. Biophys. Acta. **682** : 208-215.

Grondelle, van R., Dekker, J. P., Gillbro, T. & Sündstrom, V. (1994)
Energy Transfer and Trapping in Photosynthesis.
Biochim Biophys. Acta. **1187** : 1-65.

Gros, P., Groendijk, H., Drenth, J. & Hol, W. G. J. (1988)
Experiments in Membrane Protein Crystallisation.
J. Cryst. Growth. **90** : 193-200.

Gudowska-Nowak, E., Newton, M.D. & Fajer, J. (1990)
Conformational and Environmental Effects on Bacteriochlorophyll Optical Spectra: Correlations of Calculated Spectra with Structural Results.
J. Phys. Chem. **94** : 5795-5801.

Guo, H.C., Jardentzky, T.S., Garrett, T.P.J., Lane, W.S., Strominger, J.L. & Wiley, D.C. (1992)
Different Length Peptides Bind to HLA-Aw68 Similarly at their ends but bulge out in the middle.
Nature **360** : 364-366

Haas, D.J. & Rossmann, M.G. (1970)
Crystallographic Studies on Lactate Dehydrogenase at -75°C.
Acta. Cryst. **B26** : 998-1004.

Hamm, P., Gray, K.A., Oesterhelt, D., Feick, R., Scheer, H., & Zinth, W. (1993)
Subpicosecond Emission Studies of Bacterial Reaction Centers.
Biochim. Biophys. Acta **1142** : 99-105.

Hamm, P., Zurek, M., Mantele, W., Meyer, M., Scheer, H & Zinth, W. (1995)
Femtosecond Infrared Spectroscopy of Reaction Centres from *Rhodobacter sphaeroides* between 1000 and 1800cm-1.
Proc. Natl. Acad. Sci. (U.S.A.) **92** : 1826-1830.

Haris, P.I. & Chapman,D. (1992)
Does Fourier-Transform Infrared-Spectroscopy Provide Useful information on protein Structures.
TIBS **17** : 328-333.

Hawthornthwaite, A.M. & Cogdell, R.J. (1991)
Bacteriochlorophyll-Binding Proteins.
In. Chlorophylls, Scheer, H. (Ed.) CRC Press, Boca Raton, Florida, U.S.A. p493-528.

Hayashi, H., Noguchi, T. & Tasumi, M. (1989)
Studies on the Interrelationship of the Intensity of a Raman Marker Band of Carotenoids, Polyene Chain Structure, and Efficiency of the Energy-Transfer from Carotenoids to Bacteriochlorophyll in Photosynthetic Bacteria.
Photochem. & Photobiol. **49** (3) : 337-343.

Hoffman, N.E., Wrench, P.M., Sharples, F.P., Hiller, R.G., Welte, W. & Diederichs, K. (1996).
Structural Basis of Light-Harvesting by Carotenoids-Peridinin-Chlorophyll-Protein from *Amphidinium Carterae*.
Science **272** : 1788-1791.

Holt, S.C. & Marr, A.G. (1965)
Isolation and Purification of the Intracytoplasmic Membranes of *Rhodospirillum rubrum*..
J. Bacter. **89** (5) : 1413-1402.

Holzapfel, W., Finkele, U., Kaiser, W., Oesterhelt, D., Scheer, H., Stilz, H.U. & Zinth, W. (1990)
Initial Electron-Transfer in the Reaction Center from *Rhodobacter sphaeroides*.
Proc. Natl. Acad. Sci. (U.S.A.) **87** : 5168-5172.

Holzenburg, A., Bewley, M.C., Wilson, F.H., Nicholson, W.V. & Ford, R.C. (1993)
Three-Dimensional Structure of Photosystem II.
Nature **363** : 470-472.

Hope, H. (1988)
Cryocrystallography of Biological Macromolecules: A Generally Applicable Method.
Acta. Cryst. **B44** : 22-26.

Hu, X, Schulten, K, Koepke, J. & Michel, H. (1996)
Structure of the Light-harvesting complex-II of *Rhodospirillum molischianum*.
Biophys. J. **70** : A130.

Hu, X.C., Ritz, T., Damjanovic, A. & Schulten, K. (1997)
Pigment Organization and Transfer of Electronic Excitation in the Photosynthetic Unit of Purple Bacteria.
J. Phys. Chem. **B101** : 3854-3871.

Huber, M., Isaacson, R.A, Abresch, E.C, Gaul, D., Schenck, C.C. & Feher., G. (1996)
Electronic Structure of the Oxidised Primary Electron Donor of the HL(M202) and HL(L173) Heterodimer Mutants of the Photosynthetic Bacterium *Rhodobacter sphaeroides*: ENDOR on Single Crystals of Reaction Centers.
Biochim. Biophys. Acta **1273** : 108-128

Hudson, B.S., Kohler, B.E. & Schulten, K. (1982)
Linear Polyene Electronic Structure and Potential Surfaces.
In. Lim, E.C. (Ed.) Excited States, Vol. 6, Academic press, New York, p22-95.

Hunter, C.N., Pennoyer, J.D. & Niederman, R.A. (1982)
Assembly and Structural Organisation of Pigment-Protein Complexes in Membranes of *Rhodopseudomonas sphaeroides*.
In "Proceedings of the Special FEBS Meeting on Cell Function and Differentiation" (Ed. Evangelopoulos, E.) Alan R. Liss, Inc. New York.

Hunter, C.N. & Turner, G. (1988)
Transfer of Genes Coding for Apoproteins of Reaction Centre and Light-Harvesting LH1 Complexes to *Rhodobacter sphaeroides*.
J. Gen. Microbiol. **134** pp. 1471-1480.

Hunter, C.N., van Grondelle, R. & Olsen, J.D. (1989)
Photosynthetic Antenna Proteins: 100ps Before Photochemistry Starts.
TIBS **14** : 72-76.

Hunter, C.N. (1995)
Light-Harvesting Complex - Rings of Light.
Current Biology **5** (8) : 826-828

Inamine, G.S., Reilly, P.A. & Niederman, R.A. (1984)
Differential Protein Insertion into Developing Photosynthetic Membrane Regions of *Rhodopseudomonas sphaeroides*.
J. Cellular Biochemistry **24**(1) : 69-77.

Isler, O., Guttman, G. & Solms, U. (1971)
In. The Carotenoids. Basle and Stuttgart: Berkhauser Verlag.

Iwata, K., Hayashi, H. & Tasumi, M. (1985)
Resonance Raman Studies of the Conformations of all-*trans* carotenoids in Light-Harvesting Systems of Photosynthetic bacteria.
Biochim. Biophys. Acta. **810** (2): 269-273.

Iwata, S. Ostermeier, C., Ludwig, B. & Michel, H. (1995)
Structure at 2.8Å Resolution of Cytochrome c Oxidase from *Paracoccus denitirficans*.
Nature **376** : 660-669.

Jackson, J.B. & Crofts, A.R. (1969)
The High Energy State in Chromatophores from *Rhodobacter sphaeroides*.
FEBS Letts. **4** (3) : 185-189.

Jensen, S.L., Cohen-Bazaire, G. & Stanier, R.Y. (1966)
Biosynthesis of Carotenoids in Purple Bacteria: a Re-Evaluation Based on Considerations of Chemical Structure.
Nature **192** : 1168-1172.

Jolchine, G. & Reiss-Husson, F. (1974)
Comparative Studies on Two Reaction Center Preparations from *Rhodopseudomonas sphaeroides* Y.
FEBS Letts. **40** (1) : 5-8.

Jones, M.R., Fowler, G.J.S., Gibson, L.C.D., Grief, G.G., Olsen, J.D., Crielaard, W. & Hunter, C.N. (1992a)
Mutants of *Rhodobacter sphaeroides* Lacking One or More Pigment Protein Complexes and Complementation with Reaction Center, LH1 and LH2 Genes.
Molecular Microbiology **6** (9) : 1173-1184.

Jones, M.R., Visschers, R.W., Grondelle van, R. & Hunter, C.N. (1992b)
Construction and Characterisation of a Mutant of *Rhodobacter sphaeroides* with the Reaction Centre as the Sole Pigment-Protein Complex.
Biochemistry **31** : 4458-4465.

Jones, M.R., Heer-Dawson, M., Mattioli, T.A., Hunter, C.N. & Robert, B. (1994)
Site-Specific Mutagenesis of the Reaction Center from *Rhodobacter sphaeroides* Studied by Fourier Transform Raman Spectroscopy: Mutations at Tyrosine M210 do not Affect the Electronic Structure of the Primary Donor.
FEBS Letts. **339** : 18-24.

Jones, T.A., Zou, J.Y., Cowan, S.W. & Kjeldgaard, M. (1991)
Improved Methods for Building Protein Models in Electron Density Maps and the Location of Errors in These Maps.
Acta. Cryst. **A47**: 110-119.

Jung, M., Sommer, I., Schachner, M. & Nave, K.A. (1996)
Monoclonal Antibody O10 Defines a Conformationally Sensitive Cell-Surface Epitope of Proteolipid Protein (PLP): Evidence That PLP Misfolding Underlies Dysmyelination in Mutant Mice.
Journal of Neuroscience **16** : 7920-7929.

Kakitani, T., Hönig, B. & Crofts, A.R. (1982)
Theoretical Studies of the Electrochromic Response of Carotenoids in Photosynthetic Membranes.
Biophys. Journal **39** (1) : 57-63.

Kam, Z., Shore, H.B. & Feher, G. (1978)
On the Crystallisation of Proteins.
J. Mol. Biol. **123** : 539-542.

Karrasch, S., Bullough, P.A. & Ghosh, R. (1995)
The 8.5Å Projection Map of the Light-Harvesting Complex-I from *Rhodospirillum rubrum* Reveals a Ring Composed of 16 Subunits.
EMBO J. **14** : 631-638.

Kendrew, J.C., Dickerson, R.E., Strandberg, B.E., Hart, R.G., Davies, D.R., Phillips, D.C. & Shore, V.C. (1960)
Structure of Myoglobin, a Three-Dimensional Fourier Synthesis at 2Å Resolution.
Nature **185** : 422-427.

King, M.V., Magdoff, B.S. Adelman, M.B. & Harker, D. (1956)
Crystalline Forms of Bovine Pancreatic Ribonuclease : Techniques of Preparation, Unit Cells, and Space Groups.
Acta. Cryst. **9** : 460-464.

Kirmaier, C. & Holten, D. (1987)
Primary Photochemistry of Reaction Centres from Photosynthetic Purple Bacteria.
Photosynthesis Research **13** : 225-260.

Kirmaier, C., Laporte, L., Schenck, C.C. & Holten, D. (1995a)
The Nature and Dynamics of the Charge-Separated Intermediate in Reaction Centers in Which Bacteriochlorophyll Replaces the Photoactive Bacteriopheophytin 1. Spectral Characterization of the Transient State.
J. Phys. Chem. **99** : 8903-8909.

Kirmaier, C., Laporte, L., Schenck, C.C. & Holten, D. (1995b)
The Nature and Dynamics of the Charge-Separated Intermediate in Reaction Centers in Which Bacteriochlorophyll Replaces the Photoactive Bacteriopheophytin 2. The Rates and Yields of Charge Separation and Recombination.
J. Phys. Chem. **99** : 8910-8917.

Kleinfeld, D., Okamura, M.Y. & Feher, G. (1984)
Electron Transfer in Reaction Centers of *Rhodobacter sphaeroides*. I. Determination of the Charge Recombination Pathway of $D^+Q_AQ_B^-$ and Free Energy Relations Between $Q_A^-Q_B$ and $Q_AQ_B^-$.
Biochim. Biophys. Acta. **766** : 126-140.

Kleinfeld, D., Okamura, M.Y. & Feher, G. (1985)
Electron Transfer in Reaction Centers of *Rhodobacter sphaeroides*. II. Free Energy and Kinetic Relations Between the Acceptor States $Q_A^-Q_B^-$ and $Q_AQ_B^{2-}$.
Biochim. Biophys. Acta. **809** : 291-310.

Kleywegt, G.J. & Brünger, A.T. (1996)
Checking your Imagination: Applications of the Free-R Value.
Structure **4** (8) : 897-904.

Kleywegt, G.J. & Jones, T.A. (1996)
Efficient Rebuilding of Protein Structures.
Acta. Cryst., **D52** : 829-832.

Kleywegt, G.J. & Jones, T., A. (1997)
Good Model-Building and Refinement Practice.
Methods in Enzymology **277** In Press.

Koepke, J., Hu, X., Muenke, C., Schulten, K. & Michel, H. (1996)
The Crystal Structure of the Light-Harvesting Complex II (B800-850) from *Rhodospirillum molischianum*.
Structure **4** : 581-597.

Kok, P., Kohler, J, Groenen, E.J.J., Gebhard, R., van der Hoef, I., Lugtenburg, J, Hoff, A.J., Farhoosh, R. & Frank, H.A. (1994)
Towards a Vibrational Analysis of Spheroidene. Resonance Raman Spectroscopy of 13C-Labelled Spheroidenes in Petroleum Ether and in the *Rhodobacter sphaeroides* Reaction Centre.
Biochim. Biophys. Acta. **1185** : 188-192.

Komiya, H., Yeates, T.O., Rees, D.C., Allen, J.P. & Feher, G. (1988)
Structure of the Reaction Center from *Rhodobacter sphaeroides* R-26 and 2.4.1.: Symmetry Relations and Sequence Comparisons Between Different Species.
Proc. Natl. Acad. Sci. U.S.A. **85** : 9012-9016.

Koyama, Y., Kito, M., Takii, T., Saiki, K., Tsukida, K. & Yamashita, J. (1982)
Configuration of the Carotenoid in the Reaction Centers of Photosynthetic Bacteria: Comparison of the Resonance Raman Spectrum of the Reaction Centre of *Rhodopseudomonas sphaeroides* G1C with those of *cis-trans* Isomers of β-carotene.
Biochim. Biophys. Acta. **680** : 109-118.

Koyama, Y., Takatsuka, I., Kanaji, M., Tomimoto, K., Kito, M., Shimamura, T., Yamashita, J., Saiki, K. & Tsukida, K. (1990)
Configurations of Carotenoids in the Reaction Centre and the Light-Harvesting Complex of *Rhodospirillum rubrum* - Natural Selection of Carotenoid Configurations by Pigment Protein Complexes.
Photochem. Photobiol. **51**(1) : 119-128.

Koyama, Y. (1991)
Structures and Functions of Carotenoids in Photosynthetic Systems.
Photochem. & Photobiol. **9** : 265-280.

Koyama, Y. & Hashimoto, H. (1993)
Spectroscopy of Carotenoids.
In. Carotenoids in Photosynthesis, Young, A. & Britton, G. (Eds.), Chapman & Hall, London.

Kraulis, P.J. (1991)
Molscript- A Program to Produce Both Detailed and Schematic Plots of Protein Structures.
J. Appl. Cryst. **24** : 946-950.

Kramer, B., Kramer, W. & Fritz, H.J. (1984)
Different Base-Base Mismatches are Corrected with Different Efficiencies by the Methyl-Directed DNA Mismatch-Repair System of *Escherichia coli*.
Cell **38** (3) : 879-887.

Krauß, N., Schubert, W.D., Klukas, O., Fromme, P., Witt, H.T. & Saenger, W. (1996)
Photosystem I at 4Å Resolution Represents the First Structural Model of a Joint Photosynthetic Reaction Centre and Core Antenna System.
Nature Structural Biology **3** : 965-973.

Krinsky, N.I. (1966)
The Role of Carotenoid Pigments as Protective Agents Against Photosensitized Oxidations in Chloroplasts.
In Biochemistry of Chloroplasts, Goodwin, T.W. (Ed.), Academic Press, New York, p423-430.

Laemmli, UK (1970)
Cleavage of Structural Proteins During the Assembly of the Head of Bacteriophage T4.
Nature **227** : 680.

Lambert, I.B., Donnelly, T.H., Dunlop, J.S.R. & Groves, D.I. (1978)
Precambrian Solution Photochemistry, Inverse Segregation and Banded Iron Formations.
Nature **276** : 807-811.

Lascelles, J. (1959)
Adaptation to form Bacteriochlorophyll in *Rhodopseudomonas sphaeroides*, Changes in Activity of Enzymes Concerned with Pyrole Synthesis
Biochem. J. **72** : 508-518.

Laskowski, R.A., MacArthur, M.W., Moss, D.S. & Thornton, J.M. (1993)
PROCHECK: A Program to Check the Stereochemical Quality of Protein Structures.
J. Appl. Cryst. **26** : 283-291.

Laue, Max von (1912)
Sitz. math. phys. Klasse Bayer. Akad. Wiss., 303. (Unavailable)

Lee, J.K. & Kaplan, S. (1992a)
cis-Acting Regulatory Elements Involved in Oxygen and Light Control of *puc*-Operon Transcription in *Rhodobacter sphaeroides*.
J. Bacter. 174 : 1146-1157.

Lee, J.K. & Kaplan, S. (1992b)
Isolation and Characterisation of Trans-Acting Mutations Involved in Oxygen Regulation of *puc*-Operon Transcription in *Rhodobacter sphaeroides*.
J Bacter. **174** : 1158-1171.

Lee, C.H., Kominos, D., Jacques, S., Margolis, B., Schelessinger, J., Shoelson, S.E. & Kuriyan, J. (1994)
Crystal Structures of Peptide Complexes of the Amino-Terminal SH_2 Domain of the SYP Tyrosine Phosphatase.
Structure **2** : 423-438.

Lee, J.W, Chan, M, Law, T.V., Kwon, H.J. & Jap, B.K. (1995)
Preliminary Cryocrystallographic Study of the Mitochondrial Cytochrome *bc*1 Complex: Improved Crystallisation and Flash-Cooling of a Large Membrane Protein.
J. Mol. Biol., **252**: 15-19.

Liaan-Jensen, S. & Jensen, A. (1971)
Quantitative Determination of Carotenoids in Photosynthetic Tissues.
Methods in Enzymology **23** : 586-602.

Lien, S. & Gest, H. (1973)
Chlorophyll Synthesis in Photosynthetic Bacteria.
Bioenergetics **4** : 423-434.

Lin, S-X., Sailofsky, B., Lapointe, J. & Zhou, M. (1992)
Preparative Fast Purification Procedure of Various Proteins for Crystallisation.
J. Cryst. Growth. **122** : 242-245.

Lin, X., Murchison, H.A., Nagarajan, V., Parson, W.W., Allen, J.P. & Williams, J.C. (1994)
Specific Alteration of the Oxidation Potential of the Electron Donor in Reaction Centers from *Rhodobacter sphaeroides*.
Proc. Natl. Acad. Sci. U.S.A. **91** (22) : 10265-10269.

Littke, W. & John, C. (1986)
Protein Single Crystal Growth Under Microgravity.
J. Cryst. Growth. **76** : 663-672.

Lutz, M., Agalidis, I., Hervo, G., Cogdell, R.J. & Reiss-Husson, F. (1978)
On the State of Carotenoids to Reaction Centres of Photosynthetic Bacteria: A Resonance Raman Study.
Biochim. Biophys. Acta. **503**: 287-303.

Lutz, M., Szponarsk, W., Berger, G., Robert, B. & Newmann, J.M. (1987)
The Stereoisomerism of Bacterial, Reaction Center Bound Carotenoids Revisited: An Electronic Absorption, Resonance Raman and H-1-NMR Study.
Biochim. Biophys. Acta. **894** (3): 423-433.

Luzzati, V. (1952)
Traitement Statistique des Erreurs dans la Déterminatioin des Structures Cristallines.
Acta. Cryst. **5** : 802-810.

Mantele, W.G., Wollenweber, A.M., Nabedryk, E. & Breton, J. (1988)
Infrared Spectroelectrochemistry of Bacteriochlorophylls and Bacteriopheophytins : Implications for the Binding of the Pigments in the Reaction Center from Photosynthetic Bacteria.
Proc. Natl. Acad. Sci. U.S.A. **85** : 8468-8472.

Marrs, B. & Gest, H. (1973)
Regulation of Bacteriochlorophyll Synthesis by Oxygen in Respiratory Mutants of *Rhodopseudomonas capsulatus*.
J. Bacter. **114** : 1052-1057.

Martin, J.-L., Breton, J., Hoff, A., Migus, A. & Antonetti (1986)
Femtosecond Spectroscopy of Electron Transfer in the Reaction Center of the Photosynthetic Bacterium *Rhodopseudomonas sphaeroides* R-26: Direct Electron Transfer from the Dimeric Bacteriochlorophyll Primary Donor to the Bacteriopheophytin Acceptor with a Time Constant of 2.8 ± 0.2 psec.
Proc. Natl. Acad. Sci. **83** : 957-961.

Mathis, P. (1969)
Triplet-Triplet Energy Transfer from Chlorophyll *a* to Carotenoids in Solution and in Chloroplasts.
In: Progress in Photosynthesis Research, Vol 2, Metzner, H. (Ed.) Tübingen, Germany. pp 811-822.

Mathis, P & Kleo, J. (1973)
Triplet State of β-Carotene and of Analog Polyenes of Different Length.
Photochem. Photobiol. **18** : 343-346.

Mattioli, T.A., Hoffmann, A., Robert, B., Schrader, B. & Lutz, M. (1991)
Primary Donor Structure and Interactions in Bacterial Reaction Centers From Near-Infrared Fourier-Transform Resonance Raman- Spectroscopy
Biochemistry **30** (19) : 4648-4654.

Mattioli, T.A., Williams, J.C., Allen, J.P. & Robert, B. (1994)
Changes in Primary Donor Hydrogen-Bonding Interactions in Mutant Reaction Centers from *Rhodobacter sphaeroides* : Identification of the Vibrational Frequencies of all the Conjugated Carbonyl Groups.
Biochemistry 33 : 1636-1643.

Mattioli, T.A., Lin, X., Allen, J.P. & Williams, J.C. (1995)
Correlation Between Multiple Hydrogen-Bonding and Alteration of the Oxidation Potential of the Bacteriochlorophyll Dimer of Reaction Centers from *Rhodobacter sphaeroides*.
Biochemistry 34 (18) : 6142-6152.

McAuley-Hecht, K.E., Fyfe, P.K., Ridge, J.P., Prince, S.M., Hunter, C.N., Isaacs, N.W., Cogdell, R.J. & Jones, M.R. (1997)
Structural Studies of Wild-Type and Mutant Reaction Centres from an Antenna-Deficient Strain of *Rhodobacter sphaeroides*: Monitoring the Optical Properties of the Complex from Bacterial Cell to Crystal.
Biochemistry, Manuscript Submitted.

McDermott, G., Prince, S.M., Freer, A.A., Hawthornthwaite-Lawless, A.M., Papiz, M.Z., Cogdell, R.J. & Isaacs, N.W. (1995)
Crystal Structure of an Integral Membrane Light-Harvesting Complex from Photosynthetic Bacteria.
Nature **374** : 517-521.

McDowell, L.M., Gaul, D. Kirmaier, C., Holten, D. & Schenk, C.C. (1991)
Investigation into the Source of Electron-Transfer Asymmetry in Bacterial Reaction Centers.
Biochemistry **30** : 8315-8322.

The New Collins Concise Dictionary of the English Language (1984)
McLeod, W.T. & Hanks, P. (Eds.), Collins, London, UK.

McMaster, L. (1995)
University of Sheffield, PhD. Thesis.

McPherson, A., Koszelak, S., Axelrod, H., Day, J., Robinson, L., McGrath, M., Williams, R. & Cascio, D. (1986)
The Effects of Neutral Detergents on the Crystallisation of Soluble Proteins.
J. Cryst. Growth. **76** : 547-553.

McPherson, A. (1990)
Current Approaches to Macromolecular Crystallisation.
Eur. J. Biochem. **189** : 1-23.

McPherson, A. (1991)
A Brief History of Protein Crystal Growth.
J. Cryst. Growth. **110** : 1-10.

McPherson, P.H., Schonfeld, M., Paddock, M.L., Okamura, M.Y. & Feher, G. (1994)
Protonation and Free-Energy Changes Associated with Formation of $Q(B)H_{(2)}$ in Native and Glu-L212 to Gln Mutant Reaction Centers from *Rhodobacter sphaeroides*.
Biochemistry 33 (5) : 1181-1193.

Michel, H. (1983)
Crystallisation of Membrane Proteins.
Trends in Biochemistry **8** : 56.

Michel, H. & Deisenhofer, J. (1988)
Relevance of the Photosynthetic Reaction Center from Purple Bacteria to the Structure of Photosystem II.
Biochemistry **27** : 1-7

Michel, H. (1991)
General and Practical Aspects of Membrane Protein Crystallisation.
In Crystallisation of Membrane Proteins. Michel, H. (Ed.) CRC Press, Boca Raton, Florida, U.S.A.

Mitchell, E.P. & Garman, E.F. (1994)
Flash Freezing of Protein Crystals: Investigation of Mosaic Spread and Diffraction Limit with Variation of Cryoprotectant solution.
J. Appl. Cryst. **27** : 1070-1074.

Müh, F., Rautter, J. & Lubitz, W. (1996)
Effects of Zwitterionic Detergents on the Primary Donor of Bacterial Reaction Centers.
Ber. Bunsenges. Phys. Chem. **100** : 1974-1977.

Murchison, H.A., Alden, R.G., Allen, J.P., Peloquin, J.M., Taguchi, A.K.W., Woodburg, N.W. & Williams, J.C. (1993)
Mutations Designed to Modify the Environment of the Primary Electron-Donor of the Reaction Center from *Rhodobacter sphaeroides*-Phenylalanine to Leucine at L167 and Histidine to Phenylalanine at L168.
Biochemistry **32** (13) : 3498-3505.

Nabedryk, E., Bagley, K.A, Thibodeau, D.L., Bauscher, M., Mantele, W. & Breton, J. (1990)
A Protein Conformational Change Associated with the Photoreduction of the Primary and Secondary Quinones in the Bacterial Reaction Center.
FEBS Letts. **266** : 59-62.

Nabedryk, E., Allen, J.P., Taguchi, A.K.W., Williams, J.C., Woodbury, N.W. & Breton, J. (1993)
Fourier-Transform Infrared Study of the Primary Electron Donor in Chromatophores of *Rhodobacter sphaeroides* with Reaction Centers Genetically Modified at Residue M160 and Residue L131.
Biochemistry **32** (50) : 13879-13885.

Nagarajan, V., Parson, W.W., Gaul, D. & Schenck, C. (1990)
Effect of Specific Mutations of Tyrosine (M)210 on the Primary Photosynthetic Electron Transfer Process in *Rhodobacter sphaeroides*.
Proc. Natl. Acad. Sci. U.S.A. **87** (20) : 7888-7892.

Nagarajan, V., Parson, W.W., Davis, D. & Schenck, C.C. (1993)
Kinetics and Free-Energy Gaps of Electron-Transfer Reactions in *Rhodobacter sphaeroides* Reaction Centers.
Biochemistry **32** : 12324-12336.

Nakazato, K., Toyoshima, C., Enami, I. & Inoue, Y. (1996)
2-Dimensional Crystallization and Cryoelectron Microscopy of Photosystem II.
J. Mol. Biol. **257** :225-232.

Navaza, J. (1994)
AMoRe - An Automated Package for Molecular Replacement
Acta Cryst. **A50** : 157-163.

Niederman, R.A., Mallon, D.E. & Langan, J.J. (1976)
Membranes of *Rhodopseudomonas sphaeroides* IV. Assembly of Chromatophores in Low Aeration Cell Suspensions.
Biochim. Biophys. Acta. **440** : 429-447.

Nicholls, D.G. & Ferguson, S.J. (1992)
Bioenergetics.
Academic Press Limited, London.

Nitschke, W., Feiler, U., Lockau, W. & Hauska, G. (1987)
The Photosystem of the Green Sulfur Bacterium *Chlorobium limicola* contains two Early Electron Acceptors Similar to Photosystem I.
FEBS Letts. **218** : 283-286

Nitschke, W. & Rutherford, A.W. (1991)
Are all of the Different Types of Photosynthetic Reaction Centre Variations on a Common Structural Theme.
TIBS **16** : 241-245.

Noguchi, T., Hayashi, H. & Tasumi, M. (1990)
Factors Controlling the Efficiency of Energy-Transfer from Carotenoids to Bacteriochlorophyll in Purple Photosynthetic Bacteria.
Biochim. Biophys. Acta. **1017** (3) : 280-290.

Okamura, M.Y., Steiner, L.A. & Feher, G. (1974)
Characterisation of Reaction Centers from Photosynthetic Bacteria. I. Subunit Structure of the Protein Mediating the Primary Photochemistry in *Rhodopseudomonas sphaeroides* R-26.
Biochemistry **13** (7) : 1394-1402.

Olsen, J. & Hunter, C.N. (1994)
Protein-Structure Modelling of the Bacterial Light-Harvesting Complex.
Photochem. & Photobiol. **60** (6) : 521-535

Ossama, E.K., Chang, C.H., Tieck, D., Norris, J. & Schiffer, M. (1991)
Comparison of Reaction Centers from *Rhodobacter sphaeroides* and *Rhodopseudomonas viridis* : Overall Architecture and Protein Pigment Interactions.
Biochemistry **30** : 5361-5369.

Ostermeier, C., Iwata, S. & Michel, H. (1996)
Cytochrome c Oxidase.
Current Opinion in Structural Biology **6** : 460-466.

Otwinowski, Z. (1993)
DENZO
In Data Collection and Processing. Sawyer, L., Isaacs, N. & Bailey, S. Eds. pp56-62.
SERC Daresbury Laboratory, Warrington, UK.

Otwinowski, Z. & Minor W. (1997)
Processing of X-Ray Diffraction Data Collected in Oscillation Mode.
Methods in Enzymology **276** : 307-326.

Paddock, M.L., Rongey, S.H., Feher, G. & Okamura, M.Y. (1989)
Pathway of Proton-Transfer in Bacterial Reaction Centers : Replacement of Glutamic Acid 212 in the L-Subunit by Glutamine Inhibits Quinone (Secondary Acceptor) Turnover.
Proc. Natl. Acad. Sci. U.S.A. **86** (17) : 6602-6606.

Paddock, M.L., McPherson, P.H., Feher, G. & Okamura, M.Y. (1990)
Pathway of Proton Transfer in Bacterial Reaction Centres-Replacement of Serine-L223 by Alanine Inhibits Electron and Proton Transfers Associated with Reduction of Quinone to Dihydroquinone.
Proc. Natl. Acad. Sci. U.S.A. **87** (17): 6803-6807.

Paddock, M.L., Rongey, S.H., McPherson, P.H., Juth, A., Feher, G. & Okamura, M.Y. (1994)
Pathway of Proton Transfer in Bacterial Reaction Centers: Role of Aspartate-L213 in Proton Transfers Associated with Rereduction of Quinone to Dihydroquinone.
Biochemistry **33** (3) : 734-745.

Papiz, M. Z., Prince, S. M., Hawthornthwaite-Lawless, A. M., McDermott, G., Freer, A. A., Isaacs, N. W. & Cogdell, R. J. (1996)
A Model for the Photosynthetic Apparatus of Purple Bacteria.
Trends in Plant Science **1** : 198-206.

Pardee, A.B., Schachman, H.K. & Stanier, R.Y. (1952)
Chromatophores of *Rhodospirillum rubrum.*
Nature **169** : 282-283.

Parson, W.W., Clayton, R.K. & Cogdell, R.J. (1975)
Excited States of Photosynthetic Reaction Centers at Low Redox Potentials.
Biochim. Biophys. Acta. **387** : 265-278.

Parson, W.W. & Warshel, A. (1987)
Spectroscopic Properties of Photosynthetic Reaction Centers .2. Application of the Theory to *Rhodopseudomonas viridis*
J. Am. Chem. Soc. **109** : 6152-6163.

Petsko, G.A. (1975)
Protein Crystallography at Sub-Zero Temperatures: Cryo-Protective Mother Liquors for Protein Crystals.
J. Mol. Biol. **96** : 381-392.

Pfennig, N. & Truper, H.G. (1983)
Taxonomy of Phototrophic Green and Purple Bacteria- A Review.
Ann. Microbiol. **134B** : 9-20.

Pfister, K., Steinback, K. E., Gardner, G. & Arntzen, C.J. (1981)
Surface Enhanced Resonance Raman Scattering Spectroscopy of Bacterial Photosynthetic Membranes - Orientation of the Carotenoids of *Rhodobacter sphaeroides* 2.4.1.
Proc. Natl. Acad. Sci. U.S.A. **78** : 981-985.

Picorel, R., Lu, T.H., Holt, R.E., Cotton, T.M. & Siebert, M. (1990)
Surface-Enhanced Resonance Raman-Scattering Spectroscopy of Bacterial Photosynthetic Membranes - Orientation of the Carotenoids of *Rhodobacter sphaeroides* 2.4.1.
Biochemistry **29** : 707-712.

Pradel, J., Lavergne, J. & Moya, I. (1978)
Formation and Development of Photosynthetic Units in Repigmenting *Rhodopseudomonas sphaeroides* Wild-Type and "Phofil" Mutant Strain.
Biochim. Biophys. Acta. **502** : 169-182.

Price, N.C. (1997)
Protein Analysis by Circular Dichroism.
In Encyclopedia of Molecular Biology and Biotechnology, Meyers, R.A. (Ed.), VCH Press, Weinheim. In Press.

Pullerits, T. & Sündstrom, V. (1996)
Photosynthetic Light-Harvesting Pigment-Protein Complexes - Toward Understanding How and Why.
Accounts of Chemical Research **29** (8) : 381-389.

Rautter, J., Lendzian, F., Schultz, C., Fetsch, A, Kuhn, M., Lin., X., Williams, J.C., Allen, J.P. & Lubitz,W. (1995)
ENDOR Studies of the Primary Donor Radical Cation in Mutant Reaction Centers of *Rhodobacter sphaeroides* with Altered Hydrogen-Bond Interactions.
Biochemistry, **34** (1995) 8130-8143.

Reiss-Husson, F. & Jolchine, G. (1972)
Purification and Properties of a Photosynthetic Reaction centre Isolated from Various Chromatophore Fractions of *Rhodopseudomonas sphaeroides* Y.
Biochim. Biophys. Acta. **256** : 440-451.

Rich, P.R. (1984)
Electron and Proton Transfer Through Quinones and Cytochrome *bc* Complexes.
Biochim. Biophys. Acta. **807** : 10-

Rimai, L., Gill, D. & Parsons, J.L. (1970)
Raman Spectra of Dilute Solutions of Vitamin A Type Molecules.
J. Am. Chem. Soc. **93** (6) : 1353-1357.

Rini, J.M, Schulze-Gamen, U. & Wilson, I.A. (1992)
Structural Evidence for Induced Fit as a Mechanism for Antibody- Antigen Recognition.
Science **255** : 959-965.

Robert, B. (1996)
Resonance Raman Studies in Photosynthesis.
In: Biophysics in Photosynthesis. Amesz, J. & Hoff, A.J. (Eds.) Kluwer Scientific, The Netherlands.

Robert, M. C. & Lefaucheux, F. (1988)
Crystal Growth in Gels: Principle and Application.
J. Cryst. Growth. **90** : 358-367.

Robles, S.J, Breton, J. & Youvan, D.C. (1990)
Partial Symmetrization of the Photosynthetic Reaction Center.
Science **248** : 1402-1405.

Rodgers, D.W. (1994)
Cryocrystallography.
Structure **2** : 1135-1140.

Rodgers, D.W. (1997)
Practical Cryocrystallography.
Methods in Enzymology, **276** : 183-203.

Rosenberger, F. & Meehan, E.J. 1988
Control of Nucleation and Growth in Protein Crystal-Growth.
J. Crystal Growth **90** : 74 - 78.

Ruffle, S.V., Donnelly, D., Blundell, T.L. & Nugent, J.H.A. (1992)
A Three-Dimensional Model of Photosystem II Reaction centre of *Pisum sativum*.
Photosynth. Res. **34** : 287-300.

Sambrook, J., Fritsch, E.F., Maniatis, T (1989)
Molecular Cloning: A Laboratory manual.
Cold Spring Harbour Laboratory Press, U.S.A.

Sanger, F., Nicklen, S. & Coulson, A.R. (1977)
DNA Sequencing with Chain-Terminating Inhibitors.
Proc. Natl. Acad. Sci. U.S.A. **74** : 5463-5467.

Santini, C., Tidu, V., Tognon, G., Ghiretti, M.A. & Bassi, R. (1994)
Three-Dimensional Structure of the Higher-Plant Photosystem II Reaction Centre and Evidence for its Dimeric Organisation *in vivo*.
Eur. J. Biochem. **221** : 307-315.

Sauer, U.H. & Ceska, T.A. (1997)
A Simple Method for Making Reproducible Fibre Loops for Protein Cryocrystallography.
J. Appl. Cryst. **30** : 71-72.

Sayre, R.T., Andersson, B. & Bogorad, L. (1986)
The Topology of a Membrane Protein: The Orientation of the 32-KD QB-Binding Chloroplast Thylakoid Membrane Protein.
Cell **47** (4) : 601-608.

Schachman, H.K, Pardee, A.B. & Stanier, R.Y. (1952)
Studies on the Macromolecular Organisation of Microbial Cells.
Arch. Biochem. Biophys. **38** : 245-260

Schagger, H. & von Jagow, G. (1987)
Tricine-Sodium Dodecyl Sulphate-Polyacrylamide Gel Electrophoresis for the Separation of Proteins in a Range from 1 to 100kDa.
Ana. Biochem **166** : 368-379.

Scheer, H [Ed.] (1991)
Chlorophylls.
CRC Press, Boca Raton, Florida, U.S.A.

Schick, B. & Jurnak, F. (1994)
Extension of the Diffraction Resolution of Crystals.
Acta. Cryst. **D50** : 563-568.

Schidlowski, M. (1988)
A 3,800-Million-Year Isotopic Record of Life from Carbon in Sedimentary Rocks.
Nature **333** : 313-318.

Schumacher, A. & Drews, G. (1978)
The Formation of Bacteriochlorophyll-Protein Complexes of the Photosynthetic Apparatus of *Rhodopseudomonas capsulata* During Early Stages of Development.
Biochim. Biophys. Acta. **501** : 183-194.

Schumacher, A. & Drews, G., (1979)
Effects of Light Intensity on Membrane Differentiation in *Rhodopseudomonas capsulata*.
Biochim. Biophys. Acta. **547** : 417-428.

Shimada, K. (1995)
Aerobic Anoxygenic Phototrophs.
In: Anoxygenic Photosynthetic Bacteria, Blankenship, E.D., Madigan, M.T. & Bauer, C.E. (Eds.) , Kluwer Academic Publishers, The Netherlands, p105-122.

Shochat, S., Arlt, T., Franke, C., Gast, P., Vannort, P.I., Otte, S.C.M., Schelvis, H.P.M., Schmidt, S., Vijgenboom, E., Vrieze, J., Zinth W. & Hoff, A.J. (1994)
Spectroscopic Characterization of Reaction Centers of the (M)Y210W Mutant of the Photosynthetic Bacterium *Rhodobacter sphaeroides*.
Photosynthesis Research **40** : 55-66.

Schopf, J.W. & Packer, B.M. (1987)
Early Archean (3.3-Billion To 3.5-Billion-Year-Old) Microfossils from Warrawoona Group, Australia
Science **237** : 70-73

Siefermann-Harms, D. (1985)
Carotenoids in Photosynthesis 1. Location in Photosynthetic Membranes and Light-Harvesting Function.
Biochim. Biophys. Acta. **811** : 325-355.

Simon, R., Priefer, U. & Puhler, A. (1983)
A Broad Host Range Mobilisation System for *in vivo* Genetic Engineering: Transposon Mutagenesis in Gram Negative Bacteria.
Biotechnology **1** : 784-791.

Sinning, I. Michel, H., Mathis, P. & Rutherford, A.W. (1989)
Characterisation of Four Herbicide-Resistant Mutants of *Rhodopseudomonas viridis* by Genetic Analysis, Electron Paramagnetic Resonance, and Optical Spectroscopy.
Biochemistry **28** : 5544-5553.

Sinning, I. (1992)
Herbicide Binding in the Bacterial Photosynthetic Reaction Centre.
TIBS **17** : 150-154.

Sistrom, W.R., Griffiths, M. & Stanier, R.Y. (1956)
The Biology of a Photosynthetic Bacterium which Lacks Coloured Carotenoids.
Cell Comp. Physiol. **48** : 473-515.

Steiner, L.A., Okamura, M.Y., Lopes, A.D., Moskowitz, E. & Feher, G. (1974)
Characterisation of Reaction Centers from Photosynthetic Bacteria. II. Amino Acid Composition of the Reaction Center Protein and its Subunits in *Rhodopseudomonas sphaeroides* R-26.
Biochemistry **13** (7) : 1403-1410.

Stowell, M.H.B., McPhillips, T.M., Rees, D.C., Soltis, S.M., Abresch, E. & Feher, G. (1997)
Light-Induced Structural Changes in Photosynthetic Reaction Center: Implications for Mechanism of Electron-Proton Transfer.
Science **276** : 812-816.

Strandberg, B. (1968)
On the Crystal Structure of Globular Proteins as Determined by Means of X-Ray Diffraction: With Special Reference to the Molecular Structure of Human Erythrocyte Carbonic Anhydrase form C at 5.5Å Resolution.
Ark. Kemi. **28** : 1-12.

Sturgis, J.N. & Niederman, R.A. (1996)
The Effect of Different Levels of the B800-850 Light-Harvesting Complex on Intracytoplasmic Membrane Development in *Rhodobacter sphaeroides*.
Arch. Microbiol. **165** (4) : 235-242.

Svenson, B., Etchebest, C., Tuffrey, P., van Kan, P., Smith, J. & Styring, S. (1996)
A Model for the Photosystem II Reaction Centre Core Including the Structure of the Primary Donor P680.
Biochemistry **35** (**16**) : 14486-14502.

Swartz, H.M, Bolton, J.R. & Borg, D.C. (1972)
Biological Applications of Electron Spin Resonance.
Wiley-Interscience, John Wiley & Sons Inc., New York.

Takemoto, J. (1974)
Kinetics of Photosynthetic Protein Assembly in *Rhodopseudomonas sphaeroides*.
Arch. Biochim. Biophys. **163** : 515-520.

Tauschel, H.D. & Drews, G. (1967)
Thylakoidmorpogenese bei *Rhodopseudomonas palustris*.
Arch. Mikrobiol **59** : 381-404.

Teng, T.Y. (1990)
Mounting of Crystals for Macromolecular Crystallography in a Free-Standing Thin Film.
J. Appl. Cryst. **23** : 387-391.

Thrash, R.J., Fang, H.L.B. & Leroi, G.E. (1977)
The Raman Excitation Profile Spectrum of β-Carotene in the Preresonance Region: Evidence for a Low-Lying Singlet State.
J. Chem. Phys. **67** : 5930-5933.

Trebst, A (1986) (Unavailable)
The Topology of the Plastiquinone and Herbicide Binding Peptides of Photosystem II- A Model.
Z. Naturforsch **42C** : 742-750

Tsukihara, T, Aoyama, H, Yamashita, E., Tomikazi, T, Yamaguchi, H., Shinzawa-Itoh, K., Nakashima, R., Yaono, R & Yoshikawa, S. (1995)
Structures of Metal Sites of Oxidised Bovine Heart Cytochrome c Oxidase at 2.8Å.
Science **269** : 1069-1074

Vatter, A.E. & Wolfe, R.S. (1958)
The Structure of Photosynthetic Bacteria
J. Bacter. **73** : 480

Vriend, G. & Sander, C. (1993)
Quality Control of Protein Models - Directional Atomic Contact Analysis.
J. Appl. Cryst. **26** : 47-60.

Vos, M.H., Jones, M.R., Breton, J., Lambry, J.-C. & Martin, J.-L. (1996)
Vibrational Dephasing in Long- and Short-Lived Primary Donor Excited States in Mutant Reaction Centers of *Rhodobacter sphaeroides*.
Biochemistry **35** : 2687-2692.

Wachtweitl, J., Farchaus, J.W., Mathis, P. & Oesterhelt, D. (1993)
Tyrosine-162 of the Photosynthetic Reaction Center Plays a Critical Role in the Cytochrome-$C_{(2)}$ Mediated Rereduction of the Photooxidised Bacteriochlorophyll Dimer in *Rhodobacter sphaeroides*: 2. Quantitative Kinetic Analysis.
Biochemistry **32** (40) : 10894-10904

Wachtweitl, J., Laussermair, E., Mathis, P., Farchaus, J.W. & Oesterhelt, D. (1993)
Probing the Donor Side of Bacterial Reaction Centers : Site-Directed Mutants of Tyrosine L-162 of *Rhodobacter sphaeroides* and *Rhodopseudomonas viridis*.
Biochemical Society Transactions **21** (1) : 43-44.

Wang, S., Lin, S., Lin, X., Woodbury, N.W. & Allen, J.P. (1994)
Comparative Study of Reaction Centers from Purple Photosynthetic Bacteria - Isolation and Optical Spectroscopy
Photosynth. Res. **42** : 203-215.

Warshel, A. & Karplus, M. (1974)
Calculation of $\pi\pi^*$ Excited State Conformations and Vibronic Structure of Retinal and Related Molecules.
J. Am. Chem. Soc. **18** (4) : 5677-5689.

Weber, P. C. (1991)
Physical principles of protein crystallisation.
Adv. Prot. Chem. **41** : 1-36.

Weiss, M.S. & Hilgenfeld, R. (1997)
On the Use of the Merging R-Factor as a Quality Indicator for X-Ray Diffraction.
J. Appl. Cryst. **30** : 203-205.

Wilson, C.M. (1983)
Staining of Proteins on Gels: Comparison of Dyes and Procedures.
Methods in Enzymology **91** : 236-247.

Williams, J.C., Steiner, L.A., Ogden, R.C., Simon, M.I. & Feher, G. (1983)
Primary Structure of the M-Subunit of the Reaction Center from *Rhodopseudomonas Sphaeroides*.
Proc. Natl. Acad. Sci. U.S.A **80** : 6505-6509.

Williams, J.C., Steiner, L.A., Feher, G. & Simon, M.I. (1984)
Primary Structure of the L-Subunit of the Reaction Center from *Rhodopseudomonas Sphaeroides*.
Proc. Natl. Acad. Sci. U.S.A **81** : 7303-7307.

Williams, J.C., Alden, R.G., Murchison, H.A., Peloquin, J.M., Woodbury, N.W. & Allen, J.P. (1992)
Effects of Mutations Near the Bacteriochlorophylls in Reaction Centers from *Rhodobacter sphaeroides*.
Biochemistry **31** (45) : 11029-11037.

Witt, H.T., Krauß, N., Hinrichs, W., Witt, I., Fromme, P., Pritzkow, W & Saenger, W. (1992)
Three-Dimensional Crystals of Photosystem I from *Synechoccus sp.* and X-Ray Structure Analysis at 6Å Resolution.
In Research In Photosynthesis (Proc. IX Int. Congress Photosynthesis, Nagoya, Japan) Murata, N. (Ed), Kluwer Academic, Dordrecht, Netherlands, pp521-528.

Woese, C.R. (1987)
Bacterial Evolution.
Microbiol. Rev. **51** : 221-271.

Woodbury N.W. & Allen, J.P (1995)
The Pathway, Kinetics and Thermodynamics of Electron Transfer in Wild Type and Mutant Reaction Centers of Purple Nonsulfur Bacteria
In: Anoxygenic Photosynthetic Bacteria, Blankenship, E.D., Madigan, M.T. & Bauer, C.E. (Eds.), Kluwer Academic Publishers, The Netherlands, p527-557.

Woody, T.A. (1995)
Circular Dichroism.
Methods in Enzymology **246** : 34-70.

Wraight, C.A. (1979)
Electron Acceptors of Bacterial Photosynthetic Reaction Centres II H+ Binding Coupled to Secondary Electron Transfer in the Quinone Acceptor Complex.
Biochim. Biophys. Acta. **548** : 309-327.

Yarmus, L., Rosenthal, J. & Chopp, M. (1972)
EPR of Triplet Excitons in Tetracene Crystals: Spin Polarization and the Role of Singlet Exciton Fission.
Chem. Phys. Letts. **16** : 477-481.

Yeates, T.O., Komiya, H., Chirino, A., Rees, D.C., Allen, J.P. & Feher, G. (1988)
Structure of the Reaction Center from *Rhodobacter sphaeroides* R-26 and 2.4.1.: Protein-Cofactor (Bacteriochlorophyll, Bacteriopheophytin and Carotenoid) Interactions.
Proc. Natl. Acad. Sci. U.S.A. **85** : 7993-7997.

Young, A.C.M., Dewan, J.C, Nave, C. & Tilton, R.F. (1993)
Comparison of Radiation Induced Decay and Structural Refinement from X-ray Data Collected from Lysozyme Crystals at Low and Ambient Temperatures.
J. Appl. Cryst. **26** : 309-319.

Xiong, J., Subramaniam, S. & Govindjee (1996)
Modelling of the D1/D2 Proteins and Cofactors of the Photosystem II Reaction Center: Implications for Herbicide and Bicarbonate Binding.
Protein Science **5** : 2054-2073.

Zinth, W., Knapp, E.W., Fischer, S.F., Kaiser, W., Deisenhofer, J. & Michel, H. (1985)
Correlation of Structural and Spectroscopic Properties of a Photosynthetic Reaction Center.
Chem. Phys. Lett. **119** : 1-4.

Zou, J.Y. & Jones, T.A. (1996)
Towards the Automatic Interpretation of Macromolecular Electron-Density Maps: Qualitative and Quantitative Matching of Protein Sequence to Map.
Acta. Cryst. **D52** : 833-841.